

## STATEMENT

### **Active and Passive Membrane Properties of Motoneurons**

A thesis submitted for the degree of Doctor of Philosophy  
of the Australian National University  
December 2000

by

David W. Thurbon, BSc(Hon). (ANU)

Division of Neuroscience  
John Curtin School of Medical Research  
Australian National University  
Canberra

## STATEMENT

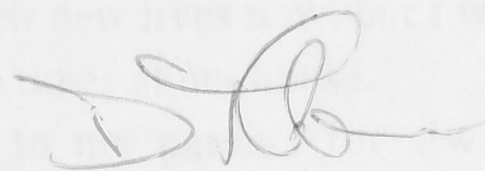
All the work described in this thesis is original. The experiments were performed by me between July 1995 and December 2000 under the supervision of Professor Stephen J. Redman (ANU, Australia) and Professor Hans-R. Lüscher (Universität Berne, Switzerland). Professor Hans-R. Lüscher was involved only with the chapter involving the determination of passive membrane properties. Professor Lüscher carried out part of the analysis and produced the figures for this chapter. His help is gratefully acknowledged. Thomas Hofstetter (Universität Berne, Switzerland) performed the morphological reconstructions for this chapter as well. During the course of this study a number of presentations were made at scientific meetings in Australia and the United States of America. The following abstracts were published in conjunction with these presentations:

Lüscher, H-R., Thurbon, D., Hofstetter, T. and Redman, S.J. (1997). Dendritic recording of action potentials and brief voltage transients in motoneurons of rat spinal cord slices. *Society for Neuroscience*, **23**:512.9.

Thurbon, D., Lüscher, H-R., Hofstetter, T. and Redman, S. J. (1997). Passive cable models of motoneurons and interneurons in rat spinal cord slices. *Society for Neuroscience*, **23**:512.1.

In addition, the following paper, relating to Chapter 3 of this thesis, has been published:

Thurbon, D., Lüscher, H-R. , Hofstetter, T. and Redman, S.J. (1998). Passive electrical properties of ventral horn neurons in rat spinal cord slices. *J. Neurophysiol.* **79**:2485-2502.



David W. Thurbon

## ACKNOWLEDGEMENTS

When I first arrived at the Australian National University at the beginning of 1989, I thought it was all going to be a simple matter of doing a three year degree course and then starting work in science. Well, didn't I find out something. Here I am in the year 2000 and my scientific career is just about to begin. It certainly has been a long time getting here and there have been so many incredibly tough times mixed in with the good times that nothing could possibly try my patience in future.

There are so many people that have contributed to my success over these years that it is virtually impossible to name them all. First and foremost I would like to acknowledge the unwavering efforts of my PhD supervisor, Professor Stephen Redman for having the patience of a saint when dealing with me. He has always remained calm and collected even during times when I screamed, shouted and swore at him horribly. Thanks Steve for giving me more chances than I ever deserved. I certainly wouldn't have made it without your guiding hand to show me the way.

Furthermore, I would like to thank Professor Hans Lüscher for coming to Australia to work with me and for his invaluable help with the passive cable studies on motoneurons. No doubt my postdoctoral studies with him in Switzerland will be successful and enjoyable.

I would also like to thank Garry Rodda, the department's technician, for all his help with my lab work and the thesis figures as well as hours of friendly conversation and input on various aspects of the experimental work and the thesis.

I would also like to convey my thanks to the people here at the Department of Neurophysiology: John Bekkers for his help with experimental techniques and his scientific conversation; John Clements for help with modelling and his program, AxoGraph; Greg Stuart for help with the lab work and modelling, and for reading the introduction; Anna Cowan and Rosemary Martin for getting me started in neuroscience; Christian Stricker for help setting up the rig; Stephen Williams for providing help with the lab work as well as his cynical comments about the people in the lab, which made me feel better when I was down.

I would also like to thank my old mates in Canberra for all the fun times, thanks Paul, Jarrod, Dennis, Caleb, Nathan, Simon, Rich, Tim and all the other people that I know around town. Thanks for the wild times. Thanks also to Hobbo for giving me a bed in Townsville while I was there.

I am also appreciative of the mateship that I developed with my fellow PhD students here at JCSMR. They have all long since gone on to their new lives now, but I will always remember them. Thanks Chris, Cathy, Luc, Greg for the times at uni house.

Above all I would like to express my thanks to my parents for always being supportive of my crazy adventures regardless of how mundane or awesome they may have been.

## ABSTRACT

This thesis describes an *in vivo* study of the passive properties of putative rat motoneurons, the action potential attenuation that occurs in the dendrites of these cells and the voltage dependent ionic channels that contribute to this attenuation.

Passive properties of putative motoneurons were determined by fitting modelled responses to the experimental voltage response to a brief current stimulus. This provided information about the passive properties of motoneurons. It was found that the somatic response of these cells to small voltage deviations near resting potential was linear. Fitting of small current pulse voltage transients with a computer model allowed the determination of the passive membrane properties. For four cells, the residuals between the experimental and fitted response suggested that homogeneous membrane properties could more accurately describe the subthreshold responses of these cells. These cells had  $R_m=5.34\pm 0.91\text{K}\Omega\cdot\text{cm}^2$ ,  $C_m=2.35\pm 0.47\mu\text{F}/\text{cm}^2$  and  $R_i=86.50\pm 21.83\Omega\cdot\text{cm}$ . Models with these membrane properties matched the cells' experimentally measured membrane time constant and input resistance with high accuracy. The average membrane time constant ( $\tau_m$ ) of these models was  $12.48\pm 2.90\text{ms}$  and the average input resistance was  $84.00\pm 18.96\text{M}\Omega$ . The passive membrane properties were used to calculate the average electrotonic length of the dendrites to their terminations and the value obtained was  $0.78\pm 0.27\lambda$ . This estimate was biased by dendrites that were removed during the slicing procedure. Calculation of the average electrotonic length without inclusion of cut dendrites gave a value of  $0.85\pm 0.14\lambda$ . Overall, these results suggest that the passive description of the motoneurone provided here is not greatly different to that provided previously for cat motoneurons with DC signals (Clements & Redman 1989, Fleshman *et al.* 1988, Ulrich *et al.* 1994). However, the higher value of capacitance reported here indicates that rapid voltage signals will be attenuated more heavily than was previously thought for these cells.

Experiments were also performed which explored the contribution of the A-type potassium conductance to action potential attenuation in the dendrites of motoneurons. This involved the use of dendritic recordings to explore action potential attenuation in the dendrites of spinal motoneurons. Dendritic electrodes could not be placed further from the soma than about  $50\mu\text{m}$ . The average distance at which recordings were made was  $37\pm 8\mu\text{m}$ . The average action potential attenuation at this distance was  $10.7\pm 6.2\%$ . This is an average of  $8.1\text{mV}$  of attenuation for a  $74\text{mV}$  action potential at the soma. Action potentials were always found to peak at the soma first followed by the dendrite indicating that the site of action potential generation is close to the soma. The average temporal separation between the action potential peaks was  $54.4\pm 45.6\mu\text{s}$  for an electrode separation of  $37\pm 8\mu\text{m}$  giving a

conduction velocity of 0.68m/s. In some cases, no temporal separation of the action potentials was observed. Blockade of the A-current produced a 4mV increase in the amplitude of the action potential indicating that the A-current contributes to the action potential amplitude at the soma. Measurement of the attenuation using soma-dendritic recordings did not reveal any differences in the amount of attenuation that occurred under control conditions and under A-current blockade. An attempt was made to determine if blocking the dendritic A-current intracellularly with 4-AP could reveal a difference in the channel density between the soma and dendrites. However, because the A-current blocker 4-AP does not cross the membrane quickly enough, this experiment was not successful.

A theoretical exploration of the effect of dendritic voltage-dependent conductances on the action potential amplitude in the dendrites was also made. It was possible to reproduce the recorded action potential waveform in the model by using contrived conductances and a simplified axonal morphology. This also produced a voltage-dependent  $\text{Na}^+$  channel which qualitatively mimicked the amplitude and time-course of currents recorded in rat motoneurons by Safronov and Vogel (1995). Modelling of the influence of dendritic  $\text{Na}^+$  and A-currents on action potential amplitude revealed that  $\text{Na}^+$  currents contribute most to action potential amplitude in the distal dendrites, while A-currents were more important at proximal locations.

---

# Table of Contents

---

<i>Statement</i>	ii
<i>Acknowledgements</i>	iii
<i>Abstract</i>	iv
<i>Table of Contents</i>	vi
<b>Chapter One: Introduction</b>	1
<b>Historical Perspective</b>	1
<b>Compartmental Models of Neurones</b>	8
<i>Problems with Compartmental Modelling I: Electrophysiology</i>	13
<i>Problems with Compartmental Modelling II: Morphology</i>	15
<b>Passive Properties of Spinal Motoneurones</b>	16
<b>Action Potential Backpropagation and Dendritic Active Conductances</b>	19
<i>Purkinje Cells</i>	22
<i>Retinal Ganglion Cells</i>	23
<i>Dorsal Horn Neurones</i>	24
<i>Thalamocortical Neurones</i>	25
<i>Neurones of the Substantia Nigra</i>	25
<i>Hippocampal Pyramidal Cells</i>	26
<i>Pyramidal Cells of the Sensorimotor Neocortex</i>	33
<b>Dendritic Active Conductances and Backpropagation in Motoneurones</b>	38
<b>Immunocytochemical Localisation of Motoneuronal Ion Channels</b>	42
<b>Concluding Comments</b>	43
<b>Chapter Two: Methods</b>	45
<b>Dissection</b>	45
<b>Recording</b>	46
<b>Histology and Morphological Reconstruction</b>	47
<b>Chapter Three: Passive Properties of Motoneurones</b>	49
<b>Introduction</b>	49
<b>Methods</b>	49
<i>Two Electrode Experiments</i>	53

	<i>Reciprocity</i>	53
	<i>Modelling Methods</i>	56
	<i>Onset and duration of Fit Interval</i>	56
	<i>Fit Acceptance and Precision of Parameter Estimation</i>	57
	<i>Determination of <math>L_{avg}</math></i>	67
	<b>Results</b>	68
	<i>Morphology</i>	68
	<i>Electrophysiological Measurements</i>	74
	<i>Compartmental Models</i>	74
	<i>Optimal Fits and Parameter Values</i>	74
	<i>Passive Electrotonic Structure</i>	87
	<i>Fitting Transients from Two Electrodes</i>	87
	<i>Test for Reciprocity</i>	91
	<b>Discussion</b>	94
	<i>Identification of Motoneurons and Interneurons</i>	94
	<i>Passive Cable Parameters</i>	95
	<i>Fitting Transients from Two Electrodes</i>	97
	<i>Reciprocity</i>	98
	<i>Electrotonic Profile of Motoneurons</i>	99
	<i>Simulation of Synaptic Input.</i>	99
	<i>The Passive Motoneurone</i>	104
	<b><u>Chapter Four: Action Potential Propagation in Motoneurone Dendrites</u></b>	107
	<b>Introduction</b>	107
	<b>Methods</b>	110
	<i>Recordings</i>	110
	<i>Isolation of the A-current</i>	110
	<i>Action Potential Amplitude Versus Membrane Potential and 4-AP</i>	112
	<i>The Effect of 4-AP on Somatic and Dendritic Action Potentials</i>	112
	<i>Blockade of the A-current with Intradendritic 4-AP</i>	113
	<b>Results</b>	113
	<i>Control Recordings at the Soma</i>	113
	<i>Action Potentials in Soma and Dendrites</i>	114

<i>Time Differences Between Somatic and Dendritic Action Potentials</i>	115
<i>Isolation of the A-current</i>	126
<i>Effect of 4-AP on Somatic and Dendritic Action Potentials</i>	127
<i>Effect of Membrane Potential on Action Potential Amplitude</i>	134
<i>Blockade of the A-current Using Intradendritic 4-AP</i>	135
<b>Discussion</b>	140
<i>Action Potential Decrement</i>	140
<i>Initiation Site of the Action Potential</i>	141
<i>The A-current in the Motoneurone</i>	141
<i>The Effect of 4-AP on Action Potential Waveform</i>	144
<i>Effect of Intradendritic 4-AP on Somatic and Dendritic Action Potentials</i>	145
<i>Conclusions</i>	145
<b><u>Chapter Five: Modelling of Action Potential Backpropagation</u></b>	147
<b>Introduction</b>	147
<b>Methods</b>	147
<i>Contrived Sodium Channel</i>	149
<i>Delayed Rectifier</i>	154
<i>Active Dendrites</i>	154
<i>Transient Potassium Current (<math>I_A</math>)</i>	155
<i>The Sodium Channel of Mainen et al. (1995)</i>	160
<i>Action Potential Amplitude Versus Dendritic Diameter</i>	161
<b>Results</b>	161
<i>Action Potential Attenuation with Distance from the Soma</i>	161
<i>Action Potential Attenuation and Dendritic Diameter</i>	189
<b>Discussion</b>	200
<i>The Simulated Action Potential</i>	200
<i>Dendritic Ion Channels</i>	200
<i>Action Potential Attenuation Versus Distance from the Soma</i>	201
<i>Comparison of the Model with that of Lüscher and Larkum (1998)</i>	202
<i>Action Potential Amplitude Versus Dendritic Diameter</i>	203
<i>Comparison of Modelled Results with Experimental Measurements</i>	203
<i>Conclusions</i>	203



<b>Chapter 6: General Discussion</b>	207
<b>Improvements to the Techniques Used</b>	209
<i>Passive Properties</i>	209
<i>Visualisation</i>	210
<i>A-currents</i>	211
<i>Modelling of Active Conductances</i>	211
<i>Further Work</i>	211
<b>Appendix One: The Biocytin/Neurobiotin Glycerol Whole Mount Technique</b>	213
<b>Materials Required</b>	213
<b>Solutions and times for slice processing</b>	214
<b>References</b>	215

### Historical Perspective

A section of neurite is essentially a cylinder of cytoplasm surrounded by a thin membrane. Electrically, the cytoplasm acts as a series resistance or core conductor with the membrane, but both resistance due to leak channels, and capacitance due to the charge separation across the membrane and its dielectric properties. This structure is recognised as an electrical cable and the transfer of applied voltage or current along this structure is defined by cable theory.

---

## Chapter One

### General Introduction

---

Axons transmit nerve impulses without decrement, often over large distances. To do this, they have a high density of sodium channels, and repeat their geometrical and electrical properties along their length. In contrast to the axon, dendrites are short, taper and have a relatively low density of voltage-dependent conductances compared with the axon (Black *et al.* 1990, Stuart & Sakmann 1994, Magee & Johnston 1995a, Bischofberger & Jonas 1997, Safronov *et al.* 1997, Martina *et al.* 2000, Williams & Stuart 2000a). Usually it is the dendrites that contain most of the membrane surface area of a neurone and it is here that the majority of synaptic contacts are made with the axon terminals of presynaptic cells. Therefore, synaptic potentials must be transmitted through the dendrites before they finally sum to produce action potentials at the axon hillock. The way in which synaptic potentials are generated and sum in the dendrites is important for determining the membrane potential that occurs at the site of action potential initiation and this in turn determines the temporal firing patterns of the neurone.

The dendritic properties important for synaptic processing can be described as either passive or active. This distinction refers to the voltage dependence of the dendritic membrane resistance. If the membrane resistance does not vary with membrane potential then the dendrites are considered passive. If the membrane resistance varies with membrane potential, as happens when voltage-dependent ion channels are present, then the dendritic properties are described as active. The passive properties of a neurone are fixed by its geometry and the physical properties of its components, the membrane, cytoplasm and extracellular fluid. If voltage-dependent ion channels are present in the membrane then the active properties imparted by these channels will be overlaid on the passive membrane properties. Neurones with active dendrites can also behave passively when membrane potential changes are too small or not in the appropriate voltage range to cause changes in the activation state of dendritic voltage-dependent ion channels. This chapter gives a historical perspective and brief description of the scientific study of passive and active properties of neuronal dendrites.

#### Historical Perspective

A section of dendrite is essentially a cylinder of cytoplasm surrounded by a tube of membrane. Electrically, the cytoplasm acts as a simple resistance or core conductor while the membrane has both resistance due to leak channels and capacitance due to the charge separation across the membrane and its dielectric properties. This structure is recognised as an electrical cable and the transfer of applied voltage or current along this structure is defined by cable theory.

The designation 'cable theory' comes from the derivation and application of the cable equation for calculations essential to the first transatlantic telegraph cable around 1855 by Professor William Thompson, later known as Lord Kelvin (1855, 1856). Thompson had used the mathematical methods pioneered by Fourier and he knew that his one dimensional cable equation was essentially the same partial differential equation that Fourier had used to describe the conduction of heat in a wire or ring. In the 1870's, Hermann (1879) and Weber (1873) were tackling the problem of electric current flow in and around an axon. They came up with the 'core conductor theory' by deriving and applying a different partial differential equation that accounted for three-dimensional space in a cylindrical coordinate system. Weber's solutions made explicit the non-uniformity of potential and current density in regions near an electrode.

Weber himself pointed out that, with increasing distance from the electrode, the potential within cylindrical cross sections of an axon becomes more uniform and the potential approaches an exponential decrement with distance along the core conductor. Thus for locations not too close to an electrode, the steady state results of the three-dimensional core conductor theory approach the simpler results of one dimensional cable theory. Later, around 1900, Hermann and others recognised that when this core conductor equation was reduced to one spatial dimension, it became equivalent to Thompson's cable equation. The conclusion from this was that the one dimensional cable theory provided an excellent approximation of the behaviour of cables for most purposes, where cable lengths are many times their diameter.

Experimental testing with single unmyelinated axon preparations by several groups in the 1930's and 1940's (e.g. Hodgkin & Rushton 1946) provided important evidence that confirmed the relevance of cable theory to nerve axons. However the application of cable theory to complex dendritic neurones only began in the late 1950's when it became necessary to interpret experimental data obtained from individual motoneurones by means of intracellular microelectrodes located in the soma. The application of cable theory to the dendrites of motoneurones was pioneered by Wilfred Rall in a series of seminal papers from 1957 to 1977 (Rall 1957, 1959, 1960, 1962a, 1962b, 1964, 1967, 1969a, 1969b, 1970a, 1970b, 1977).

The important parameters that could be calculated with Rall's equations were the electrical length of the neurone's dendritic tree, the membrane time constant and the ratio of the somatic membrane conductance to the dendritic input conductance. These three parameters gave some idea of the steady state attenuation and frequency filtering of synaptic potentials that would occur along the dendritic tree. Estimates were obtained from the whole-cell input resistance combined with exponential peeling (Rall 1969a). This method relies on the fact that the voltage decay following a current pulse can be expressed as an infinite series of exponentials:  $V(t) = C_0 e^{-t/\tau_0} + C_1 e^{-t/\tau_1} + C_2 e^{-t/\tau_2} + C_n e^{-t/\tau_n} + \dots$

Each of the time constants  $\tau_0$ ,  $\tau_1$ ,  $\tau_2$  and  $\tau_n$  are successively shorter and  $\tau_0$  is equal to the membrane time constant  $\tau_m$ . Given an experimental current clamp voltage transient, one can recover the longest time constant  $\tau_m$  by fitting a straight line to the linear portion of a semi-logarithmic plot of the transient. With low noise recordings, it is possible to separate two additional time constants ( $\tau_1$  and  $\tau_2$ ) by successive peeling of linear portions of the transient (see figure 1.1). The ratio of time constants can then be used to estimate the average electrotonic length of the neurone in question using the equations derived by Rall (1969a).

Wilfred Rall's papers developed the application of cable theory to motoneurone dendritic trees by assuming that the entire dendritic tree could be reduced to a single equivalent uniform cylinder so that the simple cable equation could be applied to determine the membrane time constant and electrical length. For the equivalent uniform cylinder constraint to be valid, two important assumptions were made about the motoneurone's dendritic tree.

The first assumption was that the surface to volume ratio of a dendrites branches must be the same as that of the parent dendrite (see figure 1.2). Mathematically this means that the diameters of the daughter branches of a dendrite raised to the  $3/2$  power would sum to be equal to the  $3/2$  power of the diameter of the parent dendrite. The second assumption for the Rall equivalent cylinder to be valid was that all dendritic terminations must occur at the same electrical length from the soma.

Although evidence now suggests that these assumptions are invalid for both motoneurones and most other neurones (e.g. Barrett & Crill 1974, Clements & Redman 1989, Nitzan *et al.* 1990, Thurbon *et al.* 1994), valuable functional insights and guidance in the design of experiments followed from cable theory results using such models and from studies that explored the effects of different synaptic input distributions over the dendritic tree of neurones (e.g. Lux *et al.* 1970, Nelson & Lux 1970, Brown *et al.* 1981a, Brown *et al.* 1981b, Durand *et al.* 1983, Turner 1984, Ulfhake & Kellerth 1984, Fleshman *et al.* 1988, Coleman & Miller 1989, Nitzan *et al.* 1990, Jackson 1992, Spruston & Johnston 1992, Staley *et al.* 1992, Burke *et al.* 1994). In dendritic trees where the branches do not conform to the  $3/2$  power law and the dendritic terminations are not all at the same electrotonic length, the dendritic tree can be collapsed into an equivalent non-uniform cylinder (Fleshman *et al.* 1988, Clements & Redman 1989). The concept of using an equivalent non-uniform cylinder to represent the dendritic tree of a neurone is valid and is a useful way to reduce dendritic complexity. It provides a simple description of the passive electrotonic structure of the cell and can be used to model the passive electrical responses that would be recorded at the soma during somatic voltage and current manipulations.

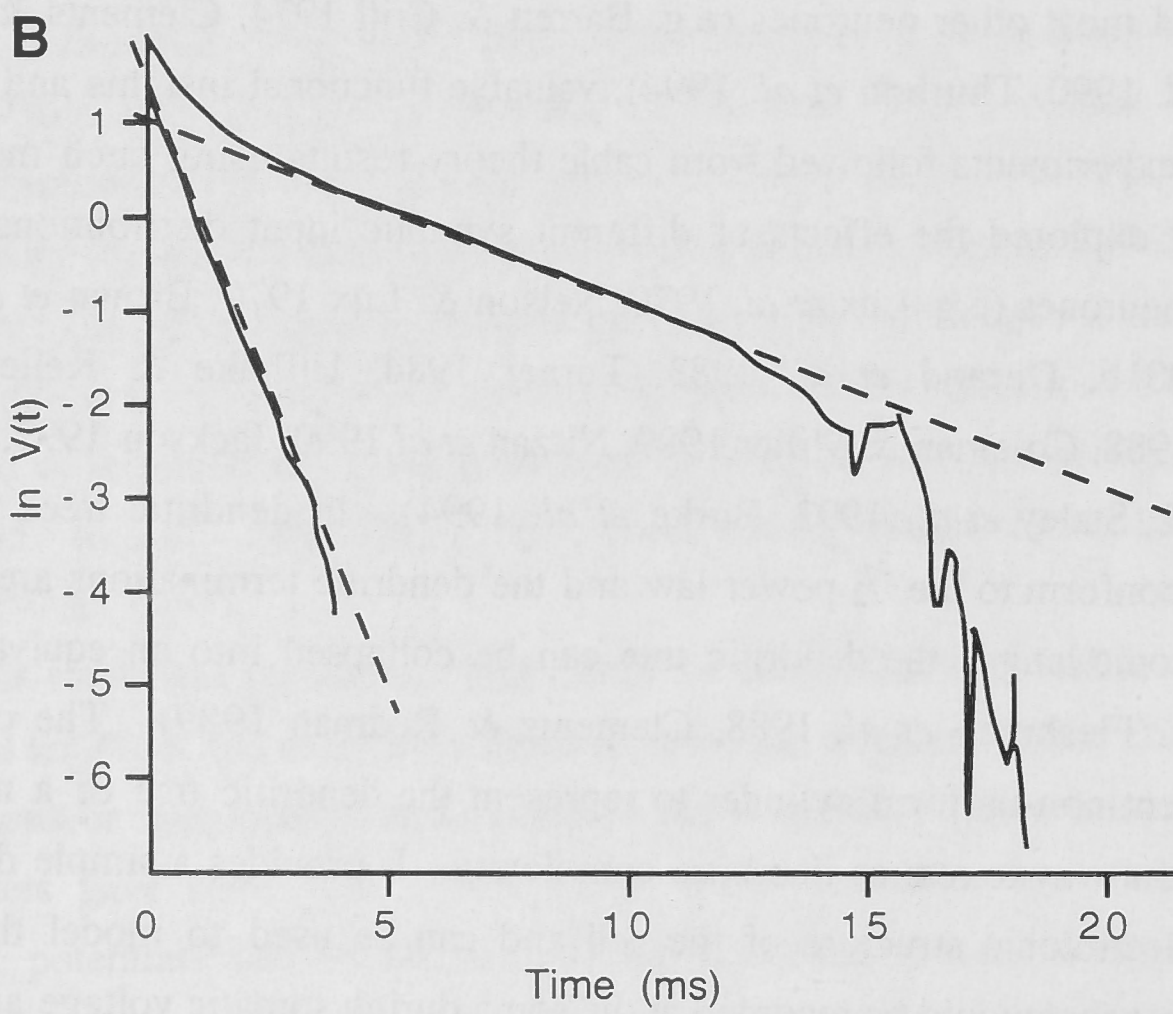
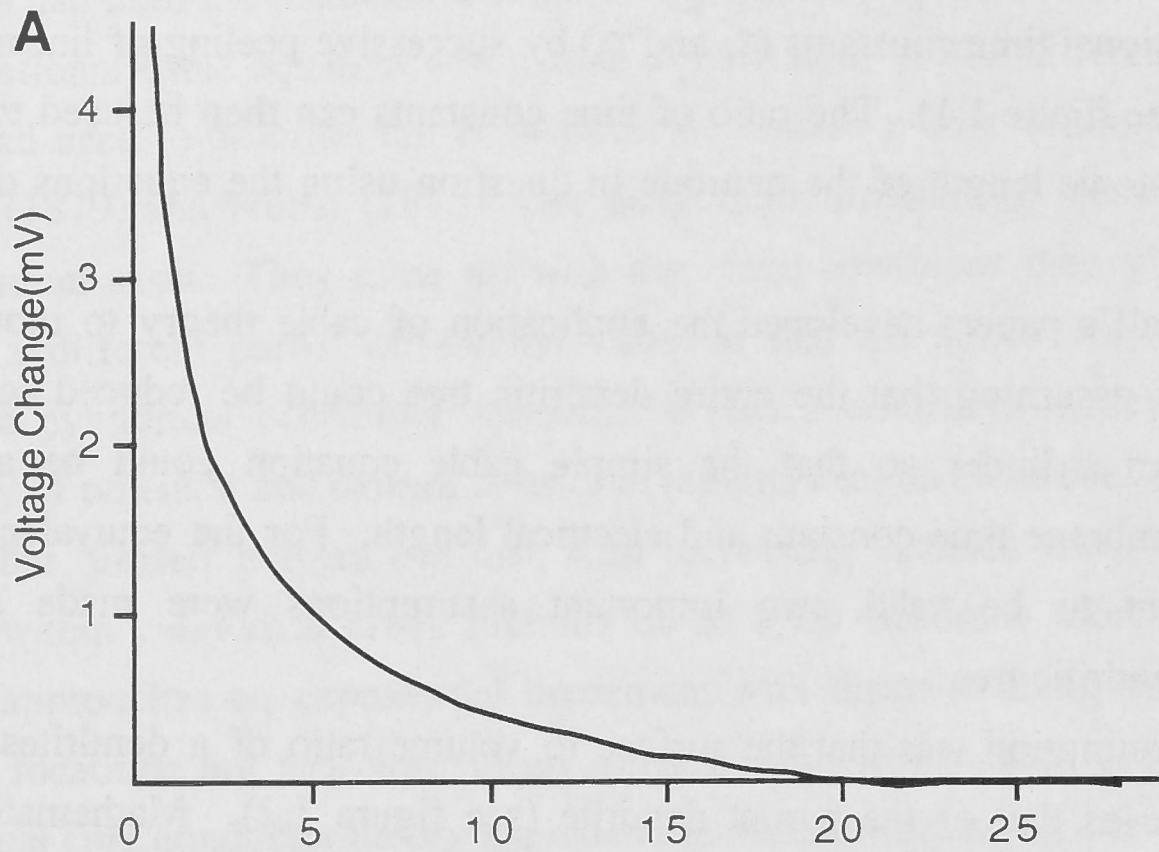


Figure 1.1. **A:** The exponential peeling method of Rall requires the analysis of voltage decay following the application of a current stimulus, in this case a 1ms hyperpolarising current pulse (voltage response is shown inverted). **B:** By making a semi-logarithmic plot of the transient, the linear portion of the transient can be fitted with a straight line and the first time constant,  $\tau_0$ , can be determined. By subtracting away the exponential defined by  $\tau_0$ , a second trace can be made and a second line fitted to define a second time constant,  $\tau_1$ . Rall (1969a) showed that when a voltage change of this kind occurs at one end of an equivalent cylinder with sealed ends, the electrotonic length of that cylinder,  $L$ , can be estimated ( $L_{\text{peel}}$ ) from the ratio of  $\tau_0$  and  $\tau_1$  using the formula:

$$L_{\text{peel}} = \pi \sqrt{\frac{1}{(\tau_0/\tau_1) - 1}}$$

(Figure from Fleshman *et al.* 1988)

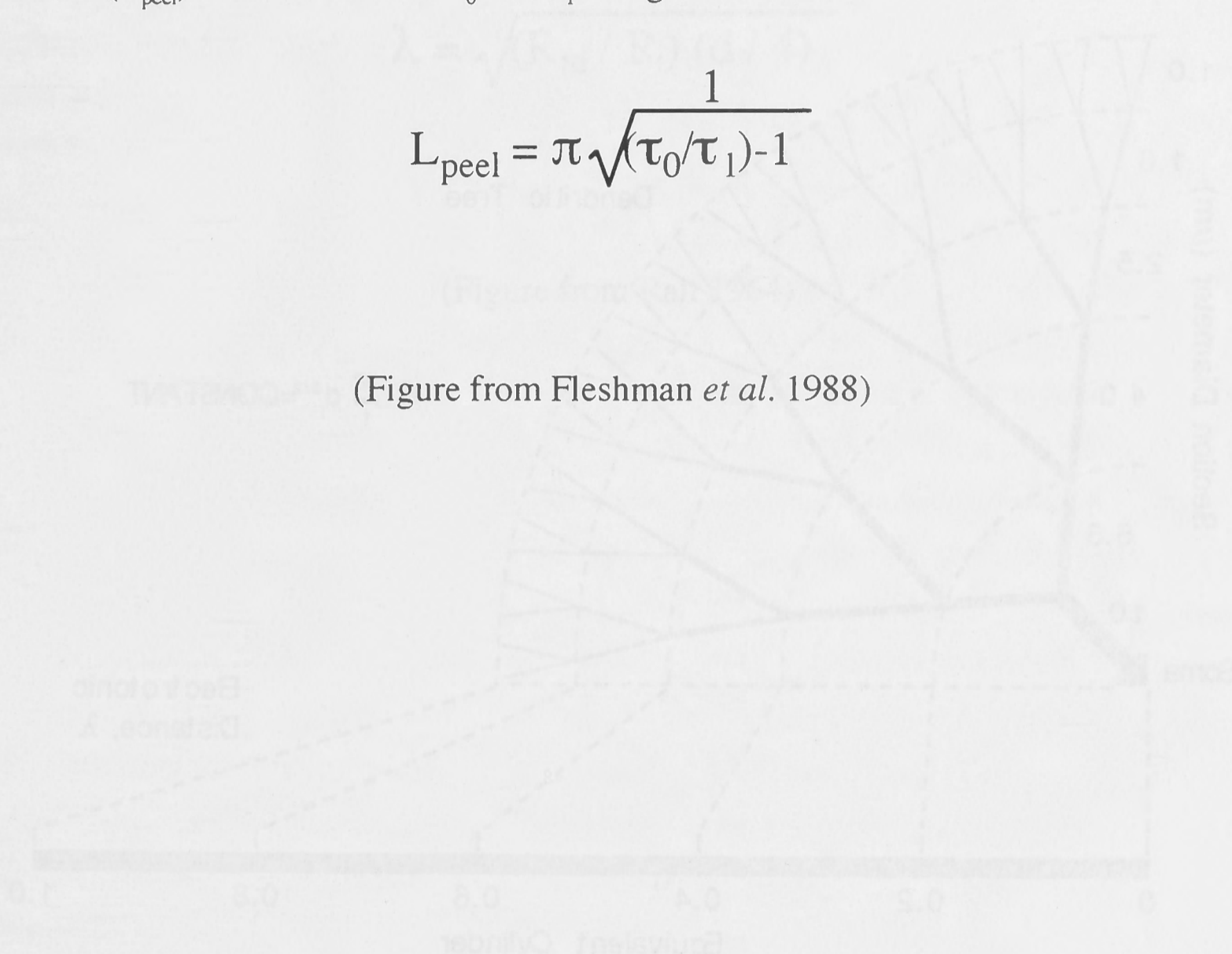


Figure 1. A. The exponential growth method of Hill requires the radius of cyg...  
 decay following the application of a constant stimulus in the case of low frequency...  
 current pulse (other response is shown in detail). B. By tracing a semi-circular...  
 plot of the diameter the larger portion of the dendrite can be fitted with a cylinder the...  
 the first time constant  $\tau_1$  can be determined. The relationship between the exponential decay...  
 by  $\tau_1$  is shown in a can be made with a semi-circular plot of diameter versus time constant...  
 $\tau_1$  (Hill, 1952) showed that when a change of this kind occurs at one end of an...  
 equivalent cylinder with equal ends, the equivalent length of the cylinder can be...  
 estimated from the ratio of  $\tau_1$  and  $\tau_2$  using the formula:

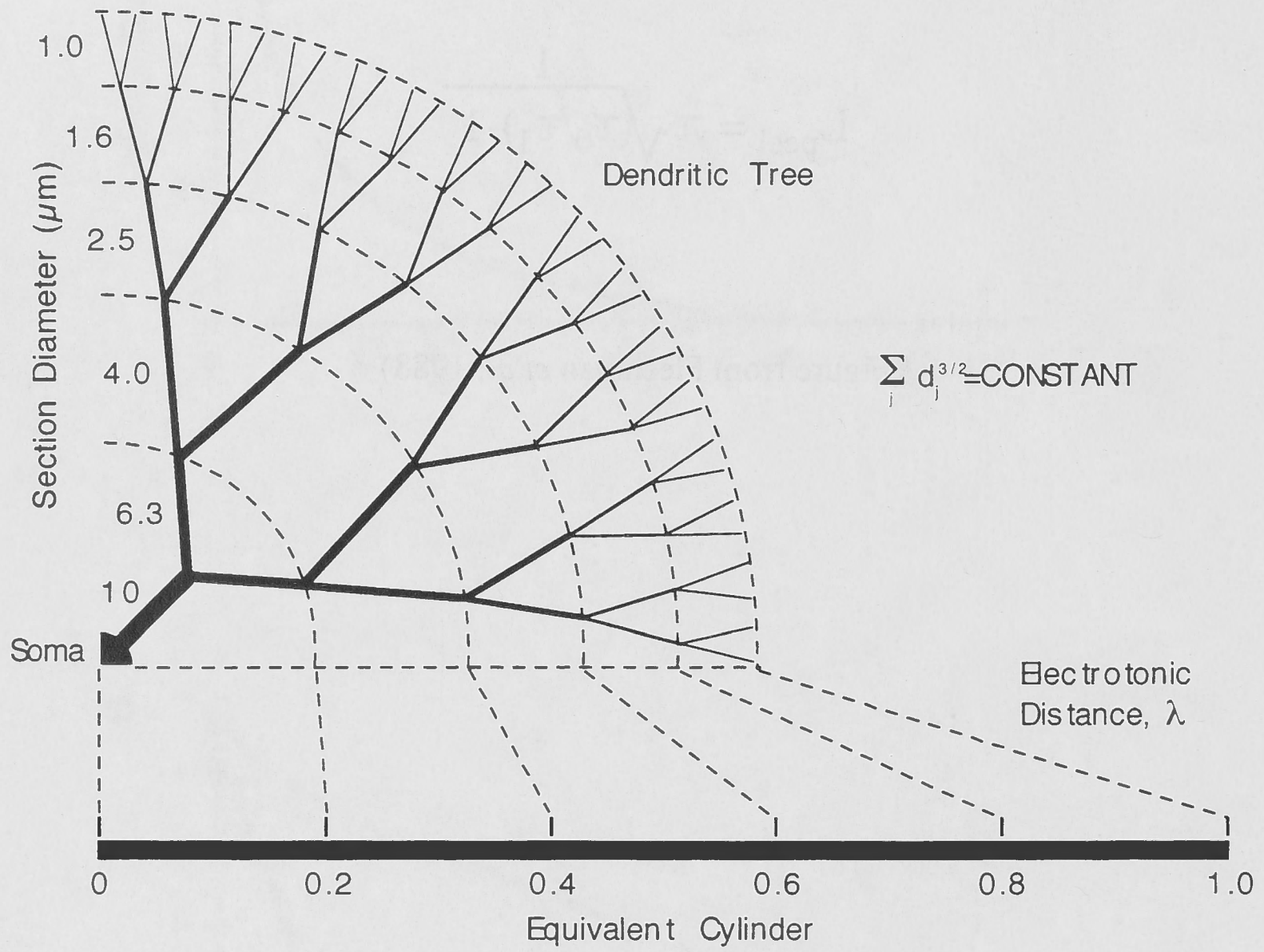


Figure 1.2. A dendritic tree that can be reduced to an equivalent uniform diameter cylinder must conform to several mathematical assumptions. First, the diameter of the parent branch raised to the  $3/2$  power must be equal to the sum of the daughter branch diameters raised to the  $3/2$  power. Second, all dendritic terminations must occur at the same electrotonic distance from the soma. The dashed lines indicate points of equal electrotonic distance in both the dendritic tree and the equivalent cylinder. Steady state electrotonic distance,  $\lambda$ , is defined by the specific membrane resistivity ( $R_m$ ), specific cytoplasmic resistivity ( $R_i$ ), and the diameter of the sections ( $d$ ), by the equation:

$$\lambda = \sqrt{(R_m / R_i) (d / 4)}$$

(Figure from Rall 1964)



Obviously, the best way to determine the electrotonic properties of a cell is to measure its morphology and electrical properties and then combine these into an electrotonic model of the cell. The first attempt to reconcile the morphology of a neurone with electrical measurements in the same neurone was by Lux *et al.* (1970) who used radiolabelled glycine injected into a cat spinal motoneurone. The tissue was then sliced very thinly and each slice was left on a photographic plate to expose for many months. Exponential peeling in combination with the equivalent cylinder model of the motoneurone derived from the measured morphology, allowed the calculation of the specific membrane resistivity and the electrotonic length of these cells. Measurements of electrotonic length derived from the morphological model combined with the estimates of  $R_m$ , gave values of electrotonic length ( $1.5\lambda$ ) that were in agreement with estimates derived from the peeling process.

The one dimensional cable theory describes current flow in a continuous passive cable using partial differential equations with the appropriate boundary conditions and can be applied to an idealised class of dendritic trees that are equivalent to unbranched cylinders. Mathematical solutions of the steady state response of such cables to various current and voltage conditions exist but become excessively complex when tapering, branching, synapses, active currents and non-steady state conditions are considered. As pointed out by Rall (1964) these complexities may be dealt with by using a compartmental model of the neurone.

### **Compartmental Models of Neurones**

A compartmental model breaks the dendritic tree of a neurone into small compartments whose responses can be dealt with separately. The advantage of a compartmental model is that it places no restrictions on the properties of the compartments except that they be isopotential. Compartments can represent any part of a neurone and may be passive or active. They may also contain a variety of synaptic inputs. Also complex dendritic and axonal branching structures, tapering and other morphological irregularities may be readily accounted for in the connection of the compartments.

In principle, a compartmental model replaces the partial differential equations of the cable theory with a series of partial difference equations. If the dendrites of a neurone are divided into sufficiently small compartments then only small errors will occur by assuming that each compartment is isopotential and spatially uniform in its electrical properties. Any non-uniformity that occurs is accounted for by numerous compartments, each with different properties.

In a section of isopotential dendrite that has a membrane resistance that is passive, the resting ionic conductances of the membrane can be represented by a single resistance ( $r_m$ ). The dielectric properties of the lipid bilayer are represented by a capacitance ( $c_m$ )

which is in parallel with the membrane resistance. The resting potential is taken to be zero since only changes in the membrane potential are important for the calculations. The cytoplasm connects the compartments together and is represented by a resistance ( $r_i$ ) connecting the compartments. It is assumed that the resistance of the extracellular medium is very low relative to  $r_i$  and therefore isopotential, so the extracellular medium is taken as a zero voltage reference.

To build a compartmental model that faithfully represents the details of neuronal morphology, the three-dimensional structure of the cell must be measured. This involves staining a single cell and recording its morphology (e.g. Lux *et al.* 1970, Barrett & Crill 1974, Durand *et al.* 1983, Turner & Schwartzkroin 1983, Turner 1984, Shelton 1985, Fleshman *et al.* 1988, Clements & Redman 1989, Nitzan *et al.* 1990, Burke *et al.* 1994, Major *et al.* 1994, Rapp *et al.* 1994, Thurbon *et al.* 1994, Carnevale *et al.* 1997, Reyes *et al.* 1998). The dimensions of the soma and the lengths and diameters of all the dendritic and axonal branches are measured. The number of compartments necessary to represent an entire neurone depends on the morphology of the cell and on computational considerations. In the case of complicated dendritic trees such as those of pyramidal cells (Turner & Schwartzkroin 1983, Major *et al.* 1994), spinal  $\alpha$ -motoneurons (Clements & Redman 1989, Ulrich *et al.* 1994) and cerebellar Purkinje cells (Shelton 1985, Rapp *et al.* 1994), hundreds or even thousands of anatomical compartments may be needed to represent the morphology accurately. For less extensively branched cells, such as vagal motoneurons and hippocampal interneurons, a few dozen compartments may be sufficient (Nitzan *et al.* 1990, Thurbon *et al.* 1994). There are tradeoffs among the number of compartments used in a model, the amount of error one can tolerate and the amount of computer memory and time required to do the analysis.

Figure 1.3 shows an example of the process of decomposing a stained neurone into geometrical subunits. Figure 1.3A shows a reconstruction of a small dendrite in which diameters have been resolved and dendritic lengths are known and have been corrected for the depth of each section into the tissue. Using these measurements, nine segments were needed to represent this dendrite and one more was used for the soma. The compartmental representation of this structure by cylinders is shown in figure 1.3B. The corresponding electrical circuit that represents this anatomical segmentation is given in figure 1.3C.

Figure 1.3 shows schematically how neuronal structures are transformed, and represented as compartmental models, but the values of the electrical elements in figure 1.3C are not yet defined. For this purpose we assume that the cell is in a resting state, that the membrane conductance is passive, and that the specific electrical properties of the membrane and cytoplasm are identical everywhere in the cell. If the values of specific membrane resistance ( $R_m$ ,  $K\Omega.cm^2$ ), specific membrane capacitance ( $C_m$ ,  $\mu F/cm^2$ ) and specific cytoplasmic resistivity ( $R_i$ ,  $\Omega.cm$ ) are known, it is possible to calculate the values

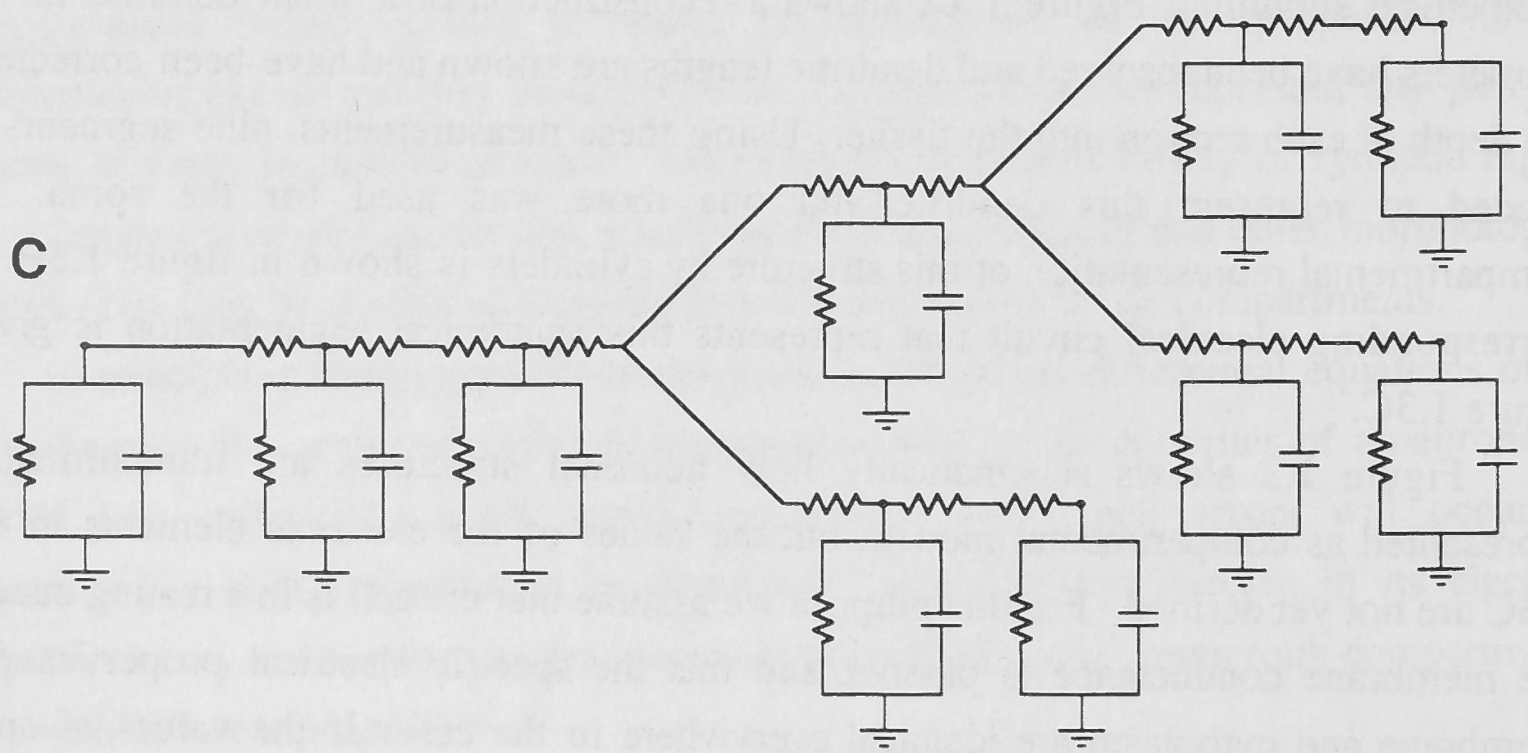
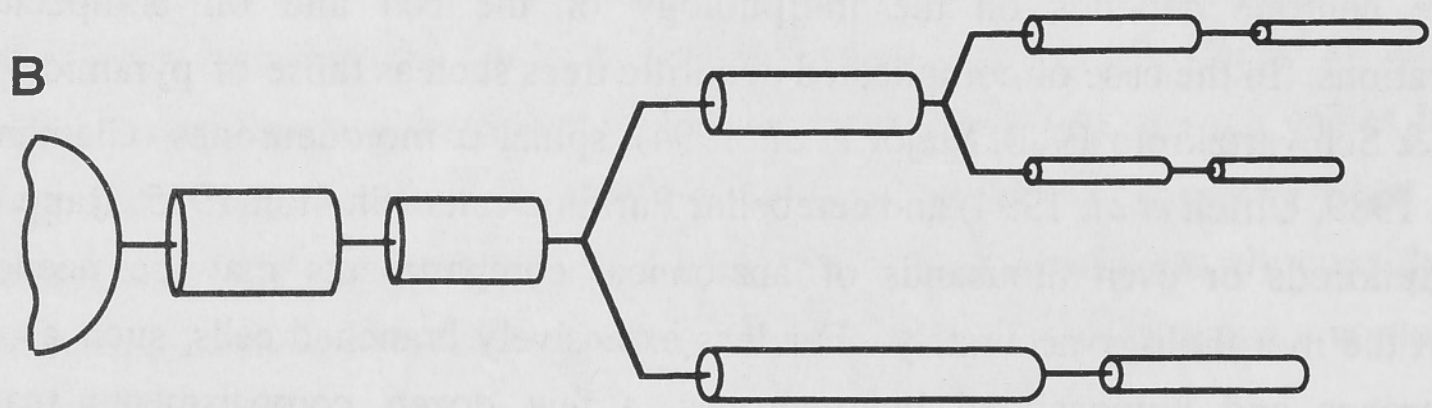
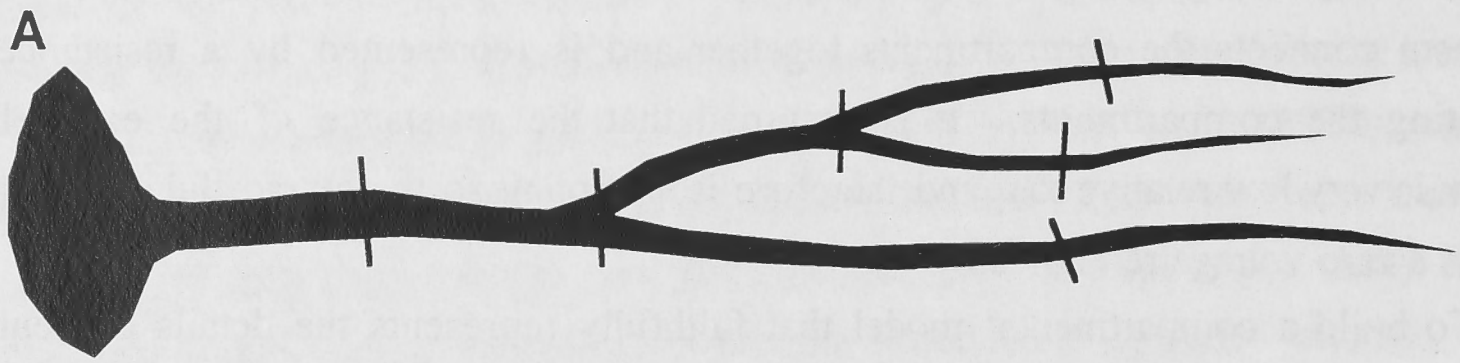


Figure 1.3. The process of converting a stained dendrite into a compartmental model. **A:** A stained dendrite and its origin at the soma. It can be divided into small sections and represented by cylinders of the same geometry as shown in **B**. These form the basis of the compartments in the compartmental model. **C:** This is the equivalent circuit, or compartmental model, of the dendrite shown in **A**. Each segment is represented by an RC circuit and is joined to other compartments by resistive links representing the cytoplasm. The values of each component in this circuit are calculated from the geometry of each segment and the values of specific membrane resistance ( $R_m$ ), specific membrane capacitance ( $C_m$ ) and specific cytoplasmic resistivity ( $R_i$ ).

(Figure from Segev *et al.* 1989)

of the circuit components (denoted as  $r_m$ ,  $c_m$  and  $r_i$ ) for each compartment in the model from the surface area, length and cross sectional area of each segment.

To represent the non-isopotentiality of the system adequately, the electrical length of the compartments should not be too long. Comparisons of responses of compartmental models with the responses obtained from analytical results for the same models (Segev *et al.* 1985) led to suggest that as a rule of thumb, compartments should be shorter than 0.2 length constants, although 0.05 or less is commonly used.

Early attempts to use compartmental models matched simple electrophysiological measurements such as input resistance and decay time constant (e.g. Lux *et al.* 1970, Barrett & Crill 1974). This made calculations simple, allowing electrotonic parameters to be determined within a reasonable period of time.

With the appearance of more powerful computers, further refinement of the study of dendritic cable properties was achieved using computer models. In this technique, detailed electrical models of the cell were made by using the cell's reconstructed morphology as the basis for the model and attempts were then made to match the response of the model to the experimental response. The first attempt to do this was by Barrett and Crill (1974) who used the cable equations to model dendritic sections and then attempted to match the modelled and experimental input resistances.

In 1989, Clements and Redman produced a procedure by which the modelled and experimental data could be fitted using an optimisation procedure. This essentially searched for values of the cable properties of the model ( $R_m$ ,  $R_i$  and  $C_m$ ) which could provide the best match to the experimental data. Once morphological measurements are entered into the computer, new values of  $R_m$ ,  $C_m$  and  $R_i$  can be applied and used to make a new compartmental model. Using this method, the electrical behaviour of the model cell to the experimental stimuli is calculated and  $R_m$ ,  $C_m$  and  $R_i$  are altered until the experimental and calculated transients match. A search is made for those combinations of  $R_m$ ,  $C_m$  and  $R_i$  that minimise the error between the experimental and theoretical transients. The values that give the best fit between transients may be considered good estimates of the specific electrical properties.

The optimisation method of Clements and Redman was rapidly accepted as the most effective way to determine cable parameters and the technique was then applied to various types of neurones (e.g. Clements & Redman 1989, Nitzan *et al.* 1990, Burke *et al.* 1994, Major *et al.* 1994, Rapp *et al.* 1994, Thurbon *et al.* 1994, Ulrich *et al.* 1994, Carnevale *et al.* 1997). Early work using the optimisation technique allowed a more detailed investigation of the passive properties of neuronal dendrites. Initially, little was known about how accurate the derived parameters were and how unique was the combination of parameters that provided the best fit to the experimental data. The problems of compartmental modelling are dealt with briefly here.

Early attempts at compartmental modelling made use of sharp microelectrodes. For a long time it was known that the soma membrane resistivity of motoneurons was lower than the dendritic membrane resistivity (Iansek & Redman 1973) but evidence that this was due to penetration of the cell with a microelectrode was not obtained until Staley *et al.* (1992) published their work on the comparison of microelectrode and whole-cell recordings. Their work indicated that a considerable somatic conductance was introduced when using sharp electrodes and this in turn activated an ion channel whose conductance reversed near the resting potential (around -75mV). The suggestion was that penetrating a cell with a microelectrode caused a hole to be formed around the penetration point that allowed  $\text{Ca}^{2+}$  into the cell and cause an activation of the  $\text{Ca}^{2+}$  dependent  $\text{K}^+$  channel. It has been suggested that the hole formed around the microelectrode is a non-specific conductance simply because it is a hole through which all ions can pass equally well. It would be expected from ionic concentrations and membrane potential that the main ions that conduct charge through the somatic leak would be calcium, sodium, potassium and chloride.

Other work by Nitzan *et al.* (1990), Pongracz *et al.* (1991), Spruston and Johnston (1992), Burke *et al.* (1994) and Thurbon *et al.* (1994) has also suggested that there is a large leak around the point of penetration of the microelectrode. Thurbon *et al.* (1994) used whole-cell recordings from CA1 interneurons and compartmental modelling to determine the passive properties of these cells. For those neurons in which a holding current was necessary to maintain membrane potential (usually indicative of electrode damage) there was less sensitivity of the fitting procedure to the upper limit of  $R_m$  than there was for neurons that did not require a holding current. Therefore, cells with a large electrode leak could have a wide range of optimal  $R_m$  values, while cells in which the leak was small had optimal values of  $R_m$  that were lower and fell within a narrow range. Thurbon *et al.* (1994) overcame this problem by using the method adopted by Clements and Redman (1989). They selected a lower value of  $R_m$  for their model such that it gave a 20% worse fit than the optimal value of  $R_m$ . In this way, a lower limit for the optimal value of  $R_m$  could be determined. When using this method it was found that cells with low leak showed little difference between the values of  $R_m$  obtained for the optimal fit and the 20% worse fit, while leaky cells had values of  $R_m$  which differed greatly between the optimal and 20% worse fit. This conclusively showed that when using compartmental models to determine the electrotonic parameters of cells in which there is a large leak conductance,  $R_m$  would be overestimated.

The finding that electrode leak could affect the quality of the derived parameters was important. It meant that earlier studies using microelectrodes and compartmental models (e.g. Fleshman *et al.* 1988, Clements & Redman 1989) had overestimated  $R_m$ .

Furthermore, studies that had used microelectrodes but had not included a leak in their model tended to have unusually high values of membrane capacitance, at least by present standards and this is now known to be caused by omitting the leak from the compartmental model (Durand *et al.* 1983, Fleshman *et al.* 1988, Burke *et al.* 1994, Thurbon *et al.* 1994). Estimates of the true value of the somatic shunt conductance would require a quantitative adaptation of the method of Svirskis *et al.* (1997) in which an electric field is applied across the preparation to induce a current transient across the shunt conductance. There has not yet been a study of membrane properties in which such a method has been employed. It may also be possible to determine the shunt conductance by placing multiple electrodes on a cell and using a compartmental model to determine the shunt.

Whole-cell recording has its own problems as well. A study by Spruston and Johnston (1992) used both whole-cell and perforated patch-clamp recording to examine the cable properties of hippocampal neurones. Their work showed that whole-cell recordings removed the activity of the voltage-dependent mixed cationic conductance ( $I_h$ ) in these cells, probably because of loss of an intracellular messenger through dilution of the cell contents with the electrode solution. They also showed that when the non-specific  $K^+$  channel blocker  $Cs^+$  was included in the bath solution, not only was the voltage-dependent conductance eliminated but also the membrane properties, notably the membrane time constant and input resistance, were increased. Several workers have used  $Cs^+$  to block voltage-dependent  $K^+$  and mixed cationic conductances in an attempt to linearise highly non-linear membrane responses so that they may examine the passive membrane properties of the cell. However,  $Cs^+$  also blocks the resting  $K^+$  leak conductance (Spruston & Johnston 1992) and therefore changes the membrane resistivity ( $R_m$ ). Under such conditions, it is not possible to make reasonable estimates of specific membrane resistivity and studies in which  $Cs^+$  has been employed (Major *et al.* 1994, Rapp *et al.* 1994) always give very high values for membrane resistivity. However, the other parameters ( $C_m$  and  $R_i$ ) are unlikely to be affected by  $Cs^+$ .

Further problems exist if the noise of the recording is too great. Under these circumstances, the confidence limits of experimentally generated transients become larger, and the number of possible combinations of  $R_m$ ,  $R_i$  and  $C_m$  that can produce optimal fits to the experimental data becomes greater. This leads to non-uniqueness in the estimates. Similar problems of non-uniqueness will occur if one tries to fit a model containing uniform passive properties to a neurone in which the passive properties vary along the dendrites.

## *Problems with Compartmental Modelling II: Morphology*

Just as improvements have been made in the electrophysiological techniques associated with compartmental modelling, so have the techniques for morphological reconstruction. Improvements in optics, reconstruction equipment and histology have been the main contributors to this improvement.

Even as recently as the early 1990's, many reconstructions were performed by slicing the tissue containing the stained cell into thin sections and reconstructing the parts of the dendritic tree present in each thin slice (e.g. Lux *et al.* 1970, Clements & Redman 1989). This introduced errors into the morphology because of the poor resolution of the depth of dendritic sections within the tissue. Once the thin slices were reconstructed, they were then assembled to produce the entire neurone's dendritic tree. More recent reconstructions have used whole-mounted tissue in combination with transducers on the microscope stage to detect the level of focus within the tissue (e.g. Nitzan *et al.* 1990, Major *et al.* 1994, Rapp *et al.* 1994, Thurbon *et al.* 1994). This has resulted in considerable improvement in the accuracy of morphological reconstructions.

To further complicate matters, many of the histological procedures used to stain for tracers such as HRP cause considerable shrinkage of the tissue due to dehydration with alcohol. This shrinkage must be taken into account if the true dendritic dimensions are to be accurately determined for the living cell. Complications may arise because shrinkage may not be the same in each plane of the tissue and the hardened HRP reaction product may not shrink but rather snap and fold as the tissue shrinks (Major *et al.* 1994). The first mention of a shrinkage free histological process being used for compartmental reconstructions was by Thurbon *et al.* (1994). It used the biocytin staining technique of Horikawa and Armstrong (1988), modified by O'Carroll *et al.* (1992) to include clearing and mounting of the tissue in glycerol. This technique does not use alcohol dehydration in the histology and has the advantage that no measurable shrinkage can be detected in the tissue (Thurbon *et al.* 1994, Ulrich *et al.* 1994, Larkum *et al.* 1998, Thurbon *et al.* 1998).

Further refinement in reconstruction has been obtained with the advent of computer aided reconstruction systems. In these systems, the neurone is traced at high magnification and a motorised microscope stage is controlled by computer to keep the computer image aligned with the tissue. Transducers detect the level of focus and allow three-dimensional, continuous reconstruction of a neurone's entire dendritic tree.

A major limitation that is present for all reconstructions is the wavelength of light, which limits the resolution of fine detail to an accuracy of about  $0.2\mu\text{m}$ . However recent advances in single and multi photon confocal microscopy may eventually increase resolution.



## Passive Properties of Spinal Motoneurones

Spinal motoneurones were the first neurones to be examined with the cable theory. The majority of the early work was carried out in cat spinal cord *in vivo* and recordings were made with sharp microelectrodes. Early attempts to determine the electrotonic properties of the motoneurone used only the exponential peeling method developed by Rall (1970b) as it applies to an equivalent cylinder representation of the neurone's dendritic tree. Nelson and Lux (1970) used this technique to measure average dendritic electrotonic length and membrane time constant. This study gave a membrane time constant for motoneurones of 4.2ms and an average electrotonic length of  $1.5\lambda$ .

Iansek and Redman (1973) used a brief intracellular current pulse to examine the membrane properties of the motoneurone. These results were analysed using the technique described by Jack and Redman (1971). The main result of their investigation was that the membrane properties of the soma and dendrites were not the same. That is, the membrane conductance of the soma and dendrites was different either because the soma had a naturally lower resistance than the dendrites, or because of a large conductance introduced by penetration of the soma with a microelectrode. Iansek and Redman (1973) also suggested that the dendritic terminations were either sealed or had high resistance terminations, and that the average electrotonic length of the dendrites was  $1.5\lambda$ .

Another attempt to reconcile the membrane properties of the motoneurone was performed by Barrett and Crill (1974). This was the forerunner of the computerised compartmental models to come, although Rall (1964) was the first to suggest compartmental models as a way to deal with the computational difficulties of complex dendritic trees. Motoneurones were stained with Procion dye and histologically processed to minimise shrinkage. Reconstructed motoneurones were found to have a profile that did not conform to the assumption of an equivalent cylinder and so this provided the first evidence that the assumptions associated with Rall's analytical model of the motoneurone were incorrect. Barrett and Crill (1974) used the reconstructed morphology to build a compartmental model in which each dendritic segment was modelled with the cable equation. They attempted to match the calculated input resistance of the motoneurone with the measured value by varying the specific membrane resistance of the model neurone. Using this method, they calculated a specific membrane resistance for the motoneurone of  $1.8\text{K}\Omega\cdot\text{cm}^2$ . By using this value in combination with the measured membrane time constant, the specific membrane capacitance was calculated to be between 2 and  $3\mu\text{F}/\text{cm}^2$ , although this was subject to errors caused by the fact that the somatic shunt caused by electrode penetration was not included in the analysis (Durand *et al.* 1983, Fleshman *et al.* 1988, Burke *et al.* 1994, Thurbon *et al.* 1998).

Ulfhake and Kellerth (1984) used the same approach as Barrett and Crill (1974) in soleus  $\alpha$ -motoneurons and compared these results with those obtained using the analytical method of Rall (1970b). The results obtained with these methods generally showed that the analytical method gives a higher  $R_m$  value than the input resistance fitting method. Furthermore, calculations of average electrotonic length made from reconstructed morphology and the calculated  $R_m$  of these cells revealed that electrotonic length was generally underestimated by the analytical technique and that motoneurons had dendrites that are several length constants long.

Fleshman *et al.* (1988) used a similar fitting method, but matched the model to the cell's input resistance, membrane time constant and the electrotonic length derived from peeling. The main finding in this study was that models in which  $R_m$  was spatially uniform did not produce a very good fit to the experimental data unless the capacitance was given highly varying values for each cell ( $1.4\text{--}8.6\mu\text{F}/\text{cm}^2$ ). To account for this, Fleshman *et al.* (1988) introduced models with non-uniform  $R_m$ , one in which  $R_m$  increased stepwise from soma to dendrite and the other in which  $R_m$  increased progressively with distance from the soma in a sigmoid fashion. Both of these models gave essentially the same electrical responses at the soma indicating that somatically recorded cell responses were relatively insensitive to the properties of the distal dendrites. Fleshman *et al.* (1988) also introduced the idea of an equivalent dendritic profile calculated from the geometry that allowed a more accurate determination of the membrane time constant  $\tau_m$ . Such an equivalent dendritic profile is useful for determining the response of the cell to electrical manipulations at the soma but cannot be used to model dendritic events. Fleshman *et al.* (1988) concluded from their work that membrane resistivity in motoneurons is probably lower at the soma than in the dendrite and that membrane resistivity varies between different types of motoneurone.

Clements and Redman (1989) further refined the model matching approach to determination of electrotonic properties by applying an optimisation method to the fitting procedure. Short current pulse and voltage clamp responses were recorded from these cells and used as the target transients for the modelling. Representations of motoneurons were built from morphological reconstructions as before. When modelling the cells,  $R_m$ ,  $C_m$  and  $R_i$  could be varied and a new electrical description of the cell could then be made. By simulating the same stimulus as had been used in the experiment,  $R_m$ ,  $R_i$  and  $C_m$  could be varied until the modelled and experimental transients overlay as closely as possible. Once this was done, the values of  $R_m$ ,  $R_i$  and  $C_m$  obtained from the modelling are assumed to be those of the living cell. Clements and Redman (1989) added a further refinement to their model. They included a somatic shunt resistance ( $r_{sh}$ ) in their model to account for a lower somatic membrane resistance due to damage from the microelectrode. They found that such a model produced better fits to their experimental data than could be

obtained if the shunt was not included. Using this approach, Clements and Redman (1989) found that dendritic  $R_m$  ranged from 7 to  $35\text{K}\Omega\cdot\text{cm}^2$  while somatic  $R_m$  was around 100 to  $420\Omega\cdot\text{cm}^2$ . Therefore, dendritic  $R_m$  was about 20 to 100 times greater than somatic  $R_m$  for different neurones. The average dendritic electrical length measured in this study was about  $1.2\lambda$  although most motoneurones had some dendritic terminations at  $2-3\lambda$ . It was suggested that the reason for the low somatic  $R_m$  was a somatic leak caused by microelectrode penetration. Clements and Redman (1989) also suggested that motoneurones are more electrically compact than had hitherto been supposed. They also tried fitting their data with a model in which  $R_m$  increased linearly with electrical distance from the soma but they found that their model was relatively insensitive to changes in  $R_m$  in the distal dendrites.

A similar study by Burke *et al.* (1994) examined cat  $\gamma$ -motoneurones. This study also found it was necessary to include a significantly lower membrane resistance at the soma than in the dendrites. When  $R_m$  was constrained to be uniform in soma and dendrites, implausibly high values of membrane capacitance were required to match the transients. Again it was concluded that the low somatic membrane resistance was due to a shunt caused by penetration with a microelectrode and that the high values of membrane capacitance required for uniform  $R_m$  models were an artifact caused by the somatic shunt.

All these approaches used intracellular microelectrodes. They suffered from: (1) large capacitive artifact distorting the early part of the voltage transient making this early part unusable for either the peeled time constant method (Rall 1970b) or the method of Jack and Redman (1971); and (2) electrode damage that led to a large non-specific conductance at the soma and subsequent  $\text{K}^+$  channel activation as shown by Rose and Vanner (1988).

Rose and Vanner (1988) performed exponential peeling of time constants in cervical motoneurones of the cat and found that a better fit to the experimental data can be obtained when a somatic shunt is included in the analysis. Campbell and Rose (1997) looked at this matter in more detail by measuring the soma to dendritic conductance ratio in the presence and absence of  $\text{Cs}^+$ . They concluded that the intracellular electrode does cause a shunt conductance at the soma but also concluded that the somatic  $R_m$  is lower than for the dendrites because of tonically active  $\text{K}^+$  channels in the somata of motoneurones.

A recent study using organotypically cultured spinal tissue has provided cable parameters for motoneurones (Ulrich *et al.* 1994). This work used whole-cell recording to eliminate problems associated with the microelectrode shunt conductance and has improved the accuracy of the passive membrane parameters obtained for these cells. Using the compartmental model approach and the transient fitting procedure of Clements and Redman (1989), these cells gave an  $R_m$  of  $17.5\pm 3.1\text{K}\Omega\cdot\text{cm}^2$  and  $R_i$  of  $308\pm 39\Omega\cdot\text{cm}$

(n=3). Calculation of the cell capacitance gave a value of  $1.08 \pm 0.23 \mu\text{F}/\text{cm}^2$  (n=6). Using these values with the reconstructed morphology allowed the mean electrotonic path length of these cells to be calculated as  $0.83 \pm 0.2\lambda$  (n=5).

These studies have provided estimates of the passive cable parameters of cat motoneurons *in vivo*, and cultured rat spinal motoneurons. The main problem with these studies is that they use either microelectrodes or cultured cells. Thus they are always either confounded by culture artifacts or by the shunt conductance introduced by penetration of the cell with a microelectrode.

### **Action Potential Backpropagation and Dendritic Active Conductances**

As mentioned previously, neuronal dendritic membrane may contain voltage-dependent conductances in addition to the passive membrane properties. The properties of these voltage-dependent conductances are overlaid on the passive properties of the dendritic membrane and so the passive properties are still an important component of the membrane response even when voltage-dependent conductances are activated. A review of the active properties of neuronal dendrites can be found in Johnston *et al.* (1996) and Häusser *et al.* (2000).

There is a great deal of evidence that the axonally generated action potential can propagate back into the dendritic tree. This 'backpropagation' of the action potential may be either passive or active depending on the properties of the dendrites. Backpropagating action potentials can cause large voltage deviations in the dendritic tree and may activate voltage-dependent conductances. For this reason, backpropagated action potentials can be useful for examining the active properties of dendrites.

The earliest work that suggested action potentials could propagate from the soma back into the dendrites was the work of Chang (1951) in which extracellular field potentials were measured in the cortex during antidromic activation of neurones. This showed that a significant amount of current flowed around the dendrites of cortical cells during antidromic activation.

During the 1950's, the work of Fatt (1957) gave results that also indicated that the action potential propagated into the dendrites. This study used extracellular electrodes to measure current flow in and around the dendritic tree of a motoneurone. Although the results provided poor resolution of the current flow around the dendrites of a motoneurone, they did suggest a significant amount of current flowing into the dendrites of these cells during action potentials.

Some of the earliest work suggesting an active contribution of the dendrites to the action potential was provided by the work of Kandel and Spencer (1961) on hippocampal pyramidal cells. They showed that a fast prepotential occurred at the initiation of the action potential in 25% of their cells and that this prepotential could be generated in

isolation to the action potential. They proposed that the apical dendrites of these hippocampal pyramidal cells contained an active region that contributed to the shape of the somatically recorded action potential and they suggested that this dendritic region could initiate action potentials.

Later, direct recordings from dendrites of cerebellar Purkinje cells (Llinás & Nicholson 1971), cortical neurones (Houchin 1973), and hippocampal pyramidal neurones (Wong *et al.* 1979) provided evidence that action potentials could be initiated in the dendrites and propagate along them. This provided the first conclusive evidence that dendrites could not be considered as simply passive structures.

Recent evidence from cerebellar Purkinje cells (Stuart & Häusser 1994), retinal ganglion cells (Velte & Masland 1999), dorsal horn neurones (Wolff *et al.* 1998), thalamocortical neurones (Williams & Stuart 2000a), substantia nigra neurones (Häusser *et al.* 1995), neocortical pyramidal cells (Stuart & Sakmann 1994, Stuart & Sakmann 1995, Schiller *et al.* 1997, Stuart & Spruston 1998, Larkum *et al.* 1999a, 1999b, Williams & Stuart 1999, Bekkers 2000b, Korngreen & Sakmann 2000, Williams & Stuart 2000b), hippocampal pyramidal cells (Westenbroek *et al.* 1990, Elliott *et al.* 1995, Magee *et al.* 1995, Magee & Johnston 1995a, Magee & Johnston 1995b, Spruston *et al.* 1995, Hoffman *et al.* 1997, Magee 1998, Urban & Barrionuevo 1998, Golding *et al.* 1999, Magee 1999, Magee & Carruth 1999, Tsubokawa *et al.* 2000), hippocampal interneurones (Martina *et al.* 2000), pyramidal cells of the entorhinal cortex (Magistretti *et al.* 1999) and motoneurones (Larkum *et al.* 1996, Westenbroek *et al.* 1998) has confirmed the existence of voltage-dependent ion channels in the dendrites of these cells and that these channels can modify synaptic potentials and backpropagated action potentials. Depending on the type of channel present, they will either attenuate or amplify voltage signals as they propagate through the dendrites. It has been shown that the ionic conductances associated with these active currents include  $\text{Na}^+$ ,  $\text{K}^+$  and  $\text{Ca}^{2+}$ . This complex mixture of active currents and their distribution in the soma and dendrites imparts added complexity to the understanding of how these channels interact to process synaptic inputs.

Interest in backpropagating action potentials has grown recently due to studies of synaptic plasticity that suggest that the action potential could be an important signal for learning in neurones. The requirement for learning postulated by Hebb (1949) was that the input of a neurone should be active at the same time that the output is active in order for learning, or synaptic modification to occur. This process is activity dependent and only those inputs that contribute to the neurone's output are modified. A coincidence detector is required to detect the presence of simultaneous synaptic neurotransmitter release and axonal action potentials. The NMDA receptor is believed to be the coincidence detector because of the way it functions. The NMDA receptor is activated by the neurotransmitter glutamate but the conductance of the channel is blocked by a

magnesium ion at the resting potential. This block is only relieved when the membrane potential is depolarised. The depolarisation associated with the backpropagating action potential is important for relieving the  $Mg^{2+}$  block of the NMDA receptor (Magee & Johnston 1997, Koester & Sakmann 1998). Furthermore, the induction of both long-term potentiation and long-term depression (LTP and LTD) requires the pairing of EPSPs with postsynaptic action potentials within a narrow time window (Markram *et al.* 1997, Bi & Poo 1998, Debanne *et al.* 1998). Therefore the NMDA receptor functions as a coincidence detector for neurotransmitter release and action potentials, with  $Ca^{2+}$  influx through the channel acting as the signal for modification of synaptic efficacy (Yuste & Denk 1995, Koester & Sakmann 1998, Schiller *et al.* 1998, Yuste *et al.* 1999). Therefore, the backpropagated action potential may provide a link between axonal action potential firing and dendritic synaptic activity. Evidence for this idea comes from experiments where blocking backpropagation prevents the induction of LTP (Magee & Johnston 1997). The backpropagated action potential may also be amplified by voltage-dependent conductances when it is coincident with EPSPs (Magee & Johnston 1997, Stuart & Häusser 2000) and further  $Ca^{2+}$  entry can occur through the action of voltage-dependent  $Ca^{2+}$  channels (Jaffe *et al.* 1992, Markram *et al.* 1995, Schiller *et al.* 1995). Together these results indicate that modification of synaptic efficacy can be regulated by the interaction between EPSPs, backpropagated action potentials and dendritic voltage-dependent conductances.

Dendritic voltage-dependent ion channels also have a very important role in modifying the amplitude and time-course of dendritically generated synaptic potentials (Magee & Johnston 1995b, Wilson 1995, Tsubokawa & Ross 1996, Hoffman *et al.* 1997, Stuart & Spruston 1998, Magee 1999, Williams & Stuart 2000b). Recent experimental evidence suggests that in some neurones, the hyperpolarisation dependent cationic conductance ( $I_h$ ) compensates for the effects of dendritic filtering on EPSP decay time-course. However, it also reduces EPSP amplitude thereby reducing the summation of EPSPs that is observed at the soma (Magee 1999, Williams & Stuart 2000b). Modelling by Cook and Johnston (1997, 1999) suggests that dendritic voltage-gated conductances could normalise EPSP amplitudes at the soma independently of their location but as yet, no experimental evidence exists to support this hypothesis. Many studies have shown that the time-course and amplitude of EPSPs can be modified by dendritic voltage-dependent conductances (Hoffman *et al.* 1997, Cash & Yuste 1998, Urban & Barrionuevo 1998, Magee 1999, Nettleton & Spain 2000, Williams & Stuart 2000b). However in pyramidal cells, subthreshold amplification of synaptic potentials is greatest near the soma and occurs through activation of axo-somatic channels (Stuart & Sakmann 1995, Andreasen & Lambert 1998). Since the distribution and density of dendritic voltage-dependent ion channels varies during development (e.g. Gao & Ziskind-Conhaim 1998) and these

channels may be modulated by neurotransmitters (e.g. Colbert & Johnston 1998, Hoffman & Johnston 1999), the role these channels play in modifying synaptic potentials will depend on the developmental and behavioural state of the cells under study.

Furthermore, if voltage-dependent ion channels are present at sufficiently high density in the dendrites, then they may produce regenerative events similar to the action potential (Chen *et al.* 1997, Schiller *et al.* 1997, Stuart *et al.* 1997a, Stuart *et al.* 1997b, Golding & Spruston 1998, Golding *et al.* 1999, Magee & Carruth 1999, Velte & Masland 1999, Williams & Stuart 1999, Martina *et al.* 2000). These dendritic action potentials are usually of smaller amplitude and longer time-course than the axonal action potential and are difficult to voltage clamp because of their electrotonic separation from the soma (e.g. Fujita 1989). They may be caused by either  $\text{Na}^+$  (e.g. Stuart *et al.* 1997b, Golding & Spruston 1998) or  $\text{Ca}^{2+}$  (e.g. Schiller *et al.* 1997) conductances and their pharmacology varies according to channel type. Because of the relatively low density of these channels in the dendritic membrane, dendritic action potential initiation usually requires strong synaptic stimulation or strong somatic depolarisation. Dendritic regenerative events may also be important for initiating the action potential by amplifying synaptic depolarisations and propagating them to the axon (Stuart *et al.* 1997b). Dendritic action potentials are also important for regulating the firing mode of pyramidal cells (Larkum *et al.* 1999, Williams & Stuart 1999). No doubt, future work will provide further evidence of the role of dendritic action potentials in the integration of synaptic inputs, regulation of firing rate and modification of synaptic efficacy.

In some cells such as neurones of the substantia nigra (Häusser *et al.* 1995), the axon arises from the dendritic tree rather than from the soma. Such morphology may be important for processing synaptic inputs. The dendritic origin of the axon will mean that synaptic inputs located on the axon bearing dendrite will have more influence on axon potential generation than synapses near to the soma as is the case in most neurones.

Action potential backpropagation has now been successfully studied in a number of cell types. Each of these studies has shown a particular set of voltage-gated ion channels in the dendrites of each neuronal type and no doubt these differences are related to the different processing strategies employed by each type of neurone. The findings of these studies are reviewed briefly here.

### *Purkinje Cells*

In studies of the cerebellar Purkinje cell, early results suggested that the action potential was initiated in the soma and spread passively into the dendrites of the cell (Hounsgaard & Yamamoto 1979, Llinás & Sugimori 1980a, 1980b). However more recent evidence has challenged this view (Regehr *et al.* 1992). Studies using simultaneous somatic and dendritic recordings (Stuart & Häusser 1994) have revealed that action

potentials always occur first at the soma and then in the dendrites, indicating that the action potential is initiated in the axon and propagates back into the dendrites. It was also found that action potential amplitude was heavily attenuated with increasing distance from the soma. Stuart and Häusser (1994) discovered that simulation of action potentials using voltage clamp in the presence of TTX produced action potentials that attenuated in a comparable manner to those evoked in the absence of TTX. This suggested that backpropagated action potentials are not amplified by dendritic  $\text{Na}^+$  channels. Furthermore, outside-out patches from dendritic membrane could detect the presence of a voltage-dependent sodium channel and it was found that the density of  $\text{Na}^+$  channels was very high near the soma and rapidly decreased as patches were placed more distally, reaching very low levels within 50-100 $\mu\text{m}$  of the soma. It was concluded that although the dendrites contain voltage-dependent  $\text{Na}^+$  channels, they make only a negligible contribution to the modification of synaptic potentials and backpropagated action potentials because of their low density in the dendrites. Modelling of action potential propagation into the dendrites of Purkinje cells gave results that were in support of passive action potential attenuation. This was consistent with the low  $\text{Na}^+$  channel density observed in the dendrites. This suggests that action potential backpropagation in Purkinje cells is passive and that the dendrites function as a relatively independent compartment for integration of synaptic inputs. Although the early work of Llinás and Sugimori (1980a, 1980b) suggested that action potentials invade Purkinje cell dendrites passively, they also found that dendritic action potentials could occur as a result of voltage-dependent  $\text{Ca}^{2+}$  channels. In their hands,  $\text{Ca}^{2+}$  action potentials became larger as recordings were made further from the soma indicating that  $\text{Ca}^{2+}$  channel density increases with distance from the soma. Llinás and Sugimori suggested that the dendritic  $\text{Ca}^{2+}$  action potentials were generated at multiple sites along the dendritic tree because of the multiple  $\text{Ca}^{2+}$  action potential components observed in the dendritic recordings. They also suggested that voltage-dependent  $\text{Ca}^{2+}$  channel activity may be modulated by granule and basket cell inhibition.

### *Retinal Ganglion Cells*

The study of dendritic backpropagation and voltage-dependent ion channels in retinal ganglion cells has only just begun (Velte & Masland 1999). It has been found in these cells that action potentials can be initiated both in the soma and in the dendrite. In about half of these cells, evoked dendritic action potentials produced a mixture of subthreshold depolarisations and action potentials at the soma. In the other half of the cells, dendritic action potentials elicited only full-blown action potentials at the soma without the subthreshold depolarisations. In about half of these all-or-none type cells, the timing of the action potential between the soma and dendrite could be shifted by varying



the depolarisation at each electrode. In the remaining half of the all-or-none cells, the somatic action potential always occurred first and was followed by the dendritic action potential regardless of the depolarisations at each electrode. These results are indicative of a high variability in the density of voltage-dependent ion channels in the soma and dendrites of retinal ganglion cells. Unfortunately, because of poor resistance and capacitance compensation, Velte and Masland (1999) could not use timing of the action potential in each electrode to determine the exact point at which the action potential was initiated. However, their recordings were of sufficient quality to determine if action potentials were being recorded first at the soma or the dendrite. In 75% of the cells, depolarisation at either the soma or dendrite produced the action potential at that site first. In the remaining 25% of cells, action potentials were always recorded at the soma first regardless of the site of depolarisation. The conclusion from this is that most retinal ganglion cells have a sufficiently high density of voltage-dependent conductances in their dendrites to produce regenerative potentials. The remaining 25% of cells that only produce somatic action potentials do not have sufficient dendritic active conductances to produce regenerative events in their dendrites.

When QX-314 was allowed to diffuse into these cells through the somatic electrode, initially action potentials could still be generated in the dendrite while somatic action potentials were blocked. This indicated that the dendrites could generate action potentials independently and could propagate them to the soma. After continued perfusion of QX-314, both the dendritic and somatic action potentials were completely blocked. This proved that the dendritic and somatic action potentials were both caused by voltage-dependent  $\text{Na}^+$  channels. Furthermore, they concluded that voltage-dependent  $\text{Ca}^{2+}$  channels do not contribute to the dendritic action potentials, since QX-314 abolished dendritic action potentials. This conclusion was supported by the short time-course of the dendritic action potentials.

#### *Dorsal Horn Neurones*

In cells of the dorsal horn (Wolff *et al.* 1998), potassium currents are distributed unevenly. The delayed rectifier seems to be predominantly in the dendrites while most of the A-current is in the soma. In this study, Wolff *et al.* (1998) were able to physically isolate the soma from the axon and dendrites by patching onto the soma and then retracting the electrode to draw the soma away from the axon and dendrites. When this was done, they found that the soma amplified depolarisations to membrane potentials within the range from about -50mV to 0mV, but the soma also attenuated large depolarisations to membrane potentials above 0mV. This was due to the proportions of  $\text{Na}^+$  current, A-current and delayed rectifier present in the soma. On this basis, they concluded that the soma would amplify postsynaptic EPSPs but would attenuate

backpropagated action potentials. Furthermore, they noted that the isolated soma could not produce action potentials even when potassium channels were blocked. Therefore the failure of the soma to generate action potentials is not due to shunting by  $K^+$  channels but instead is caused by the low somatic  $Na^+$  channel density of around 1 per  $\mu m^2$  (Safronov *et al.* 1997) compared with 3-4 per  $\mu m^2$  for pyramidal cells (Colbert & Johnston 1996) or 1000-2000 per  $\mu m^2$  for the node of Ranvier (Black *et al.* 1990). This study provides very convincing evidence that the soma acts to prevent backpropagation of the action potential in dorsal horn neurones. The distribution of channels in dorsal horn neurones, with the A-current predominantly in the soma, the delayed rectifier mostly in the dendrites and a low density of  $Na^+$  channels in the soma, is in contrast to the findings of Hoffman *et al.* (1997) for hippocampal pyramidal neurones where it was found that A-current density increased with distance from the soma. Furthermore, the pharmacology of the A-current in hippocampal pyramidal cells is different from that in dorsal horn neurones. These studies suggest that there is much heterogeneity in dendritic ion channel distribution among various neuronal types.

#### *Thalamocortical Neurones*

Williams and Stuart (2000a) examined the dendritic properties of thalamocortical neurones of the dorsal thalamus. They demonstrated with simultaneous somatic and dendritic recordings that action potentials evoked by sensory or cortical EPSPs are initiated near the soma and backpropagate into the dendrites of thalamocortical neurones. Cell-attached recordings showed that thalamocortical neurone dendrites contain a non-uniform distribution of sodium channels and a uniform density of potassium channels across the somato-dendritic area that they examined, which included half the average dendritic path length of these cells. Dendritic action potential backpropagation was active, but action potentials may fail to invade the distal dendrites. They also observed that calcium channels were non-uniformly distributed in the dendrites of thalamocortical neurones. Low-threshold  $Ca^{2+}$  channels were concentrated in the proximal dendrites and these sites are known to receive excitatory connections from primary afferents. This suggested that these  $Ca^{2+}$  channels have an important role in the amplification of sensory inputs to thalamocortical neurones. However, there is no experimental evidence as yet to suggest that this is so.

#### *Neurones of the Substantia Nigra*

Simultaneous somatic and dendritic recordings have also been performed in neurones of the substantia nigra (Häusser *et al.* 1995). For both dopaminergic and GABAergic cells of the substantia nigra the situation was variable, with action potentials in the dendritic electrode peaking before, after or even simultaneously with those in the soma.

Morphological reconstruction of these cells showed that the axon often arose from a dendrite in these cells. When an action potential peaked in the dendrite before it did in the soma, it was because the dendritic electrode was attached to the dendrite from which the axon arose. When the action potential appeared first in the soma and then the dendrite, the axon arose either from the soma or from a dendrite other than the one from which the dendritic recording had been made. If the action potential occurred simultaneously, then the axon was found to originate from the section of dendrite between the somatic and dendritic electrodes. An examination of steady state and action potential attenuation in both GABAergic and dopaminergic cells found that there was barely any difference between the attenuation of either type of signal. Steady state signals appeared to be slightly attenuated, but only because of sag conductances, while action potentials appeared to be the same amplitude regardless of the recording site. No correlation could be found between the somatic or dendritic action potential amplitude and the distance of the recording site from the soma or axon. Outside-out patch recordings of the dendritic membrane of dopaminergic neurones determined that dendritic  $\text{Na}^+$  channel density was similar in the dendrites and soma of these cells. Action potentials were actively propagated in the dendritic trees of these cells and the similarly small attenuation of the action potential in the GABAergic neurones suggested that action potentials are actively propagated in those cells as well. Also, the relatively broad action potential of these GABAergic neurones (2-3ms) was attenuated much less when TTX was used to block dendritic  $\text{Na}^+$  channels than for Purkinje cell dendritic action potentials under the same conditions (Stuart & Häusser 1994). Therefore, the dendritic physiology of substantia nigra neurones may be suited to dendritic action potential propagation. The function of an axon that originates from a dendrite is not yet understood but may be important for synaptic integration, activation of NMDA receptors, and for dendritic release of dopamine in these neurones (Johnston & North 1992, Rice *et al.* 1994).

### *Hippocampal Pyramidal Cells*

It has been suggested that the backpropagated action potential may be an important signal for Hebbian learning. In the hippocampal CA1 pyramidal cell, backpropagation of the action potential is dependent on synaptic activity (Magee & Johnston 1997) but also depends on action potential firing rates (Spruston *et al.* 1995). Single action potentials propagate into the dendritic tree with ease whereas dendritic action potential amplitude decreases rapidly during high frequency firing. Somatic action potentials do not exhibit the same decrement in amplitude during high frequency firing. Spruston *et al.* (1995) suggested that this could be due to inactivation of the dendritic voltage-dependent  $\text{Na}^+$  channels responsible for propagating the dendritic action potentials and this was confirmed in the studies of Colbert *et al.* (1997) and Jung *et al.* (1997). These studies

found that the dendritic  $\text{Na}^+$  channels inactivate rapidly and that their recovery is slow and voltage-dependent. The conclusion was that voltage-dependent  $\text{Na}^+$  channels in the axon and dendrites have different inactivation properties. Further examination of dendritic action potential decrement during trains has found that activation of protein kinase C in CA1 cells with phorbol esters reduced dendritic  $\text{Na}^+$  channel inactivation and decreased the activity-dependent attenuation of the backpropagated action potential (Colbert & Johnston 1998). This indicates that action potential backpropagation can be modulated and this may have important implications for regulation of changes in synaptic efficacy. In CA1 pyramidal cells, action potentials propagate actively into the dendrites, facilitated by a relatively constant density of voltage-dependent  $\text{Na}^+$  channels throughout the dendritic tree (Magee & Johnston 1995a). When failures of backpropagation occur, it is usually at dendritic branch points (Spruston *et al.* 1995). If synaptic inputs can cause backpropagation to fail at branch points, either by inactivating dendritic  $\text{Na}^+$  channels or by activating pathways that modify their properties, then synaptic input could act as a 'gate' that controls the number of action potentials actively propagating into individual dendritic branches.

Golding and Spruston (1998) have provided direct evidence from simultaneous dendritic and somatic recordings that excitatory synaptic inputs can elicit dendritic sodium action potentials prior to axonal action potential initiation in hippocampal CA1 pyramidal neurones. Both the probability and amplitude of dendritic action potentials depended on the previous synaptic activity and firing history of the cell. Furthermore, some dendritic action potentials occurred in the absence of somatic action potentials, indicating that their propagation to the soma and axon is unreliable. Golding and Spruston also showed that dendritic action potentials contribute a depolarisation that summates with the synaptic potential and can act as a trigger for action potential initiation in the axon.

Tsubokawa *et al.* (2000) have examined the decrement of action potential amplitude in the dendrites of CA1 cells during trains of action potentials. They found that depolarisation reduced the amplitude decrement of dendritic action potentials during trains. This depolarisation induced facilitation of action potential backpropagation could be abolished by placing the intracellular  $\text{Ca}^{2+}$  chelator BAPTA into the electrode or by using a low- $\text{Ca}^{2+}$  bath solution, indicating that  $\text{Ca}^{2+}$  influx is required. Intracellular injection of either calmodulin binding domain or the  $\text{Ca}^{2+}$ /calmodulin-kinase II (CaMKII) inhibitor 281-301 blocked the depolarisation induced facilitation. Bath application of a membrane permeable CaMKII inhibitor KN-93 also blocked the facilitation but KN-92, an inactive isomer of KN-93, had no effect. These results suggest that increases in intracellular  $\text{Ca}^{2+}$  cause facilitation of action potential backpropagation in the apical dendrite of CA1 pyramidal neurone through CaMKII dependent mechanisms.

Dendritic  $\text{Ca}^{2+}$  currents in CA1 pyramidal cells have also been examined (Magee & Johnston 1995a 1995b, Magee & Johnston 1997). Subthreshold synaptic input and backpropagating action potentials both cause dendritic  $\text{Ca}^{2+}$  influx, but when synaptic input and backpropagated action potentials occur simultaneously, the  $\text{Ca}^{2+}$  influx was significantly larger than the sum of the two independent  $\text{Ca}^{2+}$  signals (Magee & Johnston 1997). Furthermore, backpropagation is dependent on synaptic activity with synaptic depolarisation helping to amplify the backpropagated action potential. This facilitates activation of voltage-dependent  $\text{Ca}^{2+}$  channels and synaptic NMDA receptors, leading to  $\text{Ca}^{2+}$  influx and induction of long-term potentiation of synaptic strength (LTP). In the work of Magee and Johnston (1997), inhibition of backpropagation by localised application of TTX to the dendritic tree decreased  $\text{Ca}^{2+}$  influx and reduced LTP. No LTP was induced unless the backpropagated action potential reached the synaptic site while it was active and hyperpolarisation of the dendrites reduced backpropagated action potential amplitude, reduced  $\text{Ca}^{2+}$  influx and decreased LTP.

Potassium channel regulation of backpropagation and dendritic integration has also been examined in hippocampal pyramidal cells. Hoffman *et al.* (1997) have performed cell-attached patch experiments on hippocampal pyramidal cells to examine the density of A-type potassium channels in these cells. They found an increasing density of  $I_A$  in pyramidal cell dendrites. These channels caused significant attenuation of dendritic action potentials and were responsible for the majority of action potential repolarisation that occurred in the dendrites. The high dendritic density of  $I_A$  would explain why action potential amplitude decrements with distance from the soma even though  $\text{Na}^+$  and  $\text{Ca}^{2+}$  channels occur at high density in the dendrites of these cells (Magee & Johnston 1995a). Hoffman *et al.* (1997) also found that A-currents caused significant attenuation of fast EPSPs in these cells, particularly at the site of the synaptic input where changes in membrane potential are greatest. It was also found that depolarising one branch of a dendrite increased action potential amplitude in that branch while action potentials in the other branch were attenuated as normal. Hoffman *et al.* (1997) proposed that this was caused by relief of A-current activity by inactivation of the channel at depolarised potentials. They concluded that synaptic EPSPs could inactivate dendritic A-currents releasing local regions of the dendrite from the dampening effects of a high A-current density. This may allow action potentials occurring at the same time as EPSPs to increase in amplitude in a spatially restricted region of the neurone. The subsequent evoked  $\text{Ca}^{2+}$  influx through NMDA receptors and voltage-dependent  $\text{Ca}^{2+}$  channels could provide the associative signal needed to alter synaptic strength.

Because of the importance of  $I_A$  in the regulation of dendritic signal propagation, modification of the properties of the A-current by neuromodulators will be important for regulating action potential backpropagation and modification of synaptic efficacy.

Hoffman and Johnston (1998) showed that the cAMP-dependent protein kinase (PKA) and the  $\text{Ca}^{2+}$ -dependent phospholipid-sensitive protein kinase (PKC) can shift the activation curve of the A-current to more depolarised potentials in the dendrites of hippocampal pyramidal cells. This resulted in increased amplitude of backpropagating action potentials in the distal dendrites. Physiologically,  $\beta$ -adrenergic and muscarinic acetylcholine receptors would cause an increase in intracellular PKA and PKC respectively. Hoffman and Johnston (1999) reported that activation of either of these neurotransmitter systems resulted in an increase in dendritic action potential amplitude. Hoffman and Johnston (1999) also tried elevating cAMP and PKA levels by using dopaminergic agonists as well. Activation of the dopaminergic neurotransmitter system increased action potential amplitude in only a subpopulation of neurones tested.

Migliore *et al.* (1999) have examined the effect of an A-type potassium channel on action potential attenuation in a computer model of hippocampal pyramidal cells. This work has shown that A-current densities in the order of 20 to 48mS/cm<sup>2</sup> cause significant attenuation of action potential amplitude particularly in the distal dendrites even though voltage-dependent  $\text{Na}^+$  channels are present. As noted above, Hoffman *et al.* (1997) propose that EPSPs can relieve A-current activity by inactivating the channel and that this causes a spatially restricted increase in backpropagated action potential amplitude. This effect could be reproduced by the model of Migliore *et al.* (1999) by placing an A-type potassium channel into the dendritic membrane. Dendritic EPSPs inactivated the A-currents so that they could not contribute to the attenuation of the action potential amplitude. The combination of an EPSP and an action potential caused a supra-linear addition of the two potentials through the action of voltage-dependent  $\text{Na}^+$  channels and this only occurred within a certain time window in which the synaptic input and action potential occurred within 2 to 8ms of each other. Phosphorylation of  $I_A$  may be important for varying the amount of action potential backpropagation in hippocampal pyramidal cells by changing the time constant of inactivation (Covarrubias *et al.* 1994, Drain *et al.* 1994) or the activation curve of the channel (Hoffman & Johnston 1998). At a dendritic location 400 $\mu\text{m}$  from the soma, Migliore *et al.* (1999) found that slowing the inactivation time constant of the A-current resulted in no change to the action potential amplification when paired with an EPSP, whereas speeding up the A-current inactivation resulted in larger action potential amplification and a larger time window over which supra-linear addition of the two signals occurred. However at 200 $\mu\text{m}$ , changes in A-current inactivation time constant caused little changes in action potential amplitude and time-course and did not change the time window over which EPSPs and action potentials added supra-linearly. Evidence from Hoffman and Johnston (1998) has shown that activation of protein kinases can shift the activation curve of  $I_A$  to more depolarised potentials. Migliore *et al.* (1999) tested the effect of a +5mV shift of the activation curve on action potential

attenuation and EPSP pairing. This caused significantly less attenuation of dendritic action potential amplitude in the distal dendrites, eliminated the supra-linear addition of EPSPs and action potentials and reduced sensitivity to changes in the A-current inactivation time constant. Therefore, this study showed that the A-current could have important implications for Hebbian modification of synaptic strength through modification of the backpropagated action potential. Furthermore, changes in the properties of  $I_A$  through phosphorylation of the channel can alter the pattern of action potential backpropagation.

Urban and Barrionuevo (1998), using somatic and dendritic recordings in CA3 cells, found that dendritic EPSPs summed non-linearly and that blocking the A-current linearised EPSP summation. They concluded that the A-current is important for shaping dendritic EPSPs. This is in contrast to the results of Cash and Yuste (1998) where they used microiontophoresis of glutamate to mimic synaptic inputs in the dendritic tree of cultured pyramidal neurones and examined the summation of two inputs by testing their individual and combined effects. Cash and Yuste (1998) found that input summation was linear and that the position of the two inputs was not important for determining the way in which they summed. This was because small inputs did not cause sufficient changes in ionic driving forces and did not activate voltage-dependent ion channels. Larger inputs also added linearly, but this linearity was caused by balanced action of NMDA receptors and the A-current. Therefore, it appears that dendritic active conductances in combination with the properties of the postsynaptic receptors can maintain a linear summation and that dendritic morphology does not interfere with this linearity. Such a mechanism may be essential for particular neuronal computations. The results of Cash and Yuste (1998) do not appear to be a culture artifact since similar experiments in CA1 pyramidal cells in slices of hippocampus (Cash & Yuste 1999) also showed linear summation of inputs through a balance of shunting and boosting mechanisms. Perhaps there are differences in the way CA1 cells and CA3 cells sum their inputs, or perhaps Cash and Yuste were better able to control the location of their inputs by using microiontophoresis of glutamate rather than by evoking EPSPs electrically.

In the study of Magee (1998), the effect of the hyperpolarisation activated cationic current ( $I_h$ ) was investigated. It was found that the density of these channels increases six to seven times from soma to distal dendrites. The activation/inactivation curves of this channel are such that a significant proportion of somatic  $I_h$  channels (~25%) are active near the resting potential. However, the activation curve of the dendritic  $I_h$  channels is shifted to more hyperpolarised potentials by about 10mV and only about half as many dendritic  $I_h$  channels will be active at rest as in the soma (~12%). Therefore, even though the dendritic density of  $I_h$  is seven times higher in the dendrite than in the soma, the effect of these channels on resting membrane properties is only half that of somatic  $I_h$  channels.

This combination of properties and distribution was found to produce a gradient of input resistance and membrane time constant from soma to distal dendrites although some of the time constant difference was not due to the gradient of  $I_h$ . This resulted in a directionally specific effect on subthreshold voltage transients such that signals travelling from soma to dendrites are heavily attenuated while signals travelling from dendrites to soma experience less decrement. This effect could be alleviated by blockade of  $I_h$  with 3mM  $Cs^+$ . The elevated dendritic  $I_h$  density decreased EPSP amplitude and duration and reduced the time window over which temporal summation of EPSPs takes place. Backpropagated action potentials were little affected by dendritic  $I_h$  presumably because its kinetics are too slow to affect the action potential. Therefore, although  $I_h$  acts to dampen dendritic excitability, its main impact is on the subthreshold range of membrane potentials where integration of synaptic inputs takes place.

Magee (1999) has performed further work on the effect of  $I_h$  on summation of synaptic inputs and has reported that temporal summation at CA1 pyramidal cell somata does not depend on the location of synaptic input. Summation of inputs from proximal ( $\sim 30\mu m$ ) and distal ( $\sim 330\mu m$ ) dendritic locations was virtually the same up to about 100Hz stimulation. The normalisation of temporal summation broke down at stimulation frequencies above 100Hz and ensured that temporal summation of high frequency inputs remained location dependent. Spatial normalisation of temporal integration could be removed by blockade of  $I_h$  with the drug ZD7288 and resulted in greater temporal summation of synaptic inputs, particularly those from the distal dendrites. A similar experiment in which trains of EPSC-shaped currents were injected along the somato-dendritic axis showed similar summation of both proximal and distal inputs and addition of ZD7288 resulted in a progressive increase in temporal summation as the inputs were moved more distal. Furthermore, the amplitude of EPSPs does not affect temporal summation unless these EPSPs initiate dendritic action potentials. During dendritic spiking, Magee (1999) found that the normalisation of temporal summation was reduced suggesting that dendritic spiking may provide a mechanism to overcome the spatial normalisation of temporal summation. Magee (1999) found that synaptic depolarisation by EPSPs produced a deactivation of  $I_h$  resulting in a net hyperpolarising current which helped to shape synaptic input and counteract the effects of dendritic filtering. Thus, the non-uniform  $I_h$  density provides a mechanism for removing location dependence of temporal summation of EPSPs in CA1 pyramidal neurones but did not alter the location dependence of EPSP amplitude. The overall effect of  $I_h$  then will ensure that a CA1 neurone's response largely reflects the temporal pattern of the synaptic input rather than the location of that input.

Magee and Carruth (1999) have studied the effects of some dendritic voltage-gated ion channels on the regulation of action potential firing in hippocampal CA1 pyramidal



cells. They found that A-currents serve to dampen  $\text{Ca}^{2+}$  channel activity in these cells. When  $I_A$  is blocked, significant  $\text{Ca}^{2+}$  channel activation occurs in the distal dendrites during action potential backpropagation. The  $\text{Ca}^{2+}$  current generated by these backpropagated action potentials propagates back to the soma to produce a slow, prolonged after-depolarisation that is capable of initiating further axonal action potentials. Therefore, these dendritic  $\text{Ca}^{2+}$  channels can potentially regulate the firing mode of the cell in a similar way to that observed in the layer 5 neocortical pyramidal cell (Williams & Stuart 1999, see below). As previously mentioned, neuromodulatory mechanisms exist which can reduce the activation of dendritic A-currents and consequently these neuromodulators may play a role in regulating the firing pattern of hippocampal pyramidal cells.

Golding *et al.* (1999) have further examined the regulation of dendritic  $\text{Ca}^{2+}$  action potentials in CA1 pyramidal cells. They showed that calcium action potentials are initiated in the apical dendrites of CA1 pyramidal neurones and cause bursts of sodium-dependent action potentials at the soma, just as was shown by Magee and Carruth (1999). Initiation of calcium action potentials at the soma was suppressed in part by potassium channels activated by sodium-dependent action potentials. Low-threshold, putative D-type potassium channels played a prominent role in setting a high threshold for somatic calcium action potentials, thus restricting initiation to the dendrites. Once initiated, repetitive firing of calcium action potentials was limited by calcium-activated potassium channels. Thus, the concerted action of calcium- and voltage-activated potassium channels serves to spatially and temporally concentrate the membrane depolarization and calcium influx generated by calcium action potentials during strong, synchronous excitation.

The exact function of the complex mixture of dendritic ion channels is at present not clear. It is possible that the purpose of dendritic active conductances is to counteract the effect of the passive membrane properties. Cook and Johnston (1997, 1999) have explored this idea by performing modelling studies to determine the active conductances and synaptic input properties that would be necessary to counteract the passive cable filtering by the dendrites. They found that a dendrite that eliminates passive dendritic filtering requires: (1) a steady state voltage-dependent inward current that together with the passive leak current provides a net outward current and a zero slope conductance at depolarised potentials. (2) a fast, transient, inward current that compensates for dendritic capacitance and (3) both AMPA and NMDA synaptic conductances that together permit synapses to behave as ideal current sources (Cook & Johnston 1999). All three of these mechanisms are consistent with known dendritic physiology. The model made many assumptions about the mix of voltage-dependent ion channels that occur in a cell's dendrites and used a simplified morphology. However, the results of Magee (1999) suggest that for the hippocampal CA1 pyramidal cell, dendritic voltage-dependent ion

channels help to counteract the effect of passive dendritic filtering, at least on the decay time-course of synaptic potentials. There is as yet no evidence to suggest that dendritic voltage-dependent conductances help to counteract the effect of dendritic filtering on the amplitude of synaptic potentials. One other finding of the modelling study of Cook and Johnston (1999) is that dendrites which eliminate dendritic filtering effects will also backpropagate action potentials, although there is no suggestion that cells which backpropagate action potentials are necessarily able to alleviate the effects of dendritic filtering. Furthermore, dendritic voltage-dependent ion channels appear to have additional functions such as regulating the firing mode of the cell suggesting that there is still much to be understood about their importance for synaptic integration, action potential backpropagation and modification of synaptic efficacy. Magee and Cook (2000) have found in CA1 pyramidal neurones that the dendritic EPSP amplitude increases with distance from the soma, counterbalancing the filtering effects of the dendrites and reducing the location dependence of somatic EPSP amplitude. They found that a progressive increase in synaptic conductance seems to be primarily responsible for normalising the amplitudes of individual inputs. Therefore, the size of synaptic conductances is important for determining how these postsynaptic potentials will interact and propagate within the dendrites of a neurone.

#### *Pyramidal Cells of the Sensorimotor Neocortex*

An examination of action potential backpropagation in layer 5 pyramidal cells of the sensorimotor neocortex (Stuart & Sakmann 1994), has shown that action potentials are recorded first in the soma and then in the dendrite regardless of the method of stimulation or the position of the dendritic recording. This suggests that the action potential originates in the soma or axon. Dual axonal and somatic recordings in these cells have confirmed that the action potential does indeed originate in the axon. Measurements of dendritic action potential amplitude showed up to 30% decrease in action potential amplitude at distances of around 500 $\mu$ m from the soma, which is very little attenuation for a brief signal over such a long distance. Outside-out patches of dendritic membrane recorded voltage-dependent Na<sup>+</sup> channels and their density was relatively constant along the entire length of the dendritic tree (Stuart & Sakmann 1994). Blockade of these channels by perfusion of QX-314 through the dendritic electrode caused the dendritic action potential amplitude to decrease. It was therefore concluded that action potential backpropagation in layer 5 neocortical pyramidal cells is active. Further examination of these cells by Stuart and Sakmann (1995) found that EPSPs spreading to the soma are amplified by somatic and axonal Na<sup>+</sup> channels. Application of Na<sup>+</sup> channel blockers to dendritic sites did not affect amplification of EPSPs but application to the soma and axon made a large difference to the somatic EPSP amplitude. They concluded that the contribution of dendritic voltage-

dependent conductances to the amplification of the EPSP was very small compared to the large amplification that occurred in the soma.

Using simultaneous whole-cell voltage and  $\text{Ca}^{2+}$  fluorescence measurements in layer 5 neocortical pyramidal cells, Schiller *et al.* (1997) showed that distal synaptic stimulation, evoking a subthreshold depolarisation at the soma, could initiate regenerative potentials in the distal branches of the apical dendritic tuft that could be graded or all-or-none indicating that these cells have two regions for action potential initiation, one in the axon and another in the distal dendrites. Furthermore, these dendritic action potentials did not propagate actively to the soma or axon. Fluorescence measurements indicated that these regenerative potentials were associated with a transient increase in intracellular  $\text{Ca}^{2+}$  concentration that could be blocked by  $\text{Cd}^{2+}$ . Therefore, these potentials were caused by voltage-dependent  $\text{Ca}^{2+}$  channels. The  $\text{Ca}^{2+}$  channels amplify small synaptic signals in the distal dendrites without generating axonal action potentials and this could be important for modifying synaptic efficacy at these distal sites. Stuart *et al.* (1997b) found that these regenerative potentials in the apical tuft of layer 5 pyramidal cells could be independent of the axonal action potential and only produced subthreshold signals at the soma. Backpropagating action potentials in the apical tuft were also seen to have a late  $\text{Ca}^{2+}$  component that was a result of these dendritic voltage-dependent  $\text{Ca}^{2+}$  channels being activated by the backpropagated action potential. These calcium currents were particularly pronounced during bursts of somatic action potentials. The increased  $\text{Ca}^{2+}$  electrogenesis during bursts is probably due to greater activation of dendritic  $\text{Ca}^{2+}$  channels caused by the sustained depolarisation that occurs during bursts in combination with the slow kinetics of the channels. The dendritic  $\text{Ca}^{2+}$  events could be prevented by application of TTX indicating that  $\text{Na}^+$  channels are important for producing a large part of the depolarisation associated with these events. This suggests that dendritic  $\text{Na}^+$  channels are activated by synaptic depolarisation and by backpropagating action potentials and that this contributes to dendritic depolarisations that can cause  $\text{Ca}^{2+}$  electrogenesis. Thus, these results suggest a role for both dendritic  $\text{Na}^+$  and  $\text{Ca}^{2+}$  channels in the generation of these electrogenic events.

Evidence suggests that layer 5 neocortical pyramidal cells are unusual in having both an axonal and dendritic zone for the initiation of action potentials. Distal dendritic inputs, which normally appear greatly attenuated at the axon must produce large potentials at the dendritic initiation zone to evoke calcium action potentials but once this occurs, they can then generate bursts of axonal action potentials. Larkum *et al.* (1999a) have shown that a single backpropagating sodium action potential generated in the axon facilitates the initiation of these calcium action potentials when it coincides with distal dendritic input within a time window of several milliseconds. As would be expected, Larkum *et al.* (1999a) found that inhibitory dendritic input could selectively block the initiation of

dendritic calcium action potentials, preventing bursts of axonal action potentials. Thus, excitatory and inhibitory postsynaptic potentials arising in the distal dendrites can exert significantly greater control over action potential initiation in the axon than would be expected from their electrotonically isolated locations. The fact that a single backpropagating action potential paired with a subthreshold distal EPSP can produce a burst of axonal action potentials may provide a mechanism by which the main cortical output neurones can associate inputs arriving at different cortical layers within a broad time window.

In a further examination of the interaction between the axonal and distal dendritic electrogenic sites, Larkum *et al.* (1999b) found that layer 5 pyramidal neurones are very sensitive to backpropagating action potentials when they occur above a critical frequency that varied between 60 and 200 Hz for different cells. Bursts of four to five backpropagating action potentials above the critical frequency elicited large regenerative potentials in the distal dendritic regenerative zone. The critical frequency had a narrow range of around 10-20 Hz and dendritic regenerative activity caused by backpropagating action potentials led to further depolarization at the soma. The frequency sensitivity of dendritic action potentials was suppressed by blockers of voltage-gated calcium channels and by synaptically mediated inhibition. Calcium fluorescence imaging during trains of action potentials occurring at rates higher than the critical frequency revealed that the dendritic site of largest transient increase in intracellular calcium was located 400-700 $\mu\text{m}$  from the soma at the same site where calcium action potentials were initiated. This conclusively showed that the distal dendritic initiation zone can interact with the axonal initiation zone if the output of the neurone exceeds a critical frequency and that this can occur even when the inputs to the neurone are restricted to regions close to the soma. Furthermore, the large influx of  $\text{Ca}^{2+}$  produced in the distal dendrites during action potential trains occurring above the critical frequency may be important for integration of synaptic inputs and for triggering intracellular cascades that modify synaptic efficacy.

Since the activity at the initiation site for dendritic  $\text{Ca}^{2+}$  action potentials can regulate firing in the axon, modulation of action potential backpropagation may also be important for regulating the action potential bursting properties of these cells. Williams and Stuart (1999) have investigated the mechanisms underlying the generation of action potential burst firing and its postsynaptic consequences in rat layer 5 neocortical pyramidal neurones. Based upon firing and subthreshold membrane properties, layer 5 pyramidal neurones were separated into three classes; regular firing, weak burst firing and strong burst firing. The blockade of apical dendritic sodium channels by the local dendritic application of TTX greatly reduced high frequency action potential burst firing, as did the blockade of low threshold  $\text{Ca}^{2+}$  channels by local apical dendritic application of  $\text{Ni}^{2+}$ . These results indicate that burst firing results from the backpropagation of action

potentials and the associated apical dendritic depolarisation caused by the combined activity of voltage-dependent  $\text{Ca}^{2+}$  and  $\text{Na}^+$  channels. In regular firing neurones, dendritic application of  $\text{Ni}^{2+}$  did not alter action potential firing properties. In regular firing neurones, apical dendritic depolarisation at locations  $>150\mu\text{m}$  from the soma resulted in low frequency burst firing during somatic current injection while in burst firing neurones, the rate of action potential burst discharges was increased during dendritic depolarisation. Little difference in firing pattern was seen in either regular or burst firing cells if the depolarisation was placed  $<150\mu\text{m}$  from the soma. Examination of temporal summation of synaptic inputs in these cells during action potential bursts showed that temporal summation is greatest during bursting and the more action potentials that occur in a burst, the greater the temporal summation of EPSPs. This amplification of EPSPs must occur through the action of  $\text{Na}^+$  channels since it is blocked by TTX. Together these results suggest that it is the membrane potential in the distal apical dendrites that is important for regulating the firing characteristics of layer 5 pyramidal neurones and that  $\text{Ca}^{2+}$  and  $\text{Na}^+$  channels are responsible for the dendritic depolarisation that occurs in these cells during backpropagated action potentials.

To further add to the understanding of the interactions between voltage-dependent ion channels in layer 5 neocortical pyramidal neurones, Korngreen and Sakmann (2000) have made a study of potassium channels in somata and dendrites of layer 5 neocortical pyramidal cells. They showed that the amplitude of ensemble  $\text{K}^+$  currents in cell-attached patches decreased along the apical dendrite as the distance from the soma increased. Korngreen and Sakmann propose that the decrease in density of the voltage-gated  $\text{K}^+$  channels along the apical dendrite of layer 5 pyramidal neurones in concert with the high  $\text{Ca}^{2+}$  channel density in the distal dendrites helps to define a region in the distal dendrites with a lower threshold for the generation of dendritic regenerative potentials produced by  $\text{Na}^+$  and  $\text{Ca}^{2+}$  channels.

Bekkers (2000b) has made a study of the voltage-gated potassium channels in cell-attached and outside-out patches from the soma and primary apical dendrites of large layer 5 neocortical pyramidal neurones. Ensemble averages revealed that some patches contained only fast transient potassium currents similar to the A-type potassium channel ( $I_A$ ), others contained only delayed rectifier-like ( $I_{DR}$ ) channels that did not inactivate or inactivated slowly, and the remainder contained mixtures of both channel types. The amount of  $I_A$  and  $I_{DR}$  present in dendritic patches depended weakly on distance from the soma. The amplitude of  $I_A$  increased, on average, by 2.3pA per  $100\mu\text{m}$ , while the amplitude of  $I_{DR}$  decreased by 0.4pA per  $100\mu\text{m}$ .  $I_A$  and  $I_{DR}$  channels in dendritic cell-attached patches were activated by the passage of a backpropagating action potential past the tip of the patch electrode. These results show directly that these potassium channels participate in dendritic action potential repolarisation. They may also contribute to the

process of synaptic integration in these neurones. However, the functional consequences of these channels to the integration of synaptic inputs in the dendrites of layer 5 neocortical pyramidal cells is still uncertain.

Another study by Takigawa and Alzheimer (1999) used acutely dissociated dendritic segments and cell somata of rat neocortical pyramidal neurones to determine and compare the relative density of G-protein activated  $K^+$  currents in the two cellular compartments. They used agonists for adenosine,  $GABA_B$  and serotonin to activate G-protein activated  $K^+$  currents and observe their effects. Their data suggests that several neurotransmitters might employ G-protein activated  $K^+$  currents as a tool to directly modulate the electrical properties of dendrites. In concert with voltage-dependent  $K^+$  currents and the hyperpolarisation-activated cationic conductance ( $I_h$ ), G-protein activated  $K^+$  currents should dampen dendritic excitability and thus influence various aspects of dendritic signal integration. Therefore certain neurotransmitters may modulate dendritic voltage-dependent conductances and such modulation could be important for regulating the amplitude of backpropagated action potentials, thereby regulating calcium influx during synaptic activation of NMDA receptors and subsequent changes in synaptic efficacy.

In a recent study by Williams and Stuart (2000b), an investigation was made of the properties and distribution of the hyperpolarisation-activated cationic conductance ( $I_h$ ) in the axon, soma, and apical dendrites of neocortical layer 5 pyramidal neurones, and their effect on the time-course of EPSPs. They found an increase ( $\sim 9\text{pA}/100\mu\text{m}$ ) in the density of dendritic  $I_h$  channels with distance from the soma. Just as in hippocampal pyramidal cells, a significant proportion of  $I_h$  is active at the resting membrane potential ( $\sim 7\text{-}8\%$ ) although the activation properties of this channel are similar across the somato-dendritic axis unlike the  $I_h$  channels of CA1 cells. Simulation of EPSPs in the soma and dendrites resulted in somatic EPSPs of similar decay time-course regardless of their location but with rise-times that were slower for simulated EPSPs arising in the dendrites. In a passive system, distal EPSPs would be expected to show greater somatic temporal summation because of their slower decay kinetics at the soma. The normalisation of simulated EPSP half-width suggested that this might not occur in layer 5 pyramidal neurones. In a similar experiment to that of Magee (1999), Williams and Stuart (2000b) applied trains of simulated EPSPs and observed little temporal summation regardless of the location of the input. Application of the  $I_h$  blocker ZD7288 produced significant temporal summation of inputs and this summation was greatest for distal inputs. Depolarisation of the soma increased temporal summation and this could be further increased by addition of ZD7288. However, the increase in temporal summation caused by depolarisation and ZD7288 could be partially removed by TTX, suggesting that voltage-dependent  $Na^+$  channels are also important for the resulting temporal summation at depolarised membrane potentials. Thus Williams and Stuart (2000b), studying neocortical layer 5 pyramidal cells, have found

similar results to those of Magee (1999) for the hippocampal CA1 cell. That is, that these cells contain a high level of dendritic  $I_h$  that counteracts the effect of dendritic filtering on the decay time-course of synaptic inputs resulting in reduced temporal summation. So, although the high level of active  $I_h$  that is present in the distal dendrites of these cells at rest leads to a faster decay of the simulated EPSP amplitude because of higher membrane conductance, the deactivation of the channel by depolarisation leads to generation of a net outward current that shortens the decay. These data indicate that an increasing density of apical dendritic  $I_h$  channels counteracts the influence of cable filtering on somatic EPSP time-course and temporal summation in layer 5 neocortical pyramidal neurones and supports the hypothesis proposed by Cook and Johnston (1997, 1999) in which the purpose of dendritic voltage-dependent conductances is to eliminate the location dependence of synaptic input.

### **Dendritic Active Conductances and Backpropagation in Motoneurones**

Studies of action potential backpropagation in the motoneurone took place much earlier than for the cells discussed above and did not utilise dendritic recordings. Rather, these studies relied on indirect methods. The early interest in backpropagating action potentials arose because the time-course of the recorded action potential at the soma had to be explained in terms of where it was initiated and how it spread into the soma and dendrites (Brock *et al.* 1953). Various components of the rising phase of the action potential could be distinguished and were attributed to the contribution of different parts of the neurone to the shape of the action potential. The problem with this approach was that the recordings were made from the soma of motoneurones and so it was very difficult to determine how action potentials propagated in the axon and dendrites and how much contribution each compartment made to the size and shape of the action potential at the soma. Brock *et al.* (1953) concluded that the antidromic action potential time-course had various components that were caused by the action potential propagating through various parts of the neurone. The myelinated axon produced the M-spike component, the soma and dendrites produced the SD-spike component and the initial segment generated the NM-spike component, although this was later renamed the IS-spike component. They suggested that the majority of the current needed for action potential production was produced by the axon hillock, while the axon, soma and dendrites produced progressively less current per unit area and therefore had progressively lower  $\text{Na}^+$  channel density. A later paper by Fatt (1957) used extracellular recording to determine the relative contributions of the dendrites, soma and axon to the action potential. Fatt determined that the total current that flowed around a motoneurone during an action potential was about 0.2 to 0.3  $\mu\text{A}$ . Since this was such a large current, he assumed that a large part of the motoneurone had to be active. Fatt concluded that the active region was the soma but he

also realised that his technique did not have sufficient spatial resolution to provide accurate localisation of the current associated with the action potential. Fatt's recordings showed that there was a reversal of the direction of current flow that propagated along the dendritic tree indicating active backpropagation of the action potential into the dendrites of the motoneurone. He concluded that the action potential was produced predominantly in the soma while the dendrites and axon were only responsible for a small part of the current associated with the antidromic action potential.

Further attempts to define the site of action potential initiation included the work of Coombs *et al.* (1957). They showed that the steep initial rising phase of the action potential recorded in the motoneurone soma was due to the activity of the axon initial segment, while the later components were produced by the soma and dendritic membrane. Furthermore, impulses generated by the activity of the initial segment were recorded in the ventral roots before the somato-dendritic action potential. This provided further evidence that action potentials were initiated in the axon initial segment.

Overall, these early attempts to examine the temporal and spatial characteristics of action potential generation and propagation revealed that it had two components. It was suggested (Brock *et al.* 1953, Coombs *et al.* 1957) that the first component was generated in the initial segment and that the second was generated in the soma and possibly the dendrites. An alternative explanation by Fatt was that the first component arose in the soma and that the second was attributable to an active response of the dendrites.

Frank *et al.* (1959) used a voltage clamp to measure intracellular current in an attempt to clarify the issue of where the action potential was initiated. They discovered that the membrane region producing the second component of the action potential must be partly unclamped because the threshold for firing the second component was much higher than for the first, and that this component could occur even when the first component was clamped near threshold. They also deduced that the clamped area did not lie between the parts of the neurone that generated the first and second action potential components, otherwise the first component would not be able to trigger the second component during a clamp. Therefore, they concluded that the first component is generated in the axon while the second must involve no more than a part of the soma-dendritic membrane.

A later paper by Dodge and Cooley (1973) used a computer model of a motoneurone with active conductances to reproduce the action potential observed in a recorded motoneurone. To achieve this the Na<sup>+</sup> channel density had to be high in the axon, low in the soma and very low or absent in the dendrites. From this study it became apparent that the Na<sup>+</sup> channel density over the motoneurone was more localised than had previously been thought and that Na<sup>+</sup> channel density gradients could be very steep. The low dendritic Na<sup>+</sup> channel density combined with the resistive load of the dendrites meant that the action potential did not propagate effectively into the dendrites.



Early work to try to determine if voltage-dependent ion channels were present in the dendritic membrane of the motoneurone relied on attempts to produce dendritic action potentials. Kuno and Llinás (1970) found that axotomised motoneurones could produce spike-like responses to monosynaptic EPSPs. However, they could not determine the origin of these spike-like potentials other than to say that they originated in the dendrites, nor did they define the ion channel responsible. Similarly, Fujita (1989) found that by altering stimulus strength to evoke EPSPs in cat motoneurones, dendritic action potentials could be elicited. Because they were unlike the normal action potential seen in motoneurones and because of the way they interacted with IPSPs and somatically generated depolarisations, they were presumed to be dendritically generated. However, Fujita did not examine the ionic nature of these putative dendritic action potentials to determine whether the depolarising potentials were caused by  $\text{Na}^+$  or  $\text{Ca}^{2+}$  channels.

Walton and Fulton (1986) demonstrated the presence of dendritic  $\text{Ca}^{2+}$  action potentials and  $\text{Na}^+$  action potentials in neonate rat neurones. They also showed that a  $\text{Ca}^{2+}$  dependent  $\text{K}^+$  conductance ( $I_{\text{K}(\text{Ca}^{2+})}$ ) was present, which is responsible for the majority of the afterhyperpolarisation and is the major determinant of firing rate in these cells. A voltage-gated  $\text{Ca}^{2+}$  current is required to activate this conductance and blockade of this current with  $\text{Cd}^{2+}$  reduced the  $I_{\text{K}(\text{Ca}^{2+})}$  and increased action potential firing rates. However, they also noted that the  $\text{Ca}^{2+}$  current decreased as animals became older and  $\text{Ca}^{2+}$  action potentials were only detectable in 3-5 day old rats after application of potassium blockers such as  $\text{Cs}^+$ . They also observed small all-or-none action potentials in motoneurones of young rats (3-5 days) and in older rats after application of  $\text{Cs}^+$ . These action potentials had faster rise times than the dendritic  $\text{Ca}^{2+}$  action potentials and could be blocked by TTX indicating that they were sodium dependent. These findings suggest that neonatal motoneurones generate  $\text{Na}^+$  and  $\text{Ca}^{2+}$  dependent events at separate anatomical sites, probably in the dendritic membrane and that the  $\text{Ca}^{2+}$  component decreases with age. The early  $\text{Ca}^{2+}$  currents may be important for setting synaptic efficacy in the early stages of motor development.

One of the most definitive early studies on the ion channels present in rat motoneurones is that of Takahashi (1990) on neonate rat motoneurones. This work shows neonate rat motoneurones have three predominant types of potassium conductance; a  $\text{Ca}^{2+}$  dependent potassium channel ( $I_{\text{K}(\text{Ca}^{2+})}$ ), a delayed rectifier ( $I_{\text{DR}}$ ) and an A-type potassium conductance ( $I_{\text{A}}$ ). This study made no examination of  $\text{Ca}^{2+}$  current in these cells, but it did address the contribution of potassium channels to the action potential repolarisation and the afterhyperpolarisation. In neonatal motoneurones, blockade of the A-current markedly prolonged the action potential at the soma (Takahashi 1990). It was therefore concluded that in neonatal rat motoneurones  $I_{\text{A}}$  contributes significantly to action potential repolarisation.

Clements *et al.* (1986) found that internal injection of TEA into cat motoneurons increased the amplitude of dendritically generated EPSPs and prolonged their time-courses, while it had no effect on somatically generated EPSPs. This suggested the presence of a dendritic potassium channel that reduced EPSP amplitude and time-course.

Direct measurement of the backpropagation of the action potential in motoneurone dendrites has so far only been performed in motoneurons cultured from young rats (Larkum *et al.* 1996). In this study, organotypic cultures of spinal cord were used as the experimental preparation. Somatic and dendritic recordings were made with the dendritic electrode at distances varying from 30 to 423  $\mu\text{m}$  from the soma. It was found that the amplitude of the backpropagated action potential was much larger than would be expected for passive attenuation calculated from a simple passive model of the motoneurone. Addition of TTX reduced the dendritic action potential amplitude to that expected for passive propagation. This indicates that there is a  $\text{Na}^+$  channel that amplifies the action potential within motoneurone dendrites. Also, addition of QX-314 to the dendritic electrode solution gradually abolished the amplification of the backpropagated action potential and reduced it to the level expected for passive propagation. This active backpropagation was not present in all cells, and in some cases it was found that action potential backpropagation followed a purely passive decay. To answer the question of whether different dendrites of the neurone could have different conduction properties, Larkum *et al.* (1996) also used optical recordings of membrane potential using the voltage sensitive dye di-8-ANEPPS. Propagation of action potentials and of hyperpolarising pulses was compared to determine whether action potentials were conducted differently in different dendrites. It was found that action potentials declined on average 12.5% less than hyperpolarising pulses, confirming that action potentials are indeed actively backpropagated. Furthermore, the results varied for each dendrite, indicating that it is possible for different dendrites of the same neurone to have differing ability to propagate action potentials. Larkum *et al.* (1996) suggest that the  $\text{Ca}^{2+}$  influx associated with the backpropagating action potential may be important as a retrograde signal to regulate the motoneurone's computational ability.

Measurements of  $\text{K}^+$  channels in motoneurone dendrites have not been made, however a whole-cell and patch-clamp study of potassium channels in isolated somata of rat motoneurons (Safronov & Vogel 1995) found that the most predominant potassium current in the motoneurone soma is the A-current, at least in young rats. A delayed rectifier is also present, along with the voltage-activated  $\text{Na}^+$  channel. This differs from the axonal potassium channels of rat motoneurons which have been shown to contain three types of delayed rectifier with varying kinetics and that none of these corresponds to the A-current (Roper & Schwarz 1989, Safronov *et al.* 1993). These results suggest that the A-current is differentially distributed in the motoneurone. The A-current will tend to

dampen backpropagating action potentials while still allowing EPSPs to propagate to the axon initial segment.

### **Immunocytochemical Localisation of Motoneuronal Ion Channels**

Immunocytochemical techniques have been applied to the problem of identifying the type and spatial extent of dendritic ion channels. Subcellular immunocytochemistry has been performed for  $\text{Na}^+$ ,  $\text{Ca}^{2+}$  and  $\text{K}^+$  channels in the hippocampus, cerebellum, neocortex and spinal cord (e.g. Westenbroek *et al.* 1989, Hell *et al.* 1993, Sheng *et al.* 1994, Sekirnjak *et al.* 1997, Westenbroek *et al.* 1998).

Labelling of  $\text{Ca}^{2+}$  channels subtypes in the spinal motoneurone and neuromuscular junction has shown that each  $\text{Ca}^{2+}$  channel subtype is differentially distributed (Westenbroek *et al.* 1998). Class A (P- and Q-type)  $\text{Ca}^{2+}$  channels are preferentially distributed in the presynaptic boutons of motoneurons at the neuromuscular junction. Class C and D (L-type) and class E (R-type)  $\text{Ca}^{2+}$  channels were found mostly in the soma and proximal dendrites of motoneurons. The only  $\text{Ca}^{2+}$  channel present in significant quantities in motoneurone dendrites is the B-subclass (N-type) of  $\text{Ca}^{2+}$  channel (Westenbroek *et al.* 1998). This differential distribution of  $\text{Ca}^{2+}$  channel subtypes suggests distinct functional roles for the different channel types.

Immunocytochemical labelling of  $\text{Na}^+$  channel subtypes in the spinal cord has shown a differential distribution of  $\text{Na}^+$  channel types as well. Westenbroek *et al.* (1989) showed a preferential distribution of  $\text{Na}^+$  channels in the unmyelinated axons of the spinal cord and in the somata of motoneurons, but that little or no  $\text{Na}^+$  channels were present in the dendrites of these cells.

In the immunocytochemical study of  $\text{Na}^+$  channels by Caldwell *et al.* (2000) they used affinity-purified isoform-specific antibodies, and found that  $\text{Na}(\text{v})1.6$  is highly concentrated at nodes of Ranvier of both sensory and motor axons in the peripheral nervous system and at nodes in the central nervous system. The specificity of this antibody was also demonstrated with the  $\text{Na}(\text{v})1.6$ -deficient mutant mouse strain *med*, whose nodes were negative for  $\text{Na}(\text{v})1.6$  immunostaining. Both the intensity of labeling and the failure of other isoform-specific antibodies to label nodes suggest that  $\text{Na}(\text{v})1.6$  is the predominant channel type in the node of Ranvier. In the central nervous system,  $\text{Na}(\text{v})1.6$  is localized in unmyelinated axons in the retina and cerebellum and was strongly expressed in dendrites of cortical pyramidal cells and cerebellar Purkinje cells. Ultrastructural studies have shown that labeling for  $\text{Na}(\text{v})1.6$  in the dendrites of these cells occurs in both the cytoplasm and on dendritic shaft membranes. The cytoplasmic component presumably represents channels that are being transported to dendritic sites for incorporation into the membrane. Remarkably,  $\text{Na}(\text{v})1.6$  labeling was observed at both presynaptic and postsynaptic membranes in the cortex and cerebellum. Thus, a single

sodium channel isoform is targeted to different neuronal domains and can influence both axonal conduction and synaptic responses. In the motoneurone however, it appears to be present only in the axon.

Immunocytochemical labelling of  $K^+$  channels has been performed in the spinal cord by Veh *et al.* (1995). This study did not examine  $K^+$  channel distribution at high resolution, but merely found a high expression of the  $K(v)1.1$  and  $K(v)1.2$  varieties of the shaker  $K^+$  channel in the soma and dendrites of motoneurons suggesting that dendrites of motoneurons do indeed contain voltage-dependent  $K^+$  channels.

### Concluding Comments

Generally, studies of dendritic ion channels have shown a great deal of heterogeneity between cell types and this indicates that the results for one cell type cannot be transferred to another cell type. In addition, studies such as that of Häusser *et al.* (1995) where the axon originates from the dendritic tree, remind us that not all neurones have their axons attached to the soma. Therefore, until the complexities of dendritic ion channels are better understood, it is unsafe to generalise about the role these channels play in the integration of synaptic potentials in neurones and the propagation and initiation of action potentials.

As already mentioned, dendritic recordings have been achieved in neurones of the neocortex, hippocampus, cerebellum, substantia nigra, thalamus, spinal cord and retina, but little work has been done to examine the dendritic ion channels of motoneurons electrophysiologically. This study is the first of its kind to place an electrode on a motoneurone dendrite in a rat spinal cord slice and measure dendritic events.



---

## Chapter Two

### General Methods

---

This chapter deals with the general methods that were used in the experiments described in the following chapters. Each of these experimental chapters has its own specific methods relating to the work in that chapter. Experiments and modelling were carried out at the John Curtin School of Medical Research in Canberra, Australia while histological processing and reconstruction were performed at the Physiological Institute in Berne, Switzerland.

#### Dissection

Preparation of spinal cord slices was performed by first anaesthetising a 7-15 day old Wistar rat of either sex with halothane (4% in medical O<sub>2</sub>) followed by intraperitoneal injection of urethane (0.1g/mL, 0.1mL/100g body weight) and then chilling the animal for 5-7 minutes on ice until breathing had almost ceased. During this time, the rat was kept in an atmosphere of 95%O<sub>2</sub>/5%CO<sub>2</sub>. The rat was then decapitated and pinned, dorsal side up, on a cork pad.

The skin was cut along the spine and reflected along its entire length. The vertebral column and thorax were then cut at the upper thoracic level and further cuts made to separate the vertebral column including the dorsal thorax, pelvis and tail stump from the rest of the body.

The excised vertebral column was then placed in a dissecting dish lined on the bottom with Sylgard and filled with artificial cerebrospinal fluid (ACSF) containing ACSF ice crystals and therefore at about 0°C. This ACSF consisted of (in mM) NaCl 113, KCl 3, NaH<sub>2</sub>PO<sub>4</sub> 1, NaHCO<sub>3</sub> 25, glucose 11, CaCl<sub>2</sub> 1, MgCl<sub>2</sub> 6 and was used throughout the dissection and slicing of spinal cord slices. For recording, the ACSF was modified so that it contained 2mM CaCl<sub>2</sub> and 1mM MgCl<sub>2</sub>.

A ventral laminectomy was then performed by placing one tip of the scissors inside the spinal canal and cutting through the vertebrae bilaterally while pulling the excised bone up and away, leaving the exposed spinal cord intact in the pinned vertebrae

The dura mater was then split along the ventral midline for the entire length of the cord using Vanass scissors. The most rostral end of the cord was then grasped with fine forceps and lifted upwards while the nerve roots and dorsal root ganglia were freed by cutting the roots outside the dura. The excised cord was then placed in the Sylgard coated chamber and the dura mater split on the dorsal side and removed by cutting through the nerve roots, removing the dorsal root ganglia, nerve roots and dura together.

Next, the cord was hemisected for a millimetre or so at the rostral end. The pia mater was gripped with fine forceps and by pulling caudally could be completely removed,

taking all remnants of the nerve roots with it. This step is essential for clean slicing of the cord and to ensure the viability of large cells. Once the pia had been removed from the cord, two cuts were made with a scalpel to isolate the lumbar enlargement of the spinal cord (lumbar 3 to sacral 1).

The isolated spinal segment was then mounted in molten, oxygenated Agar at 36°C. The Agar (1.0g/60mL) was boiled vigorously to ensure it was dissolved and then bubbled with 95%O<sub>2</sub>/5%CO<sub>2</sub> and cooled to 36°C. At this point, it was poured into a small mould and the lumbar enlargement of the spinal cord was placed in it vertically.

The mould containing the Agar and the spinal cord section were then cooled in icy ACSF to solidify the Agar. Once cooled, a small cube of Agar containing the cord was cut from the mould with a scalpel and glued to a cutting block with cyanoacrylate glue. This was then mounted on a Camden vibrotome and transverse slices of spinal cord of 300µm thickness were made.

Once cut, slices were placed in a beaker of recording ACSF at room temperature (20-24°C) and were then incubated in a water bath at 35°C where the temperature was allowed to equilibrate and the slices were allowed to recover for 1 hour. Thereafter the slices were kept at room temperature (20-24°C) for up to 6 hours.

## Recording

For recording purposes, single slices were transferred to a holding chamber on a microscope stage and perfused at 3mL/min with ACSF maintained at 34±2°C with a Peltier device. The ACSF always contained 10µM CNQX, 100µM picrotoxin and 10µM strychnine in order to block synaptic background activity. The slice was held in place in the recording chamber with a U-shaped platinum wire supporting parallel nylon threads (Edwards *et al.* 1989). One thread was placed across the dorsal horns of the spinal cord slice and another thread across the ventral border of the spinal cord leaving most of the ventral horn free for electrode exploration.

The neurones were visualised using infra-red differential interference contrast (IR-DIC) optics on a Zeiss Axioskop microscope. This was achieved by removing the heat filter from the lamp housing to allow infra-red light to reach the field aperture and then using a 40nm bandwidth 770nm filter in the filter holder of the microscope. This gives infra-red illumination of the tissue (Stuart *et al.* 1993). All other optics were standard equipment for differential interference (Nömarski) optics. The objective was a 40x water immersion lens (Zeiss), infinity corrected and mounted on a 20mm extension tube to allow more room under the turret for micromanipulators. The image was magnified by a factor of four with a video adapter tube (Zeiss) attached to the camera port of the microscope. Images were recorded with an infra-red sensitive video camera (Hamamatsu, Model C2400-07ER, Japan) and displayed on a monitor. Images were

recorded on computer with a frame grabber (Quick Capture) and software (NIH Image 1.41).

Whole-cell recordings were made only from neurones with cell body diameter larger than 20  $\mu\text{m}$  (the major diameter in the elliptic outline) in the hope that these neurones were most likely motoneurones (Takahashi 1990). However, reliable identification of the cell type was not possible, even after staining and reconstruction (see Chapter 3). The electrodes were made from thick-wall borosilicate glass tubing (1mm inner diameter, 1.5mm outer diameter) containing a filament so that electrodes did not have to be back-filled. Electrode resistances were between 5 and 8  $\text{M}\Omega$  for electrodes attached to the soma. They were filled with a solution of the following composition (in mM): gluconic acid 135, KCl 5, MgATP 5,  $\text{MgCl}_2$  1.2, ethylene glycol-bis( $\beta$ -aminoethyl ether)-N,N,N',N'-tetra-acetic acid (EGTA) 5, N-tris(hydromethyl)methyl-2-aminoethanesulfonic acid buffer (HEPES) 5. This was adjusted to pH 7.30 using KOH and the osmolarity set to 280-290mOsM using sorbitol. In experiments where staining was necessary, Biocytin (Sigma) was added at 0.5% w/v.

The electrodes were moved with manipulators (Sutter MP285) mounted on optical columns (Spindler & Hoyer) with optical column clamps. The microscope was mounted on a sliding table so that the field of view could be moved while the electrodes were attached to the slice.

Voltage clamp and current clamp were achieved using an AxoClamp 2 and AxoClamp 2B amplifier, one for each electrode. Sweeps were viewed on an oscilloscope and digitized using an A/D converter (ITC 16, Instrutech Corp, Greatneck, N.Y., U.S.A.) attached to a computer (Macintosh Quadra 700). Data was displayed and stored to hard disk using AxoData (Axon Instruments) and analysed with AxoGraph (Dr. John D. Clements).

Current passing and voltage clamp protocols were sent to the amplifiers through the D/A converters of the ITC-16, and were controlled by AxoData.

### **Histology and Morphological Reconstruction**

In experiments in which staining had to be achieved, the electrophysiological measurements took between 20 and 30 minutes during which time the biocytin diffused into the cell. Before the electrodes were withdrawn from the cell, a video image was taken of the cell body and proximal dendrites. The slice was then removed from the recording chamber and placed in a fixative (0.1M phosphate buffer containing 4% paraformaldehyde and 4% sucrose) and the slices were then stored in this fixative in the refrigerator for up to 8 weeks. They were then sent by express mail to Berne for histological processing and reconstruction.

The biocytin filled cells were visualised with the Vectastain ABC Kit (Vector Laboratories, Burlingame, CA, U.S.A.), following a procedure described by O'Carroll *et al.* (1992) and



which is described in Appendix 1. Upon clearing, the slices became transparent and were mounted in the concave depression of a microscope slide in 100% glycerol. They were then covered with a cover slip and sealed with nail polish. The cells were then reconstructed within 24 hours. Reconstruction was made by means of a computer-assisted reconstruction system (Eutectic 3D Neurone Tracing System, Eutectic Electronics, Raleigh, NC, U.S.A.). Each cell was represented by up to 1340 data points in three-dimensional space. The dendrites were assumed to be composed of short cylindrical segments defined by two successive data points with a diameter equal to the mean of the diameters measured at these two points. The total dendritic membrane surface area ( $A_D$ ) was the sum of the surface areas of these cylindrical segments. Since it was not possible to focus through the densely stained cell body to accurately measure the thickness of the soma, the membrane surface area of the soma ( $A_S$ ) was approximated by the surface of a prolate spheroid formed by rotating an ellipse about its major axis using the formula:

$$A_S = 2\pi b^2 + \frac{2\pi ab}{\epsilon} \arcsin(\epsilon)$$

where  $a$  and  $b$  denote the length of the major and minor axis, respectively, of the ellipse representing the soma outline, and  $\epsilon = (a^2 + b^2)^{1/2}/a$ .

Comparison of the soma outline and dimensions of the proximal dendrites in the video image taken during the experiments with the corresponding outlines following the staining procedure showed no evidence for tissue shrinkage. This is consistent with observations on tissue shrinkage by other researchers using the same histological procedure (Thurbon *et al.* 1994, Ulrich *et al.* 1994). The nominal resolution of the reconstruction system was 0.2  $\mu\text{m}$  determined from the error in repeated measurement of a single section.

---

## Chapter Three

### Passive Properties of Motoneurones

---

#### Introduction

For an examination of motoneurone dendritic properties, the first information needed was the passive parameters of the cell. For this, both single and double electrode recordings were made from visualised cell bodies in the ventral spinal cord and small current pulses were applied to produce voltage responses for the transient analysis.

#### Methods

The cell bodies were approached with two electrodes from opposing sides of the bath at an angle of approximately  $30^\circ$  to horizontal. Two Axoclamp-2 amplifiers (Axon Instruments, Foster City, U.S.A.) were used. First, a seal was established with both electrodes in voltage clamp mode. After breaking into the cell with both electrodes, both amplifiers were switched to current clamp mode. A long (75ms) hyperpolarising current pulse of  $-0.1\text{nA}$  was injected through one electrode and the bridge-balance carefully adjusted, using the resulting voltage transient recorded with the other electrode as a guide. This procedure was then repeated for the other electrode. Optimal capacitance compensation was assumed when the high frequency noise increased up to fourfold without ringing. Membrane potential was held at  $-65\text{mV}$  (in all cases holding current was less than  $-150\text{pA}$ ). In 6 out of 11 cells no holding current was used. All cells could be made to fire repetitively.

Brief ( $480\mu\text{s}$ ) rectangular current pulses of  $-0.5\text{nA}$  amplitude were injected at a repetition rate of 3Hz through one of the two electrodes. 500 voltage transients of 100ms duration were recorded simultaneously with both electrodes, filtered at 10kHz, digitised at 31.25KHz ( $32\mu\text{s}$  interval) with a 16-bit A/D converter (ITC 16, Instrutech Corp., Greatneck, N.Y. U.S.A.) and stored on hard disk. A typical transient as recorded with the voltage-recording electrode is illustrated in figure 3.1A. The maximal amplitude of the voltage transient was always less than 3mV. After recording, data was analysed offline. All 500 sweeps of the cells voltage response were visually inspected for large baseline drift and action potentials, and any contaminated records were rejected. Thereafter the sweeps were averaged and the 95% confidence band computed after subtracting the average voltage over the entire time-course of the voltage response. Between 420 and 500 sweeps were used for averaging. Figure 3.1C shows a typical averaged transient as recorded with the voltage recording electrode together with its narrow 95% confidence

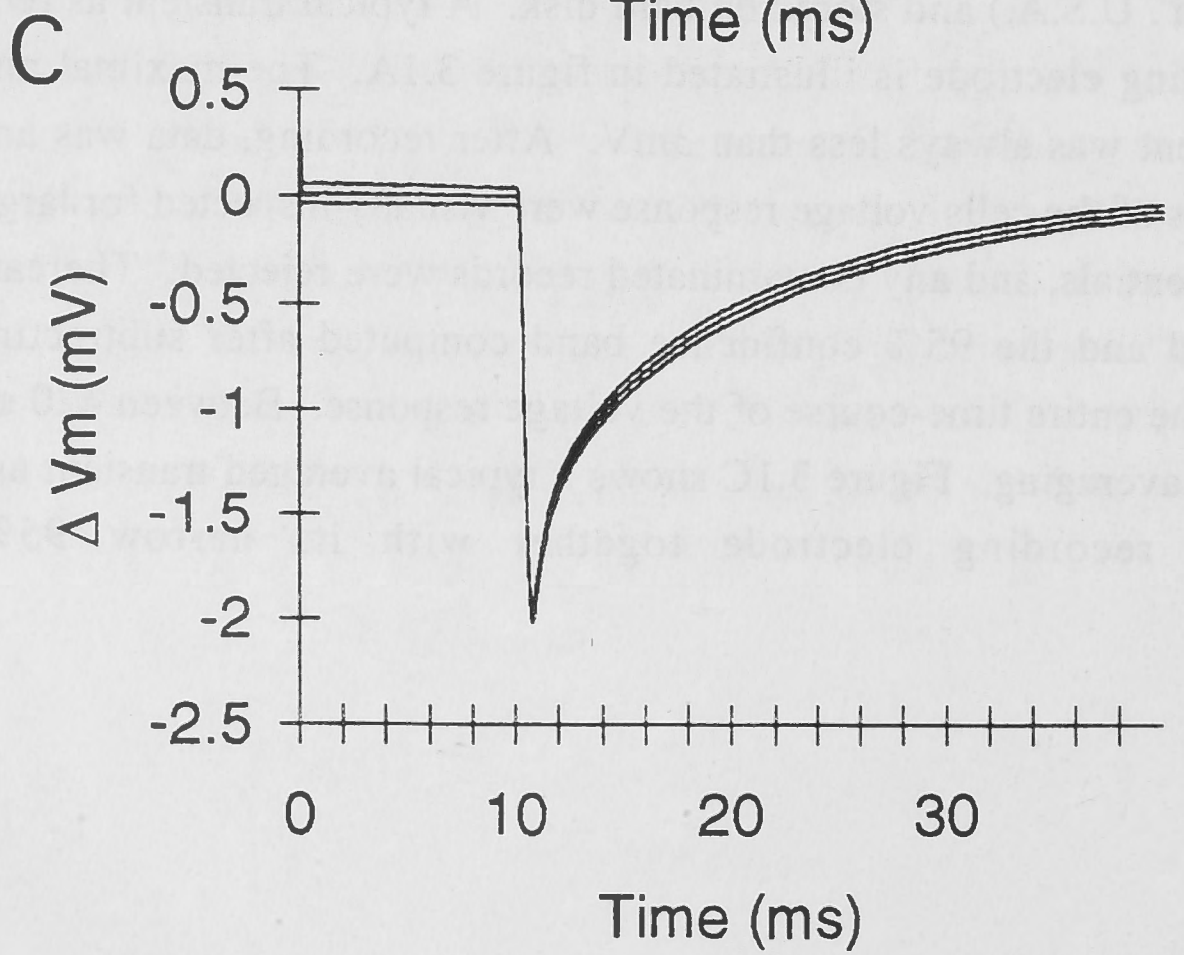
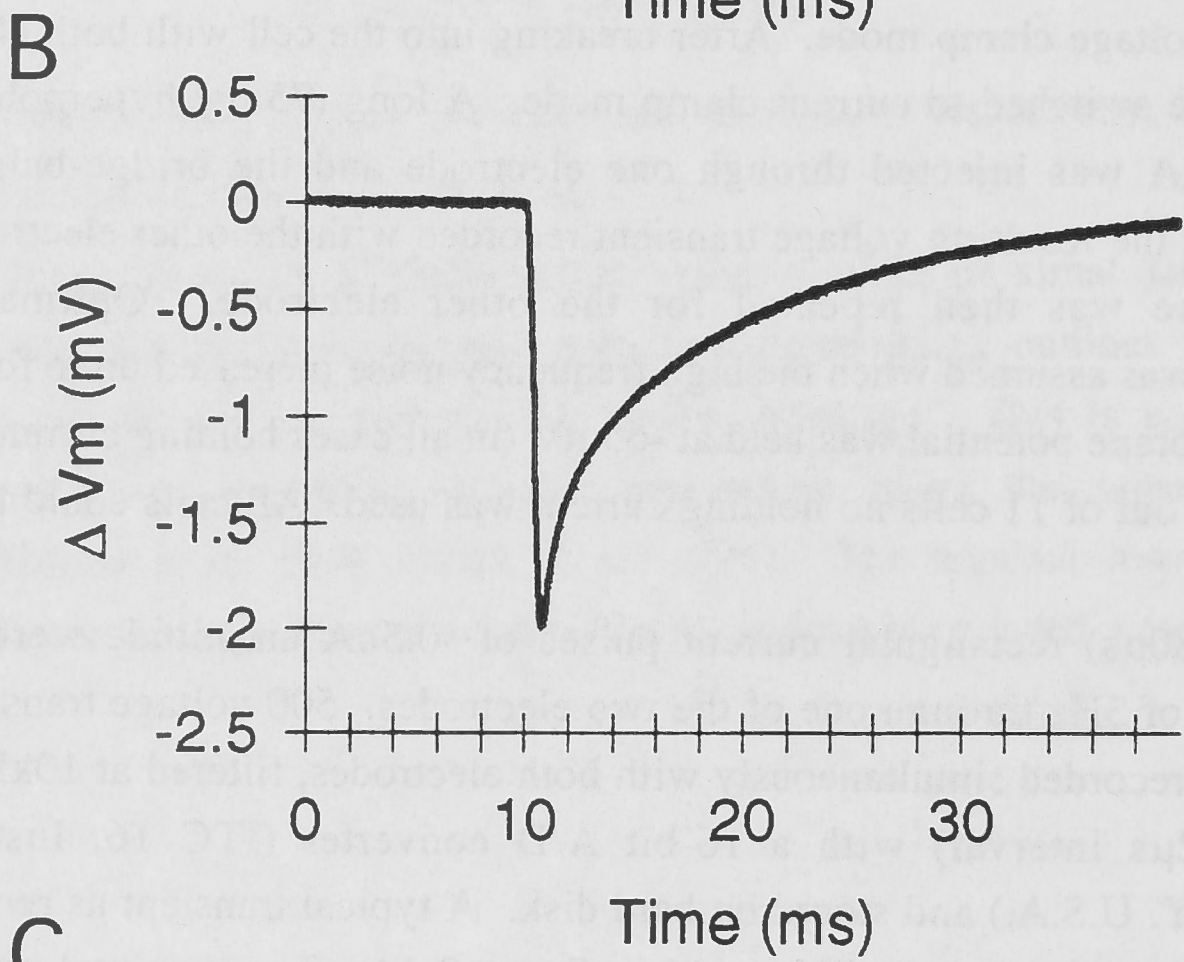
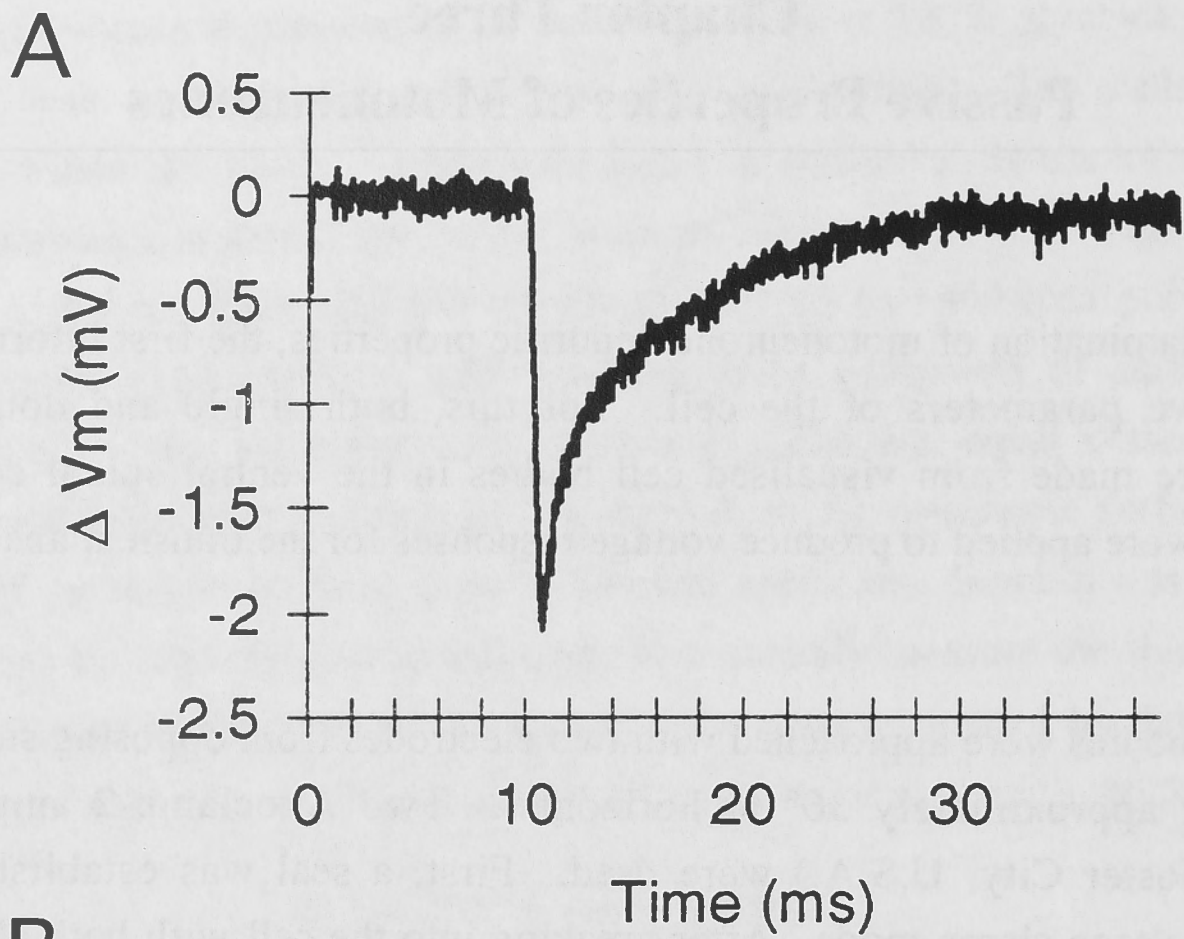


Figure 3.1. Single sweep, sub-averages and average voltage transient. **A:** Voltage response to  $-0.5\text{nA}$ ,  $480\mu\text{s}$  duration current pulse from cell C3-1311, filtered at 10KHz and digitised at 31.25KHz ( $32\mu\text{s}$  sample interval). **B:** Four sub-averages of 100 sweeps each superimposed. The near perfect superposition of the four sub-averages suggest perfect stationarity of the voltage response over time. **C:** Average voltage transient of 420 sweeps together with the 95% confidence band.

band (420 sweeps). These voltage transients were then baselined to a 1ms region immediately before the onset of the current pulse response. These uncontaminated average transients were subsequently used as the target response for the fitting procedure in the compartmental models. For such a transient to be useful as a target response for estimating the parameter values for  $R_m$  (specific membrane resistivity),  $R_i$  (specific cytoplasmic resistivity) and  $C_m$  (specific membrane capacitance) from the corresponding passive compartmental model, one must ensure stationarity of the responses over the period required to acquire the 500 responses. Comparing sub-averages of 100 responses provides a simple test for stationarity. Figure 3.1B illustrates such a test. Four consecutive sub-averages of 100 sweeps each are superimposed. The perfect superposition of all four sub-averages suggests perfect stationarity throughout the duration of the experiment.

In addition to the check for stationarity, great care was taken to ensure that the injected short hyperpolarising current did not activate (or inactivate) any voltage-dependent currents and that the recorded transients were indeed passive responses of the investigated cells. Three procedures were adopted to check the linearity of the voltage response.

(1) After collecting 500 voltage transients evoked by a  $-0.5\text{nA}$  current pulse, the same procedure was repeated with a current pulse of  $-1.0\text{nA}$  (duration always  $480\mu\text{s}$ ). The average transient was then scaled by a factor of 0.5 and superimposed on the average transient produced by the  $-0.5\text{nA}$  current pulse. The two transients always superimposed within the 95% confidence band of the small current pulse response (Fig. 3.2A). The two recordings were however never pooled and only the voltage transients to the  $-0.5\text{nA}$  current pulse were used for analysis. The near perfect superposition of the two traces add additional support for the stationarity of the voltage transients over the long time period required to acquire the transients for two different currents.

(2) The voltage transient produced by the  $-0.5\text{nA}$  current pulse was scaled by a factor of  $-1$ , plotted on a semi-logarithmic scale and visually inspected for sag. In all cells used for analysis, the late linear part of the transient could be extended well into the baseline region where noise obscured the transient (Fig. 3.2B).

(3) In 22 cells (of which 4 cells remained in the final group) voltage clamp experiments were performed either with two electrodes or one electrode (15 cells with 2-electrode, 7 cells with 1-electrode) in order to compile steady-state current-voltage relations. In all cases, the current-voltage relation was linear over the entire voltage range used and in most cases up to  $10\text{mV}$  deviation from the holding potential at  $-65\text{mV}$  (Fig. 3.2C).

Since none of the three tests could reveal any contribution of voltage activated conductances it was concluded that the voltage transients used for final analysis were

indeed passive responses of the cell's membrane, at least for the small voltage deviations used in this test. The final analysis was based on 12 cells that were chosen for their complete staining with Biocytin out of a total of 39 cells from which satisfactory electrophysiological data were obtained.

### *Two Electrode Experiments*

To further study the passive properties of motoneurone dendrites, two electrode experiments were performed in which one electrode was placed on the soma and the other electrode was placed on a dendrite. Under IR-DIC, dendrites could be seen emanating from the soma of a few cells in each ventral horn of the cord. Dendrites could be followed for up to  $50\mu\text{m}$  from the soma but generally were not visible beyond this distance. This may be because of the thin diameter of the dendrites and the fact that they do not travel parallel to the surface of the slice as do the dendrites of pyramidal cells in carefully sliced neocortex (Stuart *et al.* 1993). Therefore in this study, the maximum distance from the soma at which electrodes could be placed on a dendrite was about  $50\mu\text{m}$ . Dendritic electrodes were made finer to compensate for the thin dendrites to which they were attached and resistances for these electrodes ranged from 8-12M $\Omega$ .

While the two electrodes were attached to the cell, a current pulse of  $-0.5\text{nA}$  amplitude and  $480\mu\text{s}$  duration was applied alternately to the somatic and dendritic electrodes at a membrane potential of  $-65\text{mV}$ . Voltage responses were recorded at both electrodes during the current pulse even though voltage artifacts were present on the current injecting electrode. Pulses were applied repetitively at 3Hz and 500 responses of the voltage were recorded. The responses at both the soma and dendrite to the dendritic and somatic current pulses were averaged, after excluding any noisy records. These transients were used for the somatic and dendritic fitting procedure described below.

### *Reciprocity*

In addition, the voltage responses at each electrode were used as a test of reciprocity. Circuit theory dictates that in a passive electrical network, such as the dendrites of a passive neurone with passive membrane properties, the voltage transfer between two points in the network will be the same in both directions. In a passive neurone with two electrodes attached, this means that the somatic voltage response to dendritic current injection should be the same as the dendritic voltage response to somatic current injection. Therefore, if equal currents are injected at soma and dendrite, the responses recorded after transmission through the dendrite should have the same time-course and amplitude. This simple experiment can be used as a test for active properties in a neurone's dendrites. Since the input resistance at the dendrite is much higher than that in the soma, equal sized currents

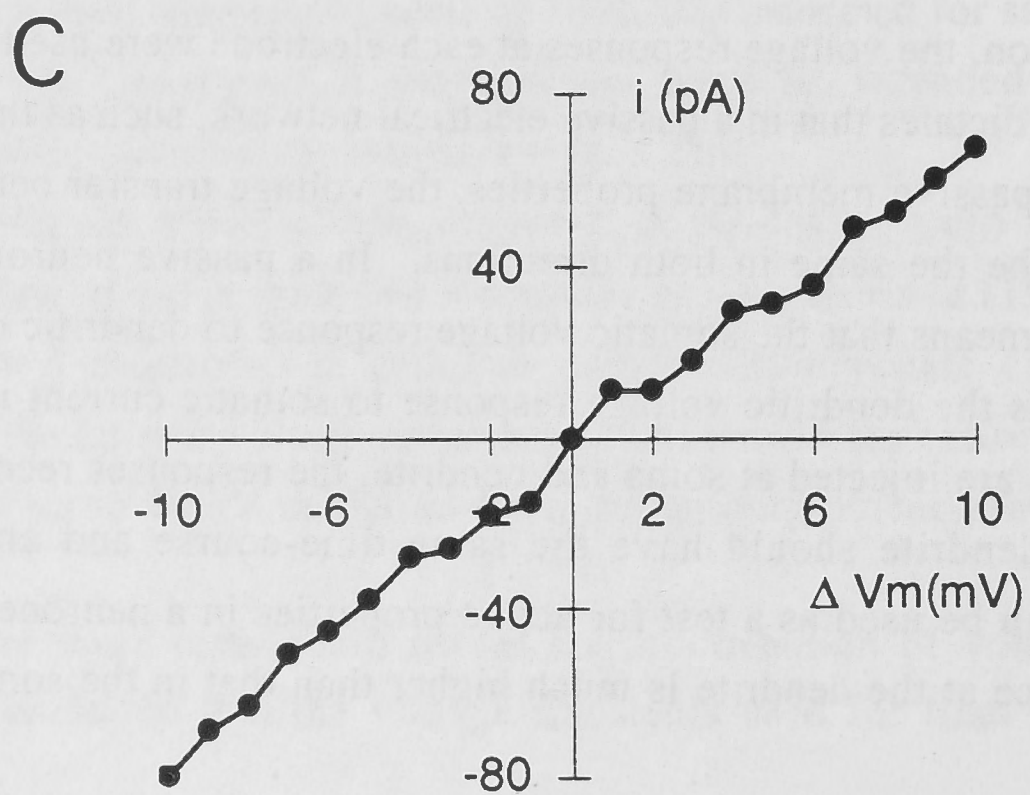
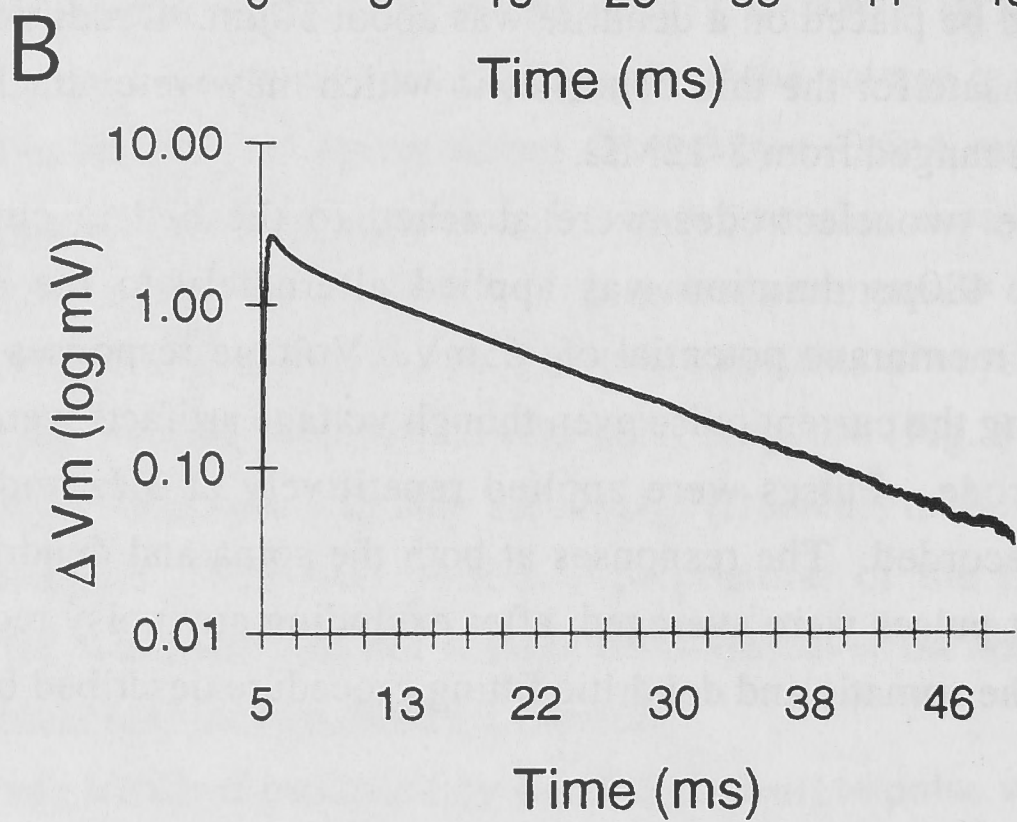
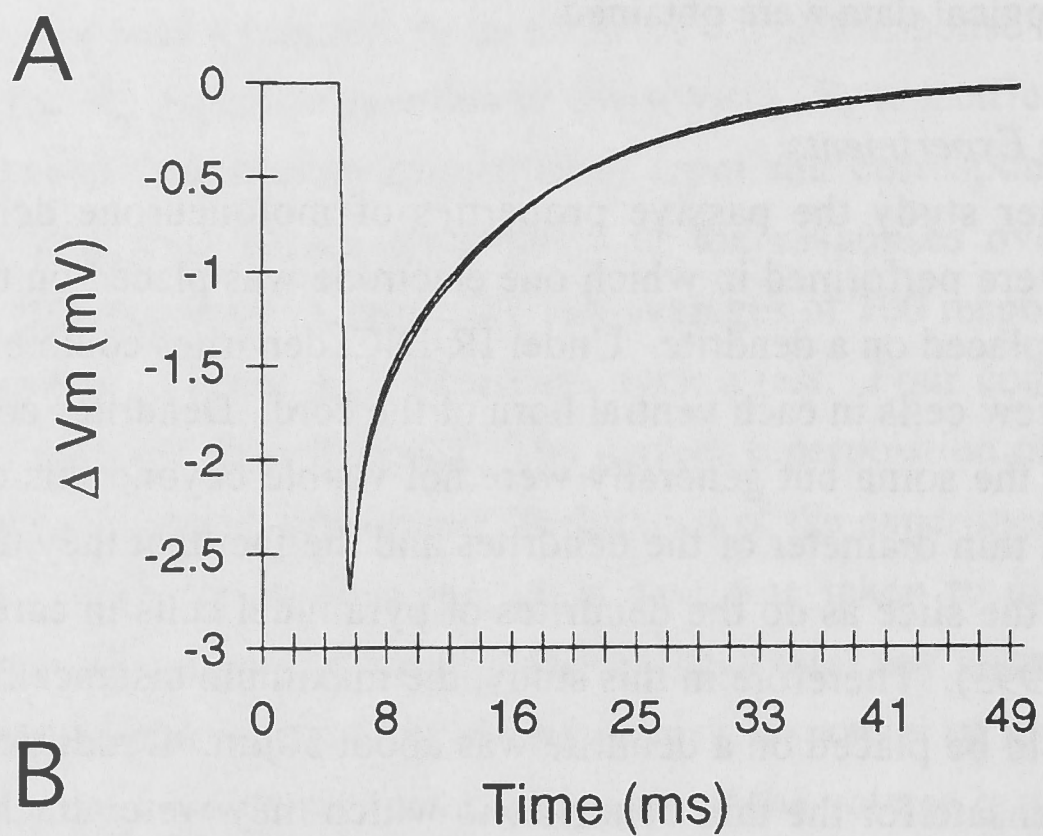


Figure 3.2. Test for linearity and sag. **A:** Average voltage response (500 sweeps) to a  $-0.5\text{nA}$ ,  $480\mu\text{s}$  duration current pulse from *cell C2-2201* superimposed with the average voltage response (500 sweeps) to a  $-1.0\text{nA}$  current pulse of same duration scaled by a factor of 0.5. The two voltage transients superimpose within the 95% confidence interval shown in fig. 3.1B. **B:** Semi-logarithmic plot of the average voltage transient (500 sweeps, same cell as in A) to a  $-0.5\text{nA}$ ,  $480\mu\text{s}$  duration current pulse scaled by a factor of  $-1.0$ . The late linear portion of the transient extends well into the noisy part where the transient approaches the baseline again. **C:** Steady-state current-voltage relation as a further test for system linearity in the voltage range used (*cell C1-1411*). Voltage steps of  $1\text{mV}$  increment and  $30\text{ms}$  duration were applied and the resulting steady-state current calculated as the mean current in a time window of  $2.0\text{ms}$  at the end of each voltage pulse. Holding potential was  $-65\text{mV}$ .



will produce larger voltage responses in the dendrite than in the soma. Thus if voltage-dependent conductances are present in the section of dendrite between the somatic and dendritic electrodes, the dendritic current pulse should cause significantly more activation of these channels than the somatic current pulse and non-identical signals will be recorded. The results of this analysis are discussed later. It should be noted at this point, that it is possible to have two voltage-dependent conductances that have the similar kinetics and which produce opposing currents. Under these conditions, the current-voltage relation of the cell will still be linear and reciprocity may still hold true.

### *Modelling Methods*

Combining physiological recordings and morphology of a neurone into a compartmental model of that cell has been described in detail by a number of researchers (Clements & Redman 1989, Segev *et al.* 1989, Major *et al.* 1994, Rapp *et al.* 1994, Thurbon *et al.* 1994, Ulrich *et al.* 1994). The common goal is to build a passive electrical model of the neurone and find its values of  $R_i$ ,  $R_m$  and  $C_m$ . This is achieved by closely matching the voltage response of the model for a given current pulse at the soma to the experimental voltage transient generated by the same current pulse (assuming uniform passive membrane properties).

The simulator NEURONE (Hines 1993) was used running under Windows95 on a 90MHz Pentium based computer. An integration time step of  $25\mu\text{s}$  was used. The fitting algorithm used to match the model's responses to the experimental target transients is supplied by NEURONE as a tool and is based on minimising a least square error function. The cell's morphology coded in a Eutectic file format was translated by a computer program called CABLE into a file which could be used directly as an input file to NEURONE specifying the three-dimensional morphology of the reconstructed cells. Each dendritic section was subdivided into segments of  $10\mu\text{m}$  length or smaller.

### *Onset and Duration of Fit Interval*

The early part of the voltage transient is most sensitive to the value of  $R_i$  (Fig. 3.3B), whereas the later part of the transient is most sensitive to the value of  $R_m$  (Fig. 3.3C) and a possible soma shunt conductance (Fig. 3.3D). The amplitude and shape of both the late and early part of the transient is important for extracting  $C_m$  (Fig. 3.3A).

The selection of the onset and end of the fit interval is therefore very crucial for the validity of the parameter values. The duration of the fit interval was chosen to be  $2\cdot\tau_m$ . If a much longer fit interval is chosen (e.g.  $3\cdot\tau_m$ ) too much weight is placed on fitting the late part of the transient while neglecting the short early part of the target response with a

subsequent error in the estimated parameter values. Long fit intervals require long simulation times as well. More crucial than the length of the fit interval however is the selection of its onset time. If the voltage transient is recorded with the current injecting electrode (Major *et al.* 1994, Rapp *et al.* 1994, Thurbon *et al.* 1994, Ulrich *et al.* 1994), the early part of the transient is heavily contaminated with the electrode artifact, even if the capacitance neutralisation is optimally adjusted. Major *et al.* (1994) have made a very careful analysis of the pipette artifacts and have chosen the onset of the fit interval to be 2.5ms after the end of the current pulse. Using a second electrode for passing the current minimises the voltage artifact on the recording electrode. Since the geometrical arrangement between the two electrodes was designed to minimise cross capacitance (180° separation in the horizontal plane, 120° separation in the vertical plane and an interposed earthed objective lens between the electrodes) the artifact caused by coupling capacitance was negligible. Even with well compensated electrodes (both capacitance and bridge) the two simultaneously recorded voltage transients could deviate for more than 20ms following the end of the current pulse (Fig. 3.4A). In this case, even a delay of 2.5ms after the onset of the current pulse could not avoid artifact contamination in the early part of the target transient (Fig. 3.4B). Using the voltage transient recorded with the second electrode as the target response overcomes this problem. However, there is still a remaining artifact caused by the residual uncompensated capacitance of the current electrode, which must be charged by the current pulse in addition to the membrane capacitance. Thus, the current actually supplied to the neurone is not a rectangular pulse, but a filtered pulse that is maintained for an unknown duration following its nominal end. Figure 3.4C compares the experimental voltage transient with the model response. It shows that the experimental transient is delayed by approximately 200µs in comparison to the model response (which uses a perfect rectangular current pulse). In this study, the onset of the fit interval was chosen to be 2.5ms after the beginning of the current pulse in order to avoid this artifact.

This selection is somewhat arbitrary, but it prevents us from overestimating  $R_i$ . The same onset of the fit interval was applied if the voltage transient recorded with the current injecting electrode was used as the target response.

#### *Fit Acceptance and Precision of Parameter Estimation*

In a first run fits were accepted if they lay within the narrow 95% confidence band around the average time-course of the experimental target transient (Major *et al.* 1994). Accepted fits were further analysed in terms of the residuals between experimental transients and the fitted model response.

The calibration of the entire data acquisition, analysis and modelling chain (i.e. amplifiers, A/D-converter, modelling and fitting software) was carefully checked using a resistor-capacitor network connected to the head stage of the Axoclamp-2 amplifiers,

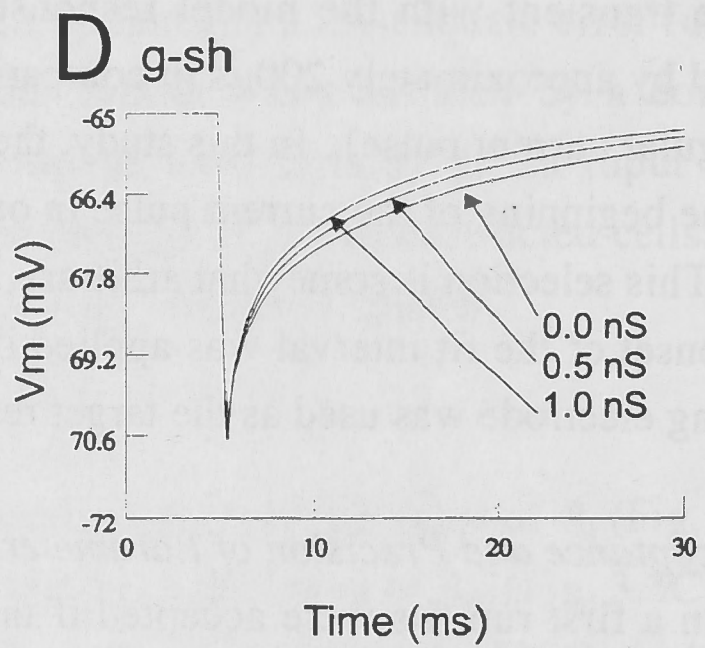
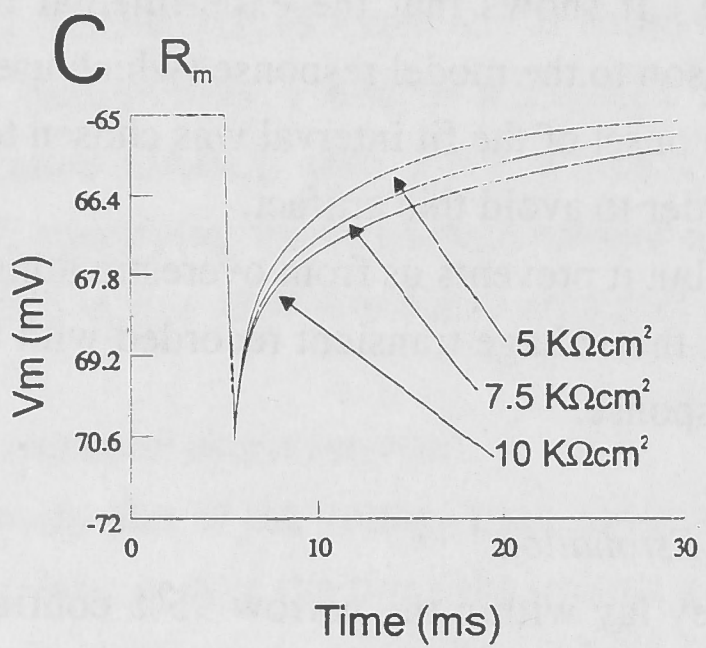
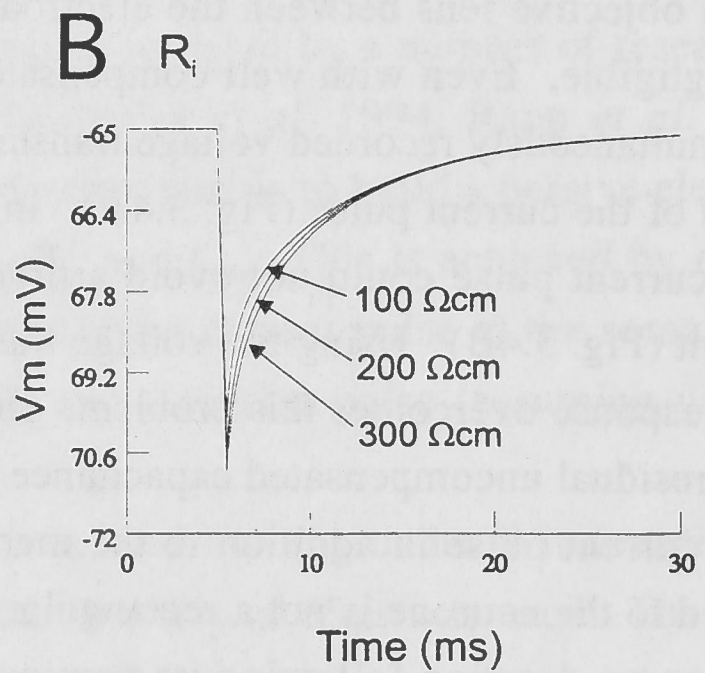
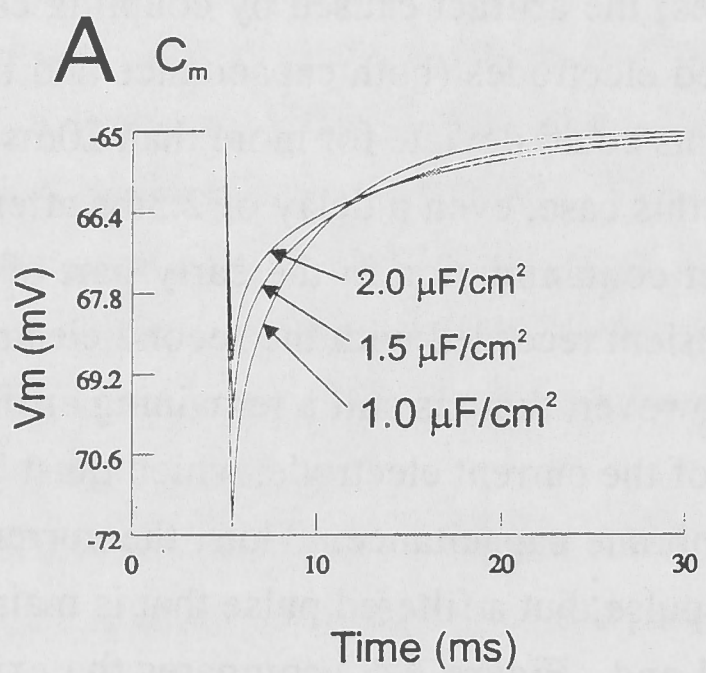


Figure 3.3. Influence of the values of  $R_m$ ,  $C_m$ ,  $R_i$  and somatic shunt conductance ( $g_{sh}$ ) on the shape of the voltage transient. Voltage response of a model (C2-2201) to a current pulse ( $480\mu s$ ,  $-0.5nA$ ) applied to the soma. **A:** Influence of different  $C_m$  on the shape of the voltage transient ( $R_m=5K\Omega.cm^2$ ,  $R_i=100\Omega.cm$ ). The early as well as the late part of the transient is affected. **B:** Influence of different  $R_i$  on the shape of the voltage transient ( $R_m=5K\Omega.cm^2$ ,  $C_m=1.5\mu F/cm^2$ ). Only the very early part of the transient is affected. **C:** Influence of different  $R_m$  on the shape of the voltage transient ( $R_i=200\Omega.cm$ ,  $C_m=1.5\mu F/cm^2$ ). Only the late part of the transient is affected. **D:** Influence of different somatic shunt conductances on the shape of the voltage transient ( $R_m=10K\Omega.cm^2$ ,  $R_i=200\Omega.cm$ ,  $C_m=1.5\mu F/cm^2$ ). The early part of the transient is not affected.



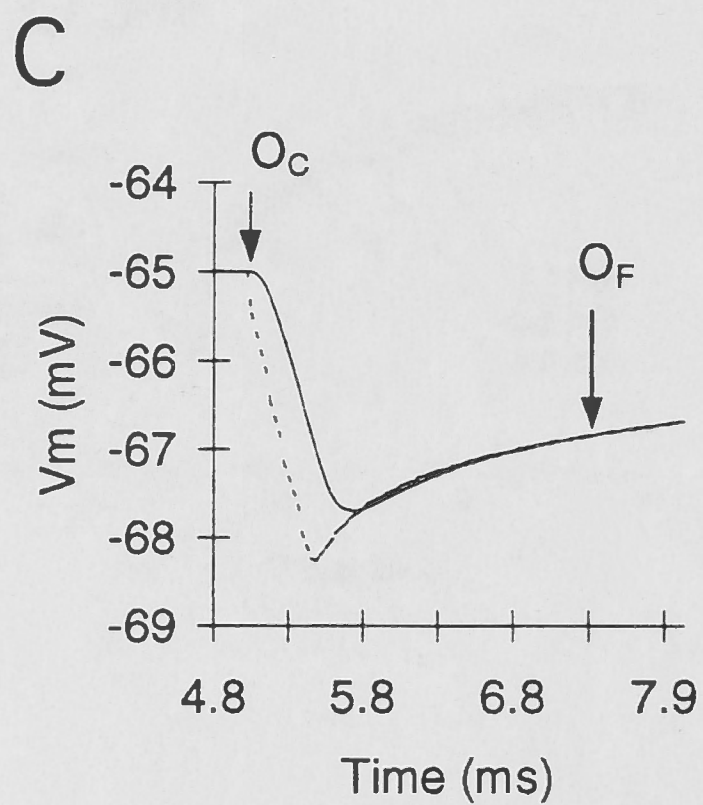
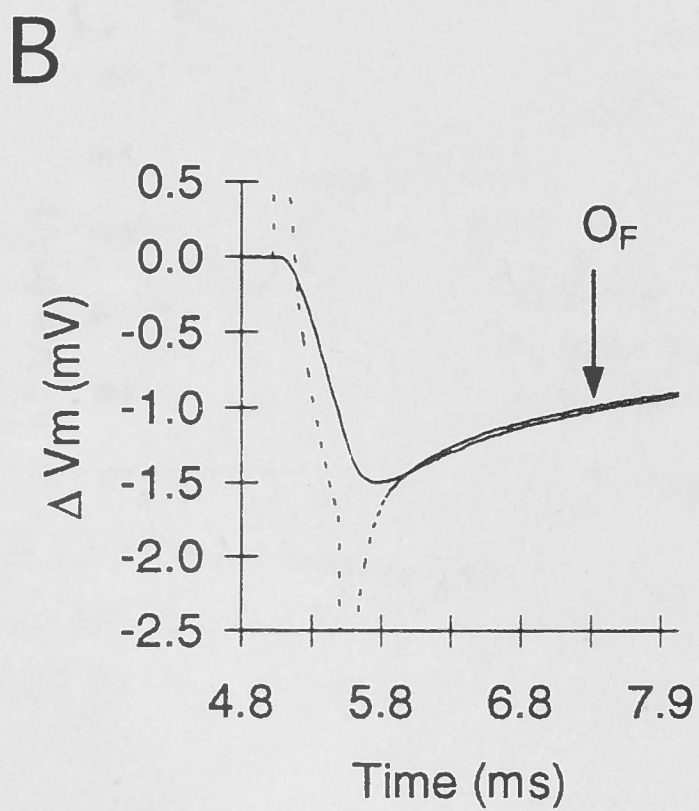
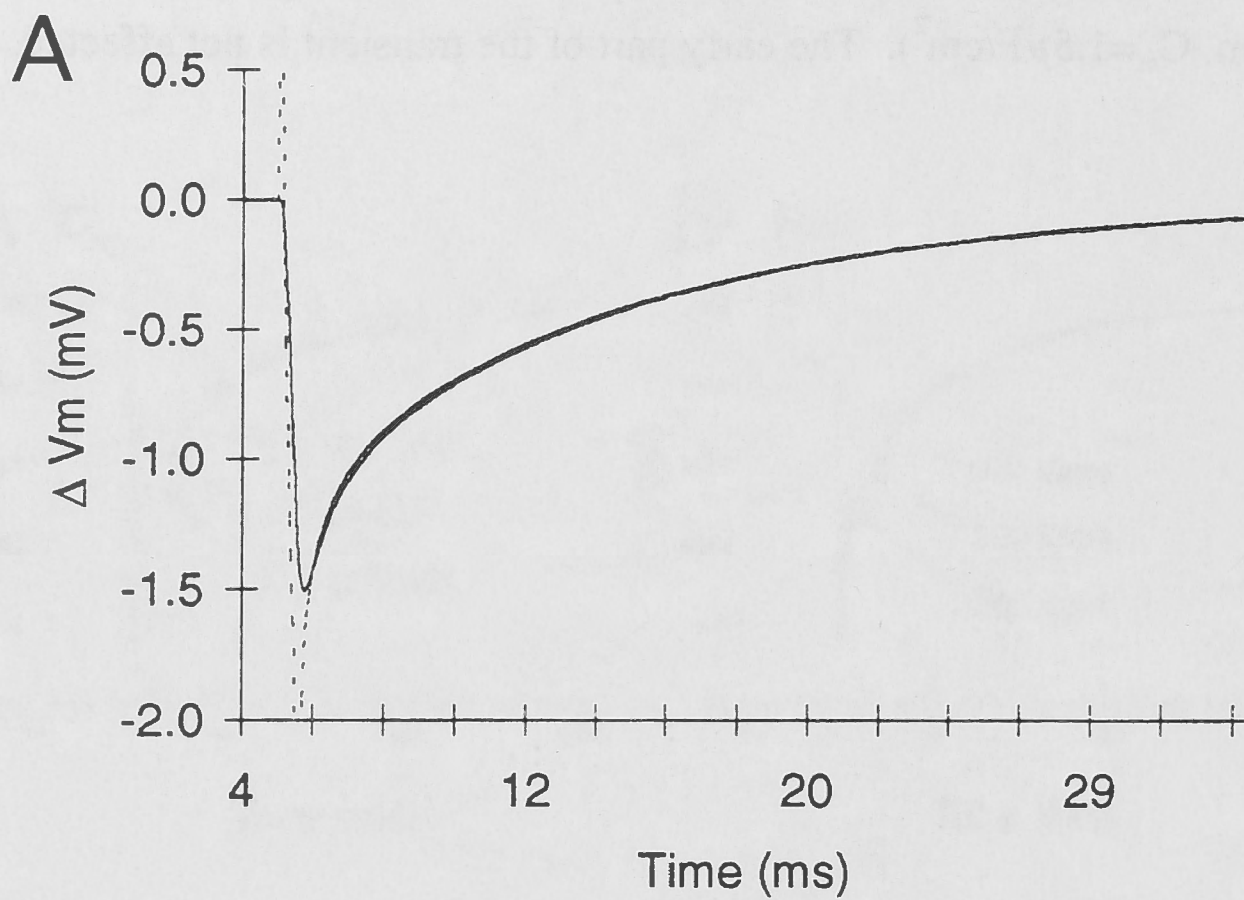


Figure 3.4. **A:** Comparison of the voltage transients recorded simultaneously via the current injecting electrode (dotted line) and via the second, voltage recording electrode (solid line). The current-on and -off artifacts are clipped. The two curves only superimpose after about 20ms from the end of the current pulse. **B:** Same recording as in A but with expanded time scale. Arrow  $O_F$  indicates onset of fit interval. **C:** Comparison of experimental voltage transient (solid line) with model response (dotted line) to the same current pulse at the completion of the fitting procedure.  $O_C$ , onset of current pulse,  $O_F$ , onset of fit interval. The experimental transient rises more slowly than the model transient and is delayed by approximately  $200\mu s$ , due to the fact that the current first has to charge the electrode capacitance and thus is no longer a rectangular pulse when charging the membrane capacitance.

and a corresponding computer model. The recovered values for the resistance and capacitance were well within the tolerance of the components used (1% resistor, 5% capacitor).

The performance of the fit algorithm was tested extensively. For several reconstructed cells compartmental models were built. Values for  $R_m$ ,  $R_i$  and  $C_m$  were assumed and incorporated into the model. A voltage transient was then generated by injecting a brief (480 $\mu$ s) current pulse (amplitude -0.5nA) into the soma of the model and this was thereafter used as the target function for the fit algorithm. The parameter search was started from many different initial values (up to 100% difference from the true values). The parameter search always converged to precisely the same values, which very closely corresponded to the true values, independent of the initial values (Table 3.1). This high precision in estimating the parameters from a noise-free transient might not be expected from an experimental, inherently noisy transient. In order to test the influence of the noise on the precision of the parameter search, noise-free transients were generated from models with assumed values for  $R_m$ ,  $R_i$  and  $C_m$ . 500 sweeps of experimental baseline noise were averaged and added to the noise-free transient. This “noisy” transient, produced by a model with known  $R_m$ ,  $R_i$  and  $C_m$  was then used as the target function for estimating the above parameters. Again, independent of the starting values, the true parameters were recovered with a very high precision (Table 3.1). Even when the noise amplitude was multiplied by a factor of 10 (simulating a worst case scenario), the “true” values of the parameters of the model could still be recovered, and the algorithm always converged to exactly the same numbers (Table 3.1). With this procedure, we could never detect a local minimum in the parameter search. Five to ten millisecond long pieces of the noise were then randomly shuffled and the fitting procedure repeated with the same initial parameter values. The differences in the recovered values of the three parameters were very small, even in the case where the experimental noise amplitude was multiplied by a factor of 10 (Table 3.2).

Two such experiments are illustrated in figure 3.5. *Cell C2-2201* was used for constructing the model. The “true” parameter values and the corresponding values of the estimated parameters are listed in table 3.1. Figure 3.5A1 uses as a target response the model’s response with added experimental noise. In figure 3.5B1, the noise amplitude is multiplied by a factor of 10. In both cases, the fit superimposes the artificial target response perfectly, and the responses cannot be distinguished. The corresponding residuals are plotted in figures 3.5A2 and B2, respectively. The residuals are equally distributed around the fit. This analysis suggests that the estimated parameter values from a noisy experimental target transient are correct within a very narrow range around the true values, if stationarity in the target response can be ensured, and if the assumption of homogeneous

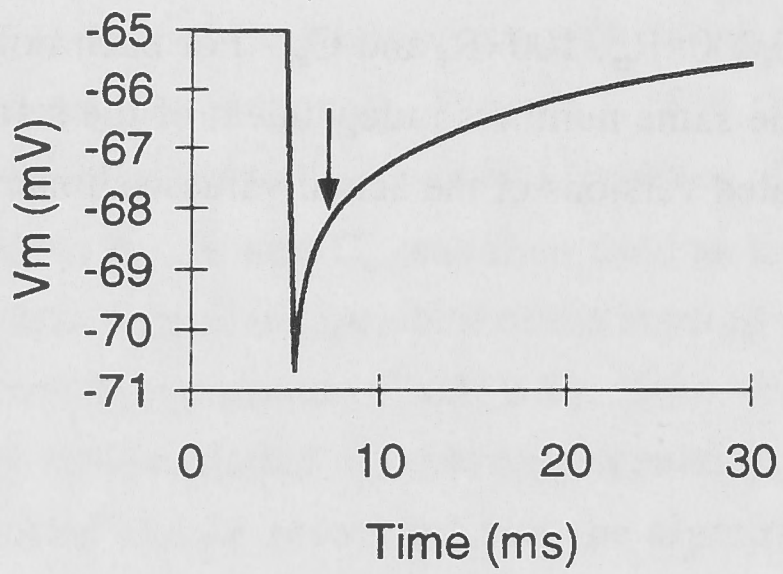
**Table 3.1:** Parameter identification is independent of start values.

Parameter	“true” value	noise-free	noise × 1	noise × 10
$10,000 \times R_m$ ( $\Omega \cdot \text{cm}^2$ )	1	1.00008	1.00007	1.00072
$100 \times R_i$ ( $\Omega \cdot \text{cm}$ )	2	1.9965	1.9948	1.9473
$C_m$ ( $\mu\text{F}/\text{cm}^2$ )	1.5	1.4997	1.4994	1.4937

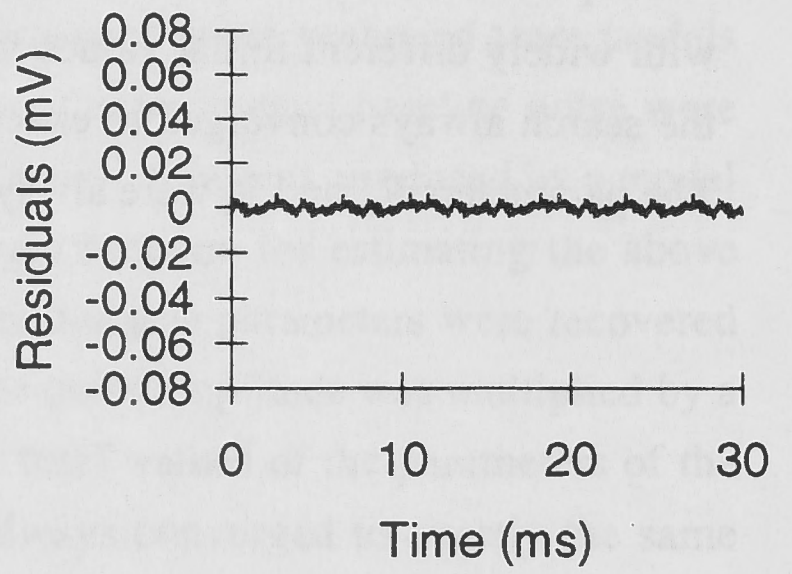
Cell C2-1211-96 was used for the model. A noise-free transient was generated with known parameters for  $R_m$ ,  $R_i$  and  $C_m$ . The parameters were then estimated by directly fitting the model’s response to this noise-free target response. In a second run experimental noise was added to the noise-free transient and was used as the target response. The parameter search was repeated for increased noise contribution (factor 10). Each search was repeated 4 times with widely different initial values for  $10,000 \times R_m$ ,  $100 \times R_i$  and  $C_m$ . For each noise level, the search always converged to exactly the same numbers independent of the start values. The parameters  $R_m$  and  $R_i$  were always scaled versions of the actual values estimated.



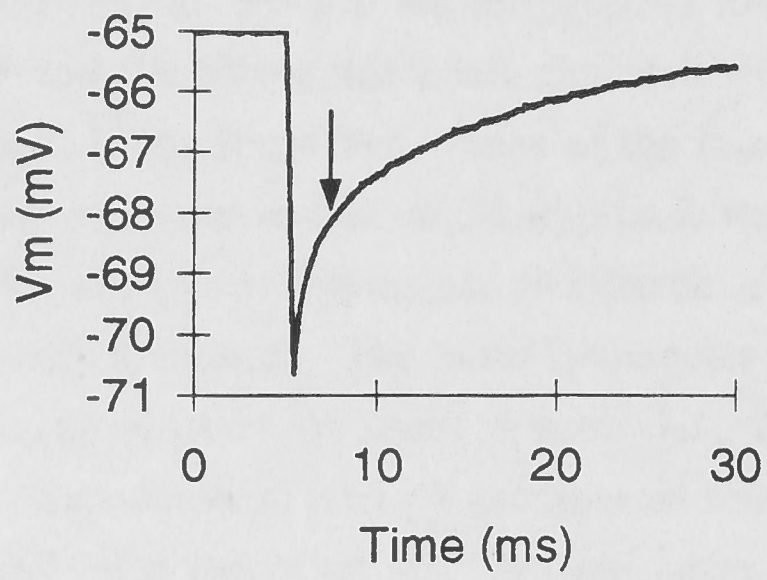
A1



A2



B1



B2

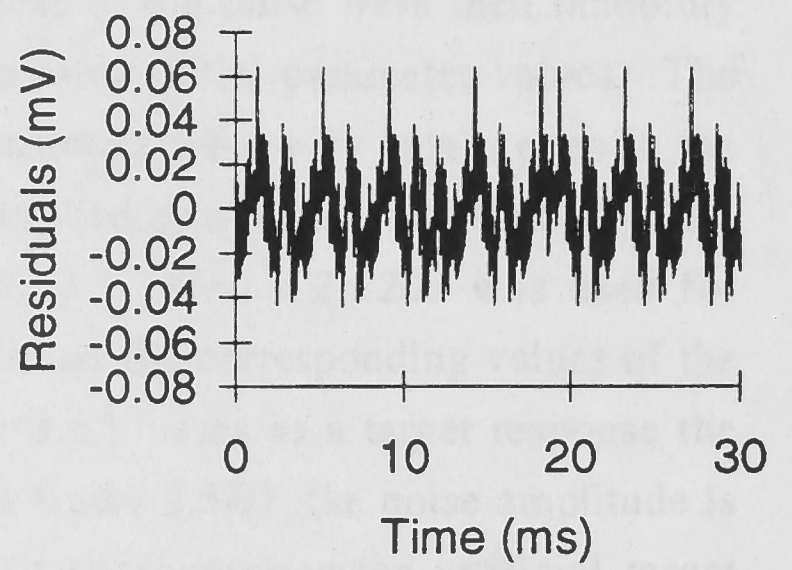


Figure 3.5. Influence of the recording noise on the precision of parameter estimation. First, a noise-free voltage transient was generated from a model cell (*C2-2201*) with known parameters for  $R_m$ ,  $R_i$  and  $C_m$  by injecting a current pulse into the soma ( $480\mu s$ ,  $-0.5nA$ ). Experimental noise was then added to the transient. This noisy transient was used as the target response to which the model's response was fitted, and the onset of the fitting interval is indicated by the arrows. **A1**: Target and fit superimpose perfectly (only one line can be seen), and the estimated values for the three parameters are very close to the "true" values (see Table 3.1). **A2**: Residuals between the target response and the fit illustrated in *A1*. **B1**: The amplitude of the noise in the target response is ten times larger than in *A1*. Fit superimposes the target response perfectly and the estimated values for the three parameters are still very close to the "true" values (see Table 3.1). **B2**: Residuals between the target response and the fit illustrated in *B1*.

**Table 3.2:** Influence of noise on the estimated parameter values.

Parameters	“true” values	start values	End values	end values	end values
$10,000 \times R_m$ ( $\Omega \cdot \text{cm}^2$ )	1	2	1.0008	0.9984	1.0007
$100 \times R_i$ ( $\Omega \cdot \text{cm}$ )	2	1	1.9473	2.0534	1.9493
$C_m$ ( $\mu\text{F}/\text{cm}^2$ )	1.5	1	1.4937	1.5095	1.4939

*Cell C2-1211-96* was used for the model. A noise-free transient was generated with known parameters for  $R_m$ ,  $R_i$  and  $C_m$ . Experimental noise multiplied by 10 was added to the noise-free transient and was used as the target response. The parameters were then estimated by directly fitting the model’s response to this target response. For each of the three different parameter searches, new noise was generated by shuffling 5 to 10ms long pieces of the baseline noise.

passive cable properties incorporated into the model is indeed correct. This procedure for testing the accuracy of the fitting algorithm does not solve the problem of possible non-uniqueness of the solutions, because different sets of parameter values may fit the transient equally well within the boundaries given by the 95% confidence band (Major *et al.* 1994, Rapp *et al.* 1994). This problem becomes obvious when additional parameters are introduced to the model, such as a shunt conductance at the soma. In these cases, it has been shown (see Fig. 3.10) that the residuals are not equally distributed around the model's transient. If the assumptions of the model do not correspond to reality (e.g. non-homogeneous passive membrane properties exist) a distinct pattern in the distribution of the residuals can be expected.

This extensive analysis of the performance of the fitting algorithm first suggests that high frequency noise in the voltage transients does not degrade significantly the values of the estimated parameters; second, that the parameters can be estimated with very high accuracy, and third, that inspection of the residuals may provide additional information about the correctness of the assumptions underlying the model if, and only if the stationarity of the recorded voltage transient over time can be guaranteed. These factors, together with the fact that the confidence band was always very narrow, and many of the "optimal" fits just grazed the upper or lower limits of the confidence band (always in the very early part of the transient), led us to abstain from exploring the parameter space systematically in order to find upper and lower limits on the estimated parameters. We believe that the model parameters obtained from the "optimal" fit are very close to the "true" model values and are compatible with an adequate description of the experimental voltage transients.

#### *Determination of $L_{avg}$*

The electrotonic length,  $L_{DP}$ , of each dendritic path of length  $x_i$  is given by

$$L_{DP} = \sum_{i=1}^N \frac{\Delta x_i}{\lambda_i}$$

where

$$\lambda_i = \sqrt{\frac{a_i \cdot R_m}{2R_i}}$$

and  $\Delta x_i$  is the length of the  $i$ 'th compartment such that  $x_i = N \Delta x_i$ , and  $a_i$  is the radius of the  $i$ 'th compartment.

## Results

### *Morphology*

Twelve cells were selected for morphological analysis from a total of 39 cells. The selection criterion was an apparent complete staining of the distal dendrites. Cells are labelled as either presumed motoneurons or interneurons. Figures 3.6 and 3.7 show examples of one presumed motoneuron and one interneuron, respectively. All cells were located in the ventral half of the spinal cord slice. During the experiment, tentative identification of motoneurons was based on the size of the cell body. After staining and reconstruction, additional identification criteria were the dendritic morphology, precise location of the cell body and axon trajectories. Large cells were found that sent their axons to the contra-lateral side, indicating that they were interneurons. Size and location of cell body is not sufficient for positive identification of motoneurons. The large neuron illustrated in figure 3.6 was located in the motor nucleus, extending its dendrites over a large area of the ventral horn. Although its axon could not be identified with certainty, it was tentatively classified as a motoneuron. The large neuron depicted in Figure 3.7 is located closer to the central canal, extending its axonal branches into the ventral horn. From its location and axon trajectory it was classified as an interneuron. Unfortunately, the electrophysiological properties of the cells could not be used for positive identification as well. Input resistance and action potential characteristics as well as other electrophysiological criteria were insufficient to positively identify cells.

As can be seen from inspection of figure 3.6E and 3.7E, a substantial portion of the dendritic tree was severed during the slicing process. This cannot be avoided because, unlike cortical pyramidal neurons or Purkinje cells, the dendritic tree of rat lumbar spinal neurons extends almost radially from the cell body (Chen & Wolpaw 1994). Selecting cell bodies deep in the slice would keep more of the dendritic tree intact. Impaired visibility of the cell body, however, made such an approach impractical. Table 3.3 summarises the morphological characteristics of the 12 cells analysed. Because all the dendrites had a smooth surface without spines or swellings, the surface area of the neurons could be estimated accurately, although the measured diameter values of the distal dendrites were affected with considerable uncertainty due to the limited resolution of the reconstruction system.

The average ratio of dendritic surface area to somatic surface area ( $A_D/A_S$ ) was  $4.25 \pm 2.01$  (SD, range 2.1-8.4), indicating that the somatic surface area contributed significantly to the total membrane surface area of the cell. In cells with no truncated dendrites, this ratio might be higher by a factor of up to two times. The small ratio of  $A_D/A_S$  and the absence of spines make these cells well suited for modelling and cable parameter identification.

Table 3.3: Morphological data

Cell	Type	Fit	A <sub>S</sub>	A <sub>D</sub>	n-stem	d-stem	n-end	mbo	d <sup>3/2</sup>	l-tot	maj-ax	min-ax	A <sub>D</sub> /A <sub>S</sub>
C3-1111	MN	yes	1287	3052	8	3.1	10	3	0.86	856	38.14	13	2.4
C2-1211	MN	yes	788	6597	3	5	14	7	1.1	2270	22	13	8.4
C1-1311	MN	yes	1128	6887	7	3.3	16	5	0.84	3056	23	17	6.1
C3-1311	MN	yes	1936	5597	7	3.4	11	3	0.68	2449	33	21	2.9
C1-1411	IN	yes	2230	10431	6	4.2	38	6	0.96	5905	38.9	21.1	4.7
C1-2101	MN	yes	2030	10481	6	4.7	21	5	0.96	3265	31.1	22.7	5.2
C2-2101	MN	yes	1824	5825	4	5	16	5	0.81	2760	28	22.2	3.2
C3-2101	IN	yes	1724	11824	3	7.1	24	7	1.19	4545	32.6	19.2	6.9
C2-2201	IN	yes	1113	3595	4	2.3	9	3	0.79	1811	27.5	14.9	3.2
C4-2201	IN	yes	3177	8940	7	3.2	14	3	0.97	3770	36.1	29.7	2.8
C2-1002	IN	yes	2906	9067	5	5.9	9	3	0.89	2809	39.8	26	3.1
C3-1002	MN	yes	3524	7544	6	5	18	5	0.95	2727	45.3	28	2.1
		<b>Mean</b>	<b>1972.25</b>	<b>7486.67</b>	<b>5.50</b>	<b>4.35</b>	<b>16.67</b>	<b>4.58</b>	<b>0.92</b>	<b>3018.58</b>	<b>32.95</b>	<b>20.65</b>	<b>4.25</b>
		SD	863.87	2752.77	1.68	1.36	8.19	1.56	0.14	1296.98	7.06	5.54	2.01

MN, presumed motoneurone; IN, presumed interneurone; Fit, gave satisfactory fit at the 95% confidence level; A<sub>S</sub>, somatic membrane surface area ( $\mu\text{m}^2$ ); A<sub>D</sub>, dendritic membrane surface area ( $\mu\text{m}^2$ ); n-stem, number of stem dendrites; d-stem, mean dendritic stem diameter ( $\mu\text{m}$ ); n-end, number of dendritic terminals; mbo, maximum branch order; d<sup>3/2</sup>, mean Rall's ratio; l-tot, total dendritic path length ( $\mu\text{m}$ ); maj-ax, soma major axis ( $\mu\text{m}$ ); min-ax, soma minor axis ( $\mu\text{m}$ ). Shaded rows indicate the cells which remained in the final analysis.

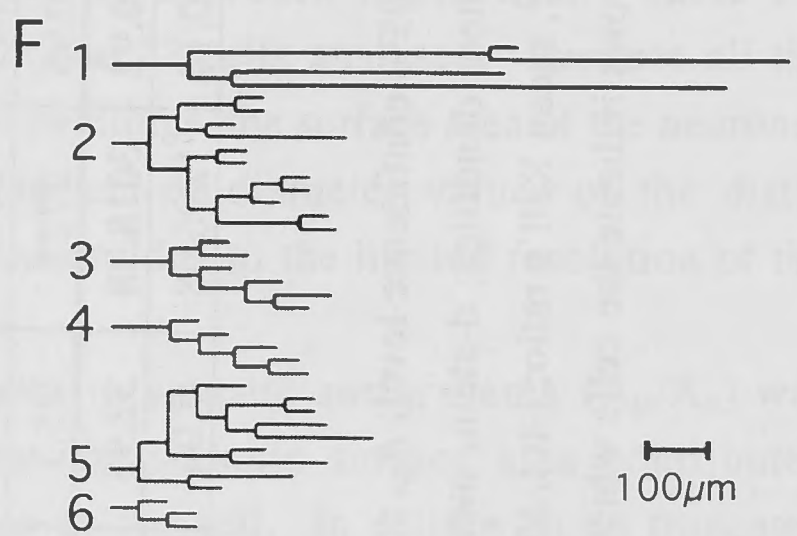
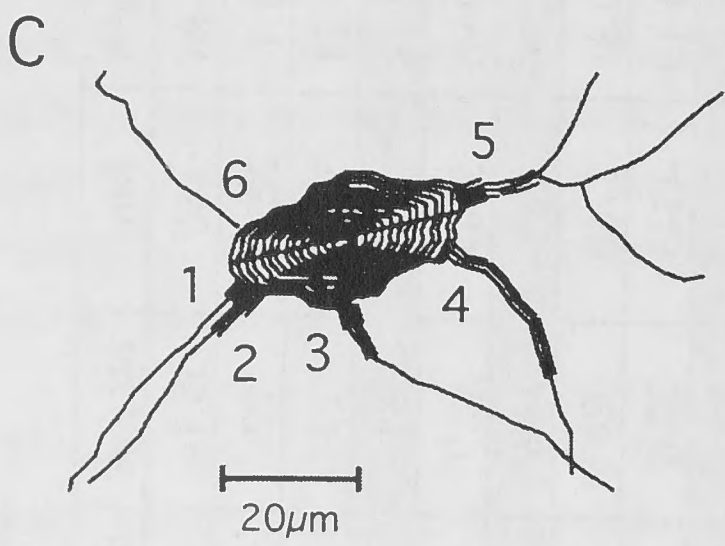
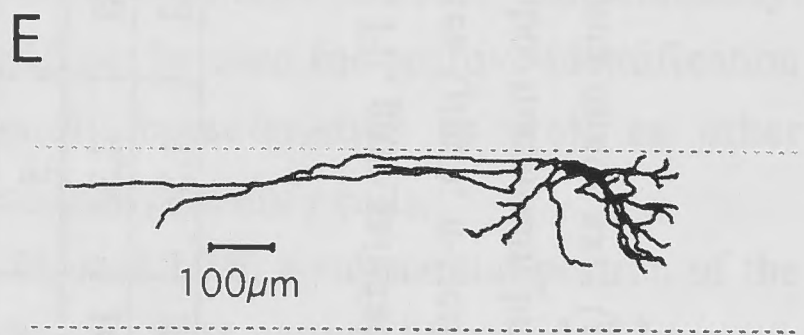
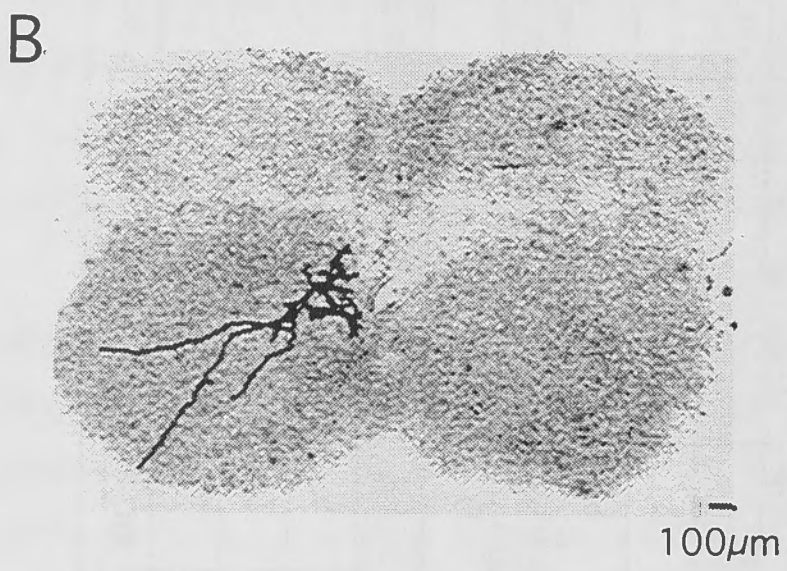
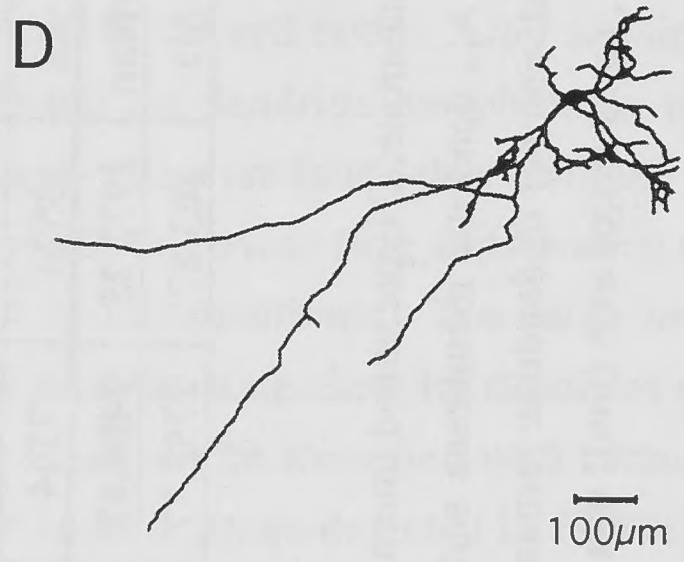
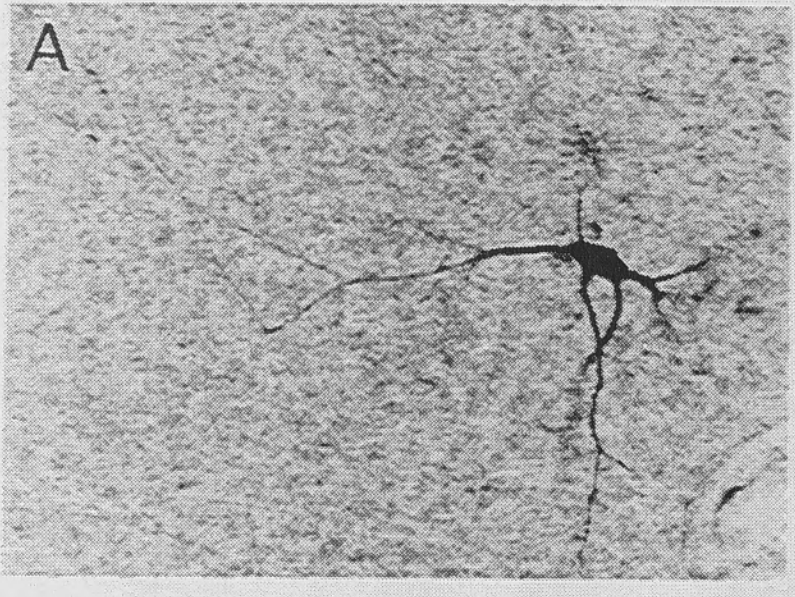


Figure 3.6. Morphology, cell location within spinal cord and reconstruction of *cell C2-1211*, a presumed motoneurone. **A:** Photomicrograph of the cell stained with Biocytin. **B:** location of the stained cell within the spinal cord slice. **C:** Reconstructed cell body and proximal dendrites with the numbering of the proximal dendrites and axon. The axon could not be identified. **D:** Reconstructed cell in the frontal plane. **E:** Reconstructed cell in a sagittal view (stippled lines mark the upper and lower surface of the slice). **F:** Dendrogram of the cell illustrated.





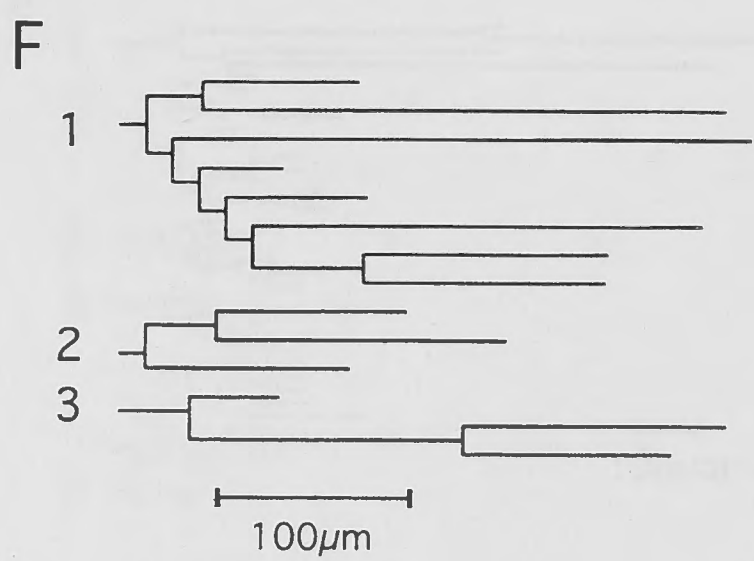
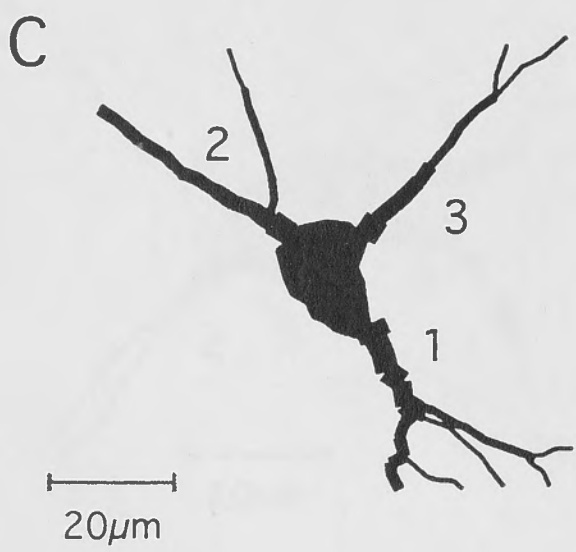
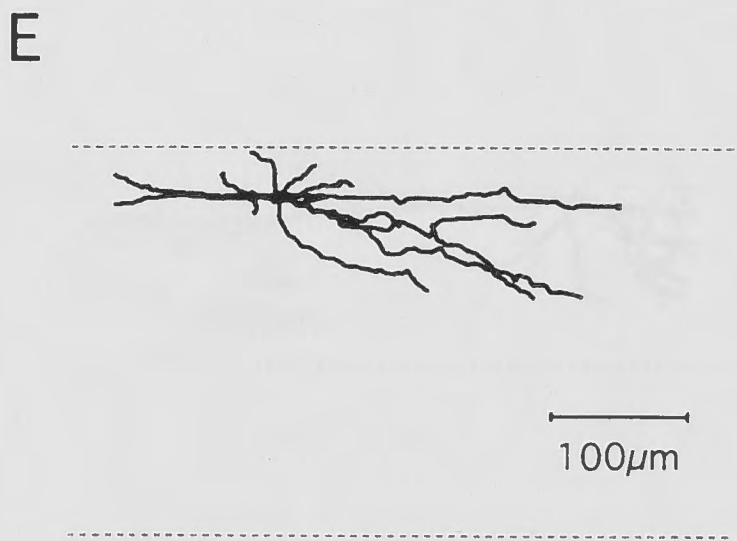
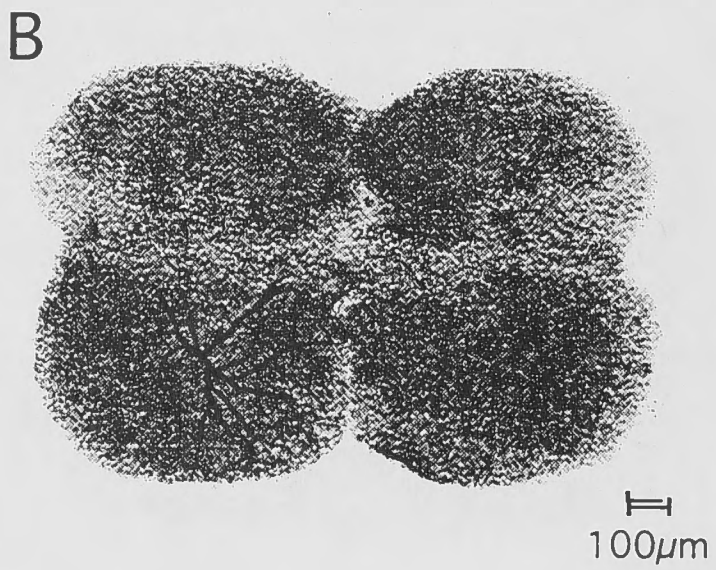
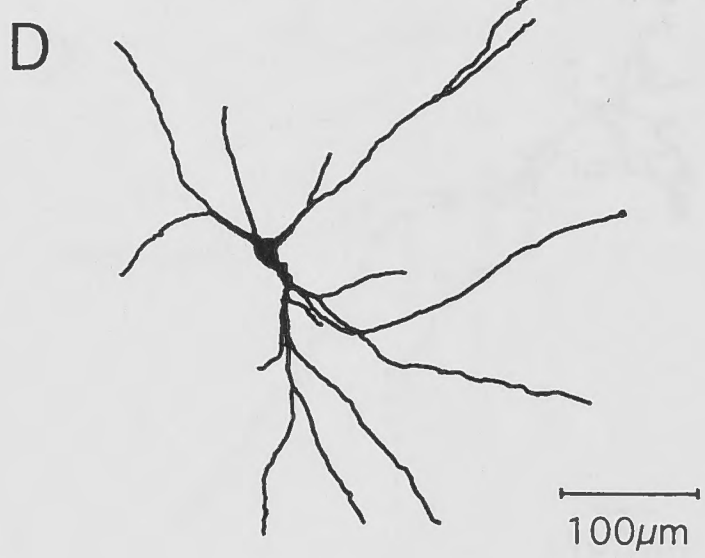
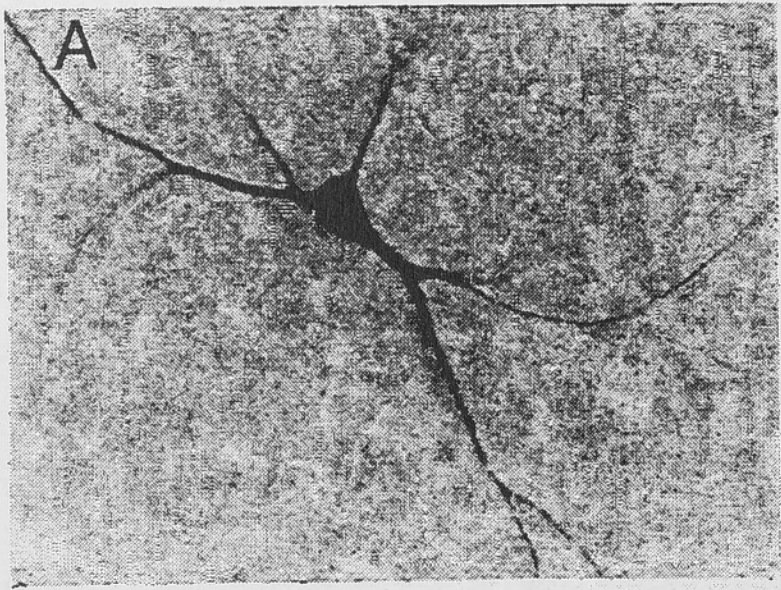


Figure 3.7. Morphology, cell location within spinal cord and reconstruction of *cell C1-1411*, a presumed interneurone. **A:** Photomicrograph of the cell stained with Biocytin. **B:** Location of the stained cell within the spinal cord slice. Note the axon trajectories extending towards the ventral horn of the spinal cord slice. **C:** Reconstructed cell body and proximal dendrites with the numbering of the proximal dendrites and axon. *Neurite no. 1* corresponds to the axon. **D:** Reconstructed cell in the transverse plane. **E:** Reconstructed cell in a frontal view (stippled lines mark the upper and lower surface of the slice). **F:** Dendrogram of cell illustrated.

### *Electrophysiological Measurements*

Electrophysiological data were obtained from 39 cells. The data of the 12 cells for which satisfactory morphological data was available are presented here. Table 3.4 indicates the input resistance and membrane time constant for each of these cells.

All cells could be made to fire repetitively. All of them could sustain high frequencies up to 350Hz. The spike frequency at the beginning of the train increased linearly with increasing current. No secondary range could be observed as has been seen in other preparations. Frequency adaptation over the period of current injection (250ms) ranged from almost no adaptation to almost complete adaptation. Following morphological reconstruction, we were unable to associate putative motoneurons or interneurons with the degree of frequency adaptation; i.e. cell type could not be determined on the basis of frequency adaptation.

### *Compartmental Models*

Compartmental modelling was used to estimate values of  $R_m$ ,  $R_i$  and  $C_m$  by directly fitting the model's voltage response to the experimentally obtained target response. This exercise depends on several assumptions. Stationarity, linear scaling, and the absence of sag in the experimental voltage response to a brief current pulse at the soma could all be tested for adequately. However, the additional assumption of homogeneous membrane properties could not be tested experimentally. Therefore, the possibility remains that the wrong models were fitted to the experiments with severe consequences on the validity of the estimated parameters. In an attempt to evaluate model adequacy, an analysis was made of the residuals between the optimal fit and the experimental target responses and these were compared to the residuals obtained by fitting known, but inadequate models to transients generated by models with homogeneous membrane properties. In a first run, fits were accepted if they did not escape the 95% confidence band (Major *et al.* 1994). Thereafter the shape of the residuals was inspected and the results classified accordingly.

### *Optimal Fits and Parameter Values*

Of the 12 cells analysed, 10 produced acceptable fits as judged by the confidence band test. Table 3.5 summarises the values obtained for  $R_m$ ,  $R_i$ , and  $C_m$ .

The mean optimal  $C_m$  of  $2.28\mu\text{F}/\text{cm}^2$  is about 3 times higher than the value determined in a similar study on hippocampal pyramidal cells (Major *et al.* 1994). Mean  $R_i$  was  $224\Omega.\text{cm}$  and  $R_m$  was  $9.23\text{K}\Omega.\text{cm}^2$ . Of the three values  $C_m$  is probably the most reliable, because it is the most robust parameter in the fitting procedure.  $R_i$  is the least reliable parameter when using a single electrode, because it is mostly determined by the

**Table 3.4:** Passive electrical parameters.

Cell	Type	$R_N$ (M $\Omega$ )	$\tau_m$ (ms)
C3-1111	MN	162	18.1
C2-1211	MN	384*	29.4
C1-1311	MN	85	14.0
C3-1311	MN	64	11.7
C1-1411	IN	117*	25.9
C1-2101	MN	93	9.7
C2-2101	MN	n.a.	13.8
C3-2101	IN	64	7.0
C2-2201	IN	127	11.9
C4-2201	IN	67	15.9
C2-1002	IN	29	4.5
C3-1002	MN	104	21.5
	<b>Mean</b>	<b>88.33</b>	<b>15.28</b>
	SD	39.31	7.41

$R_N$ , input resistance calculated from long hyperpolarising current pulses, \* slope resistance estimated from IV curves.;  $\tau_m$ , membrane time constant equated to system time constant ( $\tau_0$ ).

**Table 3.5:** Summary of the electrical parameters obtained from direct optimal fits between model and experimental responses. Fits accepted by the ~95% confidence band test.

Cell	Type	#-El.	$R_m$ (K $\Omega$ .cm <sup>2</sup> )	$R_i$ ( $\Omega$ .cm)	$C_m$ ( $\mu$ F/cm <sup>2</sup> )	Fit interval
C3-1111	MN	1	8.79	152	2.11	2.5/35
C2-1211	MN	1	26.54	482	1.3	2.5/60
C1-1311	MN	1	6.28	338	2.3	2.5/30
C3-1311	MN	2	4.24	119	2.7	2.5/25
C1-1411	IN	1	10.88	167	3.1	2.5/46
C1-2101	MN	2	5.96	78	1.7	2.5/18
C2-2101	MN	2	8.68	217	2.0	2.5/28
C2-2201	IN	2	4.95	77	2.3	2.5/25
C4-2201	IN	2	6.20	72	2.7	2.5/30
C3-1002	MN	2	9.77	541	2.6	2.5/40
		<b>Mean</b>	<b>9.23</b>	<b>224.30</b>	<b>2.28</b>	
		SD	6.45	171.78	0.54	

#-El. One or two electrode experiments;  $R_m$ , membrane resistivity;  $R_i$ , cytosolic resistivity;  $C_m$ , membrane capacitance; Fit interval: first number; onset of fit interval after beginning of current pulse (ms), second number; duration of fit interval (ms). The four cells highlighted passed the final test for model adequacy.

initial part of the transient, the part that is also affected the most by electrode artifacts. Depending on the onset time of the fit interval, some of the artifact might have been included (if the interval started too early), or alternatively, valuable information was lost if the fit interval started too late. As long as no somatic shunts are allowed in the model,  $R_m$  is robust and not affected by electrode artifacts.

Other possible sources of errors will be explored later in the discussion section of this chapter.

The results summarised in table 3.5 could be divided into two groups as judged by the distribution of the residuals between the target response and the optimal fit. Three examples of optimal fits with evenly distributed residuals are shown in figure 3.8. The left column in figure 3.8 (A1, B1 and C1) illustrate that the experimentally obtained target response (fine line) and the model response (thick line) superimpose perfectly. The corresponding residuals between target response and model response are shown in the right column of figure 3.8 (A2, B2 and C2) together with the 95% confidence band. In four of the ten cells the residuals were equally distributed around the model response as shown for the three cells in figure 3.8. This even distribution of the residuals suggests that the three parameter, homogeneous model was a very good description of the real cells.

In 6 out of 10 cells the residuals, albeit within the 95% confidence band, showed a characteristic time-course. As an example, two of these cells are illustrated in figure 3.9. Since it has already been shown that the experimental voltage transient is stationary, superimposes linearly, and is devoid of sag, thus avoiding spurious curvature in the average target response, the characteristic shape of the residuals suggests that the model used in the fitting procedure was not adequate. Non-homogeneous membrane properties are a likely cause of these residuals.

An obvious and most likely candidate for membrane inhomogeneity is a less than perfect seal at the electrode tip or a genuine low membrane resistivity of the soma. The use of two electrodes is more likely to introduce a somatic leak conductance than when one is used. Unfortunately, when a fourth parameter ( $g_{shunt}$  representing a somatic leak conductance) is introduced into the model as a free parameter, non-uniqueness in the solution becomes a very serious problem, as others have already noted (Major *et al.* 1994). We have performed an extensive analysis of the four-parameter model with artificial target responses from models with known parameters. Since variations in  $g_{shunt}$  and  $R_m$  lead to changes in the shape of the model voltage response that are virtually indistinguishable (see Fig. 3.3) almost any reciprocal pair of parameter values for  $R_m$  and  $g_{shunt}$  will result in acceptable fits. In principal,  $g_{shunt}$  can vary from zero up to the cell's total input

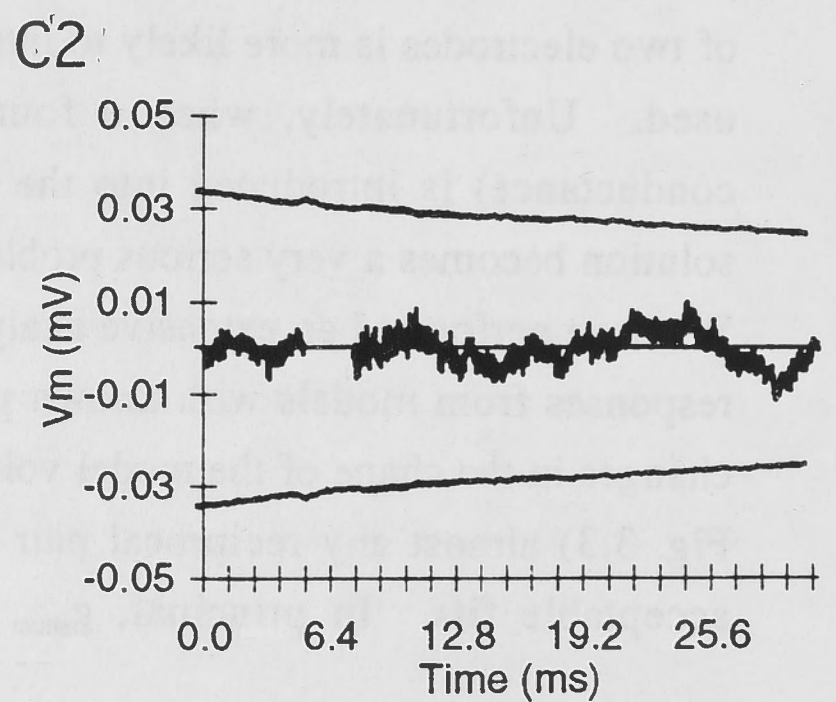
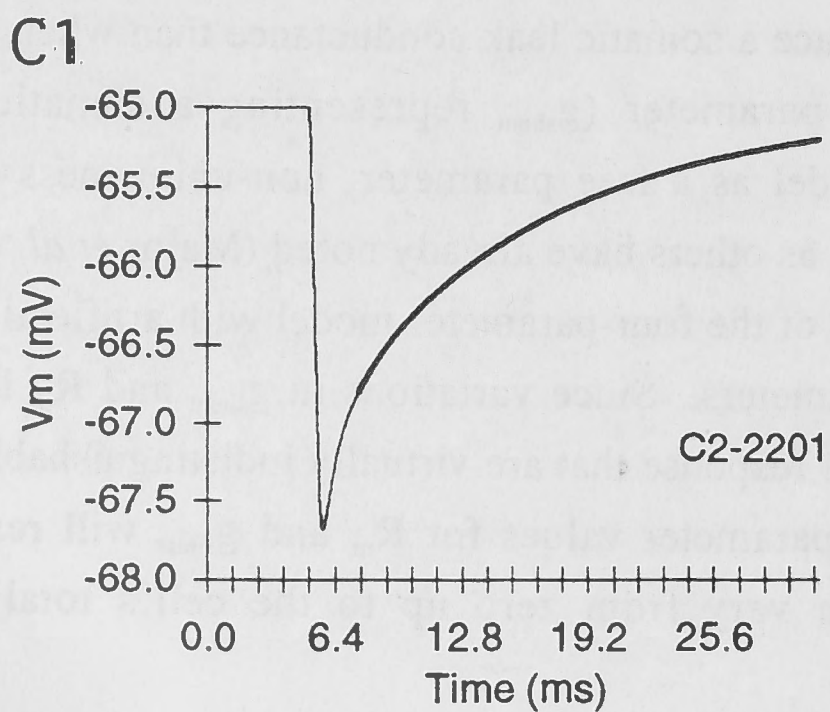
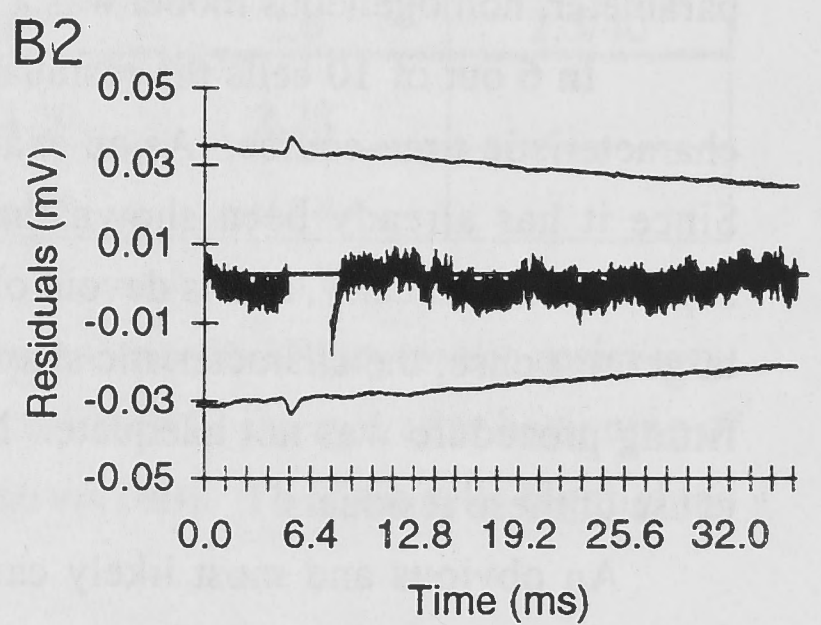
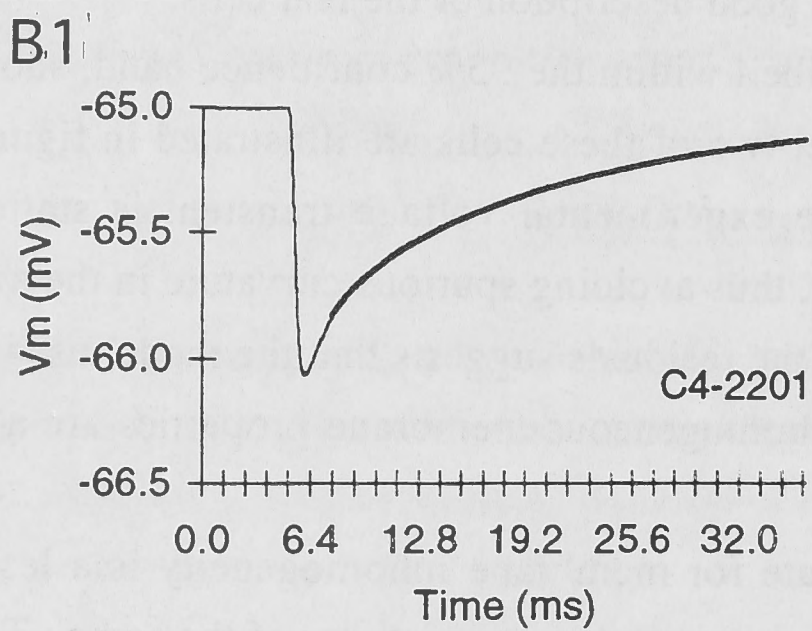
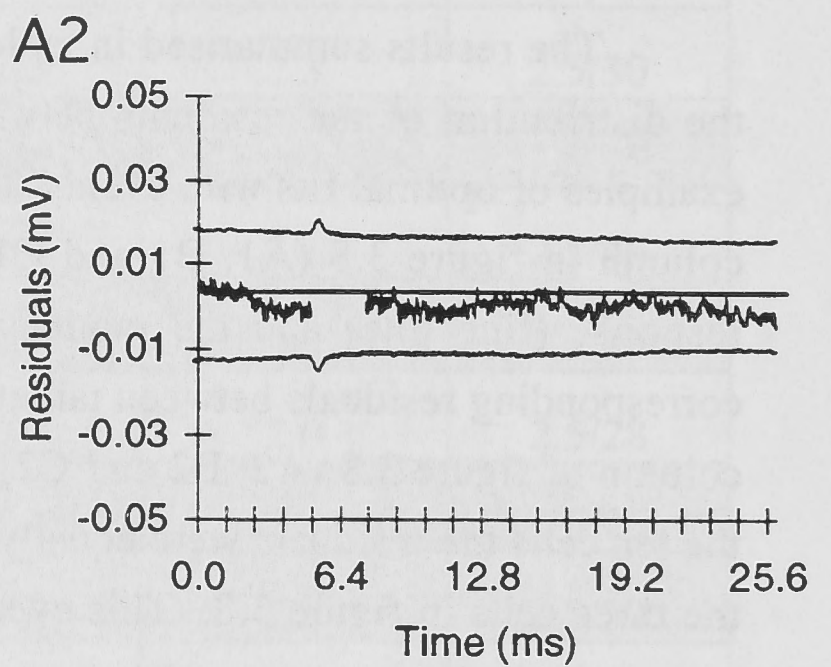
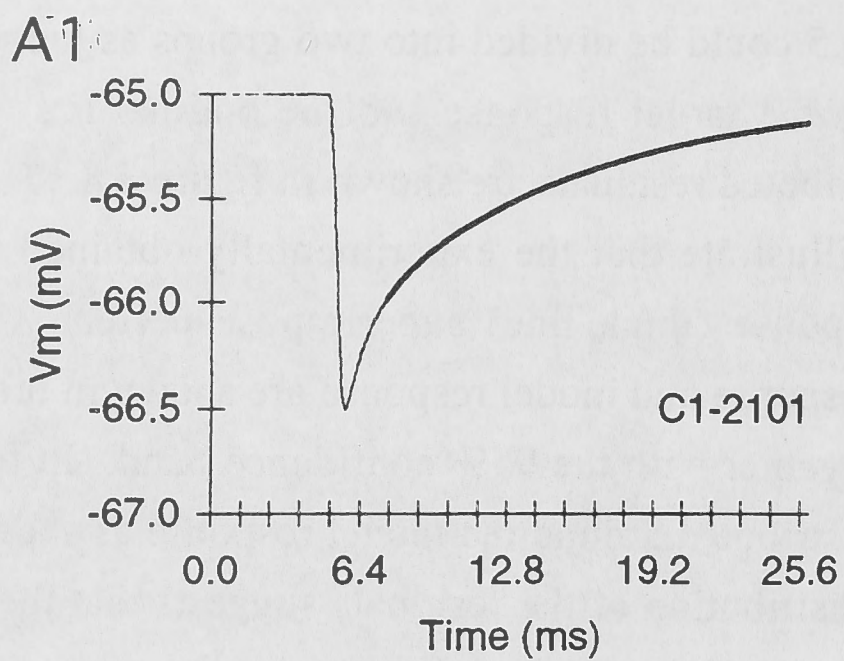


Figure 3.8. Optimal fits of three cells leaving a flat distribution of the residuals. The cell's average target responses to brief current pulses ( $-0.5\text{nA}$ ,  $480\mu\text{s}$ ) are shown as fine solid lines, whereas the optimal model responses to the same current are shown as thick solid lines. **A1**: Cell C1-2101, a presumed motoneurone. **B1**: Cell C4-2201, a presumed interneurone. **C1**: Cell C2-2201, a presumed interneurone. A2, B2 and C2 show the corresponding residuals together with the 95% confidence band. The residuals are blanked from the onset of the current pulse to the onset of the fit interval.





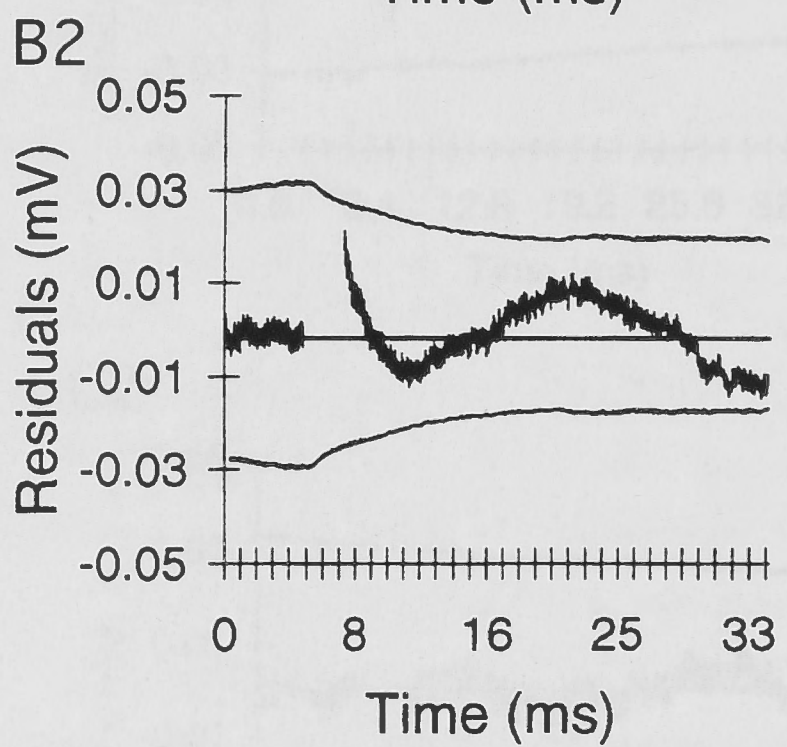
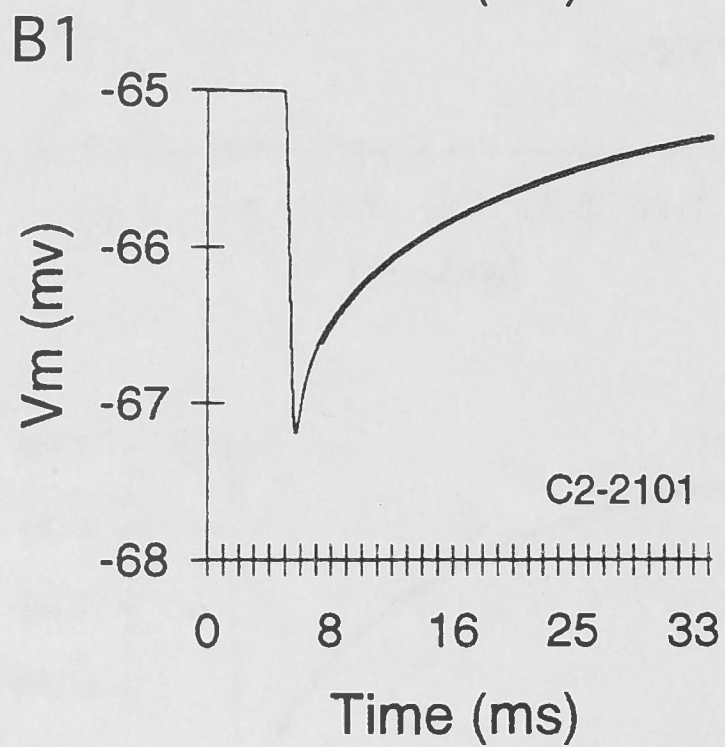
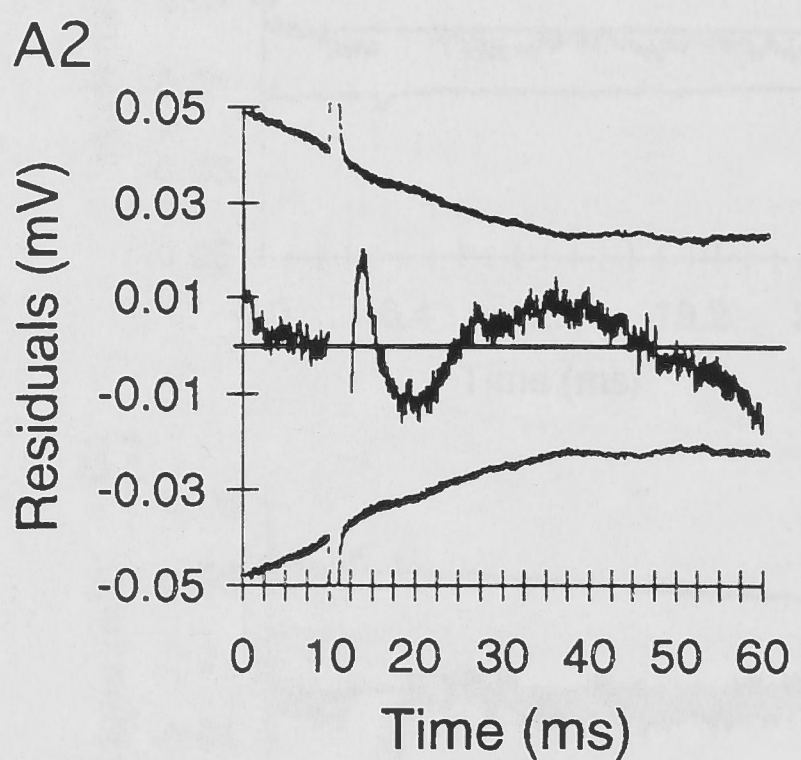
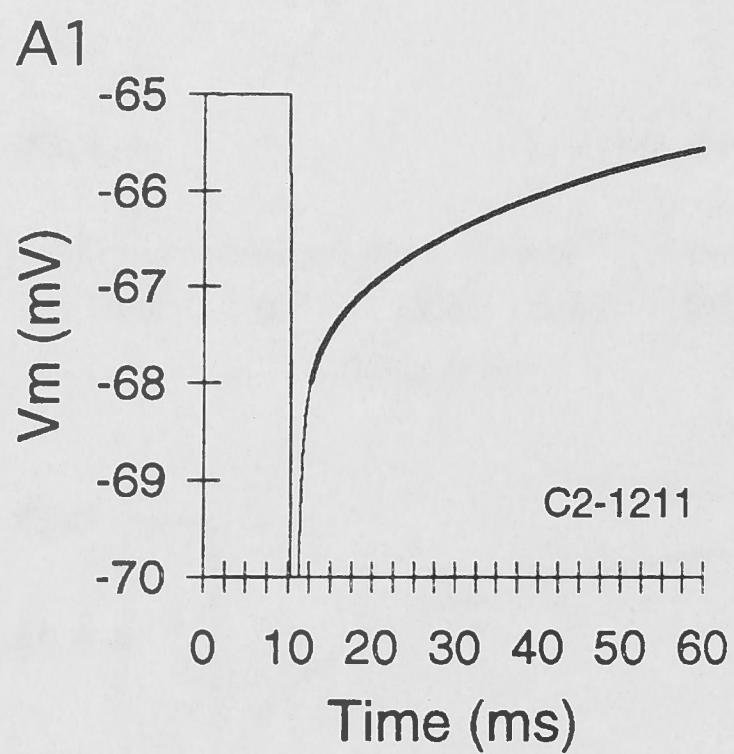


Figure 3.9. Optimal fits of two cells with a distinct time-course of the residuals. **A1:** Cell C2-1211, a presumed motoneurone. **B1:** Cell C2-2101, a presumed motoneurone. **A2 and B2:** Corresponding residuals and 95% confidence band. The residuals are blanked between the onset of the current pulse and the onset of the fit interval. The residuals stay within the confidence band but display a characteristic time-course.

conductance and still yield acceptable fits. As  $g_{\text{shunt}}$  increases,  $R_m$  increases up to extreme, implausible values.

In the six cells, where the residuals were not evenly distributed, we allowed  $g_{\text{shunt}}$  to drift away from zero. A range of values for  $g_{\text{shunt}}$  between 0.1 and 6.3nS was found. In all six cases, the mean squared error of the fit decreased as expected, but the time-course of the residuals did not even out as in figure 3.8. We must conclude, that we have no reliable way to prove whether a significant somatic shunt is present or not. Although the introduction of  $g_{\text{shunt}}$  leads to a major uncertainty in the estimation of  $R_m$ , the uncertainty in the estimated values for  $C_m$  and  $R_i$  is not large. Because of these difficulties and the uncertainties introduced by a fourth parameter we abstained from further exploration of the contribution of a somatic shunt on the parameter values, and we present the results as obtained from the three parameter, homogeneous model. We must keep in mind, however, that if a somatic shunt were present in the six cells with a characteristic time-course in the unevenly distributed residuals,  $C_m$  and  $R_i$  would have been overestimated slightly.

The introduction of any other additional parameters for taking into account membrane inhomogeneities would probably lead to similar non-uniqueness difficulties. With respect to these difficulties, a search for models that would have eliminated the characteristic time-course in the residuals would probably have been a wasted effort. However, we have attempted to identify the most likely model that, if used to fit the target transient, could explain the specific time-course of the residuals.

Taking the morphology of *cell C1-2101*, artificial, noise-free transients were generated for known parameter values of  $R_m$ ,  $R_i$  and  $C_m$  and their inhomogeneous distribution. The following inhomogeneities were considered:  $R_m$ -soma lower or higher than  $R_m$ -dendrite,  $C_m$ -soma lower or higher than in the dendrites,  $R_i$  in the soma and proximal dendrites lower or higher than in the distal dendrites. The six transients from these four-parameter models were then used to fit the voltage response of a three-parameter, homogeneous model. In all six cases, the fits were virtually indistinguishable from the target responses (within 95% confidence limits) but with characteristic distributions in the residuals (Fig. 3.10). The corresponding estimated values for  $R_m$ ,  $R_i$ , and  $C_m$  are listed in table 3.6

Unfortunately, the time-course of the residuals resulting from fitting the 'wrong' models to the target responses do not contain a unique signature that would allow unequivocal identification of the 'wrong' model. Comparing the shape of the time-courses of the residuals in figure 3.9 with the residuals in figure 3.10 however suggests that the model with a higher somatic membrane resistivity (Fig. 3.10A2) leads to a distribution of the residuals compatible with the results illustrated in figure 3.9. Although this exercise

**Table 3.6:** Estimated parameters obtained from deliberately fitting a wrong, homogeneous, 3-parameter model to target transients obtained from an inhomogeneous, 4-parameter model.

Parameter	"true" values homogeneous model	Inhomogeneous Model						Mean	SD
		$R_m$ soma ( $K\Omega.cm^2$ )	$R_m$ soma ( $K\Omega.cm^2$ )	$C_m$ soma ( $\mu F/cm^2$ )	$C_m$ soma ( $\mu F/cm^2$ )	$R_i$ proximal dendrite and soma ( $\Omega.cm$ )	$R_i$ proximal dendrite and soma ( $\Omega.cm$ )		
		20	5	1.0	2.0	100	300		
$R_m$ ( $K\Omega.cm^2$ )	10	7.83	11.24	8.76	10.24	10.11	9.97	9.56	1.21
$R_i$ ( $\Omega.cm$ )	200	302	169	565	131	112	229	251	169
$C_m$ ( $\mu F/cm^2$ )	1.5	1.68	1.43	1.76	1.48	1.41	1.48	1.54	0.15

The target transient was generated from a model with inhomogeneous membrane properties (4-parameter model). The parameter values deviated from the homogeneous model by the properties listed in the six columns (inhomogeneous model). The parameters  $R_m$ ,  $R_i$  and  $C_m$  were estimated by deliberately assuming a homogeneous, 3-parameter model.

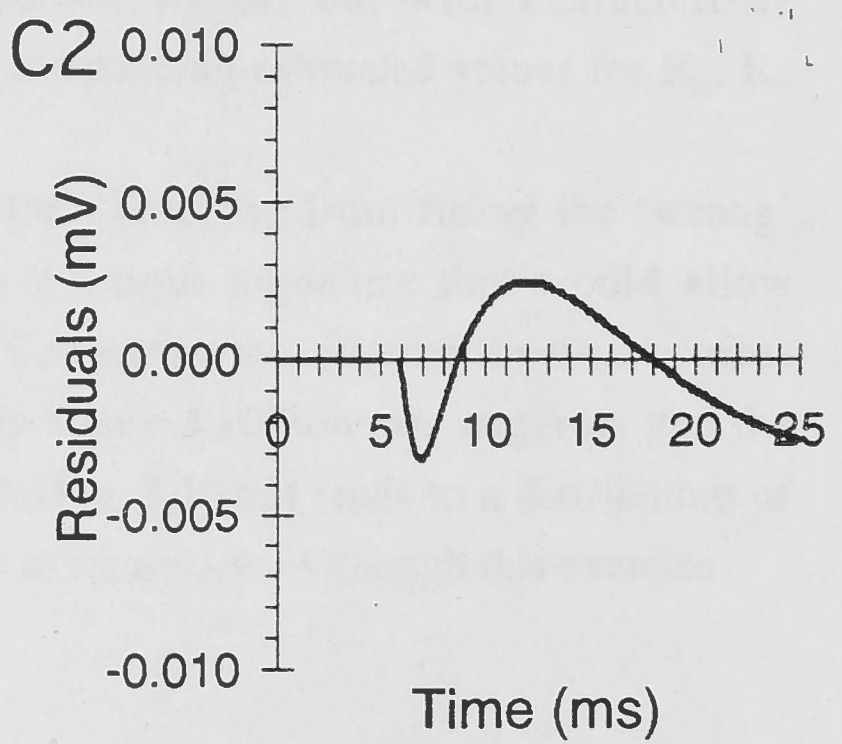
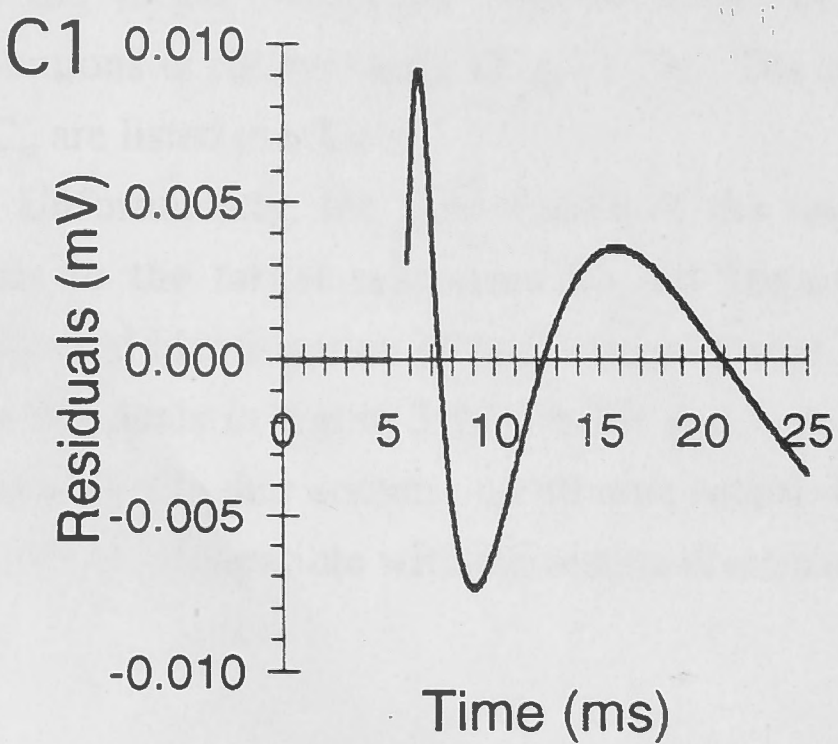
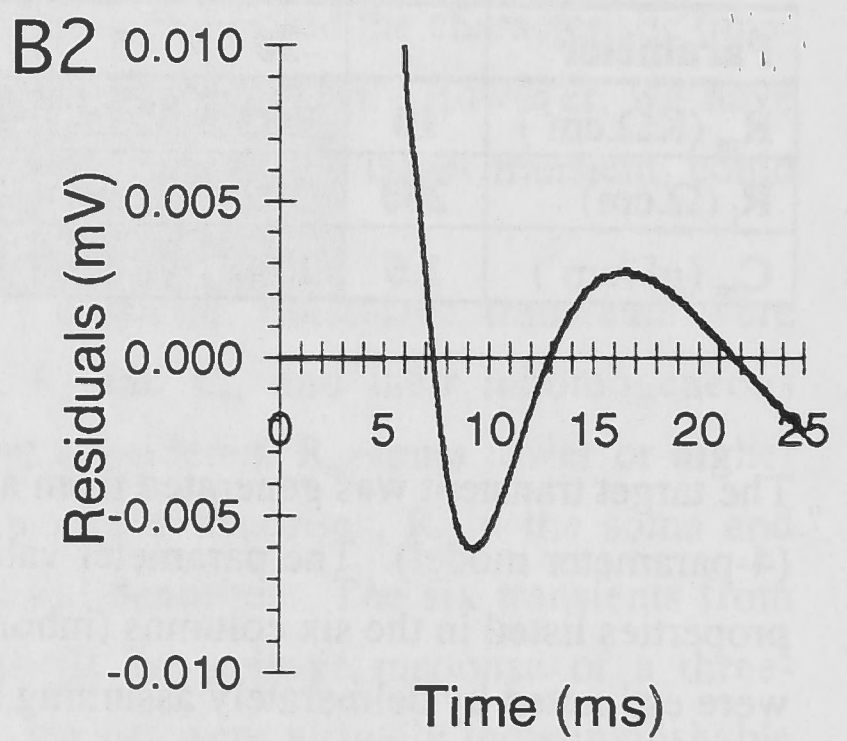
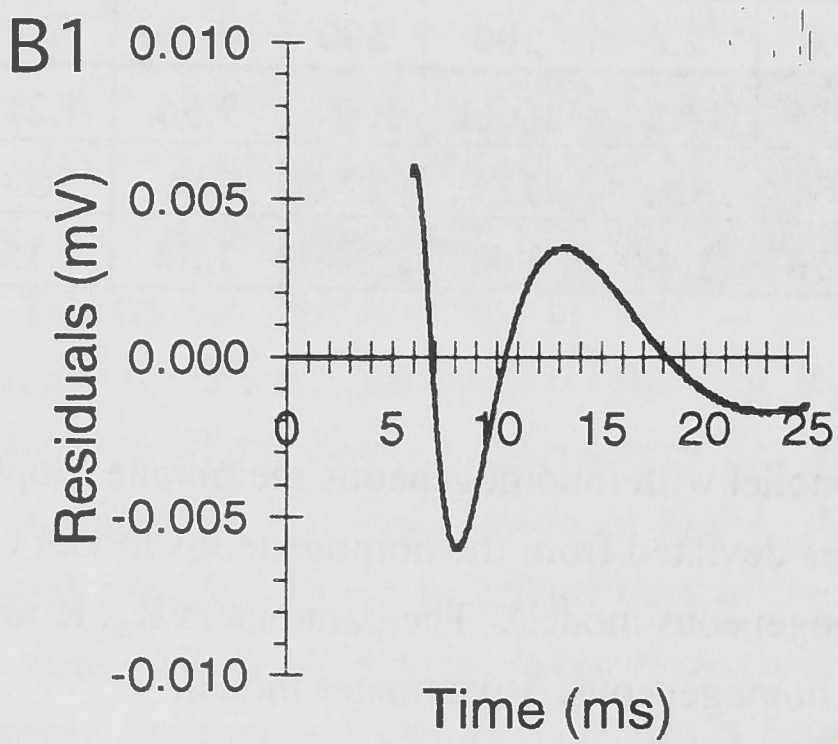
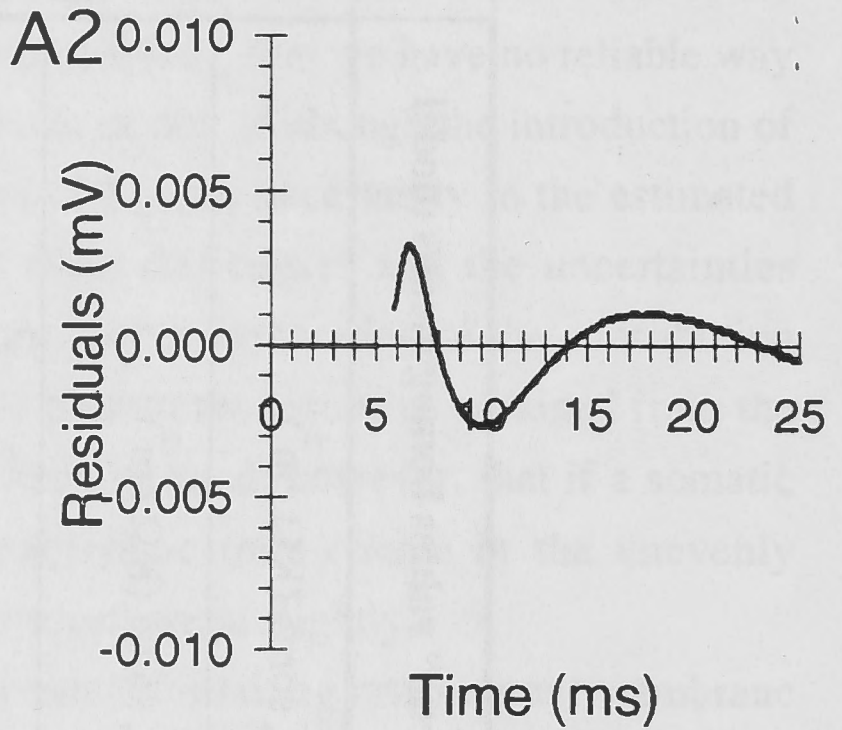
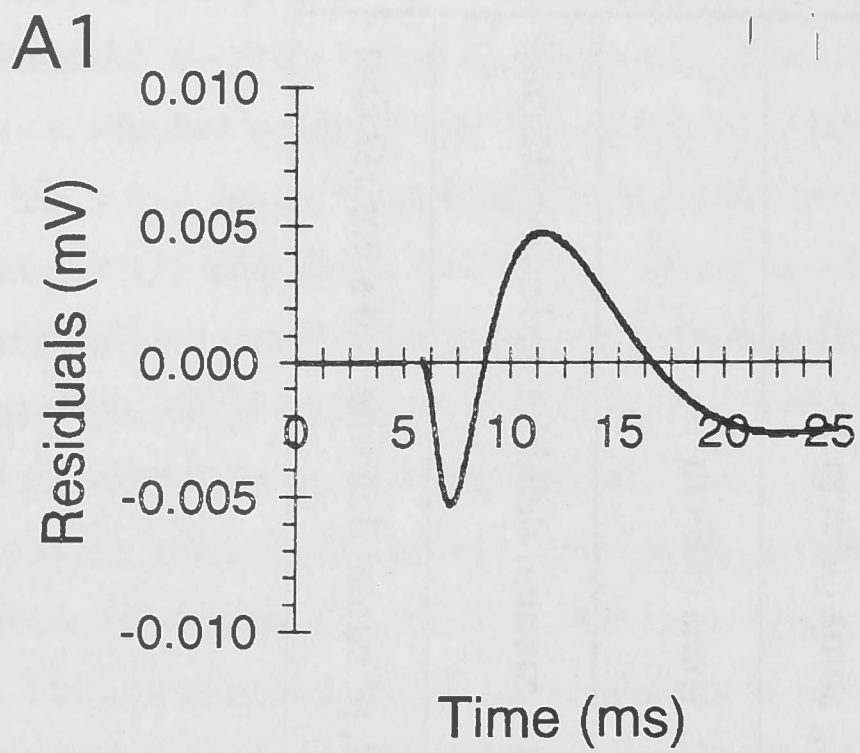


Figure 3.10. Residuals resulting from fitting a model with homogeneous cable parameters (3-parameter model) to a noise-less target response generated by a known model with non-homogeneous cable properties (4-parameter model). *Cell C1-2101* was used for the model. The following basic parameters were incorporated:  $R_m=10\text{K}\Omega\cdot\text{cm}^2$ ,  $R_i=200\Omega\cdot\text{cm}$ ,  $C_m=1.5\mu\text{F}/\text{cm}^2$ . **A:** Fit residuals from fitting a 3-parameter model to a target response produced by a model with non-homogeneous membrane resistivity. **A1:** Soma membrane resistivity lowered to  $5\text{K}\Omega\cdot\text{cm}^2$ . **A2:** Soma membrane resistivity increased to  $20\text{K}\Omega\cdot\text{cm}^2$ . **B:** Fit residuals from fitting a 3-parameter model to a target response produced by a model with non-homogeneous membrane capacitance. **B1:** Soma capacitance lowered to  $1.0\mu\text{F}/\text{cm}^2$ . **B2:** Soma capacitance increased to  $2.0\mu\text{F}/\text{cm}^2$ . **C:** Fit residuals from fitting a 3-parameter model to a target response produced by a model with non-homogeneous cytoplasmic resistivity. **C1:** Cytoplasmic resistivity of soma and proximal dendrites decreased to  $100\Omega\cdot\text{cm}$ . **C2:** Cytoplasmic resistivity of soma and proximal dendrites increased to  $300\Omega\cdot\text{cm}$ .

might push the analysis too far, inspection of the estimated parameter values in table 3.6 clearly reveals that, even in the case of an inadequate model, the retrieved parameter values are close to the values of the underlying homogeneous model. In addition, the values listed in table 3.6 illustrate whether a particular parameter value has been over- or underestimated with regard to a particular inhomogeneous model.

The analysis presented above illustrates that  $R_i$  is the most sensitive parameter to very large errors if one tries to fit the wrong model to the target response. In contrast, the estimated value of  $C_m$  turned out to be the most robust and most reliable. This has an intuitive explanation in the fact that the shape of the voltage transient is influenced over the entire time-course by  $C_m$ , unlike for  $R_m$  (late part only) or  $R_i$  (early part only) (see Fig. 3.3). Previously, a  $C_m$  value of  $4\mu\text{F}/\text{cm}^2$  was reported by Barrett and Crill (1974). More recent investigations (Clements & Redman 1989, Burke *et al.* 1994) have pointed out that these high values of  $C_m$  were the result of neglecting a somatic shunt conductance. The introduction of a somatic shunt lowered  $C_m$  close to the generally accepted value of  $1.0\mu\text{F}/\text{cm}^2$ . In order to evaluate this possibility,  $C_m$  was fixed to  $1.0\mu\text{F}/\text{cm}^2$  and  $R_m$ ,  $R_i$  and  $g_{\text{shunt}}$  (soma) became free parameters in the model. In all cases ( $n=4$ ) no acceptable fits could be obtained as evaluated by the 95% confidence test. In addition,  $g_{\text{shunt}}$  always converged exactly to the value of the cell's input conductance with a concomitant exorbitantly high value of  $R_m$  ( $> 1\text{G}\Omega.\text{cm}^2$ ).  $R_i$  settled at impossible values of  $5\Omega.\text{cm}$ . We must conclude, that omitting a somatic shunt conductance does not explain the high value of  $C_m$  found in our study.

It is possible that we have missed the most distal dendrites in the reconstruction. In order to evaluate the contribution of possibly missed distal dendrites to the estimated parameter values, we attached to all existing dendrites of a reconstructed cell  $100\mu\text{m}$  long terminal sections, with a diameter tapering from  $0.5$  to  $0.1\mu\text{m}$ . This increased the total dendritic path length by 17% and the total surface area by 5.3%. This substantial elongation of the distal dendrites changed the retrieved parameters only slightly.  $C_m$  was lowered by less than 7%. Since we have no reason to suspect that we have missed such a large part of the dendritic tree in the reconstruction process, we conclude that an incomplete reconstruction would cause insignificant overestimation of  $C_m$ .

As a result of the extensive evaluation of the fitting procedure presented above, we conclude that the parameter values of the optimal fits obtained from the four cells in which the residuals were evenly distributed around the target transient (highlighted rows in table 3.5), represent the most likely values for  $R_m$ ,  $R_i$ , and  $C_m$  (summarised in table 3.7).

### *Passive Electrotonic Structure*

The mean electrotonic path length ( $L_{avg}$ ) for the four cells remaining after the analysis detailed above was  $0.69 \pm 0.10\lambda$  (range 0.84-0.63). Due to the slicing, many dendrites were cut a short distance from the soma. The electrotonic path length of individual dendrites was therefore very different, e.g. ranging from 0.016 to  $1.25\lambda$ , in *cell C3-1311*. The fact that many dendrites were severed during the slicing process leads to an underestimation of mean  $L_{avg}$  compared to  $L_{avg}$  in the intact spinal cord. If only the uncut dendrites are taken into account, mean  $L_{avg}$  would be  $0.85 \pm 0.14$  (12 dendrites of 4 cells).

The input resistances as measured experimentally are compared to the input resistances of the models and listed in table 3.7. In the same table, the experimentally obtained membrane time constants are compared to the system time constants of the model with the corresponding parameters of  $R_m$ ,  $R_i$  and  $C_m$ . There is a very close correspondence between the experimental and modelling results. This strengthens our conclusion, that the final mean values estimated for the parameters  $R_m = 5.34 \pm 0.91 \text{K}\Omega \cdot \text{cm}^2$  (SD),  $R_i = 86.5 \pm 21.83 \Omega \cdot \text{cm}$ , and  $C_m = 2.35 \pm 0.47 \mu\text{F}/\text{cm}^2$  provide an adequate description of the cable properties of the four cells listed in table 3.7.

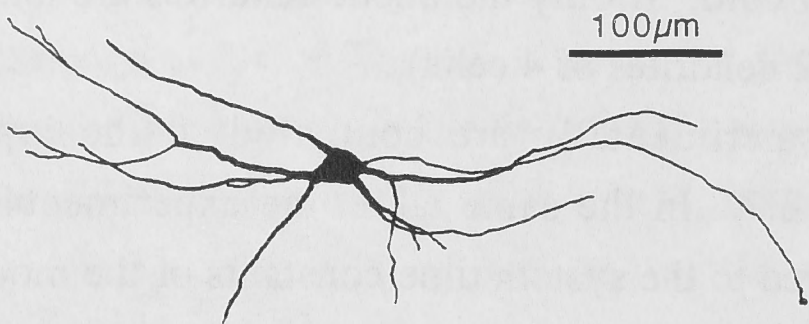
### *Fitting Transients from Two Electrodes*

Two approaches to fitting the recorded transients to the reconstructed morphology were used. In the first, the optimum electrotonic parameters were obtained for the responses generated at the dendritic electrode for the current pulse applied at the soma, and then for the response at the soma due to the dendritic current pulse. Sometimes they differed. The second approach was to obtain optimum fits to both transients simultaneously.

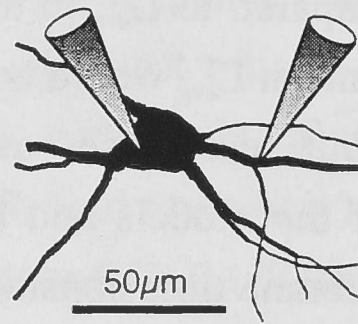
These procedures were carried out only for one single cell, *C1-2708*. The motoneurone morphology illustrated in figure 3.11A, with the electrode positions indicated in figure 3.11B (dendritic electrode approximately  $20\mu\text{m}$  from the soma) was used together with the brief current pulse responses illustrated in figures 3.11C and 3.11D, to calculate the optimum electrotonic parameters. The optimal fit to the voltage response at the dendrite due to current applied to the soma is shown in figure 3.11C and gave optimal electrotonic parameters of  $R_m = 2.8 \text{K}\Omega \cdot \text{cm}^2$ ,  $C_m = 1.4 \mu\text{F}/\text{cm}^2$  and  $R_i = 285 \Omega \cdot \text{cm}$ . When the procedure was reversed and the somatic voltage response to dendritic current injection was used as the target transient, then the optimal electrotonic parameters were  $R_m = 2.2 \text{K}\Omega \cdot \text{cm}^2$ ,  $C_m = 1.7 \mu\text{F}/\text{cm}^2$  and  $R_i = 186 \Omega \cdot \text{cm}$ . These values are close to those obtained for the dendritic transient and this indicates that the membrane properties of the dendrites, at least those  $20\mu\text{m}$  from the soma, are not greatly different from the somatic properties. When both



A

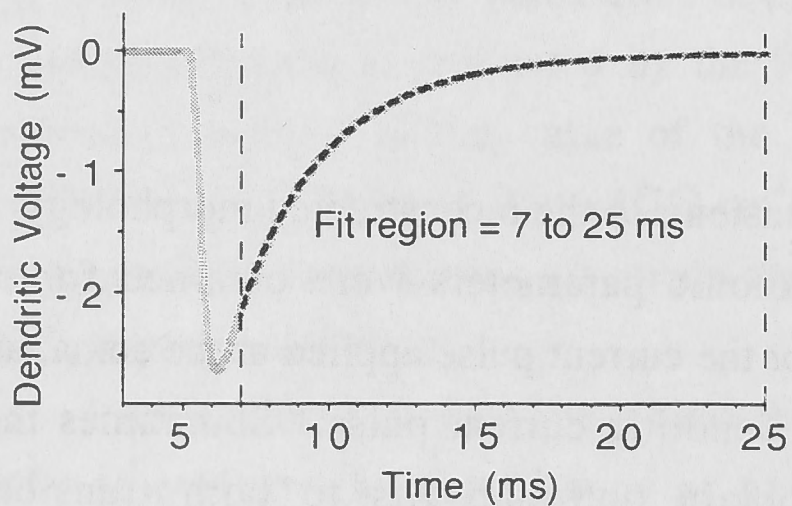


B



C

Current Injected into the Soma,  
Voltage Recorded at the Dendrite.



Fit Parameters:

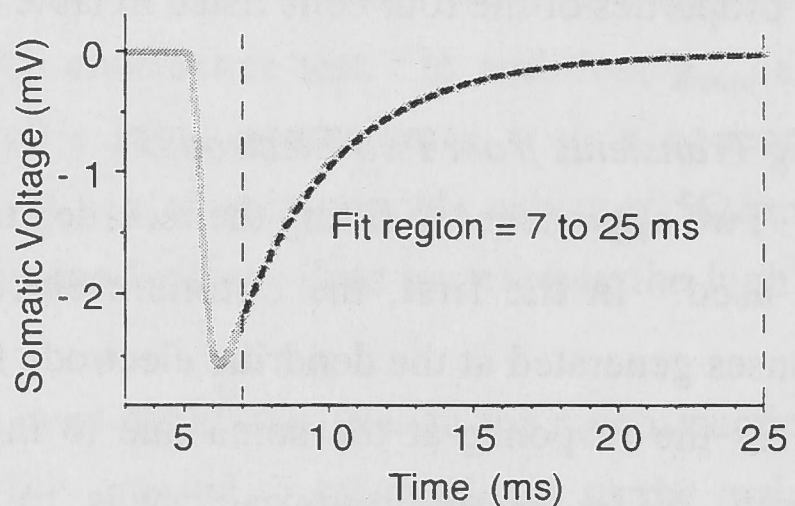
$$R_m = 2.8 \text{ K}\Omega\text{cm}^2$$

$$C_m = 1.4 \text{ }\mu\text{F}/\text{cm}^2$$

$$R_i = 285 \text{ }\Omega\text{cm}$$

D

Current Injected into the Dendrite,  
Voltage Recorded at the Soma.



Fit Parameters:

$$R_m = 2.2 \text{ K}\Omega\text{cm}^2$$

$$C_m = 1.7 \text{ }\mu\text{F}/\text{cm}^2$$

$$R_i = 186 \text{ }\Omega\text{cm}$$

Two Transient Fit Parameters:

$$R_m = 2.4 \text{ K}\Omega\text{cm}^2$$

$$C_m = 1.5 \text{ }\mu\text{F}/\text{cm}^2$$

$$R_i = 205 \text{ }\Omega\text{cm}$$

Figure 3.11. Fitting of transients from somatic and dendritic recordings. **A:** Morphology of cell *C1-2708* from which combined somatic and dendritic recordings were obtained. **B:** Reconstructed cell body and proximal dendrites of *C1-2708* showing the location of the recording electrodes. **C:** Compartmental model fitted transient (dotted line) to the dendritic voltage transient (grey line) produced by application of a current pulse ( $480\mu\text{s}$ ,  $-0.5\text{nA}$ ) to the soma. Vertical dotted lines shows the fit interval. The fit falls within the 95% confidence band (not shown) for the transient and gave  $R_m=2.8\text{K}\Omega\cdot\text{cm}^2$ ,  $C_m=1.4\mu\text{F}/\text{cm}^2$  and  $R_i=285\Omega\cdot\text{cm}$ . **D:** Compartmental model fit (dotted line) of the somatic voltage transient (grey line) produced by application of a current pulse ( $480\mu\text{s}$ ,  $-0.5\text{nA}$ ) to the dendrite. Vertical dotted lines show the fit interval. The fit is within the 95% confidence band (not shown) of the transient and gave  $R_m=2.2\text{K}\Omega\cdot\text{cm}^2$ ,  $C_m=1.7\mu\text{F}/\text{cm}^2$  and  $R_i=186\Omega\cdot\text{cm}$ . Fitting of both transients simultaneously (not shown) produced similarly good fits to the transients and gave parameter values that were midway between those for the individual fits ( $R_m=2.4\text{K}\Omega\cdot\text{cm}^2$ ,  $C_m=1.5\mu\text{F}/\text{cm}^2$  and  $R_i=205\Omega\cdot\text{cm}$ ).

**Table 3.7:** Electrical parameters obtained from compartmental computer modelling and comparison to the experimental results for the four cells finally accepted.

Cell	Type	$R_m$ ( $K\Omega.cm^2$ )	$R_i$ ( $\Omega.cm$ )	$C_m$ ( $\mu F/cm^2$ )	$\tau_m$ (Mod) (ms)	$\tau_m$ (Exp) (ms)	$R_N$ (Mod) (ms)	$R_N$ (Exp) (ms)	$L_{avg}$
C3-1311	MN	4.24	119	2.7	11.7	11.7	70	64	1.18
C1-2101	MN	5.96	78	1.7	10.1	9.7	92	93	0.61
C2-2201	IN	4.95	77	2.3	11.4	11.9	107	127	0.68
C4-2201	IN	6.20	72	2.7	16.7	15.9	67	67	0.63
	<b>Mean</b>	<b>5.34</b>	<b>86.50</b>	<b>2.35</b>	<b>12.48</b>	<b>12.30</b>	<b>84.00</b>	<b>87.75</b>	<b>0.78</b>
	<b>SD</b>	<b>0.91</b>	<b>21.83</b>	<b>0.47</b>	<b>2.90</b>	<b>2.60</b>	<b>18.96</b>	<b>29.23</b>	<b>0.27</b>

$R_m$ , membrane resistivity;  $R_i$ , cytosolic resistivity;  $C_m$ , membrane capacitance;  $\tau_m$  (Mod), membrane time constant obtained from the model;  $\tau_m$  (Exp), membrane time constant obtained from the experiment;  $R_N$  (Mod), steady-state input resistance of the model cell;  $R_N$  (Exp), steady-state input resistance of the real cell;  $L_{avg}$ , mean electrotonic dendritic path length.

responses were used as target transients for the fit procedure the electrotonic parameter values converged to values which were midway between those obtained for each of the single transients and gave parameter values of  $R_m=2.4\text{K}\Omega.\text{cm}^2$ ,  $C_m=1.5\mu\text{F}/\text{cm}^2$  and  $R_i=205\Omega.\text{cm}$ . The optimal fit to both the transients was within the 95% confidence limit of both of the transients and this indicates that there is no significant difference between the dendritic and somatic membrane properties. The fact that the two transients, when fitted individually, gave different results may be indicative of inhomogeneous passive membrane properties. However, the small separation of the electrodes in this experiment ( $\sim 20\mu\text{m}$ ) and the fact that fitting both transients simultaneously produced modelled responses that fell within the 95% confidence limits of the experimental transients, makes any attempt to reconcile any differences in membrane properties impossible.

### *Test for Reciprocity*

Reciprocity between the somatic response to dendritic current injection and the dendritic response to somatic current injection is a test for linearity of the transfer impedance between the two recording sites. To test if signal transfer between the dendrites and soma was reciprocal, current pulses of  $480\mu\text{s}$  duration were applied to the soma and dendrite of a ventral spinal neurone and the responses recorded at the other site. In figure 3.12, the voltage response at the soma to a dendritic current pulse (Fig. 3.12C) and the voltage response at the dendritic electrode to an identical somatic current pulse (Fig. 3.12B) are shown. The locations of the two electrodes on the reconstructed cell are shown in figure 3.12A and the separation of the electrodes is  $20\mu\text{m}$ . The two responses are superimposed in figure 3.12D, and they each lie within the 95% confidence limits of the other voltage transient, indicating that there is no significant difference between the two responses. This suggests that the transmission properties of the dendrite between the soma and the dendritic recording electrode are reciprocal and that the membrane resistivity is passive for small, rapid hyperpolarising excursions from  $-70\text{mV}$ . It was impossible in this experiment to use a current pulse that produced identical voltage responses in both soma and dendrite. As can be seen in figure 3.12C, the somatic voltage response is approximately  $7\text{mV}$  while the dendritic voltage response to the same current pulse is approximately  $35\text{mV}$ . Obviously, such a large hyperpolarising voltage deviation as this could cause significant activation/deactivation of dendritic voltage-dependent conductances if the kinetics are sufficiently fast. However, using a smaller dendritic current pulse to produce an identical voltage deviation in the dendrite to that in the soma would have resulted in somatic transients that were too small to be recorded reliably.

Regardless of this though, the responses at both sites were still reciprocal and fitted within the 95% confidence limits of each other, indicating that even if

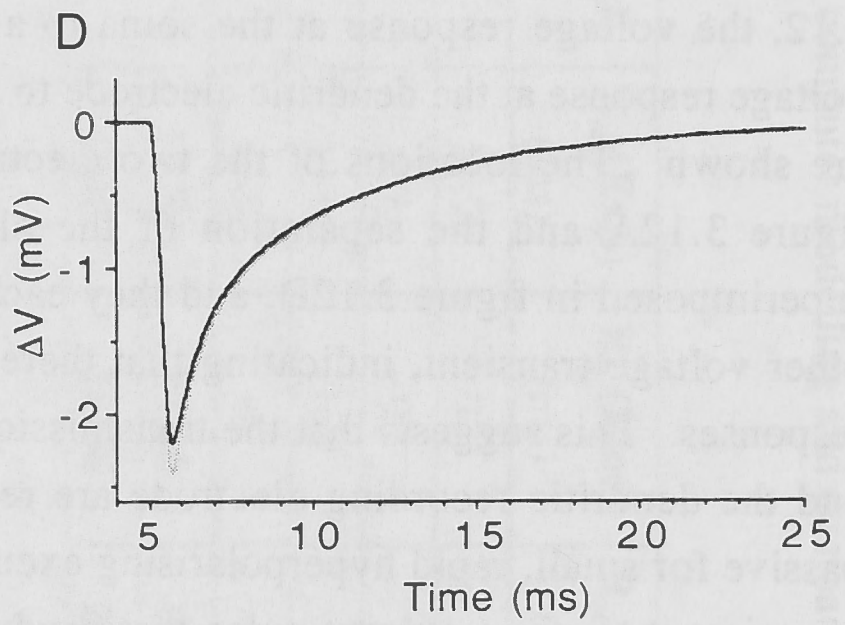
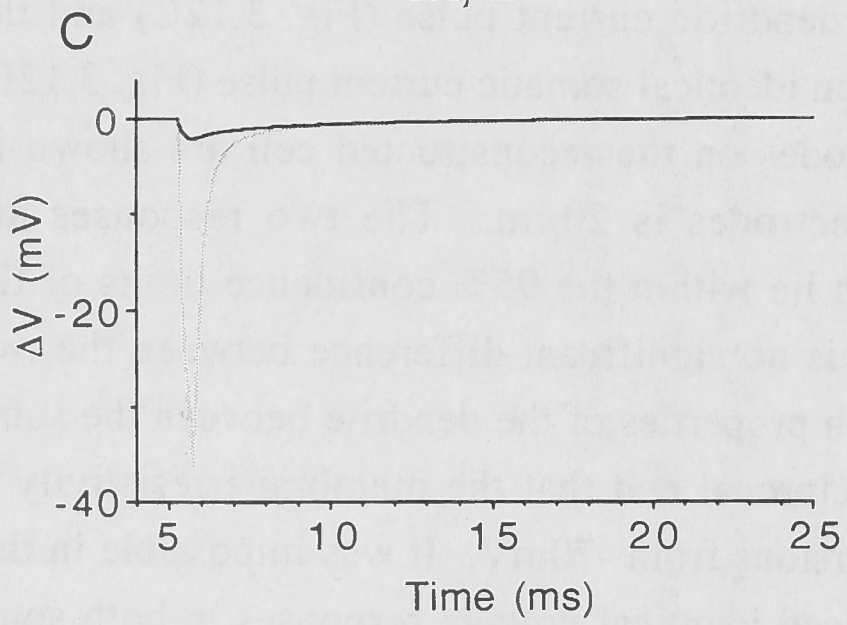
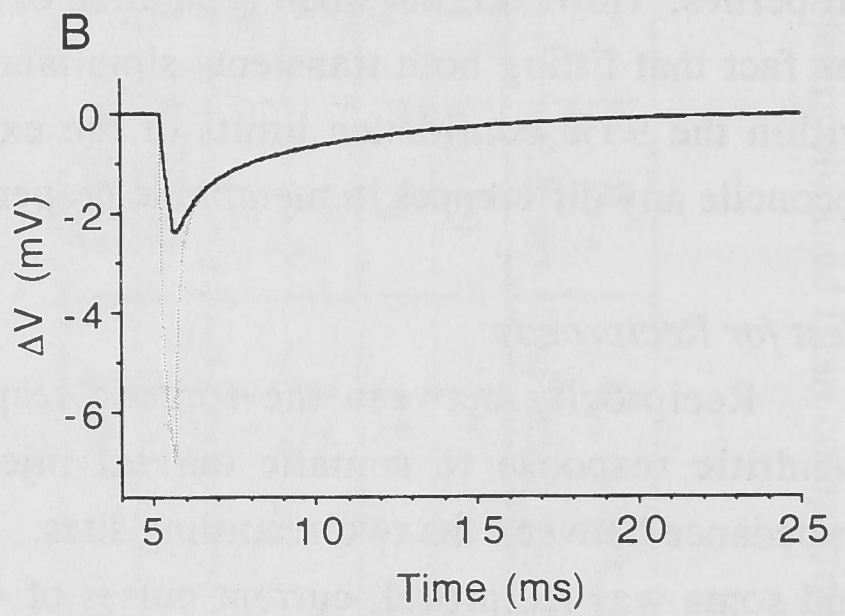
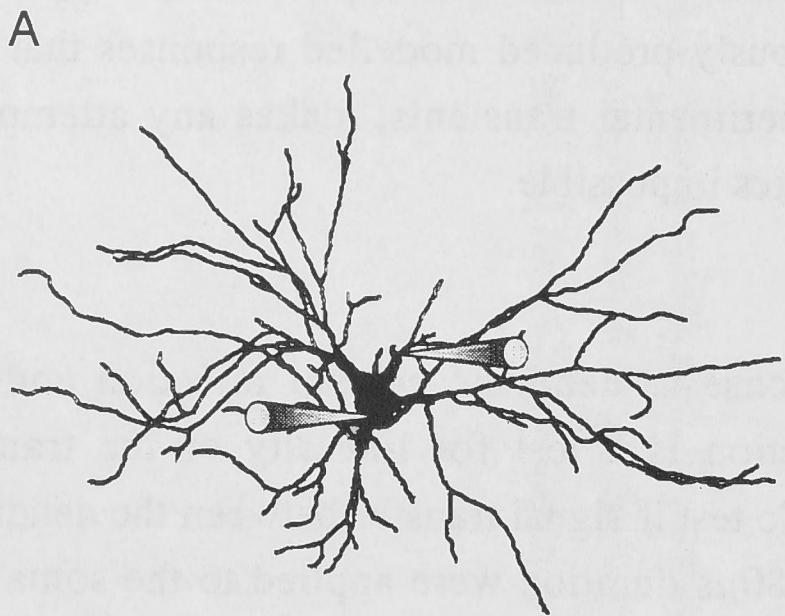


Figure 3.12. Test for reciprocity. **A:** Morphology of *cell C1-1203* showing the location of the somatic and dendritic electrodes. **B:** Somatic (grey line) and dendritic (black line) voltage transients produced by application of a current pulse ( $480\mu\text{s}$ ,  $-2.0\text{nA}$ ) to the soma of the cell shown in A. **C:** Somatic (black line) and dendritic (grey line) voltage transients produced by application of a current pulse ( $480\mu\text{s}$ ,  $-2.0\text{nA}$ ) to the dendrite of the cell shown in A. **D:** Superposition of the somatic (black line) and dendritic (grey line) responses to current injection at the dendrite and soma respectively. The transients fit within their 95% confidence intervals (not shown) indicating that signal transfer between these two sites was reciprocal.

activation/deactivation of dendritic voltage-dependent conductances does occur, it is not sufficient to affect voltage transfer.

Reciprocity was examined in 8 neurones with separations between soma and dendrite varying between 16 and 45  $\mu\text{m}$  and current steps varying from +2.0 to -2.0 nA (usually -0.1 or -0.2 nA). In all 8 experiments, reciprocity in the responses was observed. In 3 of these 8 cells, reciprocity was tested with depolarising pulses. Since reciprocity was still observed in these cells, it must be concluded that there is no difference in the activation/deactivation of voltage-dependent ion channels with either hyperpolarising or depolarising current pulses.

## Discussion

The search for the passive membrane properties and cytoplasmic resistivity of motoneurones has a long history (Rall *et al.* 1992). Technical innovations in electrophysiological measurements or morphological reconstructions have provided the impetus to improve on the inadequacies of previous measurements and this investigation is no exception. Previous measurements of the cable properties of motoneurones have had to contend with distortions to the analysis caused by electrode artifacts and tissue shrinkage. In this study, we have eliminated the latter, and minimised the former, by using an *in vitro* slice preparation and whole-cell recording with two electrodes, one for voltage and the other for current. In each of four neurones, the voltage response to a brief current pulse could be matched very precisely to the transient generated by a compartmental model for that neurone, based on the three parameters  $R_i$ ,  $R_m$  and  $C_m$ . Each of these parameters was most sensitive to the voltage response over different time periods, providing an important element of uniqueness in their determination. In six other neurones for which high quality morphological reconstruction and electrophysiology was obtained, the same precision in matching the model transient to the neurones responses could not be achieved. The mean ( $\pm$ SD) values for  $R_m$  and  $R_i$  for these neurones ( $11.8 \pm 6.7 \text{K}\Omega \cdot \text{cm}^2$  and  $316 \pm 151 \Omega \cdot \text{cm}$ , respectively;  $n=6$ ) were not significantly different from the corresponding values for the four precisely modelled neurones ( $5.3 \pm 0.9 \text{K}\Omega \cdot \text{cm}^2$  and  $87 \pm 22 \Omega \cdot \text{cm}$ ;  $n=4$ ), using a modified t-test for unequal variances (Snedecor & Cochran 1967). Similarly, the difference in the membrane capacitance was not significant ( $2.2 \pm 0.6 \mu\text{F}/\text{cm}^2$ ,  $n=6$  compared with  $2.4 \pm 0.4 \mu\text{F}/\text{cm}^2$ ,  $n=4$ ) for the two data sets.

### *Identification of Motoneurones and Interneurones*

It became clear that large neurones in the ventral horn could not be reliably identified as motoneurones, as the axons of some of these neurones crossed to the contralateral side.

These neurones must be interneurones. Only rarely could the axon be followed to the ventral root exit region and the neurones with these axons were classified as motoneurones. When the axon trajectory could not be followed, cell identification was not reliable. As there appeared to be no systematic difference between the cable parameters for putative motoneurones and interneurones, the results for both neurone types have been combined.

### *Passive Cable Parameters*

CYTOPLASMIC RESISTIVITY ( $R_i = 87 \pm 22 \Omega \cdot \text{cm}$ ).

The lower limit of this parameter is  $43 \Omega \cdot \text{cm}$ , based on the resistivity of a solution combining 50mM NaCl and 110mMKCl in 1% agar at  $37^\circ\text{C}$  (Clements & Redman 1989). As the chloride concentration in the cytoplasm is low, electrical neutrality is preserved by large negatively charged macromolecules. These less mobile charge carriers, and the presence of organelles, cytoskeletal elements and charge binding, should result in  $R_i$  being well in excess of this value. The only reported direct measure of  $R_i$  is  $70 \pm 15 \Omega \cdot \text{cm}$  in mammalian motoneurones (Barrett & Crill 1974). More recently, investigations using combined morphological reconstruction and single electrode recording from a variety of neurone types have reported  $R_i$  values in the range of 70 to  $520 \Omega \cdot \text{cm}$  (Shelton 1985, Clements & Redman 1989, Major *et al.* 1994, Thurbon *et al.* 1994, Ulrich *et al.* 1994).  $R_i$  may vary for different types of neurone if the proportion of non-conducting elements in the cytoplasm varies. It may also be reduced by dialysation, as the large cytoplasmic molecules will be diluted by the electrode solution.

The estimate for  $R_i$  is most sensitive to the initial part of the voltage decay (Fig. 3.3B), and it is this region of the response which is most affected by capacitive artifacts. Measurements using a single electrode technique are more affected by this artifact than are two electrode measurements, as charging and discharging the capacitance of the current electrode distorts the voltage transient at early times. When two electrodes are used, provided there is negligible coupling capacitance between them, the only distortion remaining arises from low-pass filtering of the current pulse by the capacitance of the current passing electrode. This results in a non-rectangular current pulse entering the neurone, and it will cause an error in the calculation for  $R_i$ . Its effect is minimised by delaying the time at which the voltage transient is modelled. None of the single electrode measurements in this study (Table 3.5) resulted in ideal fits to the model, and all of them resulted in higher values of  $R_i$  than those obtained for the four ideal results.



### MEMBRANE RESISTIVITY ( $R_m = 5.3 \pm 0.9 \text{ K}\Omega\cdot\text{cm}^2$ )

Reliable determination of this parameter represents a major challenge, even with the improved techniques used in this investigation. The main difficulty is that the presence of a leak conductance at the soma can give an artificially low value of  $R_m$  if the leak conductance is ignored (Fig. 3.3, C and D). When both  $R_m$  and somatic shunt parameters are introduced into the compartmental model, equally good fits are obtained for a large range of shunt conductance and an inversely large range of  $R_m$ . While the electrode seal resistance is known before the somatic membrane is ruptured, changes to this seal resistance may occur after rupturing the patch under the first electrode. Any leak conductance caused by rupturing the patch under the second electrode will be detected in the holding current of the first electrode, and the experiment discontinued if this occurs. In addition, the holding current must not increase during the recording. Even when these requirements are met, there is no secure way of knowing the leak resistance associated with the first electrode. For all the calculations documented in table 3.5, the leak conductance was assumed to be zero and this may cause an underestimate of  $R_m$ .

Values of  $R_m$  reported for other neurones when caesium was not present to block the resting potassium conductance range from 7 to  $220\text{K}\Omega\cdot\text{cm}^2$  (Major *et al.* 1994, Thurbon *et al.* 1994). When caesium was present in the electrode solution, Ulrich *et al.* (1994) reported a value of  $R_m=17.5\text{K}\Omega\cdot\text{cm}^2$  for cultured motoneurones. As for  $R_i$ , different neurone types may have very different resting conductances and hence different values of  $R_m$ .

### MEMBRANE CAPACITANCE ( $C_m = 2.4 \pm 0.5 \mu\text{F}/\text{cm}^2$ ).

This parameter was the most robust of the three in the fitting procedure. Major departures from uniform membrane resistance did not alter  $C_m$  very much from its true value (Table 3.6). Thus, the only potential source of significant error would be in the determination of membrane surface area, which trades off with the estimated value of  $C_m$ . A linear scaling of each compartment by a factor of 1.5 for both length and diameter would reduce  $C_m$  by a factor of 2.25, with a concomitant increase of  $R_i$  by 50 % (following the method given in Major *et al.* 1994). Such a correction of the morphology would lead to a value of  $C_m$  close to the commonly assumed value of  $1.0\mu\text{F}/\text{cm}^2$  (To conserve  $\tau_m$ ,  $R_m$  must change correspondingly). The calculation of the surface area is relatively simple for motoneurones. They do not have spines, which can make surface area calculations very difficult, and their dendrites branch infrequently. The histological procedure did not cause shrinkage, as video images of the soma and proximal dendrites taken at the beginning and end of the experiment provided an independent check on cell dimensions, as well as any

possible swelling of the cell during the experiment. Therefore, we consider an underestimation of the total surface area by a factor of 2.25 as most unlikely.

The value obtained for  $C_m$  is very different from the value of  $1\mu\text{F}/\text{cm}^2$  commonly assumed for neuronal membrane, and from the values obtained for other neurone types by similar fitting procedures to those used in this experiment ( $1.1\pm 0.2\mu\text{F}/\text{cm}^2$  for cultured motoneurons, Ulrich *et al.* 1994;  $0.7\pm 0.8\mu\text{F}/\text{cm}^2$  for CA3 pyramidal cells, Major *et al.* 1994). Other investigators using combined morphology and electrophysiological measurements on motoneurons have reported a wide range of values for  $C_m$  ( $2\mu\text{F}/\text{cm}^2$ , Lux *et al.* 1970;  $2\text{--}4\mu\text{F}/\text{cm}^2$ , Barrett & Crill 1974;  $1.8\mu\text{F}/\text{cm}^2$ , Nitzan *et al.* 1990). The capacitance of a 5.7nm thick membrane with a lipid/protein mix depends critically on the proportion of protein present. Assuming a 50/50 composition (Alberts *et al.* 1989; Ch 6), a dielectric constant for protein of 30 (Smith *et al.* 1993) and for lipid of 2 (Fettiplace *et al.* 1971), the membrane capacitance would be  $2.3\mu\text{F}/\text{cm}^2$ . If the protein component differs in different cells or in different regions of a cell, cell-to-cell variability and non-uniform distributions in  $C_m$  might be expected.

Gentet *et al.* (2000) have made direct measurements of capacitance in various cell types, including neurones of the spinal cord, using nucleated patches. For spinal neurones, the specific membrane capacitance was found to be  $0.85\pm 0.07\mu\text{F}/\text{cm}^2$  (SD,  $n=8$ ). As mentioned above, the method used in this chapter is particularly subject to errors caused by inaccuracies in estimating membrane area from the morphological reconstruction, particularly at the soma where the three-dimensional shape of the soma cannot be determined. This is important as it is the soma capacitance that dominates the cell's voltage response to transient currents at the soma. However, it is unlikely that the soma area would be overestimated by about 2.8 times ( $2.4/0.85$ ) so it must be concluded that the low value of  $C_m$  obtained by Gentet *et al.* (2000) cannot be explained here.

#### *Fitting Transients from Two Electrodes*

The procedure in which the somatic and dendritic transients were used as target responses for the fitting procedure gave results that indicate that dendritic membrane parameters are similar to those of the soma, at least for distances up to  $20\mu\text{m}$  from the soma. When each of the transients was fitted individually, the fitted parameter values were not significantly different.  $R_m$  was slightly higher and  $C_m$  slightly lower in the dendritic fit while  $R_i$  was higher. The reasons for these differences are difficult to reconcile and there are two conceivable sources for the observed differences in the somatic and dendritic parameters. Firstly, the dendritic membrane parameters may be genuinely different to those of the soma and could explain the differences between the two fits. Secondly, the different

membrane parameters recovered from the dendritic fit may have been caused by differences in leakage conductances at the two electrodes. Since the two transient fit procedure has only been performed on one cell, little can be said about differences between the fits obtained at either electrode.

It is also possible that differences in the electrical characteristics of the somatic and dendritic electrodes could also be responsible for the different parameters. The finer electrodes used for dendritic recording have a higher capacitance and a larger access resistance and produce larger electrode artifacts during current injection. As has already been noted (see Fig. 3.4), the effect of the electrodes could never be fully compensated in this experiment. Figure 3.4 shows that the capacitance of the current injecting electrode filters the injected current pulse and delays it by about  $200\mu\text{s}$ , which is a significant delay considering that the total width of the current pulse was only  $480\mu\text{s}$ . The higher capacitance of the dendritic electrode would mean that the current pulse would be more heavily filtered and delayed for longer than it was for a somatic electrode and would continue to pass current for longer once the current pulse turned off. This would cause the voltage response to have greater amplitude during the early decay phase and a more rapid decay than for a somatic electrode. Judging from figure 3.3, such changes in the voltage response would give parameter fits in which  $C_m$  was overestimated and  $R_m$  and  $R_i$  were underestimated, which is exactly what is found for the dendritic fit, suggesting that this may be the case. However, we did not perform a similar analysis to that in shown in figure 3.4 and so it is impossible to say how much contribution the dendritic electrode had to the differences in parameter estimation between soma and dendrite.

It is possible that the dendritic membrane properties are different to those of the soma, but the small electrode separation in these experiments means that it is difficult to say just how representative the dendritic fit may be of the dendritic properties at distances greater than  $20\mu\text{m}$  from the soma. When fitting was performed using both transients as targets for the fitting procedure, the values of  $R_m$ ,  $C_m$  and  $R_i$  fell in between the values obtained by fitting each transient separately. This indicates that although there may be a difference between the membrane properties of the soma and dendrites, the fitting procedure is too insensitive to be able to detect this using 95% confidence intervals as the fit criterion. All that can be said is that electrode capacitance plays a role in the differences that are seen but may not fully explain them.

### *Reciprocity*

The test of reciprocity in ventral spinal neurones provided evidence that the transfer of small rapid voltage excursions between soma and proximal dendritic locations is passive.

Even in cells where unusually large dendritic transients were generated, such as for the dendritic transient in the cell illustrated in figure 3.12 (~35mV), the reciprocity test still produced traces that superimposed. Such a test is indicative that somato-dendritic voltage transfer is reciprocal. It is impossible to say if this would be true for locations further from the soma, but it is certainly true for distances up to 45 $\mu$ m from the soma. It is still possible however, that a balance of opposing voltage-dependent conductances with identical kinetics could produce such reciprocity and this cannot be ruled out.

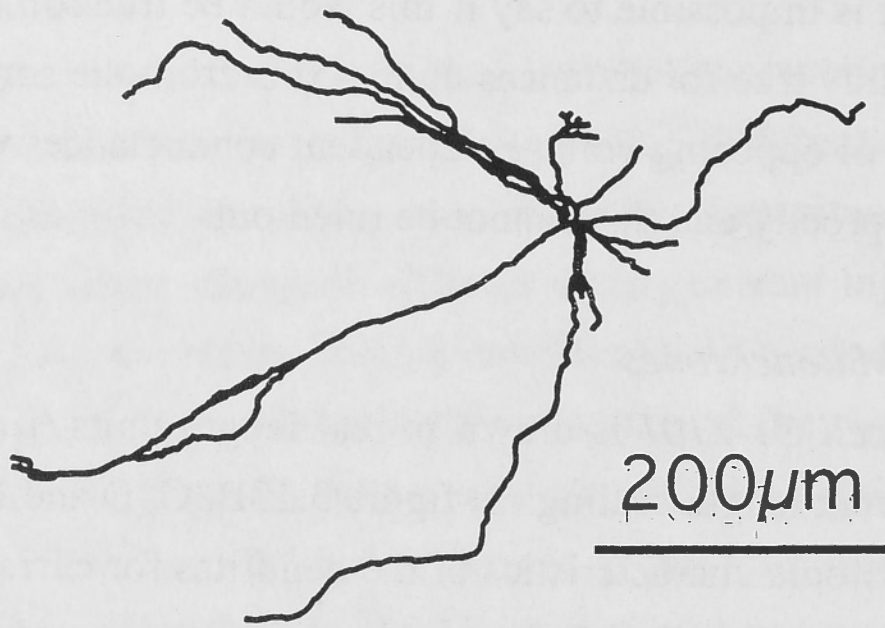
### *Electrotonic Profile of Motoneurons*

In figure 3.13A, *cell C1-2101* is drawn in real length units ( $\mu$ m). The same cell is redrawn with four different length scalings in figure 3.13B, C, D and E. The relative scales correspond to the electrotonic characteristics of the dendrites for current spreading from the dendrites towards the soma (Fig. 3.13B for steady-state current and Fig. 3.13C for 50Hz) and for current spreading distally from the soma (Fig. 3.13D for steady-state current and Fig. 3.13E for 50Hz). The scale bar corresponds to the distance over which the attenuation is  $e^{-1}$ , which is equivalent to one length constant,  $\lambda$ . This electrotonic transformation is described in Carnevale *et al.* (1997). Figure 3.13 illustrates dramatically how a neurone may be relatively compact electrotonically for DC voltages applied to the soma, but heavily attenuates AC currents spreading centrally from the dendrites. As fast synaptic potentials at their dendritic site of generation can peak in about 0.5ms, and effectively terminate in about 10ms, their frequency spectrum ranges from 25 to 500Hz. Figure 3.13 indicates that while large regions of the dendritic tree will be reasonably well clamped for DC potentials, this will not be true for fast voltage transients generated in the dendrites. The rapid decay of synaptic potentials as they spread from dendrites to soma is illustrated below in a more conventional way.

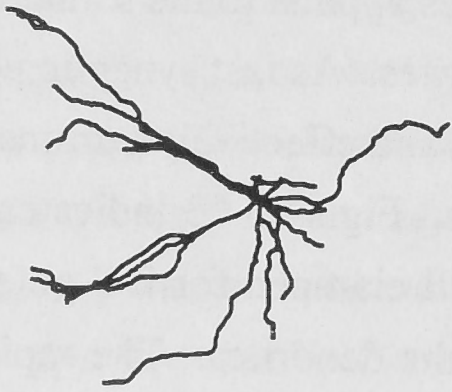
### *Simulation of Synaptic Input*

Synaptic input was simulated as a conductance change in the form of an  $\alpha$ -function with a time-to-peak of 0.3ms. In figure 3.14A an excitatory postsynaptic potential (EPSP) is plotted as recorded from the dendritic site d1, where the conductance change was applied, together with the same EPSP as it reaches the soma. As suggested by the electrotonic transform in figure 3.13, the EPSP decrements very rapidly as it spreads towards the soma. In figure 3.14B three EPSPs recorded from the soma are shown. They were elicited by the same conductance change applied either to the soma (s), to the proximal dendritic location (d1), or to the distal dendritic location (d2). In figure 3.14C the EPSP amplitude is plotted against its 10-90% rise-time as measured at the soma for the

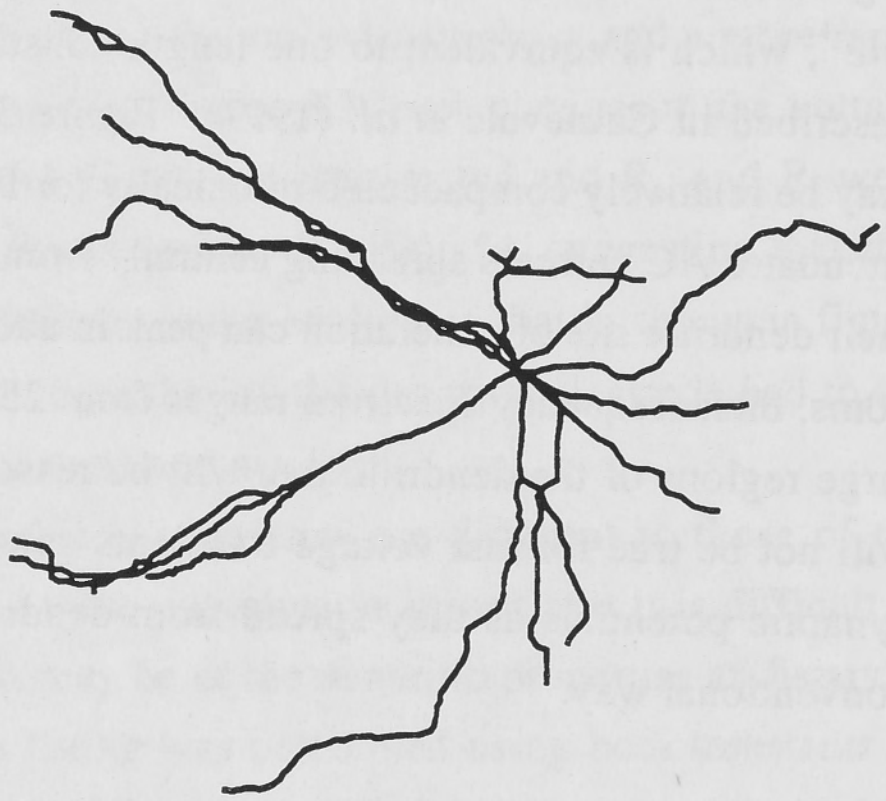
A



B



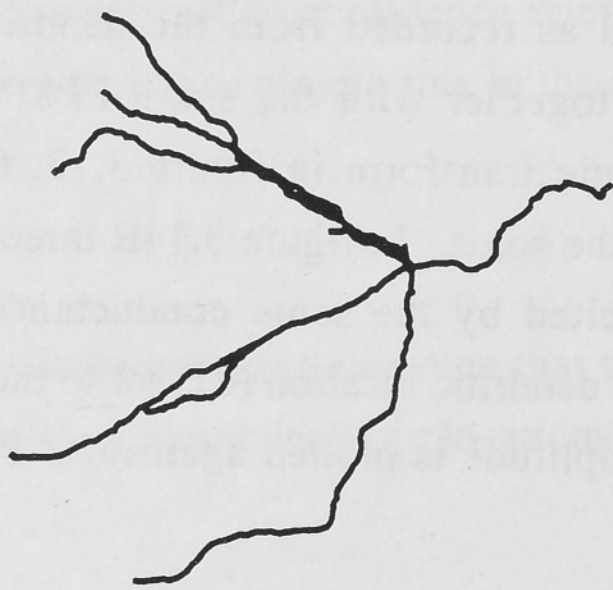
C



D



E



I

I

Figure 3.13. Electrotonic transforms for *cell C1-2101*, a presumed motoneurone. **A:** Line drawing of the reconstructed neurone. **B:** Electrotonic profile for the cell depicted in *A* for a DC potential applied to different sites on the dendrites as it decays towards the soma. **C:** Same as in *B* but for the application of a 50Hz sine wave signal instead of a DC signal. **D:** Electrotonic profile of the cell in *A* for a DC signal applied to the soma as it decays to different sites on the dendrites. **E:** Same as in *D* but for a 50Hz sine wave. The scale bar is the distance over which the voltage attenuation is  $1/e$ , which is equivalent to the length constant,  $\lambda$ . Note different scale bars for the upper and lower pairs of cells.



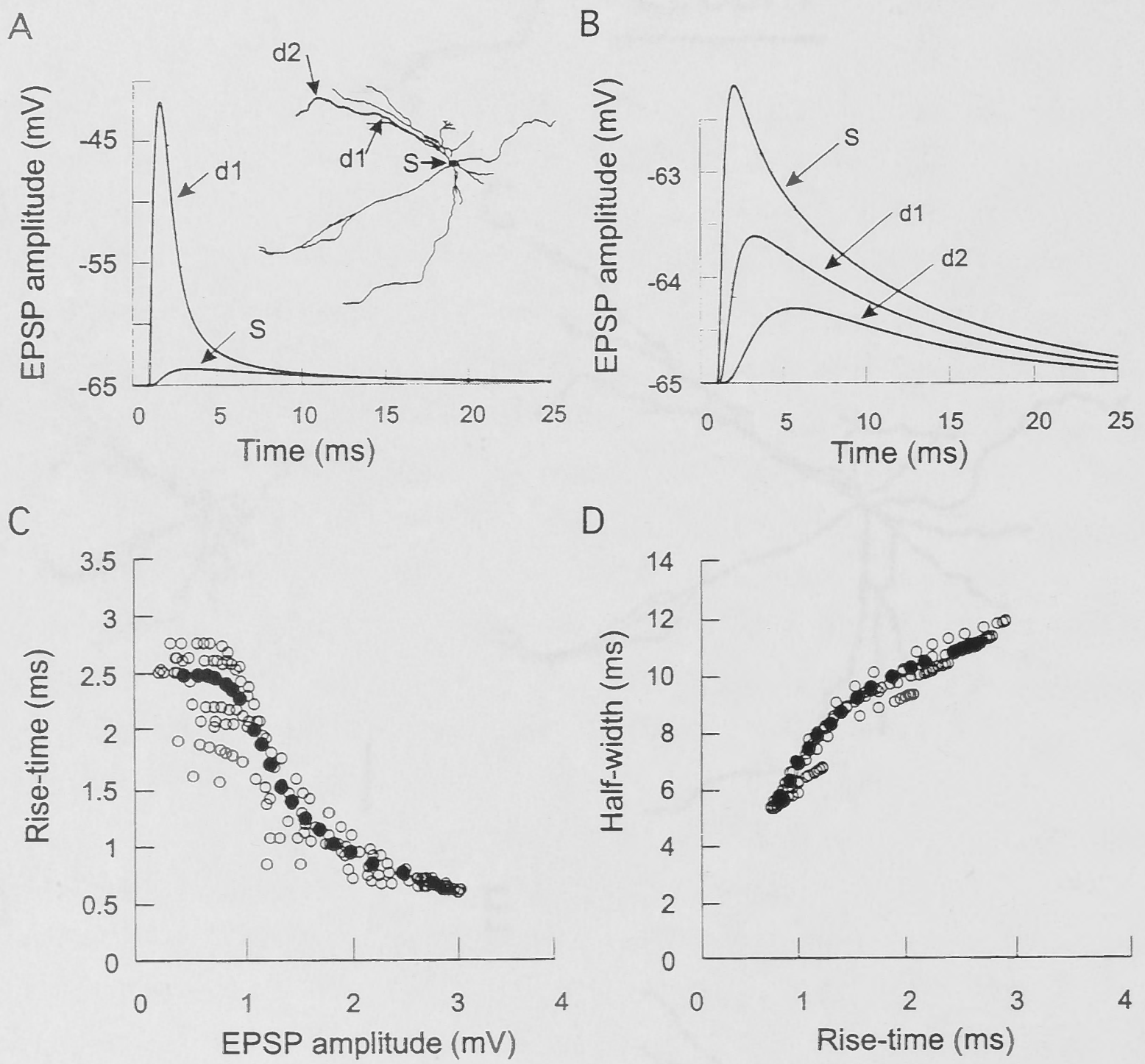


Figure 3.14. Simulated EPSPs and shape index plots for *cell C1-2101* with the passive membrane properties as listed in *table 3.7*. Synaptic input was simulated by a conductance change in the form of an  $\alpha$ -function ( $\alpha^{-1}=0.3\text{ms}$ ,  $g_{\text{max}}=10\text{nS}$ , reversal potential= $0.0\text{mV}$ , delay= $1.0\text{ms}$ ). **A:** A conductance change with the above parameters was applied to the location d1 (inset), and the resulting EPSP recorded simultaneously from the same location and from the soma are plotted superimposed. Note the very large decrement of the voltage transient from its site of generation to the soma. **B:** EPSPs recorded from the soma for a synaptic conductance change applied to the soma, location d1 and d2. **C:** Scatter plot of EPSP amplitude versus rise-time. Filled symbols represent EPSPs simulated along one particular dendritic segment (heavy line and marked with arrows in the inset of A). **D:** Scatter plot of 10-90% rise-time versus half-width. In C and D synaptic input was applied to every segment of the compartmental model for the cell.



EPSP generated in each compartmental segment of *cell C1-2101*, with an identical conductance change. The scatter plot illustrates the strong attenuation of the EPSPs as their rise-times increase. The large scatter in the data points is explained by different termination and branching conditions in different dendrites. The filled symbols following a smooth sigmoid curve represent EPSPs generated along one particular dendritic segment (thick dendrite marked with the arrows in the inset of figure 3.14A). Figure 3.14C further illustrates that a wide range of EPSP amplitudes (150 $\mu$ V-3.2mV) can be observed at the soma for synapses of equal strength (and generating a peak amplitude of 3.2mV when applied at the soma) distributed over the entire dendritic tree. Figure 3.14D plots the EPSP 10-90% rise-time versus half-width as measured in the soma for EPSPs of equal strength generated in every segment of the model. The filled symbols represent the shape index of EPSPs generated on one particular dendrite, highlighted in the inset of figure 3.14A.

### *The Passive Motoneurone*

A long standing issue in modelling passive motoneurons (as well as other neurone types) has been how to interpret the somatic shunt, and in particular whether this was an artifact of electrode penetration or a genuinely low somatic membrane resistivity. Spruston and Johnston (1992) reported that the input resistances of the principal hippocampal neurones were 3 to 10 times higher when measured by perforated patch compared with intracellular electrodes, indicating the shunt was a result of electrode damage. In other recent whole-cell recordings of voltage transients and cable analysis in hippocampal neurones, a somatic shunt has not been required (Major *et al.* 1994, Thurbon *et al.* 1994). Similarly, the best fitting results in this investigation did not require a somatic shunt, indicating a uniform  $R_m$  for motoneurone somata and dendrites. However, the possibility that  $R_m$  (and the other cable parameters) varies along dendrites remains open, as somatic measurements give limited resolution of dendritic membrane properties.

Stuart and Spruston (1998) have performed similar fitting of experimentally generated voltage transients in pyramidal cells of the neocortex using whole-cell recordings from the soma and dendrites of these cells in combination with the reconstructed morphology. They were able to get greater resolution of the dendritic membrane properties using this method. They found that  $R_i$  in their cells (70-100 $\Omega$ .cm) was similar to the values obtained here. They also found that a sigmoidally decreasing dendritic  $R_m$  gave the best fits to their data. Furthermore, this non-uniform  $R_m$  was caused by high densities of resting conductances in the distal apical dendrites of their cells, particularly  $I_h$ . Thus, the non-uniform dendritic resting conductances produce a "leaky" dendrite that increases signal attenuation in the dendrites of these cells.

The values of  $R_m$  and  $R_i$  confirm previous descriptions of the electrical compactness of motoneurone dendrites for DC signals (Fleshman *et al.* 1988, Clements & Redman 1989, Ulrich *et al.* 1994), with dendritic lengths of  $0.85 \pm 0.14\lambda$ . However, as dendritic attenuation of fast synaptic events is more sensitive to  $C_m$  than it is to  $R_m$  (Spruston *et al.* 1994), revising  $C_m$  from 1 to  $2.4 \mu\text{F}/\text{cm}^2$  implies a much greater dendritic attenuation. The example in figure 3.14 indicates peak attenuations of 20-30 fold for a fast synaptic conductance on the distal dendrites.

A large  $C_m$  value has several implications for the integrative behaviour of the neurone. It will be more difficult to support an antidromic action potential by inward currents. If a somatic action potential spreads into the dendrite passively, it will attenuate more rapidly. Synaptic potentials generated in fine dendrites will not be as large at their site of generation, and will decay more rapidly. This will provide for greater linearity in the summation of synaptic potentials in dendrites. Finally, dendritic synaptic potentials will be filtered more heavily, making it more difficult to bring the motoneurons to firing threshold.

Additionally, if voltage-dependent ion channels are present at sufficiently high density, then they may produce regenerative events similar to the action potential (Spruston *et al.* 1993). These dendritic action potentials are usually of smaller amplitude and longer time course than the axonal action potential (e.g. Fujita 1989). They may be caused by either  $\text{Na}^+$  conductances (Regehr *et al.* 1994, Smart & Häusser 1994, Spruston *et al.* 1995, Golding & Spruston 1996) or  $\text{Ca}^{2+}$  conductances (Schiller *et al.* 1997, Golding *et al.* 1999, Larkum *et al.* 1999a). These dendritic action potentials could reset the dendritic membrane potential for a short time after the spike has occurred, circumventing any synaptic potential summation that may have occurred up to that time. This strategy could be important for processing synaptic inputs. Dendritic regenerative events may also be important for initiating the action potential by amplifying synaptic depolarisations and propagating them to the axon where they can trigger an action potential (Smart & Häusser 1997). In some cells such as neurones of the substantia nigra (Häusser *et al.* 1995) the axon arises from the dendritic tree rather than from the soma and dendritic action potentials may be important for initiating axonal action potentials in the axon.

Generally, studies of dendritic ion channels have shown a great deal of heterogeneity between cell types and this indicates that the results of one cell type cannot be transferred to another cell type. Therefore, until the complexities of dendritic active properties are better understood, it is unsafe to make any generalisations about the role these channels play in the integration of synaptic potentials in neurones of different types and the propagation and initiation of action potentials.

Early work to try to define the ionic channels present in the motoneurone was done by simple experiments that attempted to determine the contribution of these channels to the



---

## Chapter Four

# Action Potential Propagation in Motoneurone Dendrites

---

### Introduction

Interest in backpropagating action potentials has grown recently due to studies in synaptic plasticity that suggest that the action potential could play an important role in learning. Backpropagated action potentials can provide the depolarisation necessary to relieve the  $Mg^{2+}$  block of the NMDA receptor allowing it to conduct  $Ca^{2+}$  ions when activated by glutamate (Magee & Johnston 1997, Koester & Sakmann 1998). This  $Ca^{2+}$  influx triggers a cascade of cellular events which lead to modification of synaptic efficacy (Yuste & Denk 1995, Koester & Sakmann 1998, Schiller *et al.* 1998, Yuste *et al.* 1999).

Dendritic voltage-dependent ion channels may also play a role in modifying the amplitude and time-course of dendritically propagated synaptic potentials (Magee & Johnston 1995b, Wilson 1995, Tsubokawa & Ross 1996, Hoffman *et al.* 1997, Stuart & Spruston 1998, Magee 1999, Williams & Stuart 2000b). Additionally, if voltage-dependent ion channels are present at sufficiently high density, then they may produce regenerative events similar to the action potential (Spruston *et al.* 1995). These dendritic action potentials are usually of smaller amplitude and longer time-course than the axonal action potential (e.g. Fujita 1989). They may be caused by either  $Na^+$  conductances (Regehr *et al.* 1992, Stuart & Häusser 1994, Spruston *et al.* 1995, Golding & Spruston 1998) or  $Ca^{2+}$  conductances (Schiller *et al.* 1997, Golding *et al.* 1999, Larkum *et al.* 1999a). These dendritic action potentials could reset the dendritic membrane potential for a short time after the spike has occurred, eliminating any synaptic potential summation that may have occurred up to that time. This strategy could be important for processing synaptic inputs. Dendritic regenerative events may also be important for initiating the action potential by amplifying synaptic depolarisations and propagating them to the axon where they can trigger an action potential (Stuart & Sakmann 1995). In some cells such as neurones of the substantia nigra (Häusser *et al.* 1995) the axon arises from the dendritic tree rather than from the soma and dendritic action potentials may be important for initiating axonal action potentials in these cells.

Generally, studies of dendritic ion channels have shown a great deal of heterogeneity between cell types and this indicates that the results of one cell type cannot be transferred to another cell type. Therefore, until the complexities of dendritic active properties are better understood, it is unsafe to make any generalisations about the role these channels play in the integration of synaptic potentials in neurones of different types and the propagation and initiation of action potentials.

Early work to try to define the ionic channels present in the motoneurone were simple experiments that attempted to determine the contribution of these channels to the

action potential waveform. Walton and Fulton (1986) demonstrated the presence of dendritic  $\text{Ca}^{2+}$  action potentials and  $\text{Na}^+$  action potentials in neonate rat motoneurons. They also showed that a  $\text{Ca}^{2+}$  dependent  $\text{K}^+$  conductance ( $I_{\text{K}(\text{Ca}^{2+})}$ ) was present, which is responsible for the majority of the afterhyperpolarisation and is the major determinant of firing rate in these cells. A voltage-gated  $\text{Ca}^{2+}$  current is required to activate this conductance and blockade of this current with  $\text{Cd}^{2+}$  reduced  $I_{\text{K}(\text{Ca}^{2+})}$  and increased action potential firing rates. However, they also noted that the  $\text{Ca}^{2+}$  current decreased as animals became older and  $\text{Ca}^{2+}$  action potentials were only detectable in 3-5 day old rats after application of potassium blockers such as TEA or  $\text{Cs}^+$ . They also observed small all-or-none dendritic action potentials in motoneurons of young rats (3-5 days) and in older rats after application of  $\text{Cs}^+$ . These action potentials had faster rise-times than the dendritic  $\text{Ca}^{2+}$  action potentials and could be blocked by TTX, indicating that they were sodium dependent. These findings suggest that neonatal motoneurons generate  $\text{Na}^+$  and  $\text{Ca}^{2+}$  dependent events at separate anatomical sites, probably in the dendritic membrane and that the  $\text{Ca}^{2+}$  component decreases with age. The early  $\text{Ca}^{2+}$  currents may be important for determining synaptic efficacy in the early stages of motor development.

Clements *et al.* (1986) found that internal injection of TEA into cat motoneurons increased the amplitude of dendritically generated EPSPs and prolonged their time-courses, while it had no effect on somatically generated EPSPs. This suggested the presence of a dendritic potassium channel that reduced EPSP amplitude and time-course.

Takahashi (1990) has examined the potassium currents present in neonate rat motoneurons. This work showed that neonate rat motoneurons have three predominant types of potassium conductance; a  $\text{Ca}^{2+}$  dependent potassium channel ( $I_{\text{K}(\text{Ca}^{2+})}$ ), a delayed rectifier ( $I_{\text{DR}}$ ) and an A-type potassium conductance ( $I_{\text{A}}$ ). Takahashi (1990) also attempted to examine the contribution of these potassium conductances to the action potential waveform. In neonatal motoneurons, blockade of the A-current markedly prolonged the action potential at the soma (Takahashi 1990). It was therefore concluded that in neonatal rat motoneurons  $I_{\text{A}}$  is the major contributor to action potential repolarisation.

Measurements of  $\text{K}^+$  channels in motoneurone dendrites have not been made, however a whole-cell and patch-clamp study of potassium channels in the somata of rat motoneurons (Safronov & Vogel 1995) found that the most predominant potassium current in the motoneurone soma is the A-current, at least in young rats. A delayed rectifier is also present, along with the voltage-activated  $\text{Na}^+$  channel. This differs from the axonal potassium channels of rat motoneurons which have been shown to contain three types of delayed rectifier with varying kinetics and that none of these corresponds to the A-current (Roper & Schwarz 1989, Safronov *et al.* 1993). These results suggest that the A-current is preferentially distributed in the motoneurone soma. This will tend to dampen

backpropagating action potentials while still allowing EPSPs to propagate to the axon initial segment.

Direct measurement of the backpropagation of the action potential in motoneurone dendrites has so far only been performed in motoneurons cultured from young rats (e.g. Larkum *et al.* 1996). In this study, organotypic cultures of spinal cord were used as the experimental preparation. Somatic and dendritic recordings were made with the dendritic electrode at distances varying from 30 to 423  $\mu\text{m}$  from the soma. It was found that the amplitude of the backpropagated action potential was much larger than would be expected for passive attenuation calculated from a simple passive model of the motoneurone. Addition of TTX reduced the dendritic action potential amplitude to that expected for passive propagation. This indicates that there is a  $\text{Na}^+$  channel that amplifies the action potential within motoneurone dendrites. Also, addition of QX-314 to the dendritic electrode solution gradually abolished the amplification of the backpropagated action potential and reduced it to the level expected for passive propagation. However this active backpropagation was not present in all cells and in some cases, it was found that action potential backpropagation followed a purely passive decay. To answer the question of whether different dendrites of the neurone could have different conduction properties, Larkum *et al.* (1996) also used optical recordings of membrane potential using the voltage sensitive dye di-8-ANEPPS. Propagation of action potentials and of hyperpolarising pulses was compared to determine whether action potentials were conducted differently to passive signals in different dendrites. It was found that action potentials declined on average 12.5% less than hyperpolarising pulses, confirming that action potentials are indeed actively backpropagated. Furthermore, the results varied for each dendrite, indicating that it is possible for different dendrites of the same neurone to have differing ability to propagate action potentials. Larkum *et al.* (1996) suggested that the  $\text{Ca}^{2+}$  influx associated with the backpropagating action potential might be important as a retrograde signal to regulate the motoneurone's computational ability.

Hsiao and Chandler (1995) have performed experiments to determine the characteristics of the A-current in guinea pig trigeminal motoneurons. They found similar results to those of Takahashi (1990). Blockade of the A-current resulted in prolonged action potentials and changes in threshold membrane potential.

In summary, there is much evidence that voltage-dependent ionic currents are present in the membrane of motoneurons and that many of these currents are localised in the dendrites of these cells. However, apart from the work of Larkum *et al.* 1996, there has been little done to further define the dendritic ionic currents of motoneurons. The experiments presented here are the first experiments ever performed in which motoneurone dendrites are recorded from *in vivo*.

## Methods

### *Recordings*

Experiments were performed as in Chapter 3 for the two electrode experiments although some modification of the experimental procedures was made. 12-14 day old rats were used rather than 7-15 day old rats. This age range was chosen to reduce developmental differences between the recorded cells and to ensure the use of the most developed cells that could be obtained while still maintaining viability of the tissue.

In these experiments, one electrode was placed on the soma and the other on a dendrite up to  $50\mu\text{m}$  from the soma. Cells were presumed to be motoneurons. However, as was mentioned in Chapter 3, the electrophysiological properties of the cells were identical and did not allow the cell type to be determined. Positive identification requires staining of the cells and observation of the morphology and axon trajectory. Even in stained cells, the axon may not be visible and the identification is uncertain. For these reasons, staining was not performed in this Chapter and cells were presumed to be motoneurons. In any one slice, dendrites could be clearly seen in only a few cells within the ventral horn, even using IR-DIC. This is probably because the dendrites of motoneurons rarely lie in the same plane as the slice, unlike the primary apical dendrites of neocortical and hippocampal pyramidal cells. Electrodes could not be placed further from the soma than  $50\mu\text{m}$  because of difficulties in visualising the thin dendrites of these cells beyond that distance and attaching a patch pipette to them. The soma electrode was attached first, followed by the dendritic electrode, as it was found that the somatic electrode was less prone to detach during explorations with a second electrode. Electrodes were filled with the same gluconic acid based solution that was used in Chapter 3. Electrode resistances were between 4 to  $6\text{M}\Omega$  for somatic electrodes and 8 to  $12\text{M}\Omega$  for dendritic electrodes. Dendritic electrodes were made with rapidly tapering shanks to reduce their stray capacitance and during recordings, the bath level was dropped to further reduce dendritic electrode capacitance. The capacitance neutralisation of the AxoClamp amplifier was then increased until the baseline noise increased up to four times that of the uncompensated level, with minimal ringing. The bath solution always contained  $10\mu\text{M}$  CNQX,  $10\mu\text{M}$  strychnine and  $100\mu\text{M}$  picrotoxin to block glutamatergic, glycinergic and GABAergic synaptic inputs respectively.

### *Isolation of the A-current*

These experiments sought to isolate and record the A-current. During these experiments, the pharmacological agents TTX ( $1\mu\text{M}$ ) and TEA ( $10\text{mM}$ ) were added to the bath solution to block voltage-dependent  $\text{Na}^+$  channels and the delayed rectifier. To compensate for the change in osmolarity caused by the high concentration of TEA the external  $\text{Na}^+$  concentration was reduced from  $113\text{mM}$  to  $103\text{mM}$ . The influence of

voltage-dependent  $\text{Ca}^{2+}$  channels and the  $\text{Ca}^{2+}$  dependent potassium conductance on the membrane current was abolished by adding  $300\mu\text{M Ni}^{2+}$  to the bath solution as well as removing  $\text{Ca}^{2+}$  from the external solution and replacing it with  $2\text{mM Co}^{2+}$ . To prevent precipitation of cobalt phosphate ( $\text{Co}_3(\text{PO}_4)_2$ ), no phosphate ( $\text{NaH}_2\text{PO}_4$ ) was included.

A somatic whole-cell electrode was attached to the soma of motoneurons. Once the ion channel blockers had been applied to the tissue, a voltage clamp protocol was used to obtain A-current recordings. Voltage clamp recordings were made on an AxoPatch 200 amplifier. Cells were held at  $-60\text{mV}$  and a  $150\text{ms}$  prepulse to  $-110\text{mV}$  was applied. This was done to ensure the maximum A-current would be available for activation. This prepulse was then followed by a  $50\text{ms}$  pulse to a membrane potential sufficient to activate the A-current. The procedure was repeated to cover the range of membrane potentials from  $-60\text{mV}$  to  $+30\text{mV}$  with a  $10\text{mV}$  separation between each potential (10 different pulse amplitudes). This voltage protocol is illustrated in figure 4.6A. Since  $10\text{mM TEA}$  does not completely block the delayed rectifier (Safronov & Vogel 1995, Bekkers 2000a), the A-current recordings were contaminated by a residual component of the delayed rectifier. To obtain a current trace useful for subtraction, a similar voltage protocol to the one just described, but modified to inactivate the A-current, was used to obtain records suitable for subtracting the contribution of unblocked currents other than the A-current. The protocol uses a prepulse to  $-110\text{mV}$  which is only  $100\text{ms}$  long and is followed by a  $50\text{ms}$  pulse to  $-30\text{mV}$  to inactivate the A-current. The duration and potential were chosen to cause maximal inactivation of the A-current while causing minimal activation of the delayed rectifier. This voltage protocol is illustrated in figure 4.6B. These two protocols were strung together  $50\text{ms}$  apart and were run simultaneously so that A-current recordings and records for subtraction were obtained at the same time. This voltage protocol was repeated at  $1\text{Hz}$  and the membrane current sampled at  $10\text{KHz}$ . Ten traces were recorded for each of the ten different pulse amplitudes from  $-60\text{mV}$  to  $+30\text{mV}$  and these were later used for averaging. Subtraction of the part of the records in which the A-current was inactivated from that in which the A-current was present produced current traces which were only contaminated by leak and capacitive artifacts caused by the  $50\text{ms}$  prepulse to  $-30\text{mV}$  and the step from this prepulse to the test potential. These artifacts were reduced by subtracting the current trace in which the prepulse to  $-30\text{mV}$  was followed by a step to  $-60\text{mV}$  (no delayed rectifier current). This produces a constant sized capacitive artifact. This can be explained as follows. Consider the capacitance artifact produced by the step from  $-110\text{mV}$  to the test potential,  $V_p$ . The size of the capacitive artifact will be equal to  $V_p+110$  multiplied by a constant,  $C$ . Therefore the size of the capacitive artifact is  $C(V_p+110)$ . In the prepulse data, the size of the capacitive artifact is  $C(V_p+30)$ . Subtraction of these gives  $C(V_p+110)-C(V_p+30)=80C$ . Therefore, this subtraction technique leaves capacitive artifacts that have a constant amplitude (Bekkers 2000a). This



experiment was repeated in the presence of 4-AP to conclusively show that the recorded current was indeed the A-current. Reversibility of the 4-AP block could not be obtained because it took too long to wash out 4-AP once the tissue had been exposed to it.

#### *Action Potential Amplitude Versus Membrane Potential and 4-AP*

To determine if the membrane potential affects the amplitude of the somatic action potential, experiments were performed in which action potentials were initiated at various holding potentials. For these experiments,  $\text{Ca}^{2+}$  channels were blocked, as described previously, to remove any possible confounding influence of  $\text{Ca}^{2+}$  currents and the  $\text{Ca}^{2+}$  dependent potassium current on the amplitude of the action potential.

The protocol for recording consisted of performing a whole-cell somatic recording from a motoneurone in current clamp mode and holding its membrane potential at -80, -70, -60 or -50mV. Steps of current of 5ms duration were used to elicit single action potentials on the rising phase of the voltage charging curve. This procedure was repeated at 1Hz for at least six records so that measurements of action potential properties could be averaged. Once control records had been recorded in low  $\text{Ca}^{2+}$  solution, 4-AP was added to the bath and the procedure was repeated.

For the analysis, records in which the membrane potential was not held within 4mV of the desired values were discarded. Threshold potential amplitude was determined as the difference between the baseline membrane potential and the foot of the action potential. The action potential amplitude was measured from the foot of the action potential to its peak. The total amplitude to the peak of the action potential was the sum of the threshold amplitude and the action potential amplitude.

#### *The Effect of 4-AP on Somatic and Dendritic Action Potentials*

To determine the effect of the A-current on the action potential, experiments were performed in which action potentials were recorded in the soma and dendrite in the presence and absence of 4-AP. Whole-cell electrodes were attached to the soma and dendrite of a motoneurone and action potentials were recorded in both electrodes with only the synaptic blockers CNQX (10 $\mu$ M), strychnine (10 $\mu$ M) and picrotoxin (100 $\mu$ M) included in the bath. Action potentials were recorded in current clamp mode with the membrane potential set to -65mV. Current steps of 5ms duration and of sufficient amplitude to generate a single action potential were injected into the cell through the somatic electrode and the action potential was recorded at both the soma and dendrite. The voltage in each electrode was sampled at 31.25KHz (32 $\mu$ s interval) and action potentials were elicited at 1Hz intervals. During recording, the polarity of the injected current was reversed for a few records so that the passive charging curve of the cell could be obtained. These were later averaged and the charging curves subtracted from the action potential

recordings so that the action potential waveform could be separated from the neurone's sub-threshold response. Once a control recording had been performed, action potentials were then recorded under  $\text{Ca}^{2+}$  channel blockade as described above. Blocking calcium currents was necessary to remove any confounding influence of the  $\text{Ca}^{2+}$  dependent potassium conductance on the action potential waveform. 4-AP was then added to the bath at a concentration of 4mM and somatic and dendritic action potentials were recorded again.

#### *Blockade of the A-current with Intradendritic 4-AP*

As a final attempt to determine if motoneurons have a different density of A-current in their dendrites to that in the soma, an experiment was performed in which 4-AP was included in the dendritic electrode solution at a concentration of 4mM. Although 4-AP is normally applied externally, Hille (1992) states that it is membrane permeable although there is no data to suggest just how membrane permeable this drug really is. Because of this property of 4-AP it was decided to try an experiment using intradendritic 4-AP. The rationale behind this experiment is that 4-AP diffusing from the dendritic electrode will cross the membrane to the external face and block dendritic A-currents. The dendritic A-currents will experience the highest concentration of 4-AP first and will be blocked before those in the soma are affected by 4-AP. If dendritic A-currents are present, then dendritic action potentials should show a change in width before those in the soma. As the 4-AP diffuses towards the soma, somatic channels will start to be blocked. Therefore, use of intradendritic 4-AP should show a difference in the time-course of change in action potential width between the dendrite and soma as the drug diffuses from the dendritic electrode tip towards the soma.

These experiments were performed in the presence of  $0\text{Ca}^{2+}/2\text{mMCo}^{2+}$  and  $300\mu\text{M Ni}^{2+}$  to remove any confounding effect of  $\text{Ca}^{2+}$  currents and the  $\text{Ca}^{2+}$  dependent potassium conductance.

## **Results**

### *Control Recordings at the Soma*

To ensure that the dendritic electrode capacitance could be adequately compensated, control recordings were performed in which both electrodes were placed on the soma of the cell. The result of an experiment of this kind is shown in figure 4.1. This shows a cell with two electrodes attached to the soma. One is a somatic electrode of  $4.6\text{M}\Omega$  resistance and the other is a high resistance electrode normally used for dendritic recording that had a resistance of  $10.2\text{M}\Omega$ . The action potentials shown in figure 4.1B superimpose perfectly indicating that the dendritic electrode capacitance could be adequately compensated. The somatic electrode capacitance could always be compensated with smaller capacitance

compensation than that required for dendritic electrodes. Also, in recordings where two somatic electrodes were placed on the soma, the current injecting and voltage recording electrodes could always be capacitance compensated to produce the same voltage waveform during various types of voltage and current manipulations.

To ensure that the action potential amplitude was not affected by prolonged whole-cell recording, an experiment was performed in which action potentials were recorded at the soma over an extended period without any pharmacological or electrophysiological manipulation of the cells. Whole-cell recordings were made from the soma of motoneurons in current clamp mode. Action potentials were elicited using 5ms current steps at a membrane potential of -65mV. This was repeated at 0.2Hz. The amount of current needed to reliably generate single action potentials varied from 0.5nA to 1.4nA. Action potential amplitude was measured from the foot of the action potential to its peak. This was then plotted as a function of time to see if there was any change in action potential amplitude with time. The results for three cells are shown in figure 4.2. Visual inspection of the traces shows that there is considerable variability in the amplitude of the action potential under control conditions, but that the average action potential amplitude does not change with time, indicating that prolonged whole-cell recording does not affect action potential amplitude. This procedure was successfully repeated in three cells that showed no change in access resistance, leakage current or capacitance compensation. The time over which the action potentials were recorded varied from 205 to 435 seconds.

Figure 4.3 shows examples of images taken during recording from the soma and dendrites of a spinal motoneuron. In each cell, there is an electrode attached to the soma, and also to a dendrite. These images give some idea of the difficulties involved in visualising these dendrites. As can be seen in both images, the single dendrite seen emanating from the soma of these cells can be followed for only a short distance before it can no longer be seen. No amount of focussing or adjustment of the IR-DIC optics could allow these dendrites to be visualised any further than about 50 $\mu$ m from the soma. It was rare to see more than one dendrite emanating from the soma of these cells.

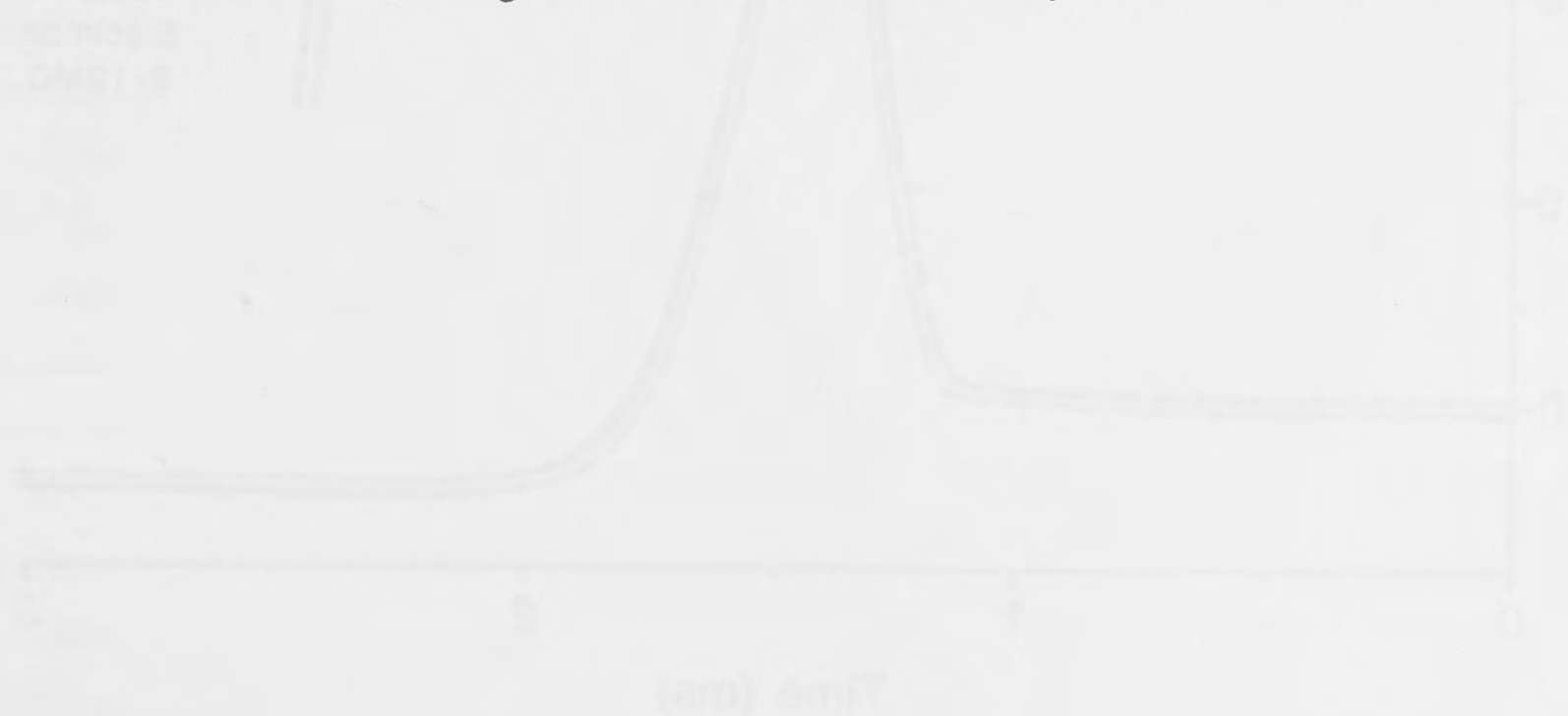
#### *Action Potentials in Soma and Dendrites*

Simultaneous recording of action potentials in the soma and dendrites of motoneurons under control conditions showed that there was some attenuation of action potential amplitude in the dendrites, even over the small distances at which these recordings were made from the soma. Typical action potentials from the soma and dendrites of motoneurons are shown in figure 4.4. The average amplitude of somatic action potentials was  $74.0 \pm 7.9$ mV (SD, n=9) while that of dendritic action potentials was  $65.9 \pm 6.5$ mV (SD, n=9). A Student's t-test of the amplitudes showed that they were significantly different at a confidence level of between 15 and 20% ( $t=0.978$   $v=16$ ). The

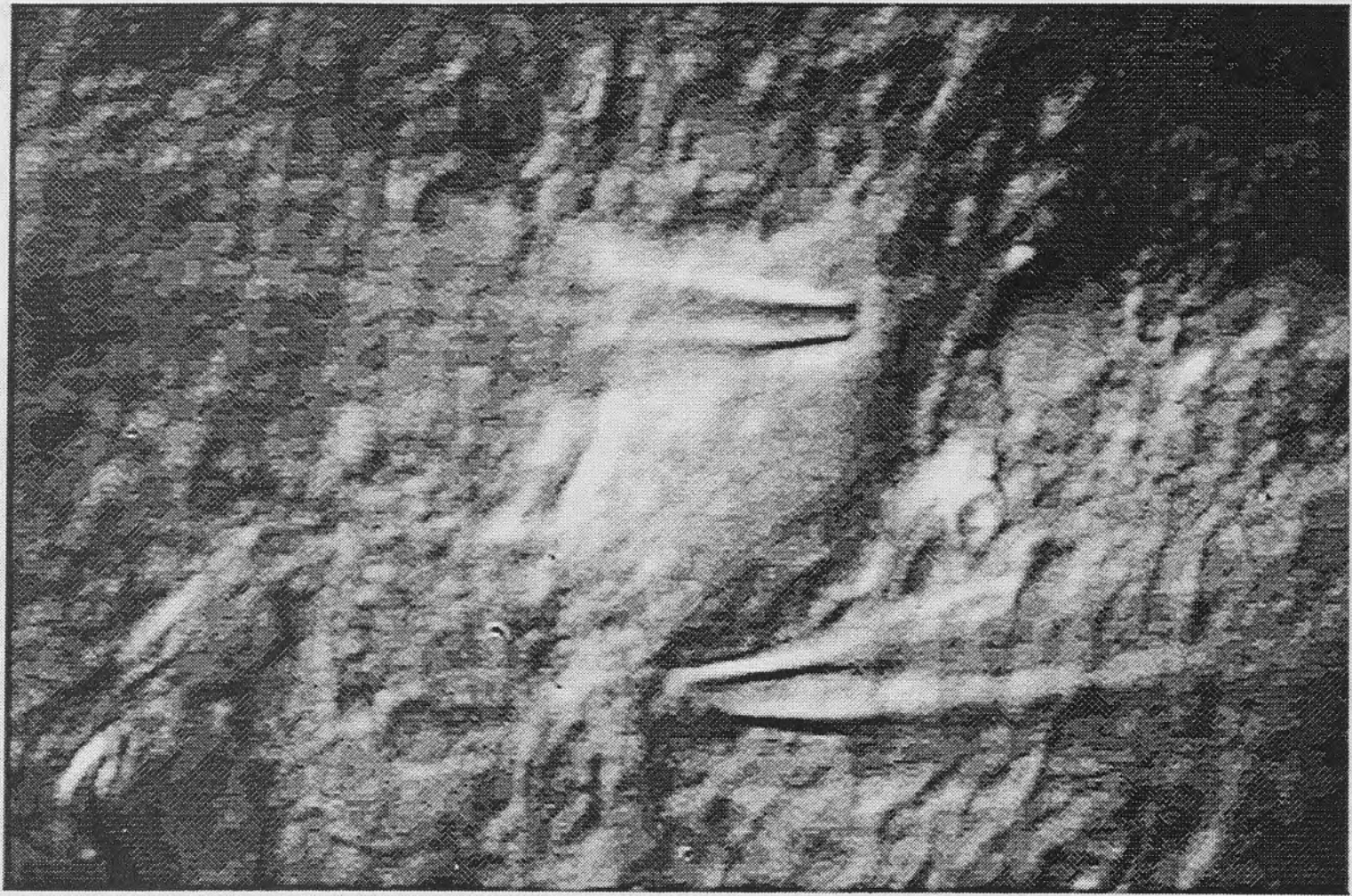
average attenuation from soma to dendrite was  $10.7 \pm 6.2\%$  (ratio of dendritic to somatic action potential amplitude =  $0.893 \pm 0.062$ ). The average distance at which the dendritic electrode was placed from where the dendrite emerged from the soma was  $37 \pm 8 \mu\text{m}$  (SD,  $n=9$ ).

#### *Time Differences Between Somatic and Dendritic Action Potentials*

Measurement of the time difference between the somatic and dendritic action potentials showed that the peak of the somatic action potential was always recorded before or simultaneously with the peak of the dendritic action potential, suggesting that the action potential is initiated in the soma before the dendrites. A recording from one cell showing temporal separation of the somatic and dendritic action potentials is shown in figure 4.5. It is possible that the action potential was initiated in a dendrite of the motoneurone and that the dendritic electrode was always attached to a different dendrite. This would result in action potentials that appeared to originate in the soma even though their true point of origin was a dendrite. However, there were no examples in which the dendritic action potential occurred before the somatic action potential ( $n=9$ ) and it is considered unlikely that I would not record from the active dendrite in a sample of nine cells. Because of the proximity of the dendritic recording to the somatic recording and the sample interval used in these experiments ( $32 \mu\text{s}$ ) the interval between the peak of the somatic and dendritic action potentials was averaged. The average temporal separation was  $54.4 \pm 45.6 \mu\text{s}$  (SD,  $n=9$ ) for electrodes separated by  $37 \pm 8 \mu\text{m}$  ( $n=9$ ). In some experiments, no temporal separation of the somatic and dendritic action potentials could be detected. Such small temporal separation of the two action potentials is to be expected when one considers the small separation of the electrodes in these experiments. Calculation of the velocity of action potential propagation in the dendrites gave  $0.68 \text{m/s}$ . This velocity is considerably faster than the  $0.24 \text{m/s}$  obtained for Purkinje cells by Stuart and Häusser (1994); comparable to the values of  $0.7\text{-}1.0 \text{m/s}$  obtained by Fatt (1957) and well within the range of  $0.213$  to  $0.96 \text{m/s}$  (average  $0.47 \pm 0.248 \text{m/s}$ ) obtained by Larkum *et al.* (1996).



A



B

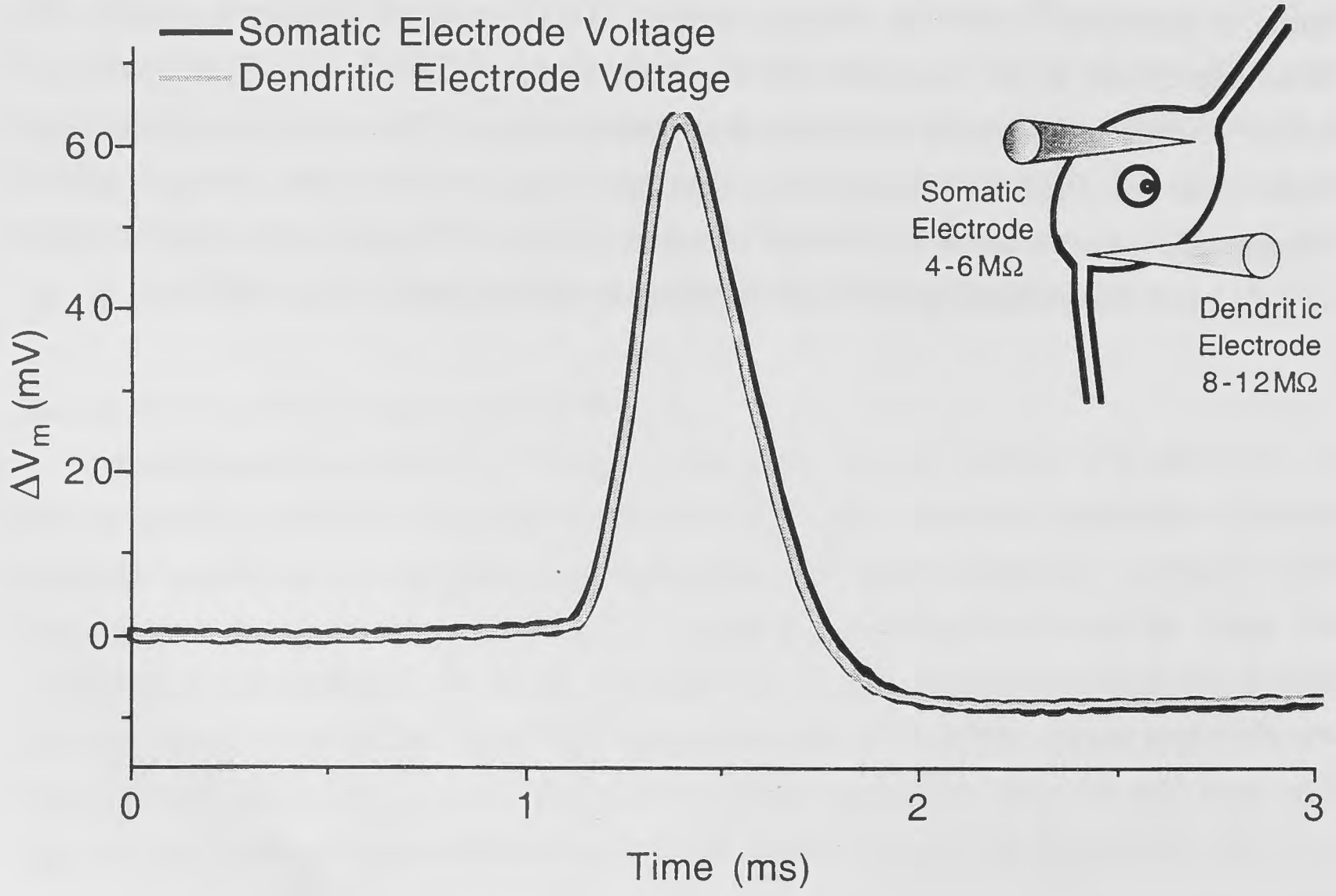
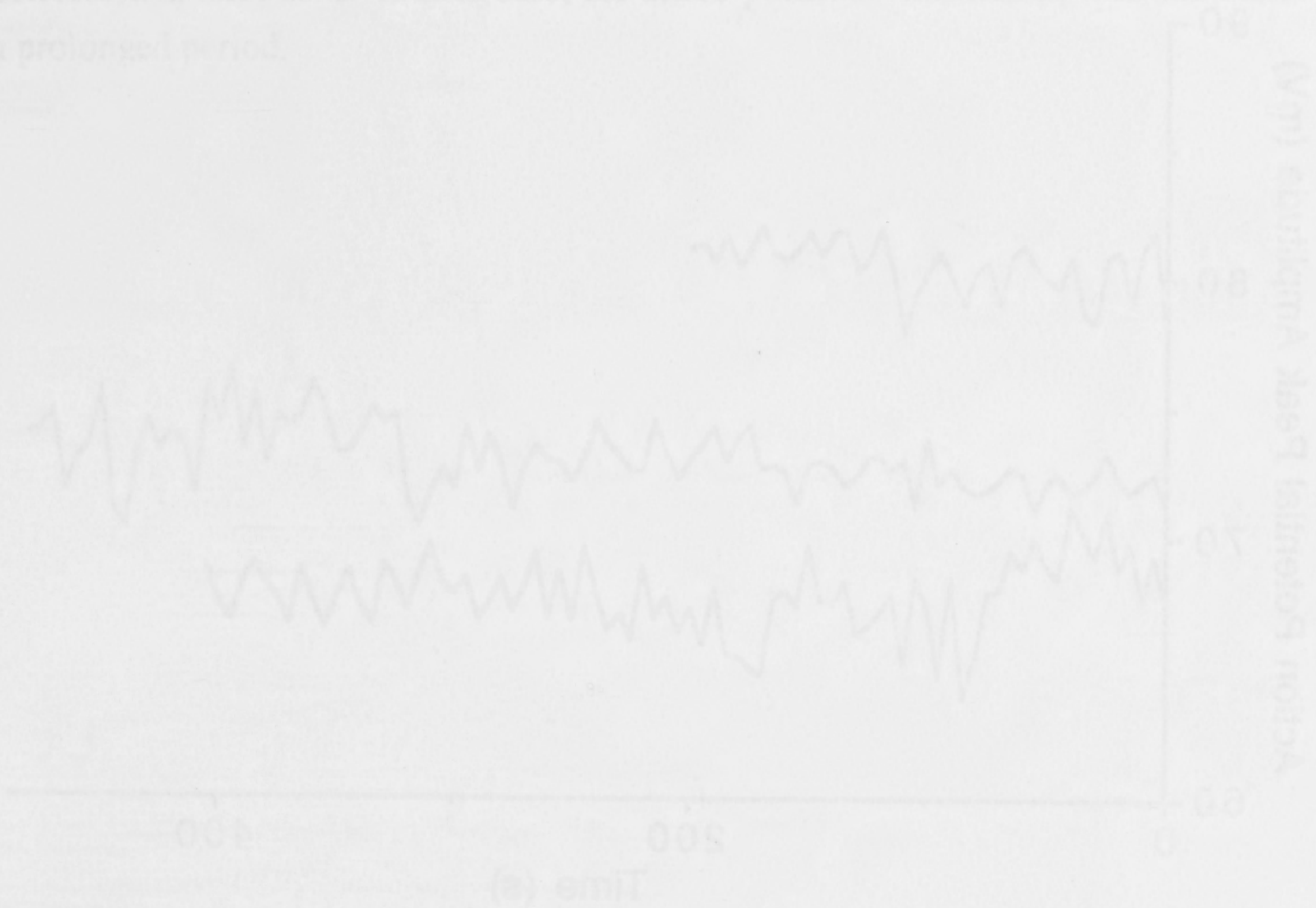


Figure 4.1. Dual somatic recordings. **A:** The soma of a cell with two electrodes attached, one a somatic electrode of  $4.6\text{M}\Omega$  resistance and the other an electrode normally used for dendritic recording with a resistance of  $10.2\text{M}\Omega$ . **B:** Action potentials recorded from the two electrodes. The inset shows the approximate position of the electrodes on the cell shown in A. The action potentials recorded in each electrode superimpose perfectly indicating that the dendritic electrode capacitance can be adequately compensated.



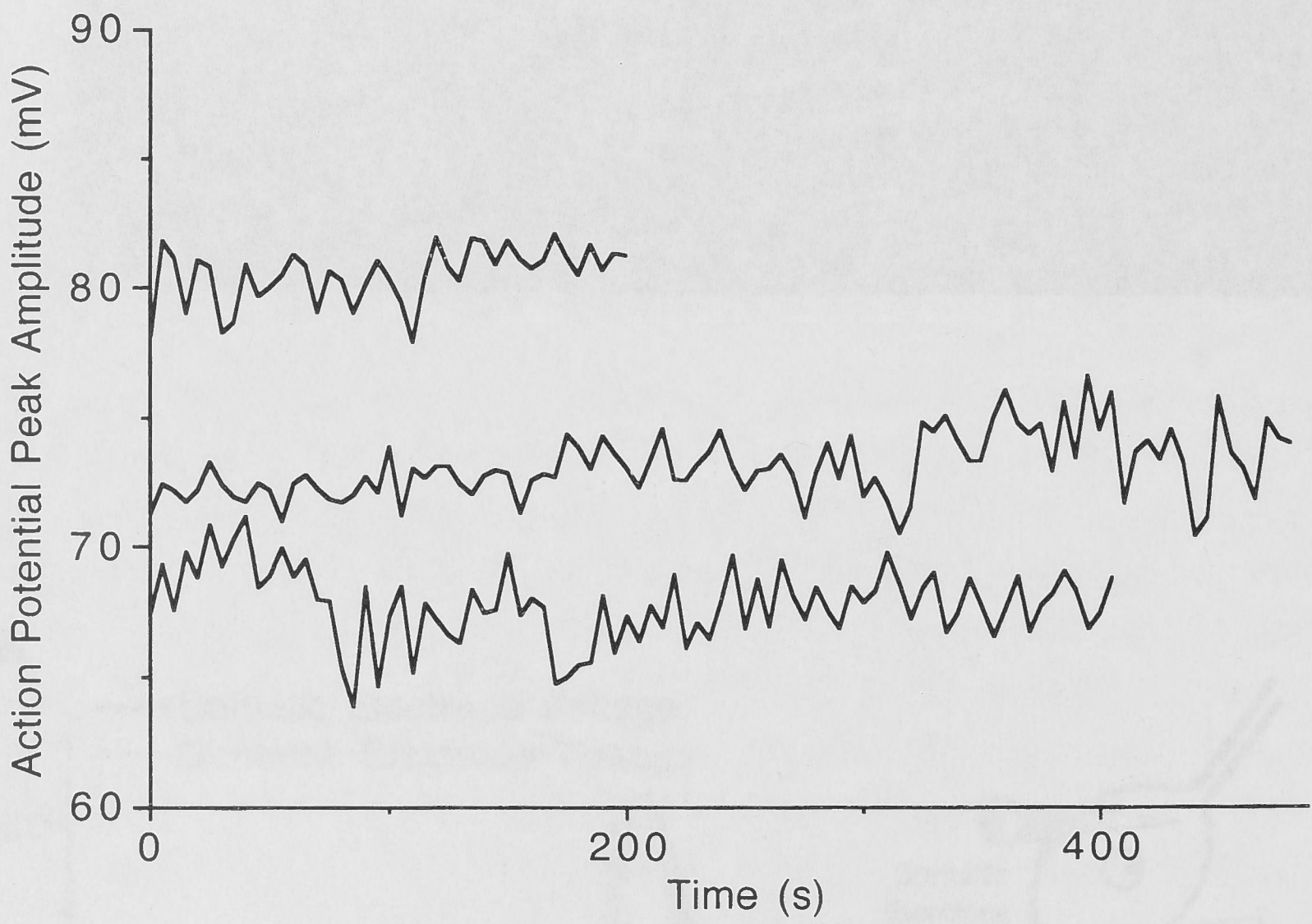


Figure 4.2. Action potential amplitude during prolonged whole-cell recording. This figure shows the action potential amplitude as measured from the foot of the action potential to the peak for three cells which did not show changes in access resistance, leakage current or capacitance compensation. These recordings were taken at 0.2Hz. This experiment was performed to assess whether diffusion of the electrode contents into the cell during whole-cell recording would affect the action potential amplitude. This was performed as a control for later experiments. Action potential amplitude varies by less than 5mV from one action potential to the next. Visual inspection of the amplitudes shows that the action potential amplitude does not change with time indicating that prolonged whole-cell recording does not affect action potential amplitude. This experiment was performed in three cells. In each case, the action potentials maintained their amplitude for a prolonged period.





20 $\mu$ m

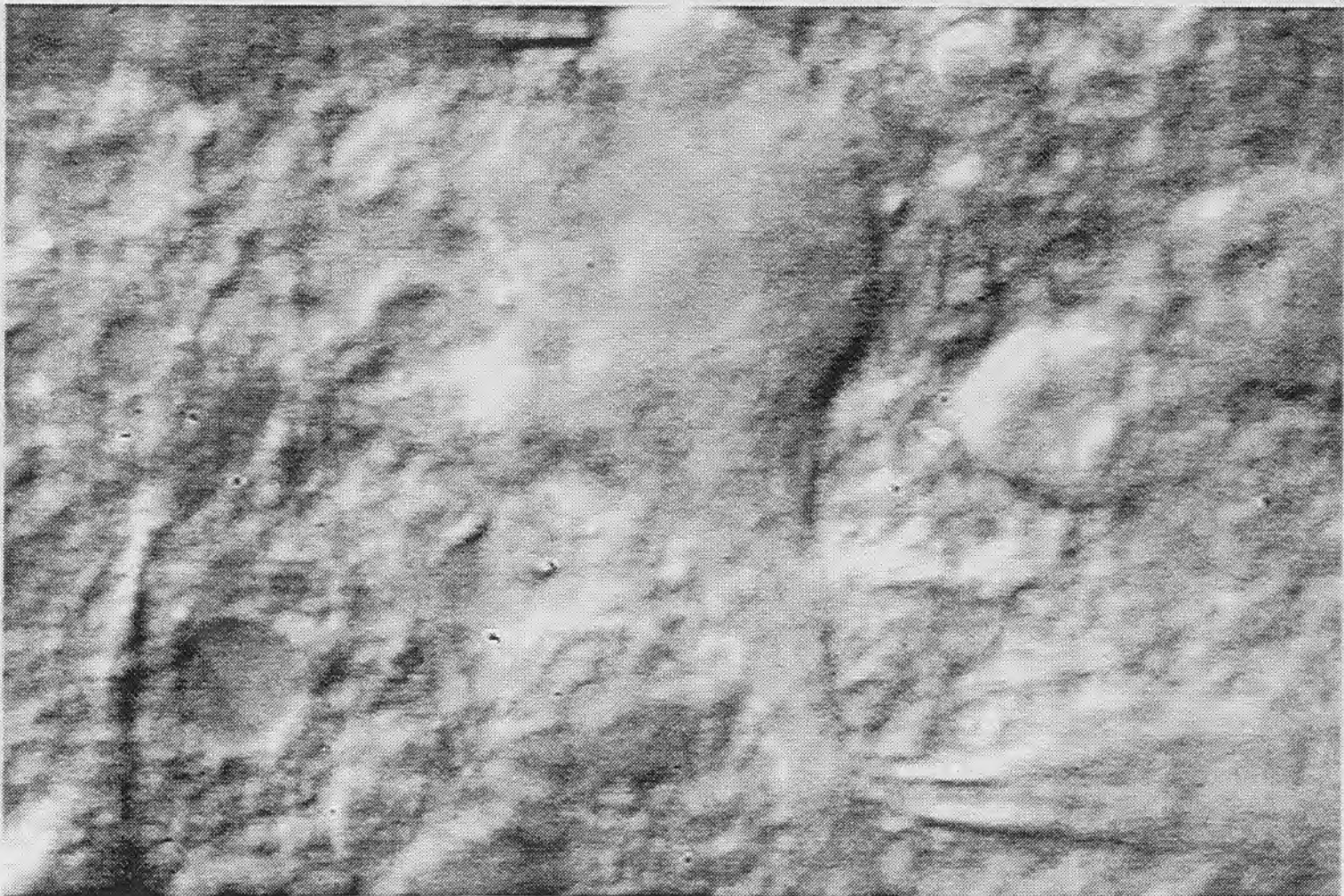
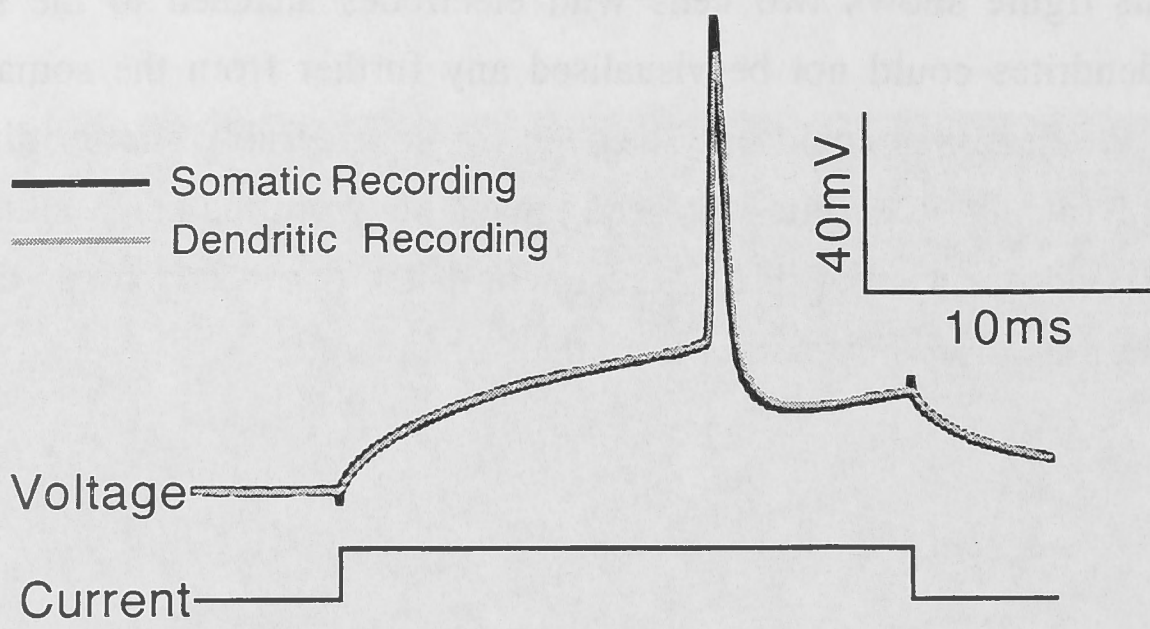


Figure 4.3. This figure shows two cells with electrodes attached to the soma and a dendrite. The dendrites could not be visualised any further from the soma than about  $50\mu\text{m}$  and often the dendrites could only be seen for considerably shorter distances than this. Usually only a single dendrite was seen emanating from the soma although in rare cases up to three dendrites were visible. Adjustment of the optics and focus did not allow the dendrites to be visualised any further from the soma than this.

The average membrane time constant ( $\tau_m$ ) of the recorded cells was  $10.5 \pm 1.5$  msec. The average membrane time constant ( $\tau_m$ ) of the recorded cells was  $10.5 \pm 1.5$  msec. The average membrane time constant ( $\tau_m$ ) of the recorded cells was  $10.5 \pm 1.5$  msec.



A



B

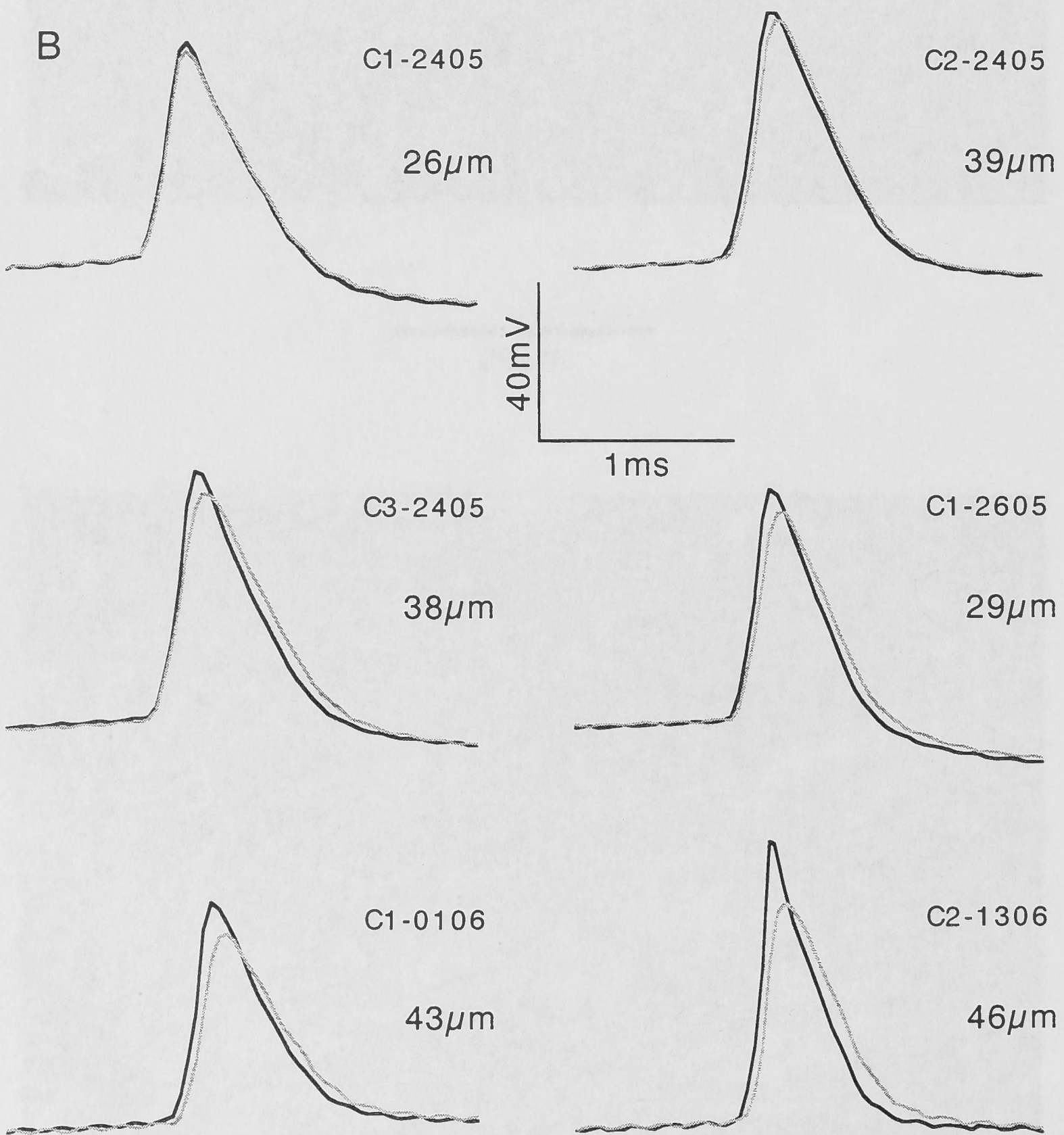
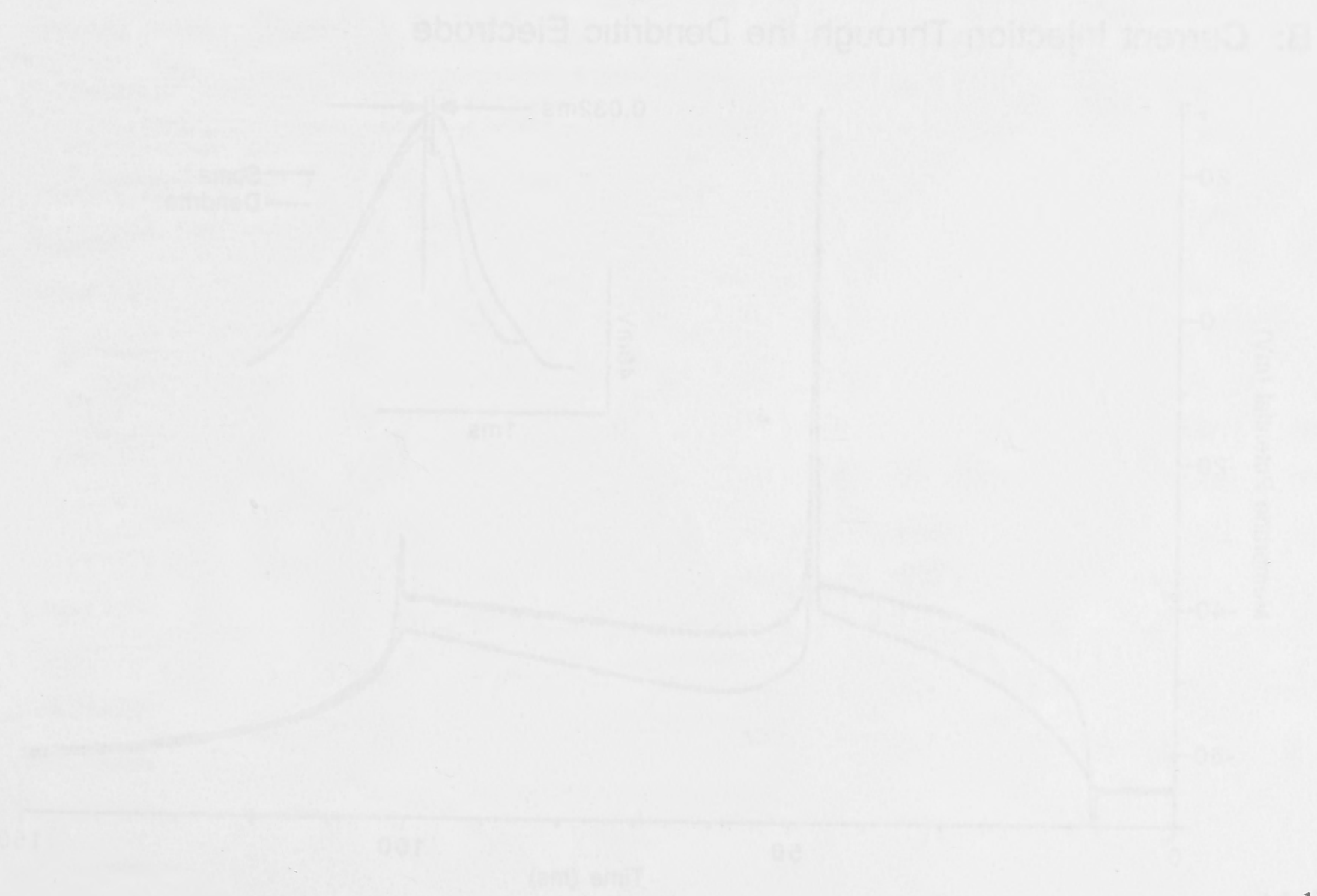
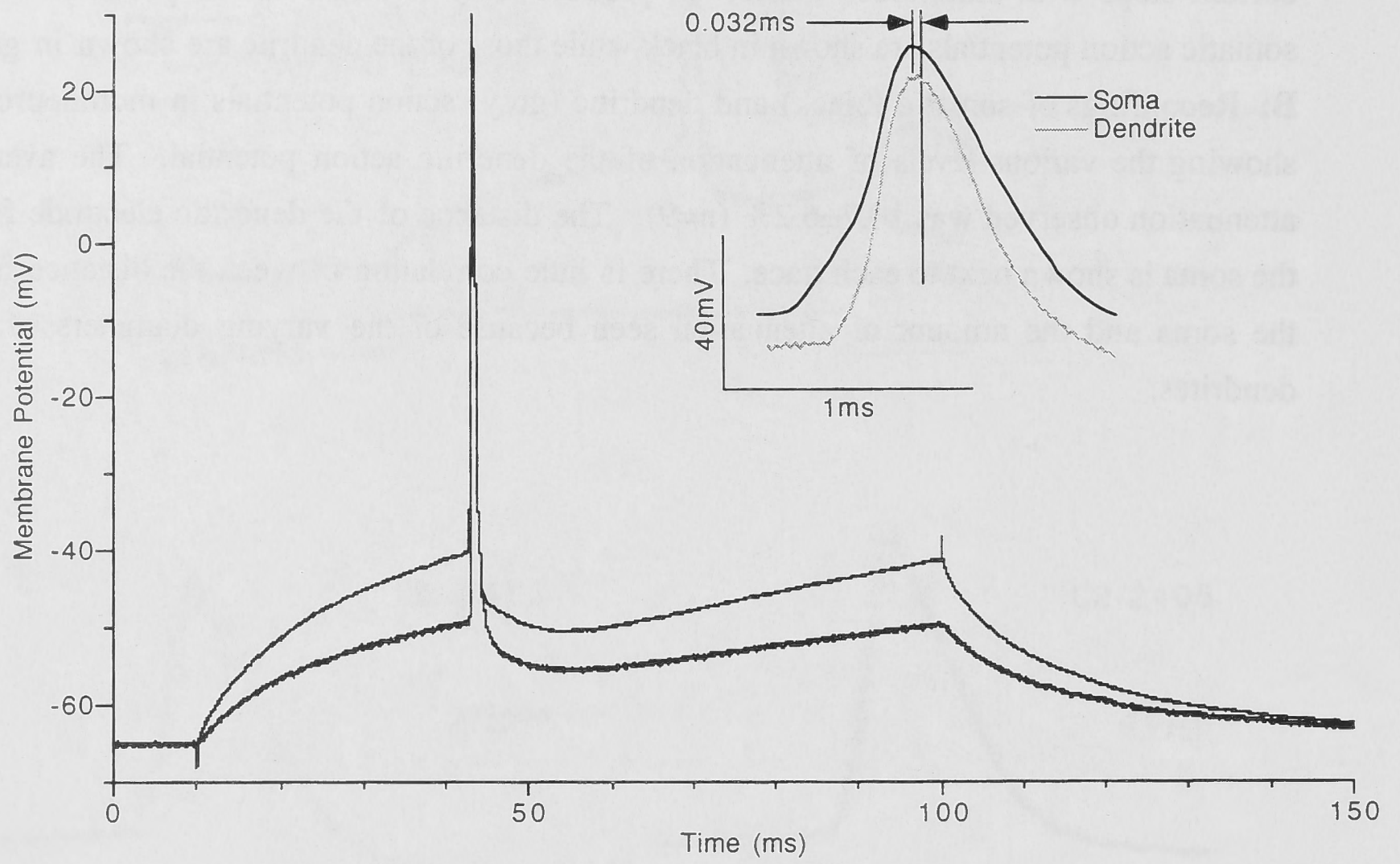


Figure 4.4. Action potentials recorded in the somata and dendrites of motoneurons. **A:** The protocol for production of action potentials in this experiment consisted of 20ms current steps with amplitudes chosen to produce only a single action potential. The somatic action potentials are shown in black while those of the dendrite are shown in grey. **B:** Recordings of somatic (black) and dendritic (grey) action potentials in motoneurons showing the various levels of attenuation of the dendritic action potential. The average attenuation observed was  $10.7 \pm 6.2\%$  ( $n=9$ ). The distance of the dendritic electrode from the soma is shown next to each trace. There is little correlation between the distance from the soma and the amount of attenuation seen because of the varying diameters of the dendrites.



### A: Current Injection Through the Somatic Electrode



### B: Current Injection Through the Dendritic Electrode

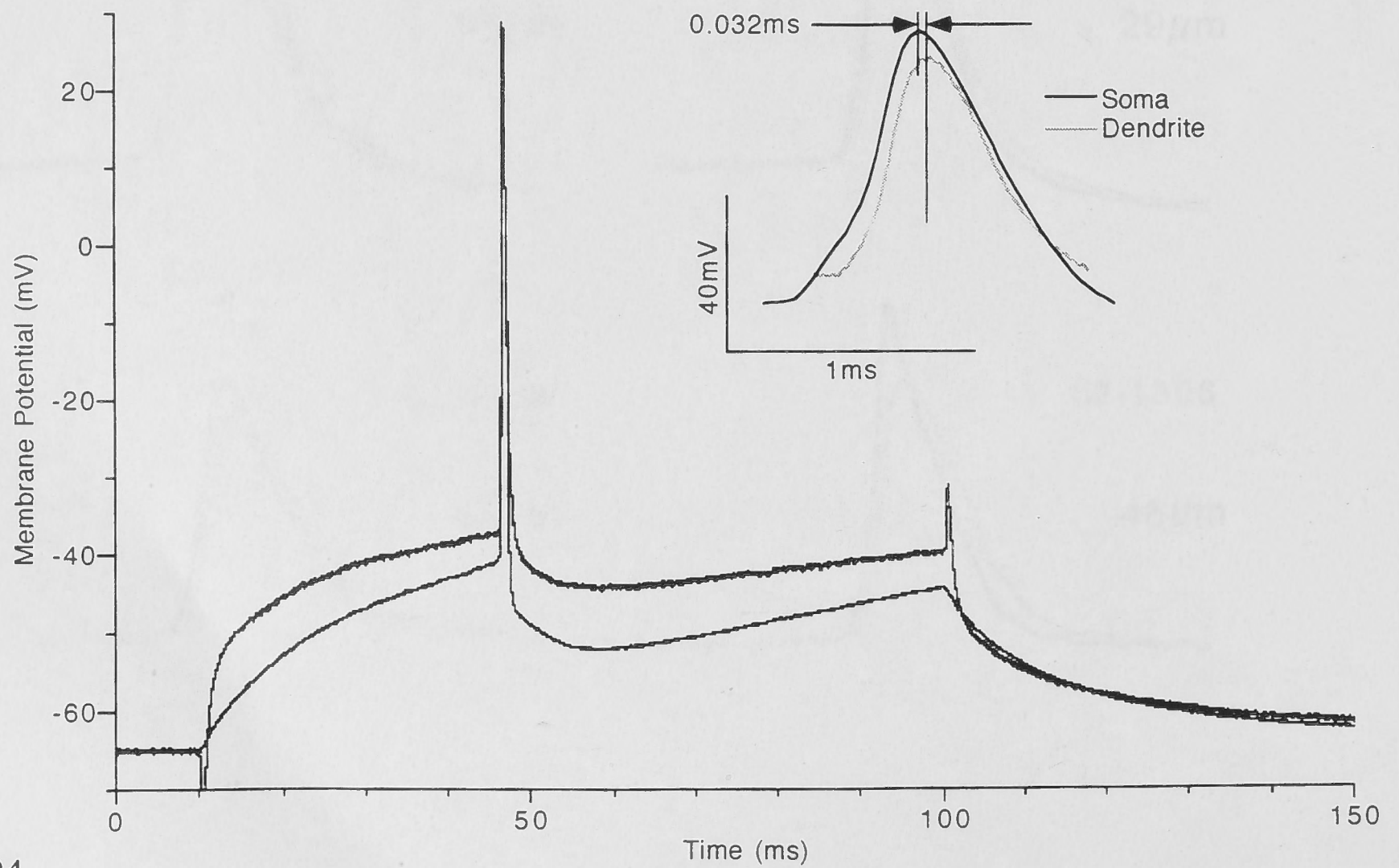


Figure 4.5. Temporal separation of the somatic and dendritic action potentials. **A:** Action potentials induced by current injection into the soma. The inset shows the action potentials on an expanded timescale. **B:** Action potentials induced by current injection in the dendrite. The inset shows the action potentials on an expanded timescale. The somatic action potential always occurs before the dendritic action potential regardless of the site of current injection. None of the cells examined (n=9) showed dendritic action potentials which occurred before the somatic action potential, suggesting that the site of action potential generation is close to the soma rather than in a dendrite.

### *Isolation of the A-current*

This experiment sought to demonstrate that an A-current could be recorded at the soma using only a somatic electrode. The voltage clamp protocol and the current recorded in one cell during this protocol are shown in figure 4.6A. There is a significant component of the delayed rectifier that is not blocked by 10mM TEA (Safronov & Vogel 1995) and this distorts the recording of the A-current. There is also significant distortion of the recording by capacitive transients and leakage current artifacts as well. In order to subtract away the capacitive transients, leakage currents and delayed rectifier, another voltage protocol was used to produce records suitable for subtraction. This protocol is shown in figure 4.6B. It is the same protocol that was used before, however the prepulse to -110mV is now only 100ms long and is followed by a 50ms step to -30mV. The potential and duration of this -30mV, 50ms prepulse were chosen to cause maximal inactivation of the A-current without any significant effect on the amount of activatable delayed rectifier (Hsiao 1998, Bekkers 2000a). As can be seen in the recordings in 4.5B, the traces no longer contain a component of the A-current and have only a delayed rectifier component and capacitive and leak artifacts. Subtraction of these traces using the procedure described in the methods revealed a family of A-currents that have increasing amplitude with increasing depolarisation. Examples of the current traces produced by this method are shown in figure 4.7A. This is the A-current. This experiment was performed on five different cells and gave similar results to those shown in figure 4.7A. The amplitude of the A-current increases as the test potential is depolarised (bottom trace=-60mV, top trace=+30mV) and the rise-time and decay-time decrease with increasing depolarisation. This procedure was repeated in five cells. For the largest and fastest A-current recorded (step from -110mV to +30mV), the average maximum current was  $1.30 \pm 0.49$  nA, the 10-90% rise-time was  $0.90 \pm 0.32$  ms and the decay time constant was  $5.12 \pm 1.34$  ms (SD, n=5). In the example shown in the figure, the peak of the A-current during the largest depolarisation (-110 to +30mV) occurs at 3.45ms. For the five cells examined, the average time to peak during the largest depolarisation was  $3.38 \pm 1.16$  ms. Conclusive proof that this current was the A-current was obtained by repeating the experiment during application of 4mM 4-AP to the tissue. An example of the subtracted current that is obtained after application of 4-AP is shown in figure 4.7B. 4-AP blocks the majority of the A-current. Washout of 4-AP and recovery of the A-current could not be performed because 4-AP did not wash out quickly enough for a satisfactory experiment of this kind to be performed. It should be noted that the current that is recorded under these non-isopotential conditions will be slower than that which would be recorded if the A-current could be perfectly clamped. Therefore these whole-cell A-current recordings do not represent the true kinetics and amplitude of the A-current.

### *Effect of 4-AP on Somatic and Dendritic Action Potentials*

Motoneurons are known to have a relatively high density of A-current, at least in their somata (Takahashi 1990, Safronov & Vogel 1995). Since the attenuation of the action potential that was seen in dendritic recordings was so small, I decided to examine the effect of blocking the A-current to see what contribution it made to the action potential waveform. Figure 4.8A shows a somatically and dendritically recorded action potential under control conditions. The separation of the electrodes in this experiment was  $32\mu\text{m}$  and the attenuation of the action potential from soma to dendrite was 6.4%. The increase in 20% width of the action potential was 3.9%. There was also a long lasting afterhyperpolarisation following the action potential that did not decay back to baseline during the 15ms interval of recording that followed action potential initiation. Figure 4.8B shows the effect of 0mM external  $\text{Ca}^{2+}$ /2mM  $\text{Co}^{2+}$  and  $300\mu\text{M Ni}^{2+}$  on the action potential waveform. The long lasting component of the afterhyperpolarisation caused by the  $\text{Ca}^{2+}$  dependent potassium conductance was removed and replaced with a short lasting afterhyperpolarisation that decayed back to the resting potential within a few milliseconds. During  $\text{Ca}^{2+}$  blockade, action potential amplitudes did not change from their values under control conditions although they were broadened by approximately 0.3ms (7.1%) at 20% of their peak amplitude due to removal of the repolarising influence of the  $\text{Ca}^{2+}$  dependent potassium conductance. The attenuation of the action potential was also increased to 13.6% in this particular example. Addition of 4-AP to the bath gave the data in figure 4.8C. The action potential width at 20% of its peak amplitude was increased by nearly five times from the value under control conditions and the afterhyperpolarisation was abolished. However the action potential amplitude was no different from that seen under control conditions. Action potential attenuation under these conditions was 8.9% for this cell and the increase in 20% width was 3.8%.

This experiment was repeated in a total of 8 cells for which stable recordings could be obtained. The results for all cells were similar and showed little effect of blocking the A-current on the action potential amplitude. Therefore, the data from all 8 cells was pooled. In this experiment, the average electrode separation was  $27.6\pm 6.2\mu\text{m}$  (SD, n=8). The average attenuation under control conditions was  $8.6\pm 5.3\%$  and the average difference in 20% width between soma and dendrite was  $3.9\pm 0.4\%$ . Under  $\text{Ca}^{2+}$  blockade the average attenuation was  $9.6\pm 5.4\%$  and the average 20% width difference between soma and dendrite was  $5.8\pm 0.5\%$ . Under 4-AP conditions the average action potential attenuation was  $9.2\pm 6.1\%$  and the 20% width difference between soma and dendrite was  $4.5\pm 1.6\%$  (SD, n=8). A Student's t-tests of the action potential amplitude attenuation under the various conditions showed no statistical difference between the various conditions.



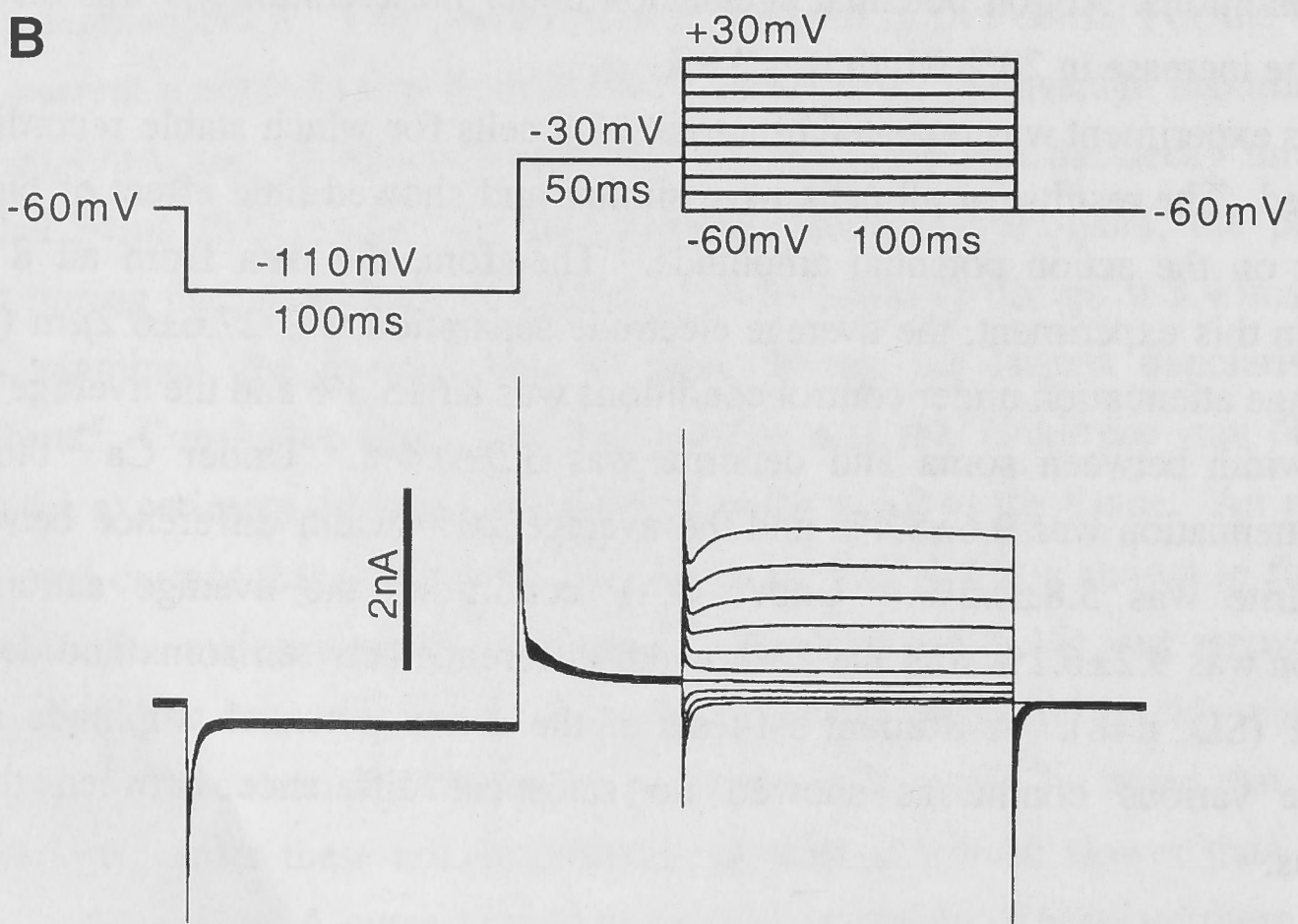
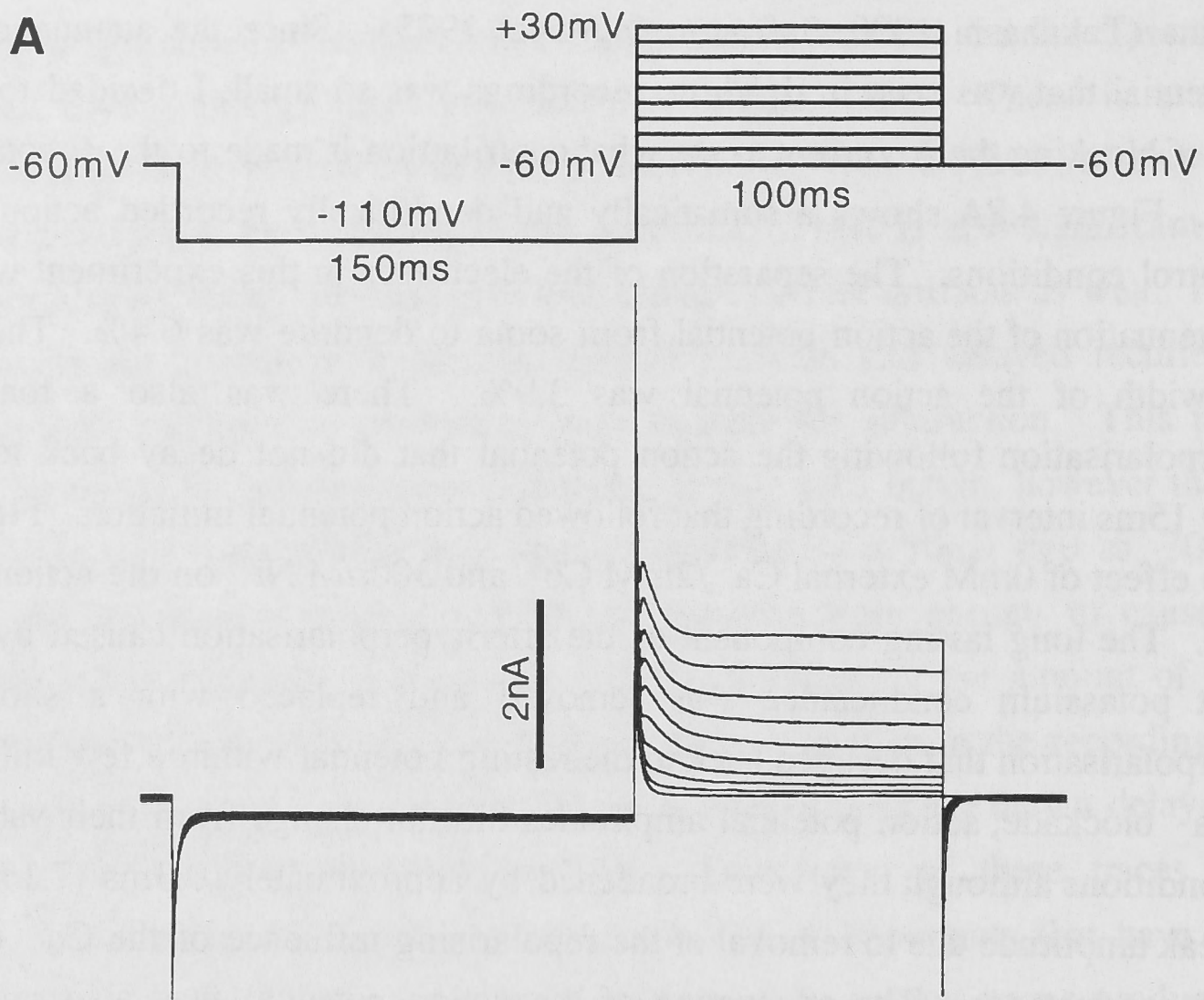


Figure 4.6. Voltage protocols for isolation of the A-current. **A:** The top trace is the voltage clamp protocol used for recording the A-current in motoneurons. It consists of a prepulse to  $-110\text{mV}$  for  $150\text{ms}$  followed by voltage steps to potentials ranging from  $-60\text{mV}$  to  $+30\text{mV}$  for  $100\text{ms}$ . The hyperpolarisation is used so that the maximum amount of A-current will be available for activation during the depolarising steps. The lower trace shows the current recorded in a single cell using the voltage protocol shown. Each trace shown in the figure is an average of 10 traces recorded in the cell. The traces show that an A-current is present but it is mixed with the delayed rectifier current. **B:** The top trace shows the voltage protocol used to produce recordings for subtraction. The protocol is the same as in A, except that the prepulse to  $-110\text{mV}$  is now only  $100\text{ms}$  long and is followed by a  $50\text{ms}$  step to  $-30\text{mV}$ . The step to  $-30\text{mV}$  was chosen to inactivate the A-current while leaving the delayed rectifier intact. The bottom trace shows the current recorded during this voltage protocol. The  $-30\text{mV}$  prepulse shows some A-current activity but this is inactivated by the time the various voltage steps are performed. The voltage steps from  $-60\text{mV}$  to  $+30\text{mV}$  show no A-current activity and the current recorded is purely capacitive artifact, leak and a component of the delayed rectifier. Subtraction of this trace from the trace in A, along with subtraction of the capacitive artifact associated with the  $-30\text{mV}$  prepulse, allowed full recovery of the A-current.



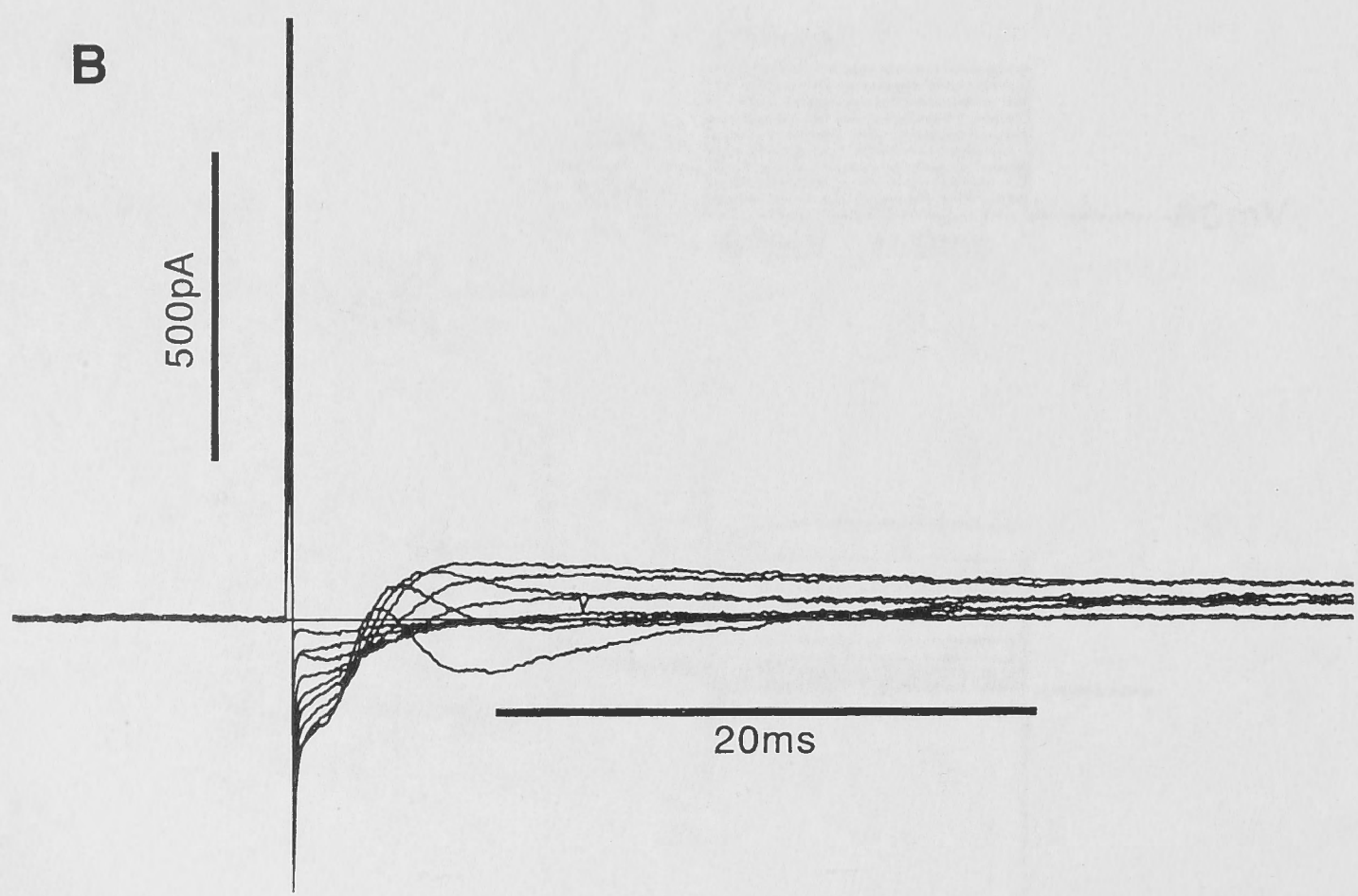
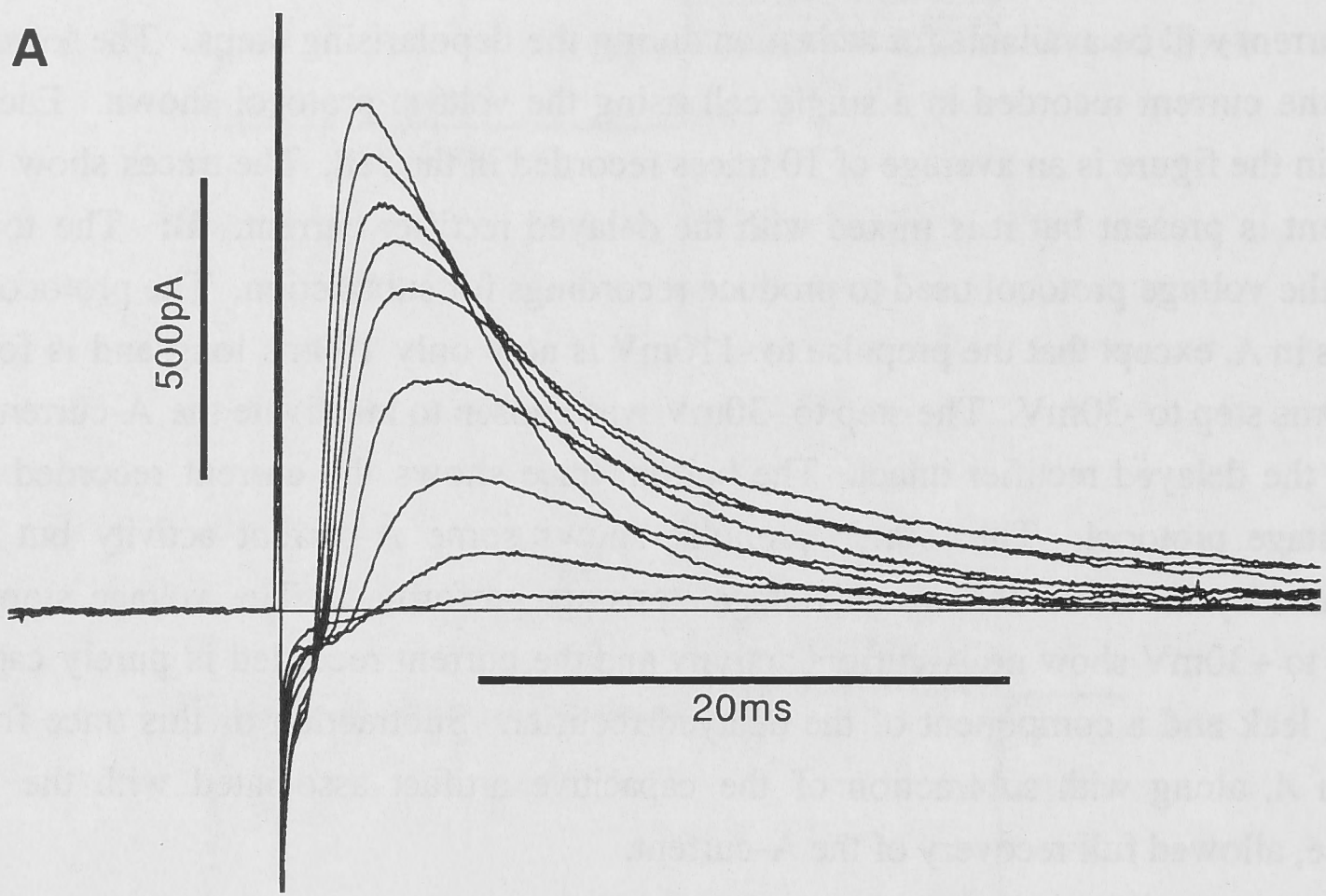


Figure 4.7. **A:** The A-current recorded from a single cell using the protocols shown in figure 4.6. The rise- and decay-times and the time to peak of the A-current decrease as greater depolarisation is used to activate the A-current. The amplitude of the current increases with progressively larger depolarisations as well. The time to peak for the largest, fastest current (voltage step from  $-110\text{mV}$  to  $+30\text{mV}$ ) is  $3.45\text{ms}$ . The peak current of this trace is  $0.85\text{nA}$  and the 10-90% rise-time and decay time constant are  $0.91\text{ms}$  and  $4.28\text{ms}$  respectively. **B:** The A-current recorded using the same protocols as in A, but now in the presence of  $4\text{mM}$  4-AP. The current is almost completely abolished by 4-AP. This conclusively demonstrates that the current is indeed the A-current. Reversal of the effect of 4-AP could not be achieved in these cells because of the long time needed to wash out 4-AP from the tissue.



Soma

Dendrite

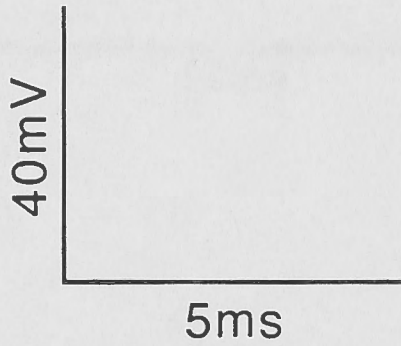
**A Control**

Electrode Separation =  $32\mu\text{m}$

Amplitude =  $78\text{mV}$   
20% width =  $0.49\text{ms}$

Amplitude =  $73\text{mV}$   
20% width =  $0.51\text{ms}$

**B  $\text{Ca}^{2+}$  blockers**



Amplitude =  $81\text{mV}$   
20% width =  $0.79\text{ms}$

Amplitude =  $70\text{mV}$   
20% width =  $0.85\text{ms}$

**C 4-AP &  $\text{Ca}^{2+}$  blockers**

Amplitude =  $79\text{mV}$   
20% width =  $2.27\text{ms}$

Amplitude =  $72\text{mV}$   
20% width =  $2.36\text{ms}$

Figure 4.8. **A:** Action potentials recorded in the soma and dendrite of a large ventral horn neurone under control conditions. The electrode separation is  $32\mu\text{m}$ . The attenuation of action potential amplitude from soma to dendrite was 6.4% and the difference in action potential width at 20% of its peak amplitude was 3.9%. **B:** Action potentials recorded in the soma and dendrite of the same cell as in A, but in the presence of  $0\text{mM Ca}^{2+}$ ,  $2\text{mM Co}^{2+}$  and  $300\mu\text{M Ni}^{2+}$ . The action potential attenuation was 13.6% and the difference in action potential width at 20% of its peak amplitude was 7.1%. **C:** Action potentials in soma and dendrite in the presence of  $\text{Ca}^{2+}$  blockers and  $4\text{mM 4-AP}$ . The attenuation of the action potential amplitude was 8.9% and the difference in 20% width was 3.8%. There was no significant difference in the attenuation of the action potential under the various conditions.

This experiment shows that the major role of the A-current in motoneurons is to repolarise the action potential. It is also an important contributor to the first few milliseconds of the afterhyperpolarisation. This experiment conclusively demonstrates that the A-current does not provide a large contribution to the action potential amplitude. The suggestion from the data is that the A-current does not significantly affect action potential amplitude because its kinetics are too slow for it to turn on in time to affect the peak of the action potential. Washout of 4-AP was not possible in these experiments so I could not try to reverse the effect of 4-AP. As can be seen in figure 4.8, there is no difference in the effect of 4-AP on the somatic and dendritic action potential. The afterhyperpolarisation is reduced at both locations and the action potential amplitude is attenuated by the same proportion as in control solution.

#### *Effect of Membrane Potential on Action Potential Amplitude*

Since the attenuation of the action potential amplitude that was seen in dendritic recordings was so small, especially considering that motoneurons are believed to contain a high density of A-type potassium current in their somata and perhaps their proximal dendrites as well (Takahashi 1990, Viana *et al.* 1993, Safronov & Vogel 1995), experiments were performed to determine why there was so little dendritic action potential attenuation. If a dendritic A-current is present in these cells, then I might expect a large attenuation of dendritic action potential amplitude. As a first test to examine the contribution of the A-current to the action potential waveform at the soma, experiments were performed in which action potentials were initiated from different resting membrane potentials. Cells were held at -80, -70, -60 or -50mV and 5ms pulses of current of sufficient amplitude to elicit a single action potential were applied. This procedure was repeated with and without 4mM 4-AP present in the bath.

The experimental results from a single cell are shown in figure 4.9. This shows the action potentials obtained at each of the four membrane potentials both before and during external application of 4mM 4-AP. Control records were recorded in the presence of  $\text{Ca}^{2+}$  blockers. In this particular cell, the threshold potential is the same regardless of the initial membrane potential (threshold=-42mV). This means that the amplitude of the charging curve needed to reach threshold increases in proportion with the increasing hyperpolarisation of the holding potential. The action potential amplitude in this cell is the same at each membrane potential indicating that changing membrane potential does not alter the amplitude of the action potential. Under 4-AP conditions, the action potential amplitude does not change, but in this particular cell, the threshold amplitude increases. In this cell, the leak current increased slightly in the presence of 4-AP and therefore more current was required to initiate an action potential. This result is not typical of the cells studied. Most showed little or no change in action potential amplitude and threshold

amplitude in the presence of 4-AP. The pooled data for all of the cells are shown in figure 4.10A. This plot shows the threshold amplitude, action potential amplitude and total amplitude for all the cells examined (n=9). This figure clearly shows that as the initial membrane potential is hyperpolarised, the threshold amplitude increases but action potential amplitude remains relatively constant. Therefore the majority of the change in total amplitude that is seen at each membrane potential is due to changes in threshold. Figure 4.10B shows the pooled data for action potential amplitude in the presence and absence of 4-AP on an expanded scale. There is relatively little difference in action potential amplitude at each of the different membrane potentials both under control conditions and in the presence of 4mM 4-AP. The maximum difference in action potential amplitude between the different membrane potentials is approximately 1mV. An analysis of variance of the action potential amplitudes under control conditions at each membrane potential could not reveal any significant differences between the amplitudes. Nor could an analysis of variance of the action potential amplitudes under 4-AP conditions at each membrane potential reveal any significant differences between the amplitudes. Figure 4.10B indicates that 4-AP increases action potential amplitude. A Student's t-test of the action potential amplitudes at each membrane potential under control and 4-AP conditions showed that the amplitudes were significantly different ( $p < 0.05$ ) except for the amplitudes at -60mV which were not significantly different ( $p > 0.25$ ). Therefore, it must be concluded that membrane potential does not alter action potential amplitude under either control or 4-AP conditions. However, 4-AP significantly increases action potential amplitude at each potential although the average increase is only about 4mV. Therefore, it is concluded that the A-current activates too slowly to be able to significantly affect the peak of the action potential but some A-current is activated by the time the action potential peaks and decreases its amplitude by a few millivolts.

#### *Blockade of the A-current Using Intradendritic 4-AP*

To determine if the dendritic density of  $I_A$  was different from that of the soma, experiments were performed in which the dendritic electrode contained 4mM 4-AP. The rationale behind this experiment is that 4-AP from the dendritic electrode will block the dendritic A-current before the 4-AP has time to diffuse to the soma and block the somatic A-current. Measurements of somatic and dendritic action potentials while the 4-AP filled electrode is attached to the cell should show an effect on the dendritic action potential before there is an effect at the soma. A simpler experiment would be to pressure eject 4-AP onto the dendrite while recording from both the soma and dendrite. However, the proximity of the dendritic and somatic recordings meant that any attempt to pressure eject 4-AP onto the dendrite would result in 4-AP also being ejected onto the soma and it was therefore impossible to selectively apply the 4-AP to the dendrite externally.



Before 4-AP

During 4-AP

-80mV

-70mV

-60mV

-50mV

50mV  
10ms

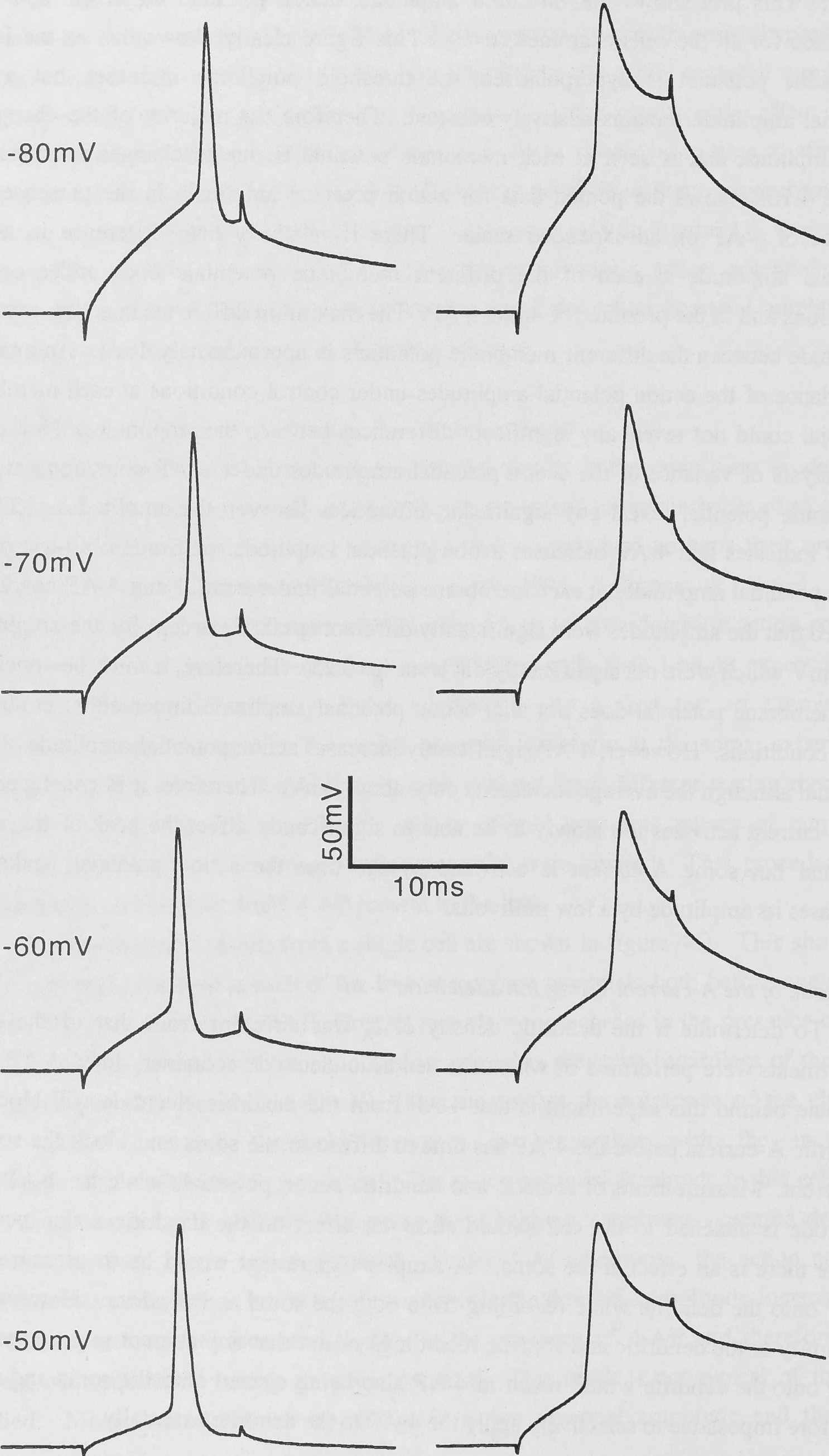


Figure 4.9. Action potentials elicited at various initial membrane potentials in the presence and absence of 4-AP. The four initial membrane potential values are indicated at the left. The left column shows action potentials in the presence of  $\text{Ca}^{2+}$  blockers but in the absence of 4mM 4-AP. Threshold membrane potential for initiation of action potentials remained relatively constant so that as the membrane potential is hyperpolarised, the amplitude of the charging curve increases. However, the amplitude of the action potential does not change. In the right column, the action potentials are elicited at the same membrane potentials as on the left but the bath now contains both  $\text{Ca}^{2+}$  blockers and 4mM 4-AP. The results are similar to those under control conditions except that the action potential is now prolonged. The threshold amplitude increases with hyperpolarisation while the action potential amplitude does not change. In this particular cell, the threshold amplitude is slightly increased in 4-AP over the control conditions because 4-AP increased the leakage current. The major affect of 4-AP that can be seen is that the repolarising phase of the action potential is greatly prolonged.



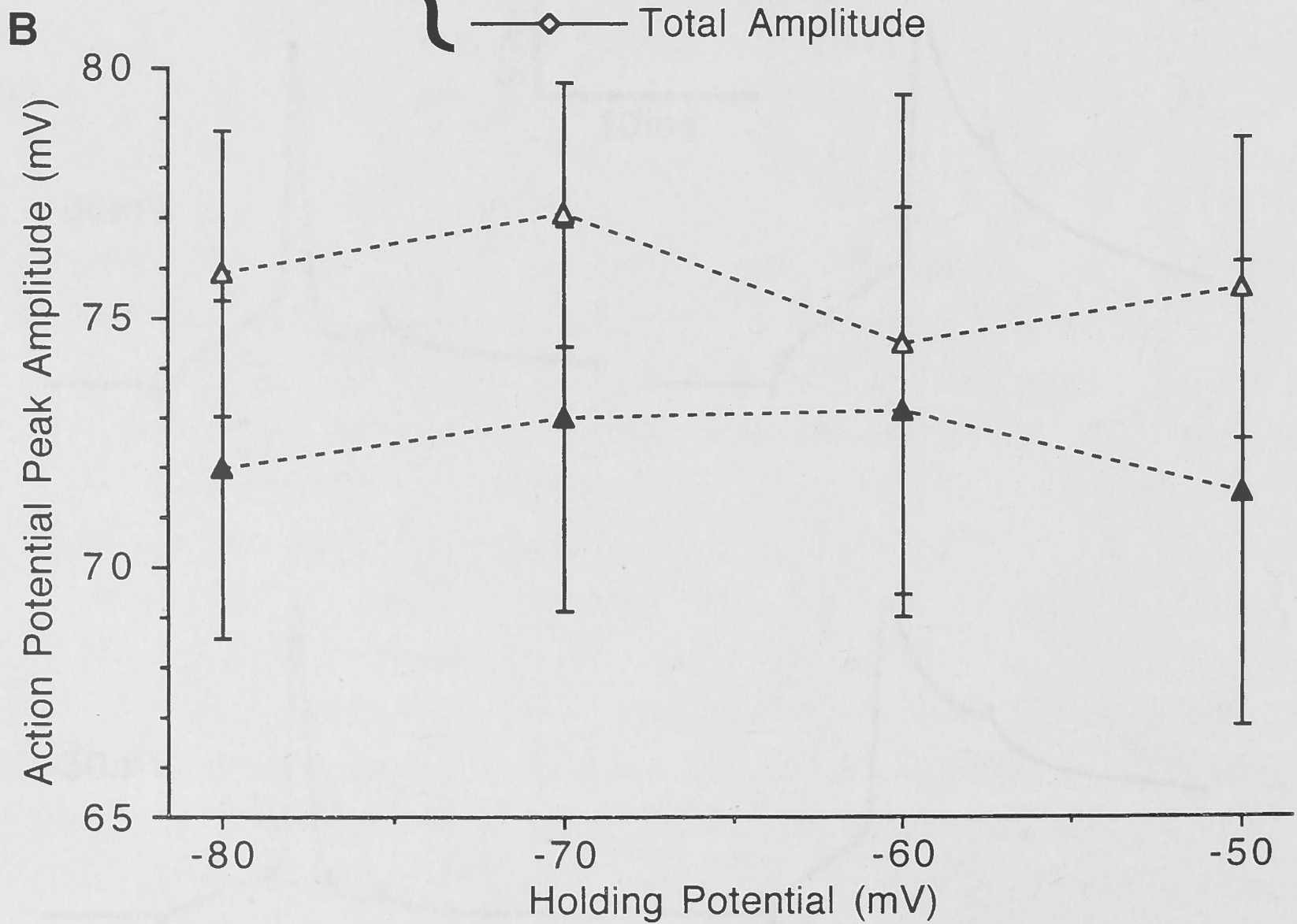
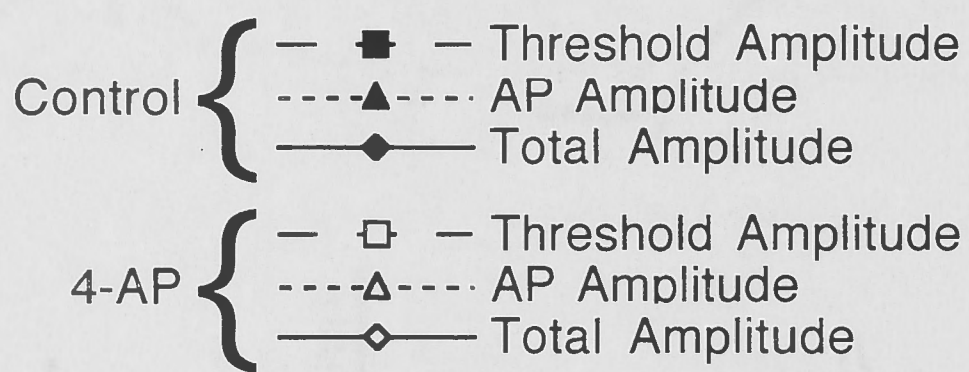
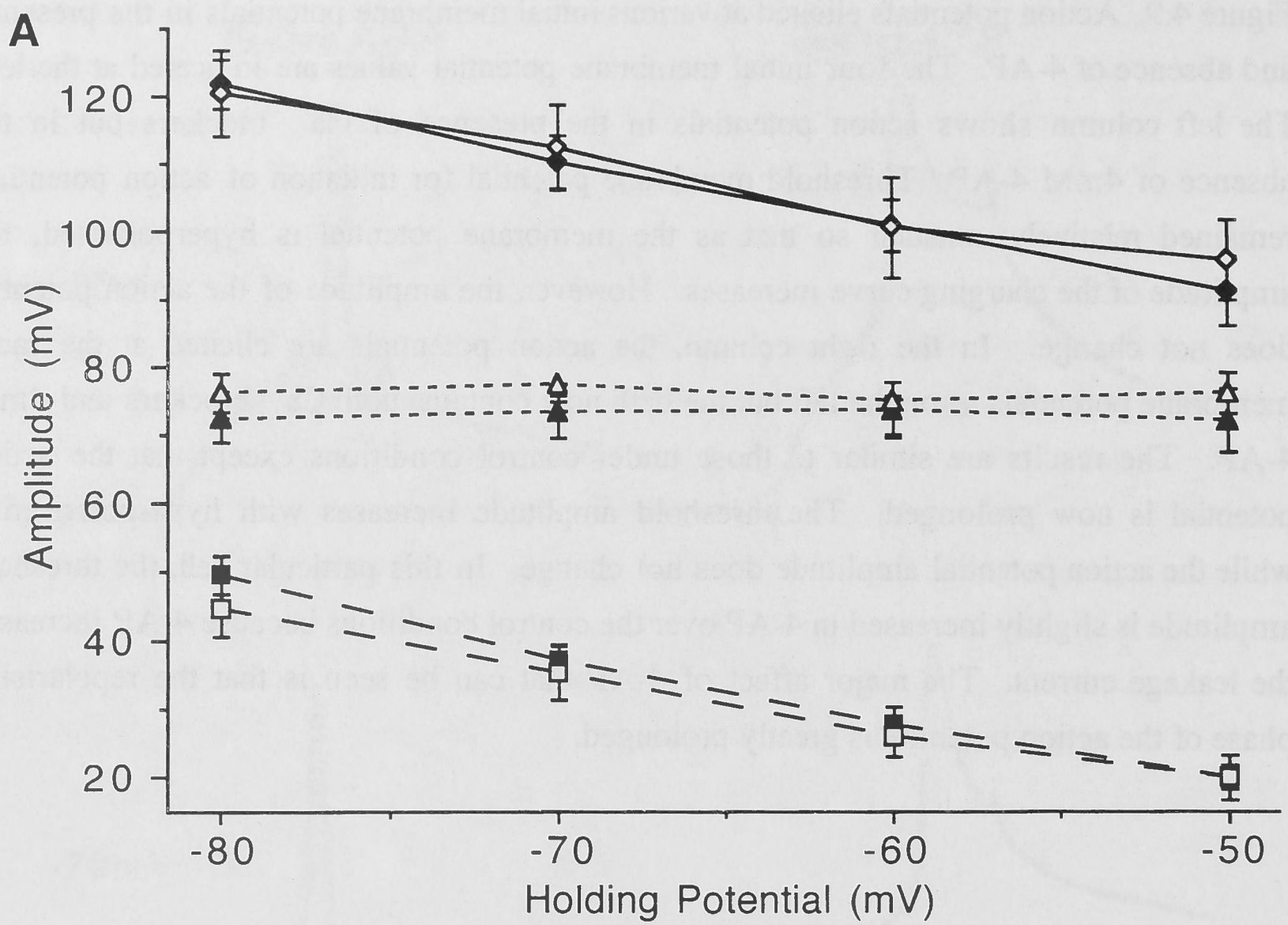


Figure 4.10. Threshold amplitude, action potential amplitude and total amplitude with and without 4-AP, plotted against initial membrane potential. **A:** This plot shows data pooled from nine cells. The solid lines are total amplitude, the short dashed lines are action potential amplitude and the long dashed lines are threshold amplitude. Threshold amplitude is measured from the baseline membrane potential to the foot of the action potential. Action potential amplitude was measured from the foot of the action potential to the peak. Total amplitude is the sum of the threshold amplitude and action potential amplitude. Closed symbols represent experiments performed in the presence of  $\text{Ca}^{2+}$  blockers only (control conditions) and the open symbols represent experiments in which 4mM 4-AP was added to the bath. The error bars represent the standard error of the mean. Total amplitude and threshold amplitude both increase with hyperpolarisation while action potential amplitude remains relatively constant. It is obvious from this result that changing initial membrane potential serves only to change the size of the charging curve needed to reach threshold. **B:** The action potential amplitudes under control and 4-AP conditions at each membrane potential on an expanded scale. The action potential amplitude does not change with alterations of the initial membrane potential, but 4-AP increases the action potential amplitude by approximately 4mV.

Figure 4.11 shows three cells in which this experiment was successfully performed. The somatic and dendritic action potential amplitude is stable throughout the recordings because these recordings do not have changes in the capacitance compensation, leakage current or access resistance. Action potential 20% width is already extended from that in control conditions because these experiments are performed in  $\text{Ca}^{2+}$  channel blocker solution ( $0\text{mM Ca}^{2+}/2\text{mM Co}^{2+}/300\mu\text{M Ni}^{2+}$ ). In these cells, the somatic and dendritic action potential width at 20% of its peak amplitude always changes at the same rate, indicating that 4-AP diffuses from the dendritic recording site to the soma very rapidly. The differences in the time over which the block occurs can be attributed to different rates of diffusion of 4-AP from the electrode tip into the dendrite, which in turn is related to the access resistance. These experiments sought to determine if the dendritic action potential would change its properties before the somatic action potential. Since no difference could be observed, no conclusion can be made about a possible difference in density of  $I_A$  in the soma and proximal dendrites of these cells.

## Discussion

The experiments described in this chapter were designed to determine if the A-type potassium conductance contributed to the backpropagated action potential amplitude in spinal motoneurons. Because blockade of the A-current altered both the somatic and dendritic action potentials, it was necessary to record both action potentials simultaneously to obtain meaningful data. I demonstrated that this was possible, and then used 4-AP and changes in membrane potential to investigate the role of the A-current on the backpropagation of the action potential.

### *Action Potential Decrement*

The average amount of action potential attenuation that was observed in these cells was  $10.7\pm 6.2\%$  with the dendritic electrodes placed at an average distance from the soma of  $37\pm 8\mu\text{m}$ . If this rate of attenuation were constant along the dendritic tree, then it would suggest total abolition of the action potential at about  $400\mu\text{m}$ . Larkum *et al.* (1996) have performed a similar experiment in cultured motoneurons and were able to record from dendrites up to  $423\mu\text{m}$  from the soma. They found relatively little decrement in action potential amplitude and sometimes no decrement at all for distances up to more than  $100\mu\text{m}$  from the soma. They also provided conclusive proof that in some dendrites of cultured motoneurons, the action potential is actively backpropagated and that  $\text{Na}^+$  channels are responsible for boosting the action potential. Optical recording of action potential backpropagation showed that the amplitude decrement was not uniform in all dendrites. This suggested that  $\text{Na}^+$  channels are not uniformly distributed in the dendrites of the motoneurone, although this may be an artifact introduced by cell culture. The action

potentials recorded by Larkum *et al.* (1996) at 50 $\mu$ m from the soma have a similar amplitude to the action potential amplitudes recorded in this Chapter.

A simple experiment to determine if Na<sup>+</sup> channels are responsible for action potential amplification in the dendrites would be to externally apply TTX to the cell and apply the action potential waveform as a voltage clamp at the soma. The problem with this experiment is that the voltage produced by such a voltage clamp does not faithfully reproduce the voltage distribution that is produced during an action potential. The action potential is generated by conductance changes rather than a voltage clamp. Therefore the current produced during an action potential under voltage clamp will not be the same as the current produced by voltage-dependent conductances during an action potential and the channel activation that occurs will not be the same as that which occurs during an action potential.

#### *Initiation Site of the Action Potential*

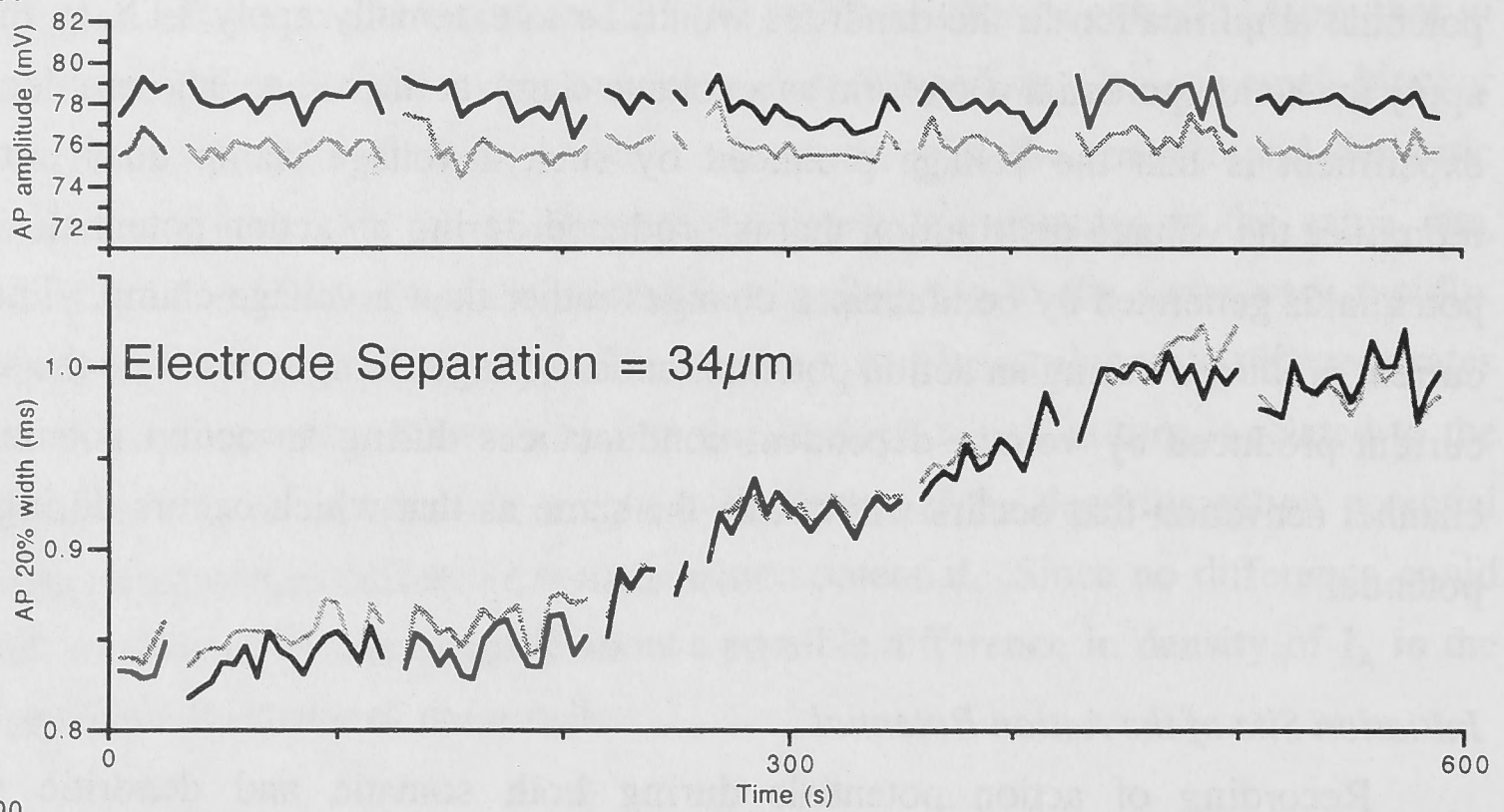
Recording of action potentials during both somatic and dendritic stimulation invariably produced action potentials that peaked in the soma before the dendrite. This is consistent with the data of Larkum *et al.* (1996). This suggests that the action potential in the motoneurone is initiated at or near the soma. Larkum *et al.* (1996) have demonstrated that action potentials may be initiated in the distal dendrites of cultured motoneurons, however these potentials are mediated by Ca<sup>2+</sup> channels and have different kinetics to the Na<sup>+</sup> action potential.

#### *The A-current in the Motoneurone*

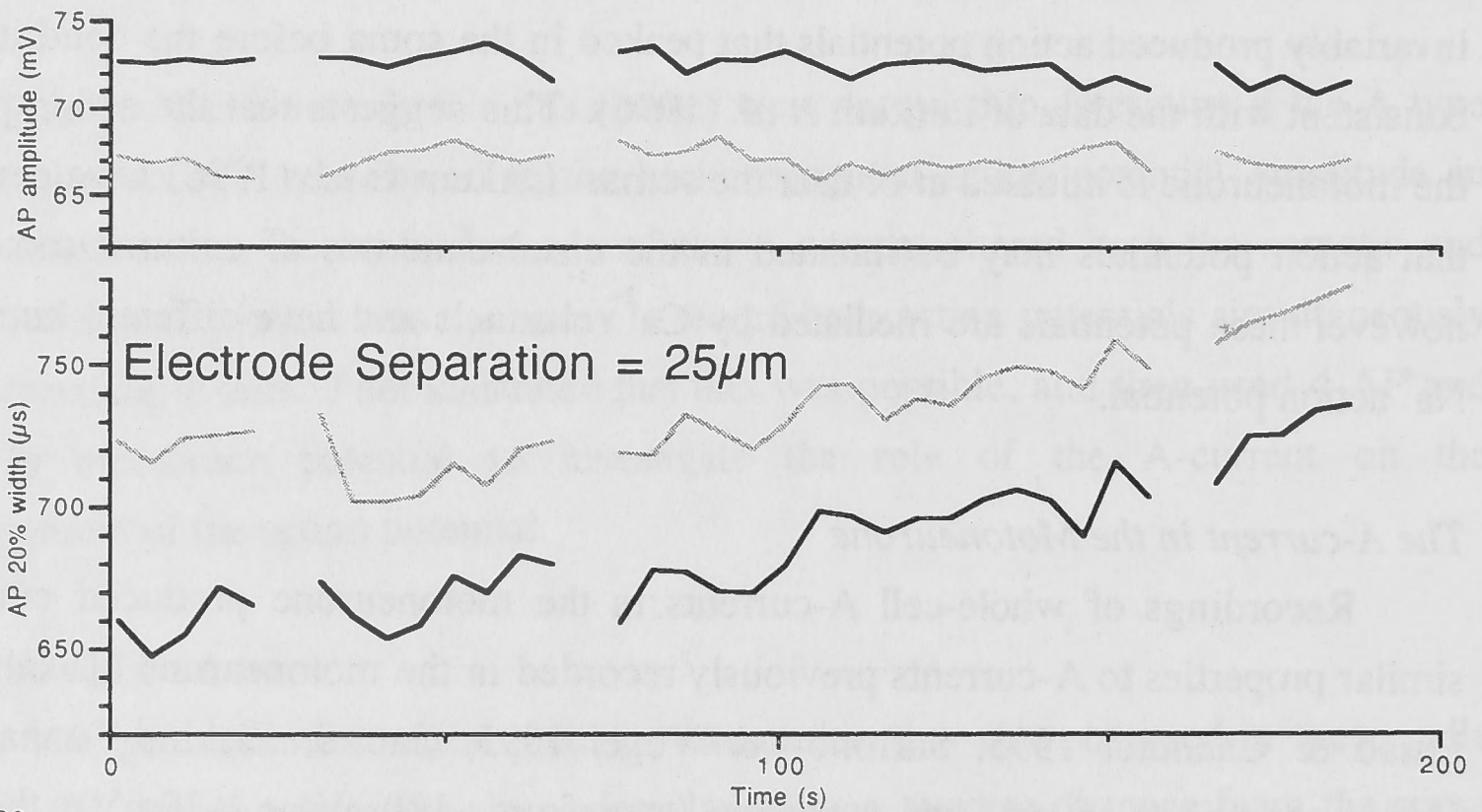
Recordings of whole-cell A-currents in the motoneurone produced currents with similar properties to A-currents previously recorded in the motoneurone (Takahashi 1990, Hsiao & Chandler 1995, Safronov & Vogel 1995, Gao & Ziskind-Conhaim 1998). Under conditions of maximal activation (step from -110mV to +30mV), the recorded current reached its peak at 3.38 $\pm$ 1.16ms and had a decay time constant of 5.12 $\pm$ 1.34ms. This is considerably slower than the whole-cell A-current recorded by Gao and Ziskind-Conhaim (1998) but similar to that obtained by Hsiao and Chandler (1995) and Takahashi (1990). This current could be largely blocked by external application of 4-AP providing conclusive evidence that this current was the A-current. Because of the non-isopotential conditions under which this current was recorded, the time-course of the current is prolonged relative to that which would be recorded if the current could be properly clamped. The kinetics of the current at an individual point on the neurone will therefore be

— Soma  
- - - Dendrite

C2-24/5/00



C1-24/5/00



C1-26/5/00

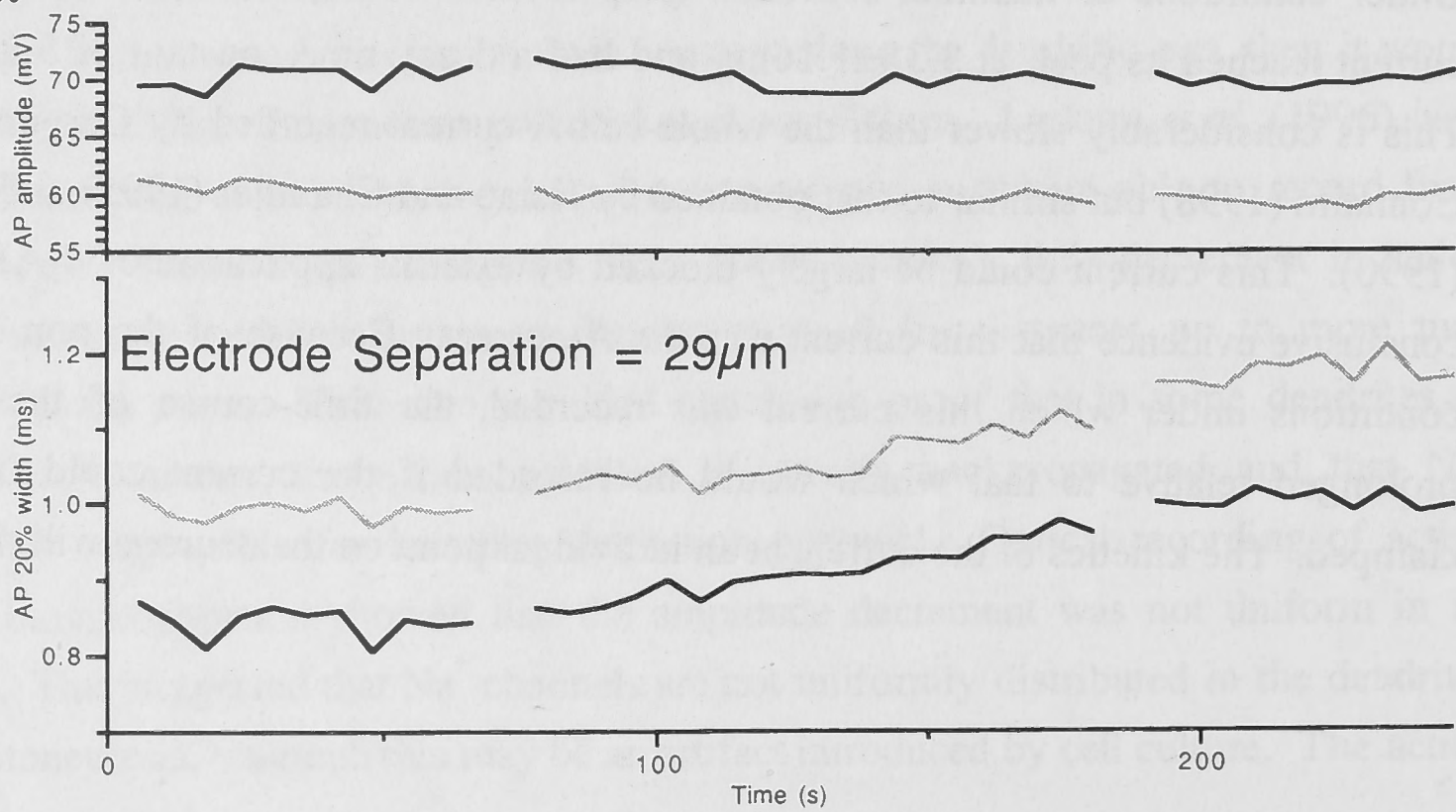


Figure 4.11. Action potential amplitude and 20% width during intradendritic application of 4-AP. This figure shows three cells in which somatic and dendritic action potential recordings were made while the dendritic electrode contained 4mM 4-AP. The top traces for each cell are the action potential peak amplitude and the bottom traces are the action potential width at 20% of its peak amplitude. Traces in black represent recordings at the soma and those in grey are those recorded from the dendrite. Breaks in the plots represent short breaks in the recording. In each case, action potential amplitude is relatively constant during the recording. The action potential 20% width however, increases with time because of blockade of  $I_A$  by 4-AP. There is no difference in the time-course of the increase in action potential width at either location.



considerably faster than that recorded here. It should be remembered however, that when an action potential invades the soma, it will also change the voltage in other non-isopotential regions of the neurone and therefore the A-current experienced by an action potential will have a similar time-course to that recorded here. Therefore, although the A-current may activate rapidly during fast depolarisations, the action potential may not induce such a rapid A-current because of the non-isopotential distribution of the action potential in the axon, soma and proximal dendrites.

#### *The Effect of 4-AP on Action Potential Waveform*

Experiments in which the A-current was blocked revealed that the A-current provides only a few millivolts contribution to the amplitude of the action potential in both the soma and dendrite (see figs 4.8 and 4.10). There were variations from cell to cell however, but the results were consistent for all cells. Any variations are considered to be random errors caused by differences between cells rather than any particular populations of cells with different properties. This result is consistent with previous studies that have used 4-AP at a concentration of up to 5mM to block the A-current (Takahashi 1990, Hsiao & Chandler 1995). The major function of the A-current in the motoneurone, as judged from these experiments and those of previous workers (Takahashi 1990, Viana *et al.* 1993, Hsiao & Chandler 1995), is to repolarise the action potential. Viana *et al.* (1993) have shown that the  $\text{Ca}^{2+}$  dependent potassium conductance is important for regulating the firing rate of motoneurons. Application of  $\text{Ca}^{2+}$  blockers to motoneurons blocked the  $\text{Ca}^{2+}$  dependent potassium conductance, abolishing the long lasting afterhyperpolarisation leaving only a fast afterhyperpolarisation (figure 4.8). This resulted in action potentials that were prolonged by approximately 7% at 20% of their peak amplitude. Application of 4mM 4-AP to the cells revealed the contribution of the A-current to the action potential waveform. The action potentials broadened by five times and the fast afterhyperpolarisation was removed. There was only a small effect of either  $\text{Ca}^{2+}$  blockers or 4-AP on the amplitude of the action potential. This provides conclusive evidence that the A-current affects action potential amplitude in motoneurons, but only by a few millivolts. The fact that the somatic action potential is relatively unaffected by 4-AP suggests that the kinetics of the A-current are too slow to allow it to significantly affect the action potential amplitude. It is also possible that the amplitude of the A-current is much smaller than that of the  $\text{Na}^+$  current and so even if the kinetics were faster, the small amplitude of the A-current in would not significantly alter the action potential amplitude. 4-AP did not affect dendritic action potential amplitude differently to the soma and this suggests again that the kinetics of the A-current are too slow to significantly affect the dendritic action potential amplitude or that the amplitude of the current is small compared to the  $\text{Na}^+$  current. It would be interesting to examine the effect of 4-AP on backpropagated action potentials at locations further out on the dendritic tree where the

slower time-course of the dendritic action potential may allow the action potential to be more heavily attenuated by the A-current.

#### *Effect of Intradendritic 4-AP on Somatic and Dendritic Action Potentials*

The attempt to block dendritic A-currents with intracellularly applied 4mM 4-AP was not entirely successful. 4-AP is a membrane permeant drug (Hille 1992), however the permeability is relatively low. For this experiment to be successful, the diffusion of 4-AP across the membrane must be as fast or faster than the diffusion from the dendritic electrode tip to the soma. The time-course over which A-current block is observed is prolonged over a period varying from 205 to 435 seconds (fig 4.11). It was not certain during this experiment just how fast the 4-AP diffused from the dendritic electrode to the soma. In figure 8 of Larkum *et al.* (1996), an experiment is shown in which QX-314 is applied through a dendritic electrode and the effect on somatic and dendritic action potentials is observed. The maximal effect of QX-314 on the somatic action potential amplitude was seen within 6.5 seconds with the dendritic electrode placed 138 $\mu$ m from the soma. If I place an electrode on a motoneurone dendrite at a distance of 50 $\mu$ m, and assuming a similar rate of diffusion for 4-AP in these cells to that for QX-314 in cultured motoneurons, and assuming a linear relation between diffusion time and distance from the soma, then 4-AP would diffuse from the dendritic electrode to the soma within 2.4 seconds. Since this is two orders of magnitude faster than the time for 4-AP to diffuse across the plasma membrane to the external face and block A-currents, it must be concluded that it is not possible to determine any difference between the dendritic and somatic A-current density using this method.

#### *Conclusions*

These experiments sought to determine the contribution of the A-current to the attenuation of backpropagated action potentials in the dendrites of presumed rat motoneurons. Various experiments were tried to determine if there was a contribution of the A-current to the action potential peak amplitude recorded at the soma. In each case, the effect on the action potential peak amplitude was only a few millivolts. Further experiments were performed to determine if the density of the A-current is different between the soma and dendrite. Because of the proximity of the dendritic recordings to the soma, it was not possible to determine any difference in the density of A-current at either location.

Therefore, the most that can be said is that the A-current in the motoneurone is the major contributor to action potential repolarisation and contributes only a few millivolts to the amplitude of the action potential. Dendritic recordings from locations more distant from the soma than were achieved here may be able to find a contribution of the A-current to action potential amplitude where the action potential waveform is more prolonged.



---

## Chapter Five

# Modelling of Action Potential Backpropagation

---

### Introduction

There have been many recent studies that have explored the influence of dendritic voltage-dependent conductances on action potential backpropagation. These have demonstrated that dendritic voltage-dependent conductances play an important role in modifying the action potential waveform as it propagates into the dendritic tree. Two currents that are important for influencing the dendritic action potential are the  $\text{Na}^+$  channel ( $I_{\text{Na}}$ ) and the A-current ( $I_{\text{A}}$ ). These currents are particularly well suited to modifying the dendritically propagated action potential because of their fast kinetics, which allow them to be activated during the rapid voltage changes that occur during an action potential.

Chapter 4 presented data that indicated that the A-current helps to shape the action potential waveform in motoneurones. The next step then was to determine how much attenuation would be expected for action potentials at the distances at which these recordings were made, that is up to  $50\mu\text{m}$  from the soma, and what density of A-current would be required to produce this attenuation. To achieve this, computer modelling of action potential backpropagation has been performed. This chapter examines the influence of some dendritic voltage-dependent conductances on action potential backpropagation in motoneurones

### Methods

To determine the possible extent of action potential attenuation, computer modelling of action potential backpropagation was performed. The first step was to mimic the voltage waveform of the action potential at the soma of the motoneurone. Measurement of the somatic action potential in 9 cells at a membrane potential of  $-65\text{mV}$  gave an average amplitude ( $\pm\text{SD}$ ) of  $74\pm 7.9\text{mV}$ , half-width of  $0.31\pm 0.066\text{ms}$  and base-width of  $0.67\pm 0.12\text{ms}$ . To model the attenuation of the action potential, *cell C1-2101* was used because it had typical motoneurone morphology and typical membrane properties. The passive properties of this cell were set to the values determined for this cell in Chapter 3, with  $R_{\text{m}}=5960\Omega\cdot\text{cm}^2$ ,  $R_{\text{i}}=78\Omega\cdot\text{cm}$  and  $C_{\text{m}}=1.7\mu\text{F}/\text{cm}^2$ . It was necessary to introduce an axon hillock into the morphology to be able to produce the correct action potential waveform. The axon hillock did not have realistic morphology. The axonal and hillock morphology of cat motoneurones has been extensively studied (e.g. Conradi *et al.* 1979, Kellerth *et al.* 1979, Lagerbäck 1985, Westrum 1993). However, data for rat motoneurones is scant and the only paper with good morphological data is that of Lahjouji *et al.* (1997) in which abducens motoneurones were studied. Measurements by Lahjouji *et al.* (1997) give an axon hillock diameter at the soma of  $3.2$  to  $5.6\mu\text{m}$ , length of  $4.2$  to  $7.6\mu\text{m}$  and final diameter of  $1.4$  to  $2.9\mu\text{m}$ . This study used dehydration of the tissue to

produce material suitable for electron microscopy. Therefore, the true dimensions may be up to twice this value (personal observations). When realistic hillock morphology was used with the reconstructed motoneurone morphology, it was not possible to simulate the rapid time-course of the action potential that was observed in recorded cells. Therefore a simple cylindrical hillock was used with a diameter of  $5\mu\text{m}$  and length of  $20\mu\text{m}$ . With just an axon and no hillock, the recorded action potential waveform could not be reproduced. Both the axon and hillock were given the same passive properties as the rest of the neurone.

To produce action potentials with the recorded time-course, voltage-dependent  $\text{Na}^+$  channels and delayed rectifier  $\text{K}^+$  channels were inserted into the axon, axon hillock and soma. An attempt was made to create realistic models of ion channels using the data of Safronov and Vogel (1995) from rat motoneurons to generate the somatic action potential. However the descriptions of these currents is incomplete and therefore it was not possible to create accurate models of these channels. Therefore, the channels used in this model were taken from the study by McCormick and Huguenard (1992). To be able to reproduce the rapid action potential waveform observed in motoneurons, it was necessary to modify these  $\text{Na}^+$  and  $\text{K}^+$  currents. This was achieved by speeding up the inactivation of the sodium channel and the activation of the delayed rectifier by 40% (see below). This had the advantage that the currents produced by these modified channels more closely matched the data of Safronov and Vogel (1995) for the ion channels of motoneurons. Therefore, the characteristics of the membrane current used to produce the action potential were not those measured in motoneurons, but were modified from those measured in cortical pyramidal cells to reproduce the action potential waveform and had properties similar to those measured in motoneurons. Without these modifications, it was impossible to reproduce the rapid action potential. The modified  $\text{Na}^+$  channel is referred to in this Chapter as the contrived sodium channel.

An attempt was made to use the  $\text{Na}^+$  channel described by Mainen *et al.* (1995) but this channel only produced abortive action potentials when the model was run at  $34^\circ\text{C}$ . For  $\text{Na}^+$  channels, the maximum conductance density at the hillock was set to  $5.0\text{S}/\text{cm}^2$ , for the axon it was  $1.0\text{S}/\text{cm}^2$  and in the soma it was  $1.5\text{S}/\text{cm}^2$ . For delayed rectifier  $\text{K}^+$  channels, the maximum conductance density at the hillock was set to  $1.6667\text{S}/\text{cm}^2$ , for the axon it was  $0.3333\text{S}/\text{cm}^2$  and in the soma it was  $0.5\text{S}/\text{cm}^2$ . Therefore, the ratio of the sodium conductance to the delayed rectifier was always kept at 3:1. It was necessary to use this combination of sodium and potassium conductance densities and channel distribution to be able to reproduce the action potential waveform. Although the conductance densities were slightly higher than accepted values ( $\text{Na}^+=3.0\text{S}/\text{cm}^2$ , Mainen *et al.* 1995) and did not have a realistic distribution, it did not matter for this study as the purpose was only to reproduce the action potential waveform at the soma. The action potential in a motoneurone is actually generated by a complex mixture of ion channel types including the sodium channel, A-current, delayed rectifier and calcium dependent potassium conductance (Walton & Fulton 1986, Takahashi 1990). Such a mixture would

be impossible to reproduce in a model with the data that is currently available. Therefore, the action potential waveform was mimicked using only sodium and delayed rectifier channels with their kinetics modified to produce the correct waveform. The modelled action potential waveform had an amplitude of 67mV, half-width of 0.234ms and base-width of 1.237ms. Comparison of the simulated action potential with that recorded from motoneurons showed that the amplitude and half-width were slightly smaller, while the base-width was significantly greater in the model. This is as close as the model could be matched to the recorded response without knowing the ion channels involved in action potential generation, their properties, density and distribution as well as the axonal and hillock morphology.

The modified ionic conductances were also placed in the dendritic membrane to determine their effect on the backpropagated action potential amplitude. The channel of Mainen *et al.* (1995) was also used in the dendritic membrane as a comparison between the different sodium channel types.

A comparison of the recorded and simulated action potentials is shown in figure 5.1.

#### *Contrived Sodium Channel*

The contrived sodium current ( $I_{Na}$ ) used for both action potential generation and one of the dendritic  $Na^+$  conductances was calculated using the formula:

$$I_{Na} = g_{Na} \cdot m^3 \cdot h \cdot (V_m - E_{Na})$$

where  $g_{Na}$  is the maximum  $Na^+$  conductance,  $m$  and  $h$  are the activation and inactivation variables respectively,  $V_m$  is the membrane potential and  $E_{Na}$  is the equilibrium potential for  $Na^+$ , which was set to +50mV. The steady-state activation variable ( $m_\infty$ ) and the time constant of activation ( $\tau_m$ ) were calculated using:

$$m_\infty = \alpha_m / (\alpha_m + \beta_m)$$

$$\tau_m = 1 / (\alpha_m + \beta_m)$$

where  $\alpha_m$  and  $\beta_m$  are the forward and reverse reaction rates calculated as:

$$\alpha_m = 0.091(V_m + 38) / (1 - \exp(-(V_m + 38)/5))$$

$$\beta_m = 0.062(V_m + 38) / (1 - \exp((V_m + 38)/5)).$$

The steady-state inactivation variable ( $h_\infty$ ) and the time constant of inactivation ( $\tau_h$ ) were calculated using:

$$h_\infty = \alpha_h / (\alpha_h + \beta_h)$$

$$\tau_h = 1 / (\alpha_h + \beta_h)$$

where  $\alpha_h$  and  $\beta_h$  are forward and reverse reaction rates calculated as:

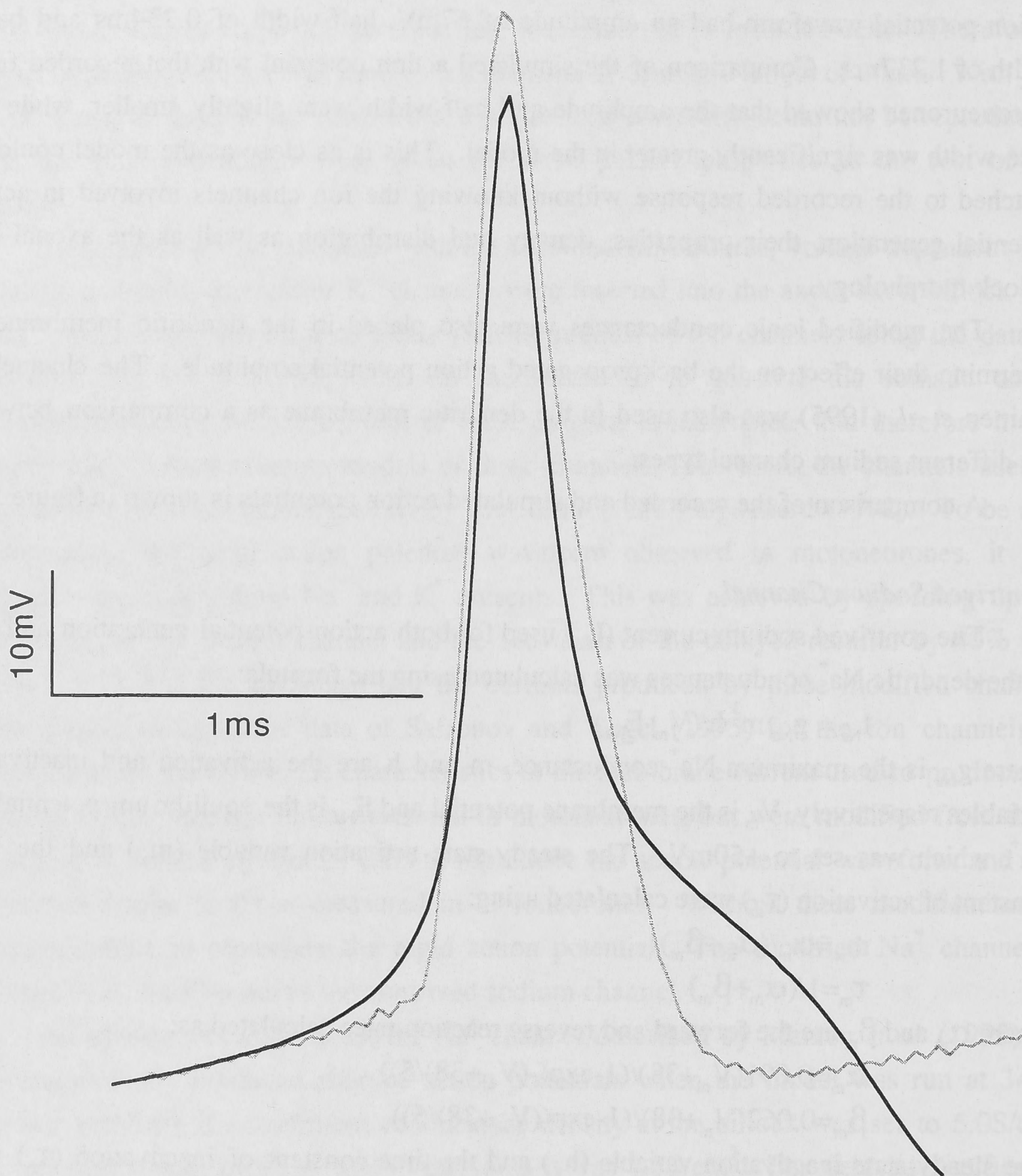
$$\alpha_h = 0.0238 \cdot \exp(-(V_m + 55)/15)$$

$$\beta_h = 2.898 / (1 + \exp((17 - V_m)/21))$$

$\alpha_m$ ,  $\beta_m$ ,  $\alpha_h$  and  $\beta_h$  were all based on values at 23.5°C. Once  $\tau_m$  and  $\tau_h$  had been calculated, they were adjusted for 34°C using a  $Q_{10}$  of 3.0 as follows:

$$\tau_{new} = \tau_{old} / (3.0^{(34-23.5)/10}).$$

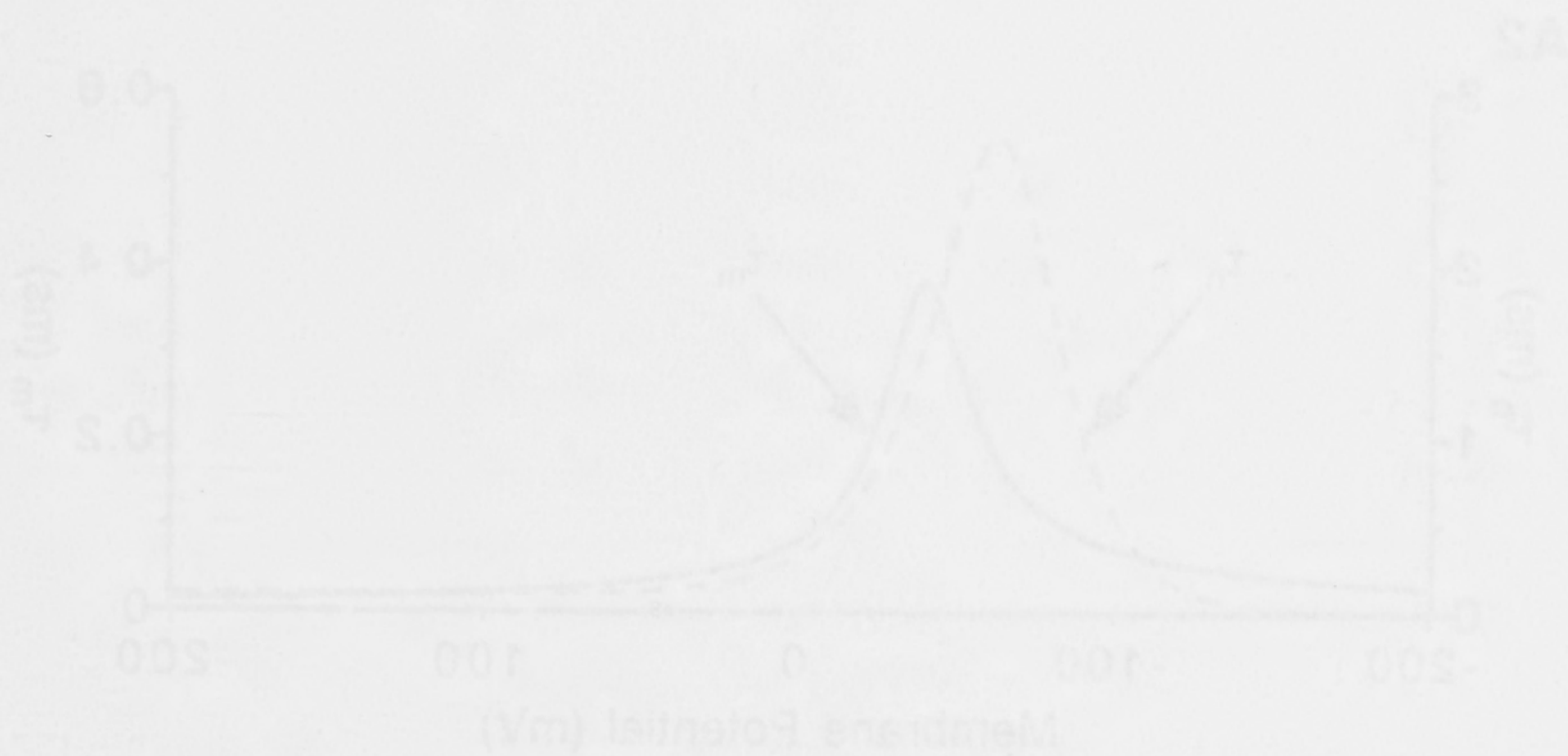
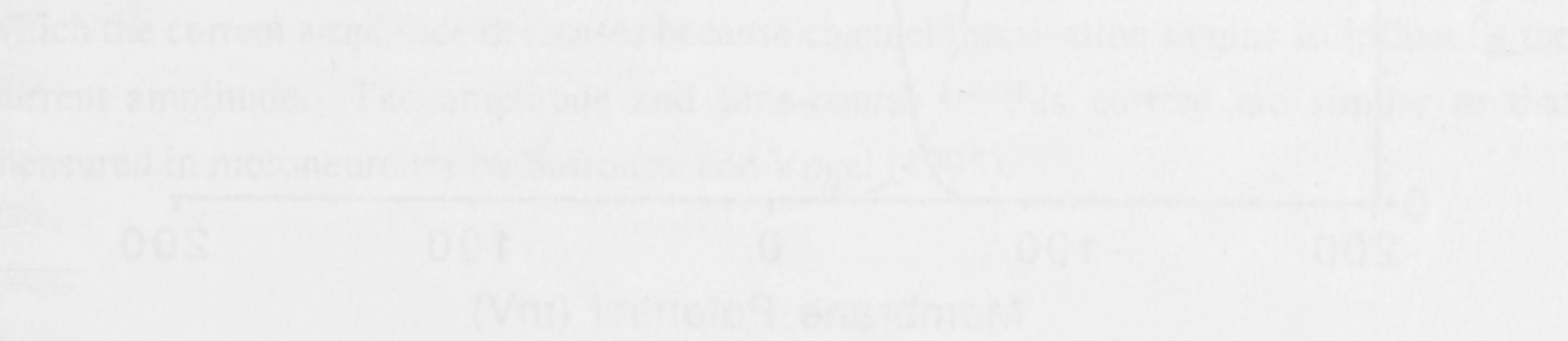
The kinetics and activation/inactivation curves for  $I_{Na}$  are shown in figure 5.2.



Recorded Action Potential  
(Grey Trace)  
 Amplitude =  $74 \pm 7.9\text{mV}$   
 Half-width =  $0.31 \pm 0.066\text{ms}$   
 Base-width =  $0.67 \pm 0.12\text{ms}$

Simulated Action Potential  
(Black Trace)  
 Amplitude =  $67\text{mV}$   
 Half-width =  $0.234\text{ms}$   
 Base-width =  $1.237\text{ms}$

Figure 5.1. A comparison of the simulated action potential (black trace) and the recorded action potential (grey trace). The half-width and amplitude of the two action potentials are closely matched. The base-width of the simulated action potential is 0.567ms wider than that of the recorded action potential, but only because of a change in the voltage gradient at the very end of the action potential. This figure shows that the waveform of the action potential can be reproduced with reasonable accuracy by the model.





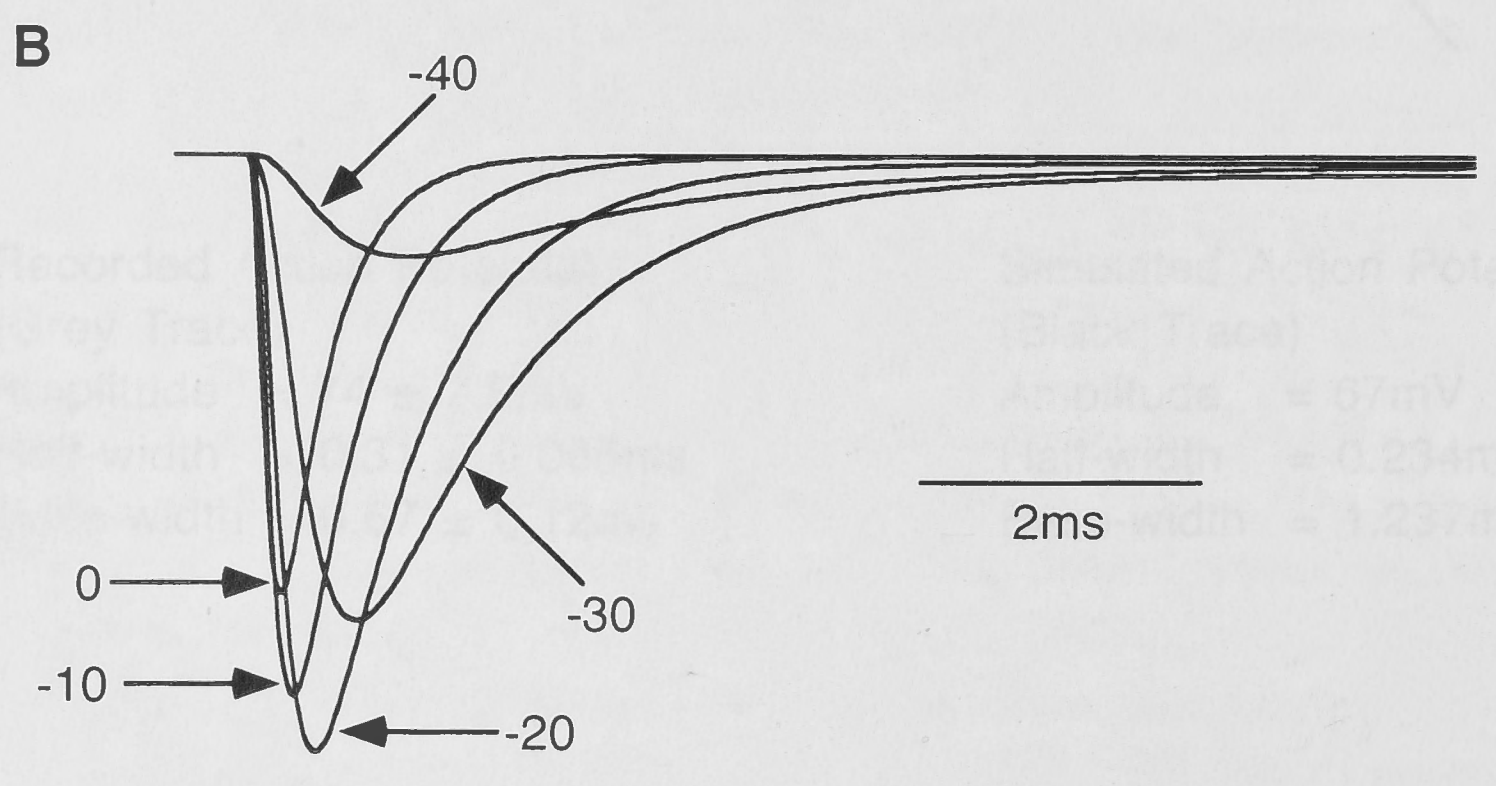
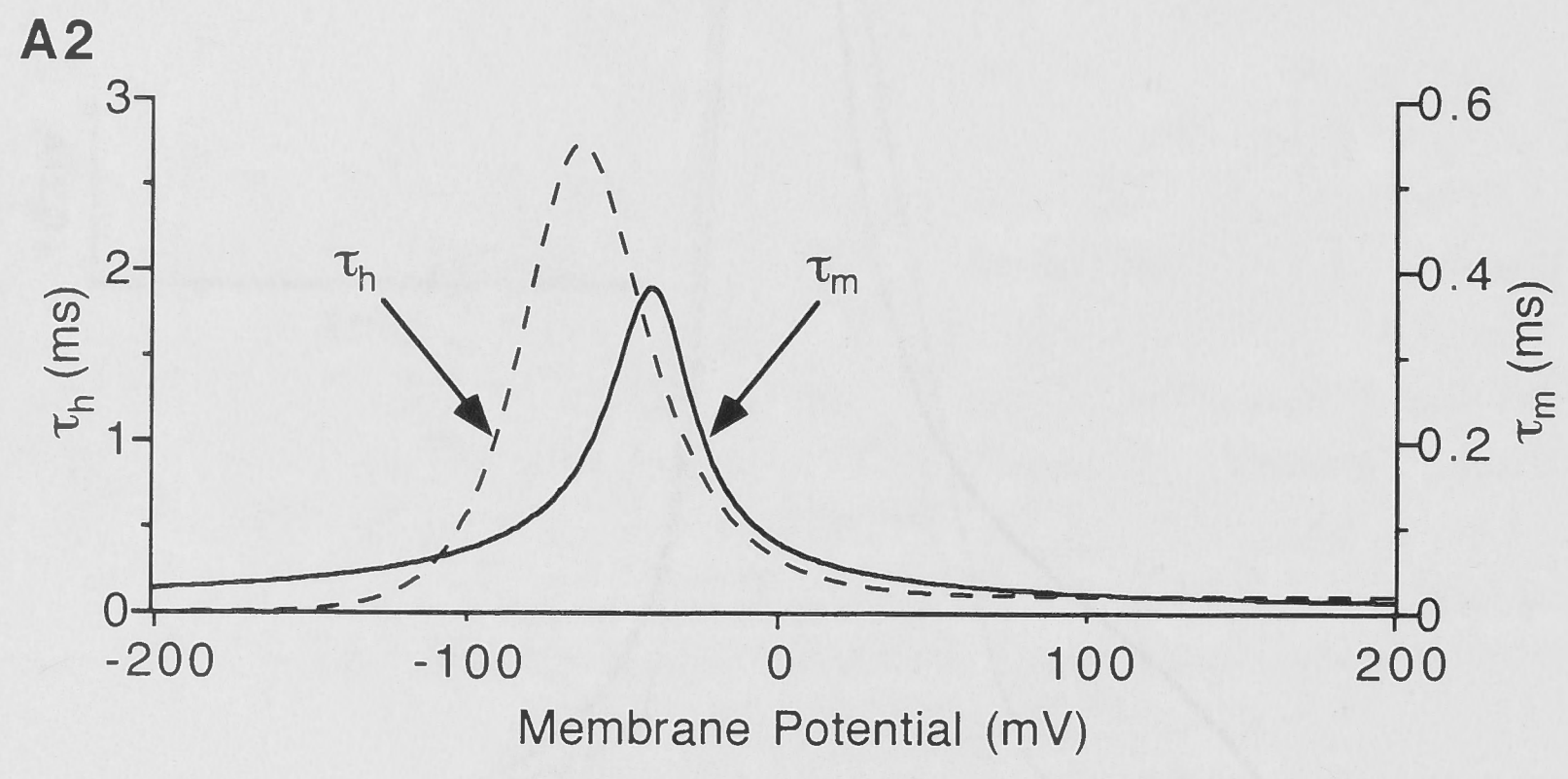
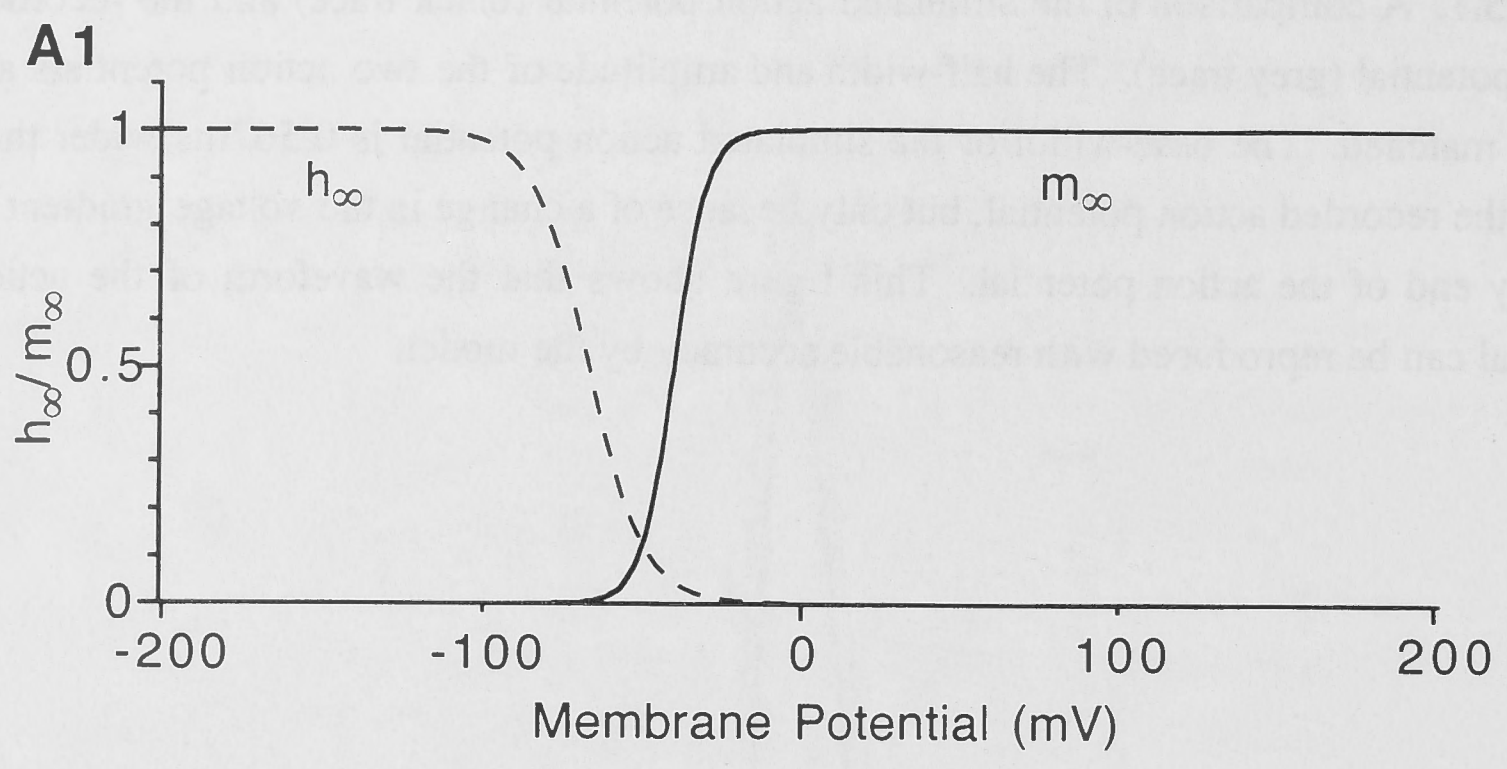


Figure 5.2. **A1:** The steady-state activation and inactivation curves of the contrived  $\text{Na}^+$  channel. **A2:** Activation and inactivation time constants for the simulated  $\text{Na}^+$  channel. Note the different scales for the activation and inactivation time constants. **B:**  $\text{Na}^+$  currents generated under voltage clamp in an isopotential compartment by stepping to membrane potentials of -40, -30, -20, -10 and 0mV from a holding potential of -120mV. Note that the amplitude of the current increases with depolarisation up to -20mV, after which the current amplitude decreases because channel inactivation begins to influence the current amplitude. The amplitude and time-course of this current are similar to that measured in motoneurons by Safronov and Vogel (1995).

### Delayed Rectifier

The delayed rectifier current ( $I_{DR}$ ) used for action potential generation was calculated using the formula:

$$I_{DR} = g_K \cdot n^4 \cdot (V_m - E_K)$$

where  $g_K$  is the maximum  $K^+$  conductance,  $n$  is the steady-state activation variable,  $V_m$  is the membrane potential and  $E_K$  is the equilibrium potential for  $K^+$  which was set to  $-90mV$ . The steady-state activation variable ( $n_\infty$ ) and the time constant of activation ( $\tau_n$ ) were calculated using:

$$n_\infty = \alpha_n / (\alpha_n + \beta_n)$$

$$\tau_n = 1 / (\alpha_n + \beta_n)$$

where  $\alpha_n$  and  $\beta_n$  are the forward and reverse reaction rates calculated as:

$$\alpha_n = 0.014(V_m + 45) / (1 - \exp(-(V_m + 45)/5))$$

$$\beta_n = 0.007 \cdot \exp(-(V_m + 50)/40)$$

$\alpha_n$  and  $\beta_n$  were based on values for  $23.5^\circ C$ . Once  $\tau_n$  was calculated, it was adjusted for  $34^\circ C$  using a  $Q_{10}$  of 3.0 as follows:

$$\tau_{new} = \tau_{old} / (3.0^{(34-23.5)/10})$$

The kinetics and activation curves for  $I_{DR}$  are shown in figure 5.3.

When this current was used in combination with the contrived  $Na^+$  current and the passive model of *C1-2101*, the action potential had an amplitude of  $67mV$ , half width of  $0.234ms$  and base-width of  $1.237ms$  which is as close as it could be made to the experimentally recorded action potential.

### Active Dendrites

To model active dendrites, either  $I_{Na}$  or  $I_A$  were placed in the dendrites and soma at a constant density. For the simulation of  $I_{Na}$  in the dendrites two conductance densities,  $2.8$  and  $9.0mS/cm^2$  (Magee & Johnston 1995a, Bischofberger & Jonas 1997), were used throughout the soma and dendritic tree and the action potential amplitude examined for each. The kinetics of the  $Na^+$  channel was identical to that used to produce the somatic action potential. For the simulation of  $I_A$  in the dendrites, two conductance densities ( $2.6$  and  $9.0mS/cm^2$ ) were used throughout the soma and dendritic tree and the action potential amplitude was examined with these two constant densities. The density of  $2.6mS/cm^2$  was calculated from the data of Hoffman *et al.* (1997) using the single channel conductance ( $7.5pS$ ) while the density of  $9.0mS/cm^2$  was assumed to be the upper limit of  $I_A$  density just as for the  $Na^+$  channel. The kinetics of  $I_A$  was slower than that of the  $Na^+$  channel and had a voltage activation range that was more depolarised.

### Transient Potassium Current ( $I_A$ )

The model of  $I_A$  used for this study was identical to the description of  $I_A$  used by Huguenard and McCormick (1992) from thalamic relay neurones.  $I_A$  was calculated using the formula:

$$I_A = g_A \cdot m^4 \cdot h \cdot (V_m - E_K)$$

where  $g_A$  is the maximum  $K^+$  conductance,  $m$  and  $h$  are the activation and inactivation variables respectively,  $V_m$  is the membrane potential and  $E_K$  is the equilibrium potential for  $K^+$  which was set to  $-90\text{mV}$ . The steady-state activation variable ( $m_\infty$ ) and the time constant of activation ( $\tau_m$ ) were calculated using:

$$m_\infty = 1 / (1 + \exp(-(V_m + 60) / 8.5))$$

$$\tau_m = 1 / ((\exp((V_m + 35.82) / 19.69)) + (\exp(-(V_m + 79.69) / 12.7)) + 0.37)$$

The steady-state inactivation variable ( $h_\infty$ ) was calculated explicitly using:

$$h_\infty = 1 / (1 + \exp((V_m + 78) / 6))$$

For the transient potassium channel, the voltage-dependence of the time constant of inactivation was complex. For membrane potentials of  $-63\text{mV}$  and more depolarised,  $\tau_h$  was calculated using:

$$\tau_h = 1 / ((\exp((V_m + 46.05) / 5)) + \exp(-(V_m + 238.4) / 37.45)).$$

For potentials more hyperpolarised than  $-63\text{mV}$ ,  $\tau_h$  was set to a constant value of  $19\text{ms}$ .

These  $\tau_m$  and  $\tau_h$  values were all based on measurements at  $23.5^\circ\text{C}$  so that once  $\tau_m$  and  $\tau_h$  were calculated, they were adjusted for  $34^\circ\text{C}$  using a  $Q_{10}$  of 3.0:

$$\tau_{\text{new}} = \tau_{\text{old}} / (3.0^{((34-23.5)/10)})$$

The kinetics and activation/inactivation curves for  $I_A$  are shown in Fig 5.4.

For all of these simulations, the passive equilibrium potential (membrane potential) was set to  $-65\text{mV}$  as in the experiments and  $E_K$  was set to  $-90\text{mV}$ .

To initiate action potentials, a current clamp stimulus of the same duration as the experiment ( $5\text{ms}$ ) was used with an amplitude of  $1.0\text{nA}$ , which is comparable to the current amplitude used to obtain experimental action potentials.

The first assessment of action potential attenuation in the dendritic tree consisted of measuring the action potential peak voltage as a function of distance from the soma. Recordings were made at 200 points on the morphology of *cell C1-2101*. These recordings were spaced approximately  $10\mu\text{m}$  apart for the first  $100\mu\text{m}$  of the dendritic tree, after which the recording points were approximately  $40\mu\text{m}$  apart. This was done to assure sufficient resolution of changes in action potential amplitude at locations close to the soma where dendritic electrodes were placed.

Recordings of action potential amplitude at all 200 points on the dendritic tree were made for five situations of active conductance: passive membrane (no active conductances),  $g_{\text{Na}} = 2.8\text{mS}/\text{cm}^2$ ,  $g_{\text{Na}} = 9.0\text{mS}/\text{cm}^2$ ,  $g_A = 2.6\text{mS}/\text{cm}^2$  and  $g_A = 9.0\text{mS}/\text{cm}^2$ . To further clarify the plot, a single dendrite of *C1-2101* was chosen and action potential

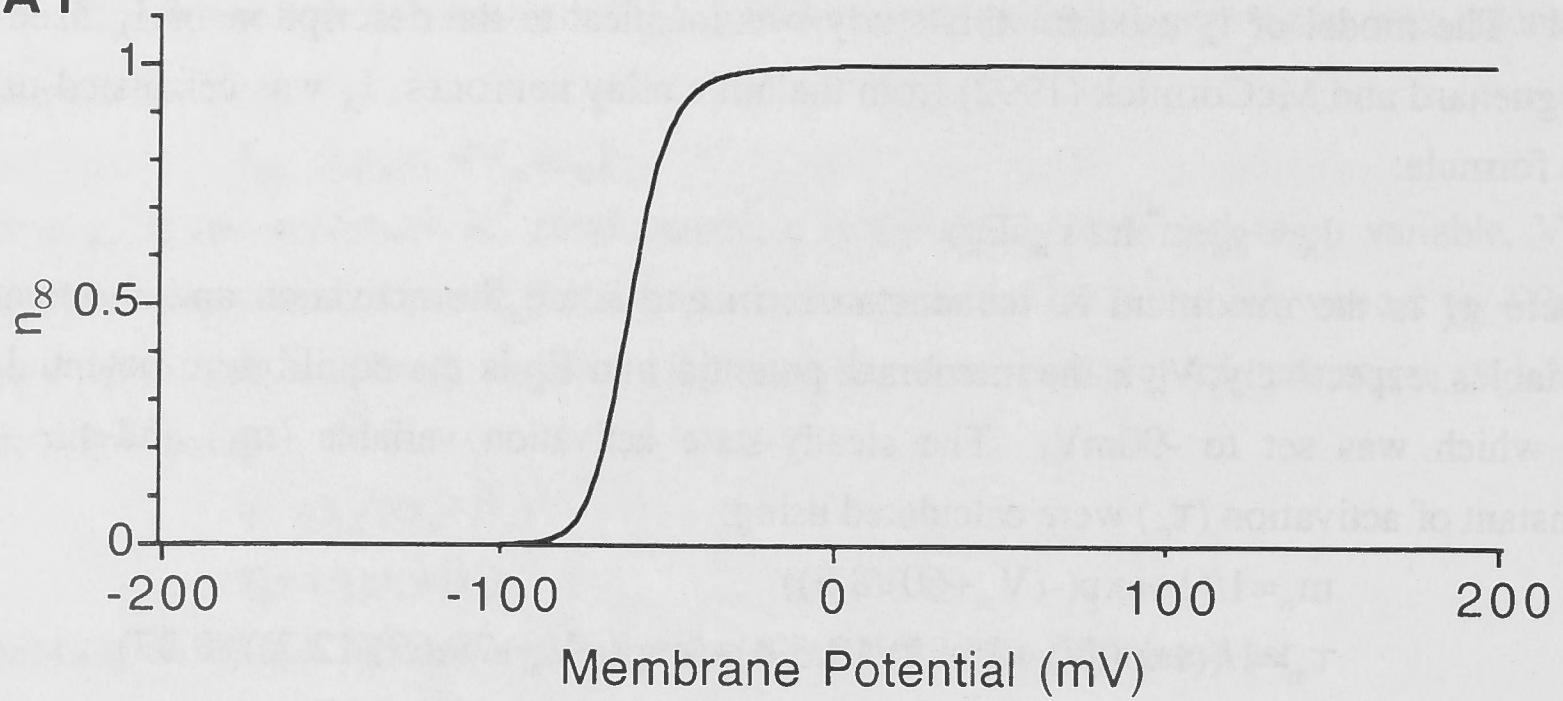
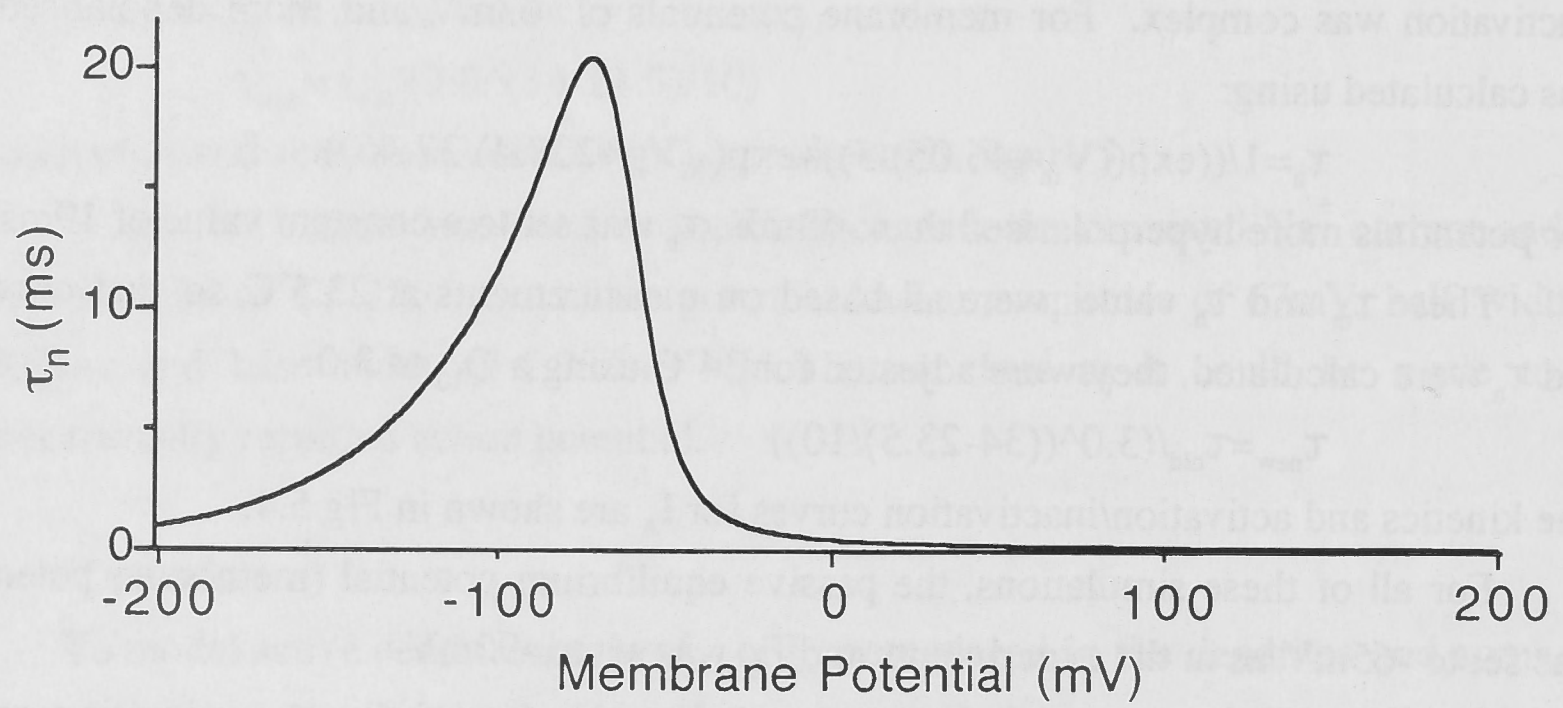
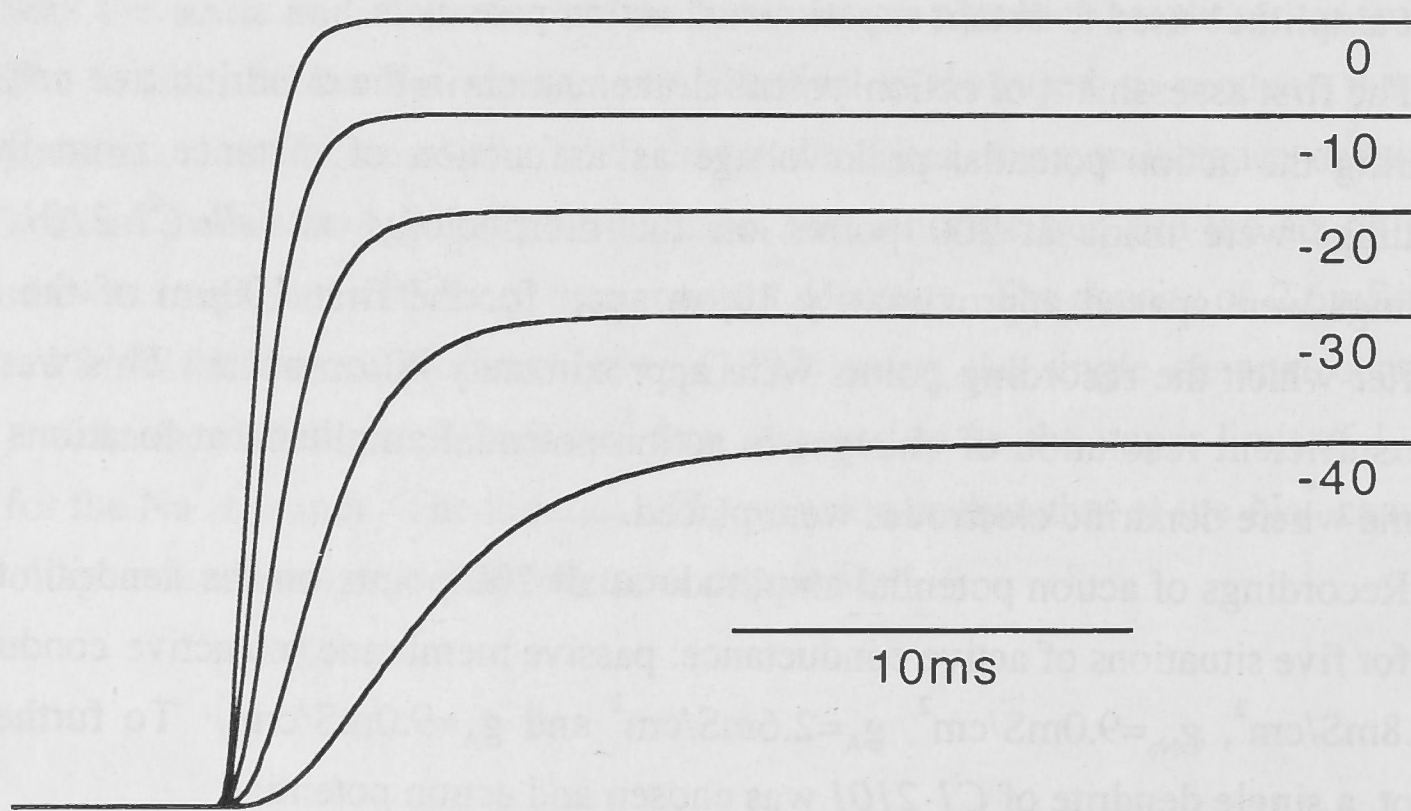
**A1****A2****B**

Figure 5.3. **A1:** The steady-state activation curve of the simulated delayed rectifier. **A2:** The activation time constant of the simulated delayed rectifier. This was increased by 40% from the value of McCormick and Huguenard (1992) to allow accurate reproduction of the action potential waveform. **B:** The delayed rectifier current generated under voltage clamp in an isopotential compartment by stepping to membrane potentials of -40, -30, -20, -10 and 0mV from a holding potential of -120mV.



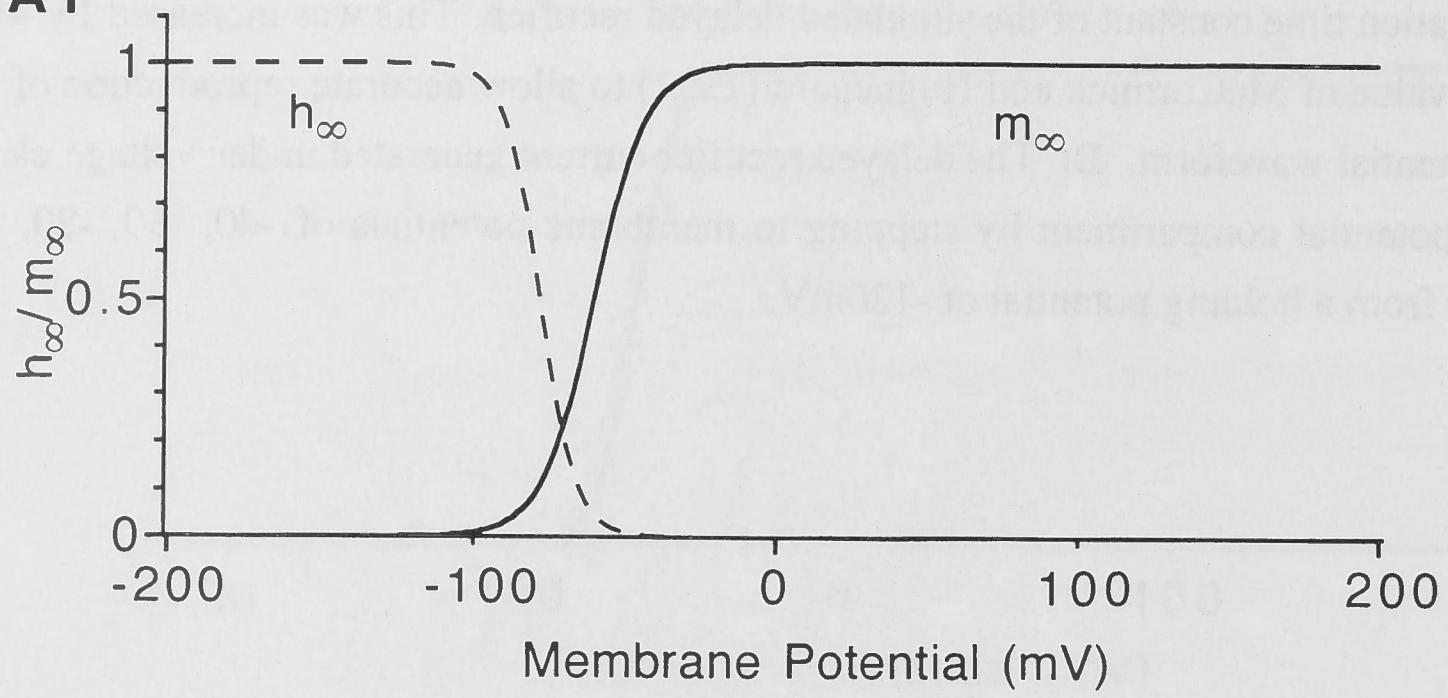
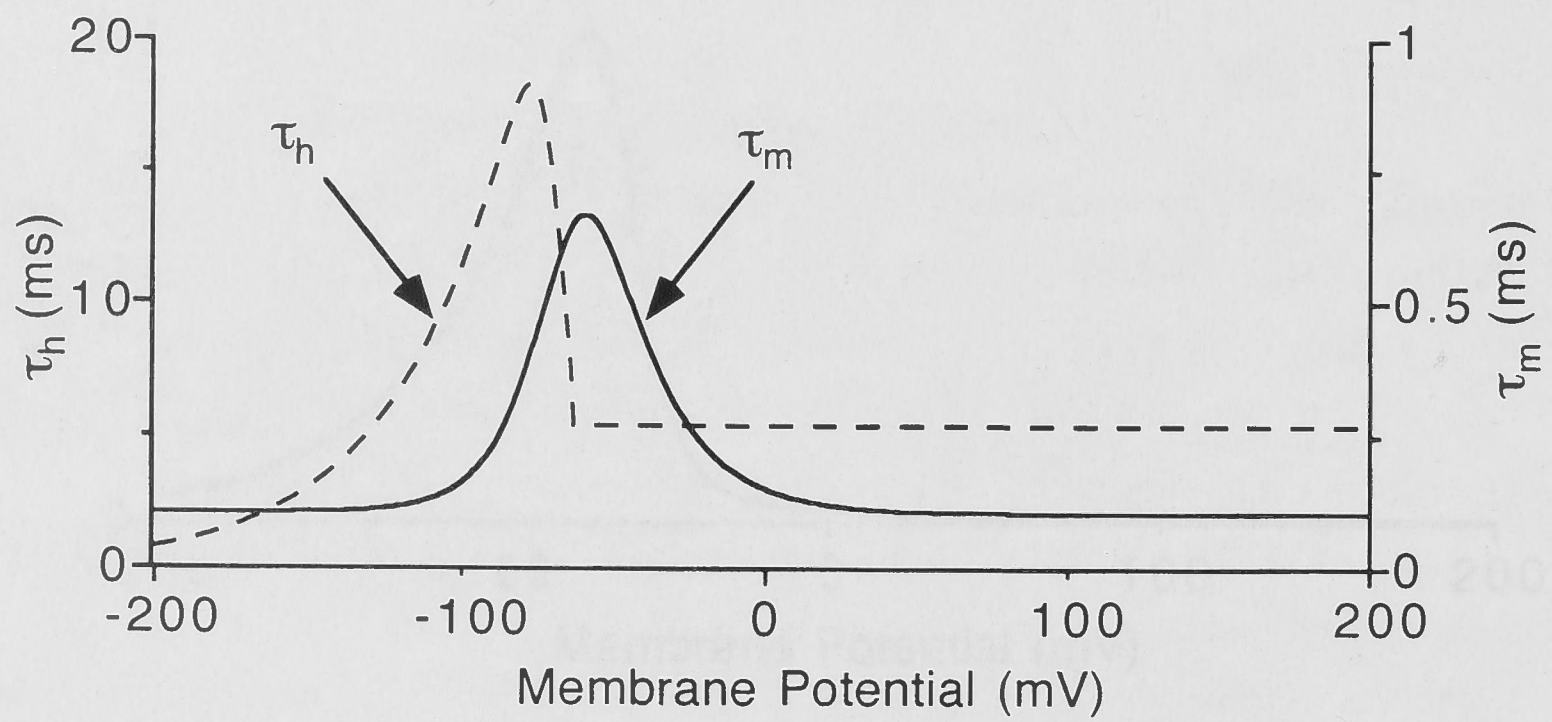
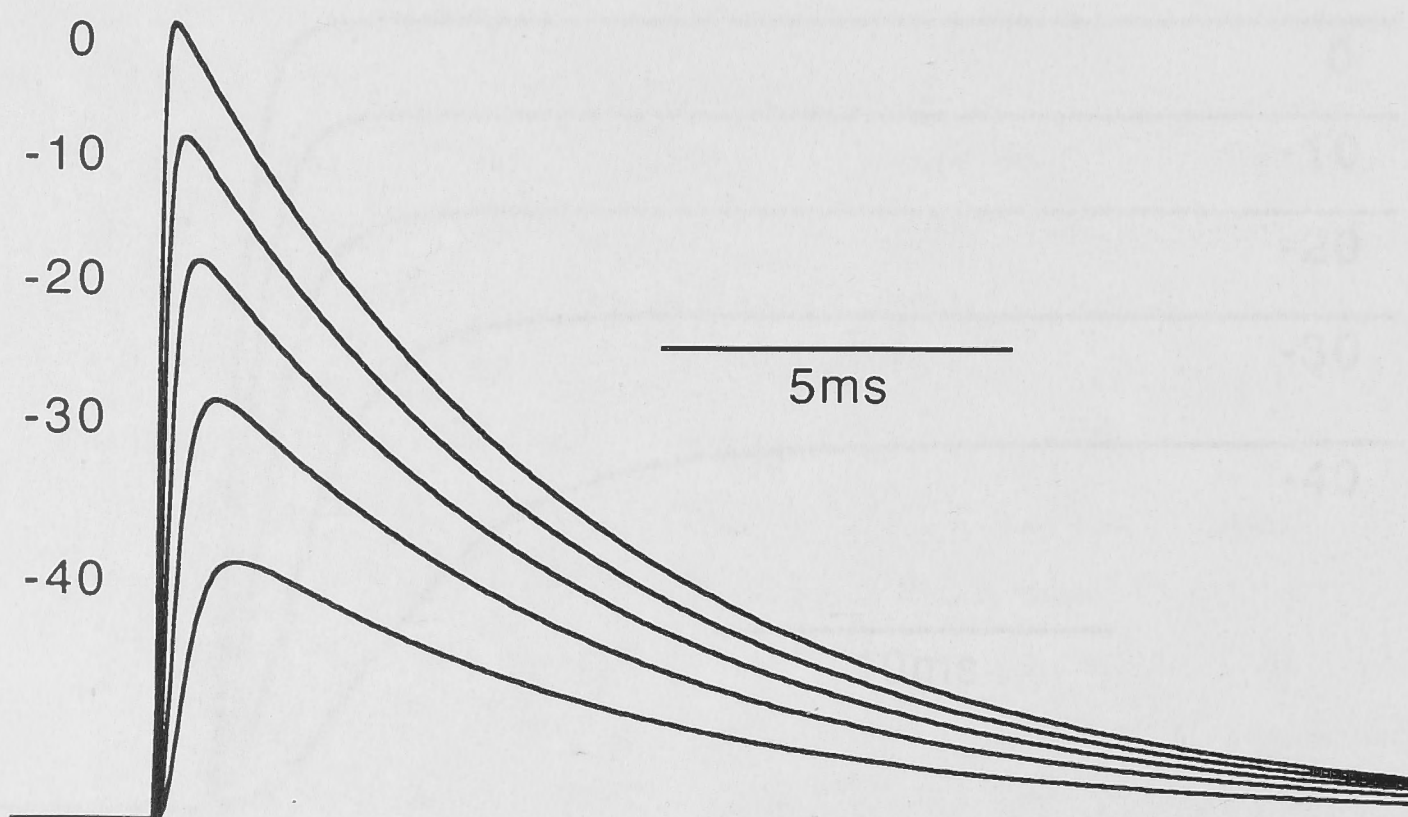
**A1****A2****B**

Figure 5.4. **A1:** The steady-state activation and inactivation curves for the simulated A-type potassium channel. **A2:** The activation and inactivation time constants for the simulated A-type potassium channel. Note the different time scales for the activation and inactivation time constants. **B:** A-type potassium current generated in an isopotential compartment under voltage clamp by stepping to membrane potentials of -40, -30, -20, -10 and 0mV from a holding potential of -120mV. Note that unlike the contrived  $\text{Na}^+$  channel, the A-type potassium channel does not show any decrease in amplitude during the largest depolarisations.



amplitude was examined at various distances along this dendrite from the soma to its termination.

As an addition to this modelling, the procedure was repeated using the Na<sup>+</sup> channel model of Mainen *et al.* (1995). This channel model has been used in the modelling of action potential backpropagation in motoneurons performed by Lüscher and Larkum (1998). Modelling of action potential backpropagation was performed with this Na<sup>+</sup> channel in the dendrites as a comparison with the other sodium channel and for comparison with the work of Lüscher and Larkum (1998).

#### *The Sodium Channel of Mainen et al. (1995)*

The current produced by the Na<sup>+</sup> channel of Mainen *et al.* ( $I_{Na}$ ) was calculated using the formula:

$$I_{Na} = g_{Na} \cdot m^3 \cdot h \cdot (V_m - E_{Na})$$

where  $g_{Na}$  is the maximum Na<sup>+</sup> conductance,  $m$  and  $h$  are the activation and inactivation variables respectively,  $V_m$  is the membrane potential and  $E_{Na}$  is the equilibrium potential for Na<sup>+</sup>, which was set to +50mV. The steady-state activation variable ( $m_\infty$ ) and the time constant of activation ( $\tau_m$ ) were calculated using:

$$m_\infty = \alpha_m / (\alpha_m + \beta_m)$$

$$\tau_m = 1 / (\alpha_m + \beta_m)$$

where  $\alpha_m$  and  $\beta_m$  are the forward and reverse reaction rates calculated as:

$$\alpha_m = 0.182(V_m + 35) / (1 - \exp((V_m + 35)/9))$$

$$\beta_m = 0.124(V_m + 35) / (1 - \exp((V_m + 35)/9)).$$

The steady-state inactivation variable ( $h_\infty$ ) was calculated explicitly as:

$$h_\infty = 1 / (1 + \exp((V_m + 65)/6.2)).$$

The time constant of inactivation ( $\tau_h$ ) was calculated using:

$$\tau_h = 1 / (\alpha_h + \beta_h)$$

where  $\alpha_h$  and  $\beta_h$  are forward and reverse reaction rates calculated as:

$$\alpha_h = 0.024(V_m + 50) / (1 - \exp((V_m + 50)/5))$$

$$\beta_h = 0.0091(V_m + 75) / (1 - \exp((V_m + 75)/5)).$$

$\alpha_m$ ,  $\beta_m$ ,  $\alpha_h$  and  $\beta_h$  were all based on values at 23.5°C. Once  $\tau_m$  and  $\tau_h$  had been calculated, they were adjusted for 34°C using a  $Q_{10}$  of 2.3 as follows:

$$\tau_{new} = \tau_{old} / (2.3^{(34-23.5)/10}).$$

The kinetics and activation/inactivation curves for Mainen's  $I_{Na}$  are shown in figure 5.5.

This channel was inserted into the dendrites and the action potential peak voltage was determined in every dendrite of *C1-2101* as a further assessment of how action potential amplitude changes with distance from the soma.

The differences between the contrived Na<sup>+</sup> channel and the channel of Mainen *et al.* (1995) can be seen by comparing figures 5.2 and 5.5. The voltage activation and inactivation curves of the contrived channel are hyperpolarised by about 15mV relative to the Na<sup>+</sup> channel of Mainen *et al.* and the activation curve has a shallower slope. The time

constants for activation and deactivation are also hyperpolarised by about 15mV. The activation time constant of the contrived channel is approximately 2.5 times that of the channel of Mainen *et al.* and has a narrower voltage range over which the time constant value is increased. The inactivation time constant of the contrived channel is shorter than that of the channel of Mainen *et al.* by about 5 times and has a broader range over which the time constant value is increased. The inactivation of the contrived channel begins to reduce the current flowing through the channel once the depolarisation is sufficient to shift the potential to regions where the inactivation time constant becomes very small. This results in crossover of the currents produced with different depolarisations (see fig 5.2). This crossover was also seen in the channel of Mainen *et al.* (1995) (see fig 5.5).

### *Action Potential Amplitude Versus Dendritic Diameter*

The second assessment of action potential attenuation related the amplitude of the action potential to the average dendritic diameter along all the dendritic sections to a particular distance from the soma. This allowed an assessment of the effect of dendritic diameters on action potential attenuation at a particular distance from the soma. Two distances were arbitrarily chosen for this analysis, 50 and 200 $\mu\text{m}$ . The 50 $\mu\text{m}$  point was chosen because this was the maximum distance at which the dendritic electrode could be placed from the soma. The 200 $\mu\text{m}$  point was chosen to explore action potential amplitude changes at more distal sites. Since action potential attenuation along a dendrite will depend on the diameter of the dendrites that it passes through, dendritic diameter was averaged at every 10 $\mu\text{m}$  along the dendritic tree including the diameter of the dendrite at the soma. This produced 6 points for 50 $\mu\text{m}$  and 21 points for 200 $\mu\text{m}$ . This provided some idea of the diameter of the dendrites that the action potential passed through before it reached the recording point (either 50 or 200 $\mu\text{m}$ ) and how these diameters affect action potential attenuation.

## **Results**

### *Action Potential Attenuation with Distance from the Soma*

Figure 5.6 shows the calculated peak voltage of the action potential versus distance from the soma for various active and passive membrane properties. Figure 5.6A shows the peak voltage of the action potential in every dendrite of *C1-2101* while figure 5.6B shows the peak voltage of the action potential in a single dendrite of *C1-2101* as marked in the inset of figure 5.6A. The black squares show the attenuation under passive conditions. Action potential amplitude decreases most rapidly over the first 100 $\mu\text{m}$  of the dendritic tree. Addition of  $I_{\text{Na}}$  to the dendritic tree (orange diamonds=2.8mS/cm<sup>2</sup> and red triangles=9.0mS/cm<sup>2</sup>) increased action potential amplitude but did so in a distance

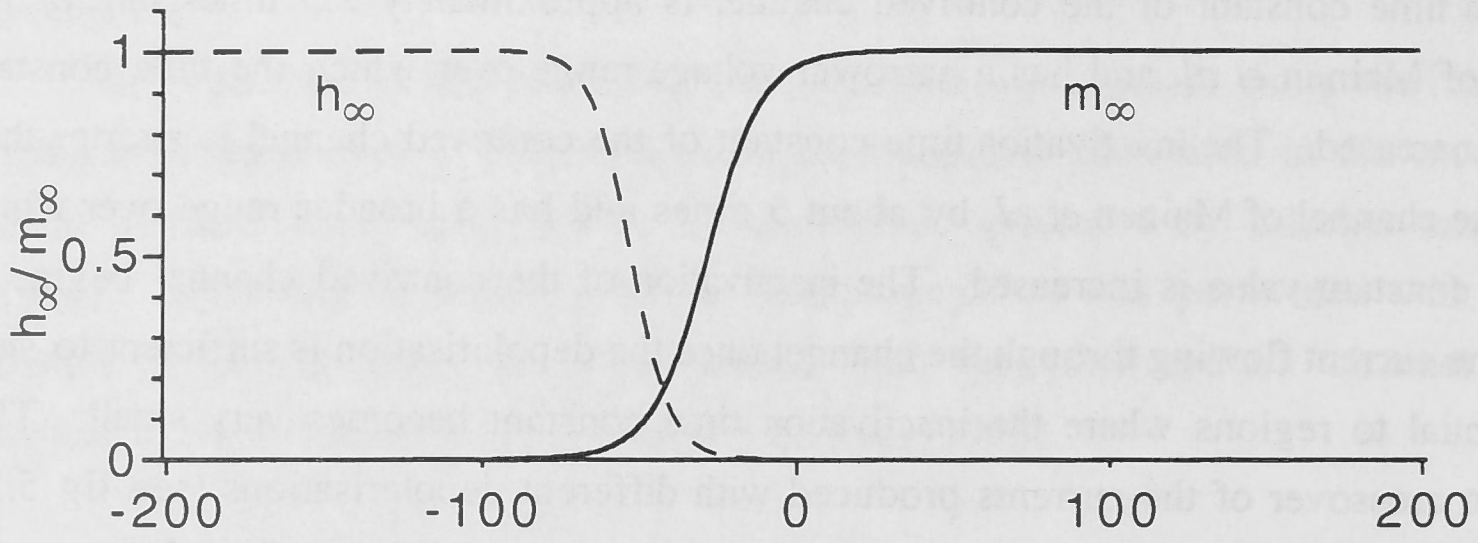
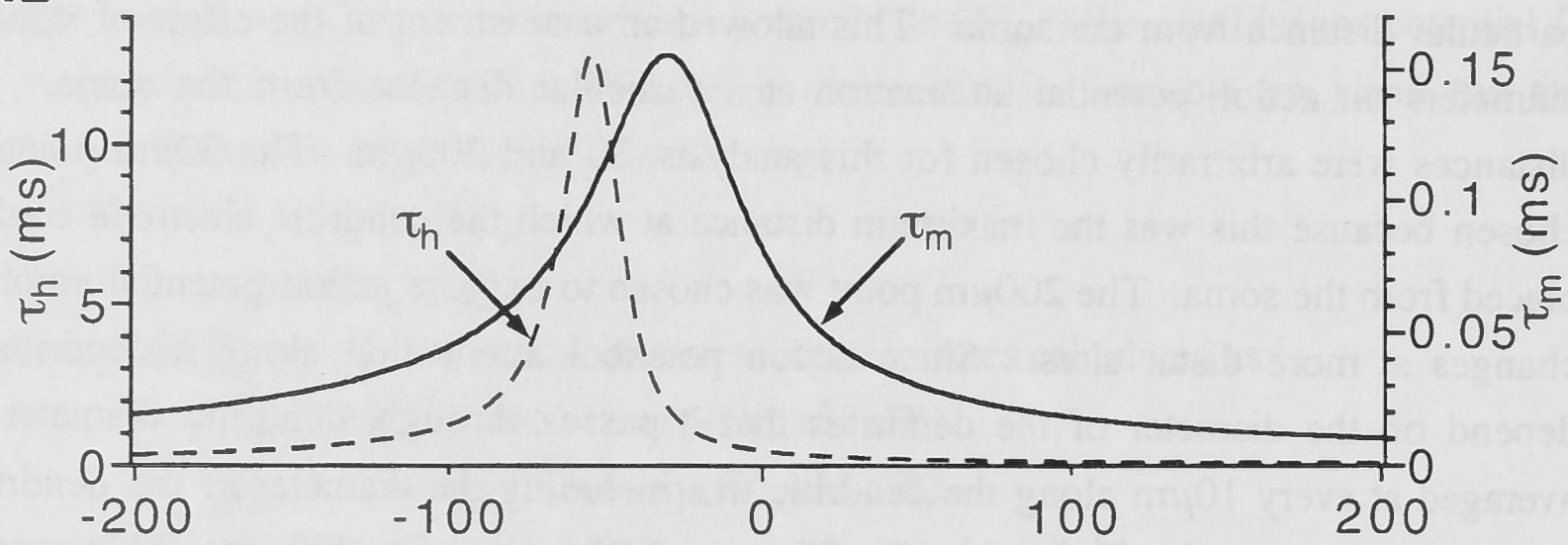
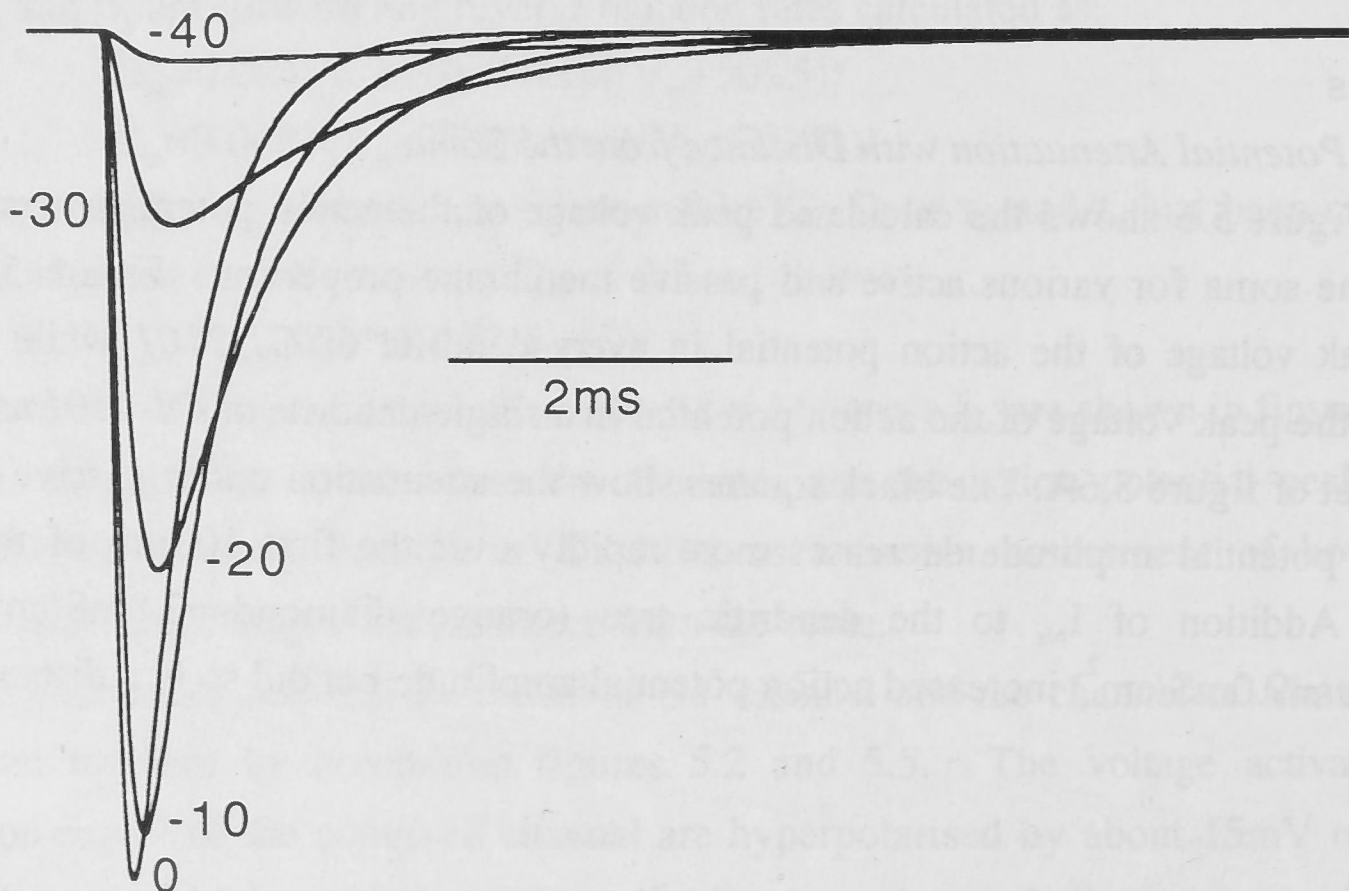
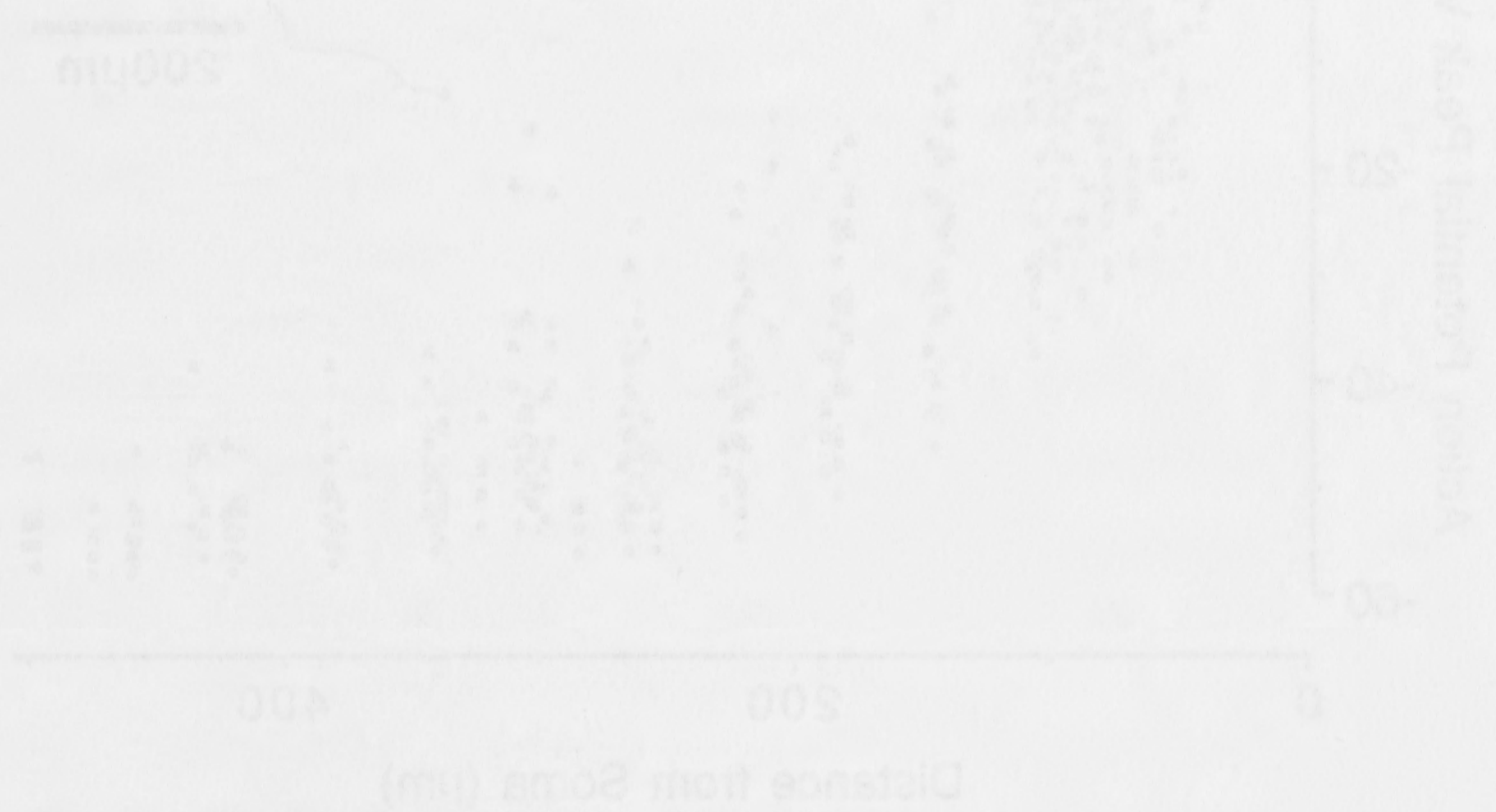
**A1****A2****B**

Figure 5.5. **A1:** The steady-state activation and inactivation curves for the simulated sodium channel of Mainen *et al.* (1995). **A2:** The activation and inactivation time constants for the simulated sodium channel of Mainen *et al.* (1995). Note the different time scales for the activation and inactivation time constants. **B:** Sodium current generated in an isopotential compartment under voltage clamp by stepping to membrane potentials of -40, -30, -20, -10 and 0mV from a holding potential of -120mV. Note that the amplitude of the current decreases during the largest depolarisations, just as for the contrived Na<sup>+</sup> channel.

Figure 2.1. A. The steady-state current and membrane current for the standard sodium channel of Hain et al. (1987). B. The membrane and membrane time constants for the standard sodium channel of Hain et al. (1987). C. The membrane time constants for the sodium and potassium time constants. D. Sodium current generated in an axon with a constant current injection. The current is injected at potentials of -40, -30, -20, and -10 mV and only from a holding potential of -100 mV. The amplitude of the current increases during the largest depolarization, just as for the control Na channel.



Figure 5.6. A: A non-pyramidal peak voltage versus distance from the soma for every dendrite of cell 51-1104 and no effect of active dendritic conductances. The legend shows the symbols for each dendrite. Parameters were  $\tau_{Na} = 2.5 \text{ ms}$ ,  $\tau_{K} = 9.0 \text{ ms}$ ,  $\tau_{Ca} = 100 \text{ ms}$ ,  $\tau_{Mg} = 10 \text{ ms}$ ,  $\tau_{Cl} = 10 \text{ ms}$ ,  $\tau_{leak} = 10 \text{ ms}$ ,  $\tau_{AHP} = 10 \text{ ms}$ ,  $\tau_{Mg} = 10 \text{ ms}$ ,  $\tau_{Cl} = 10 \text{ ms}$ ,  $\tau_{leak} = 10 \text{ ms}$ ,  $\tau_{AHP} = 10 \text{ ms}$ . B: A non-pyramidal peak voltage versus distance from the soma for every dendrite of cell 51-1104 and no effect of active dendritic conductances. The legend shows the symbols for each dendrite. Parameters were  $\tau_{Na} = 2.5 \text{ ms}$ ,  $\tau_{K} = 9.0 \text{ ms}$ ,  $\tau_{Ca} = 100 \text{ ms}$ ,  $\tau_{Mg} = 10 \text{ ms}$ ,  $\tau_{Cl} = 10 \text{ ms}$ ,  $\tau_{leak} = 10 \text{ ms}$ ,  $\tau_{AHP} = 10 \text{ ms}$ .



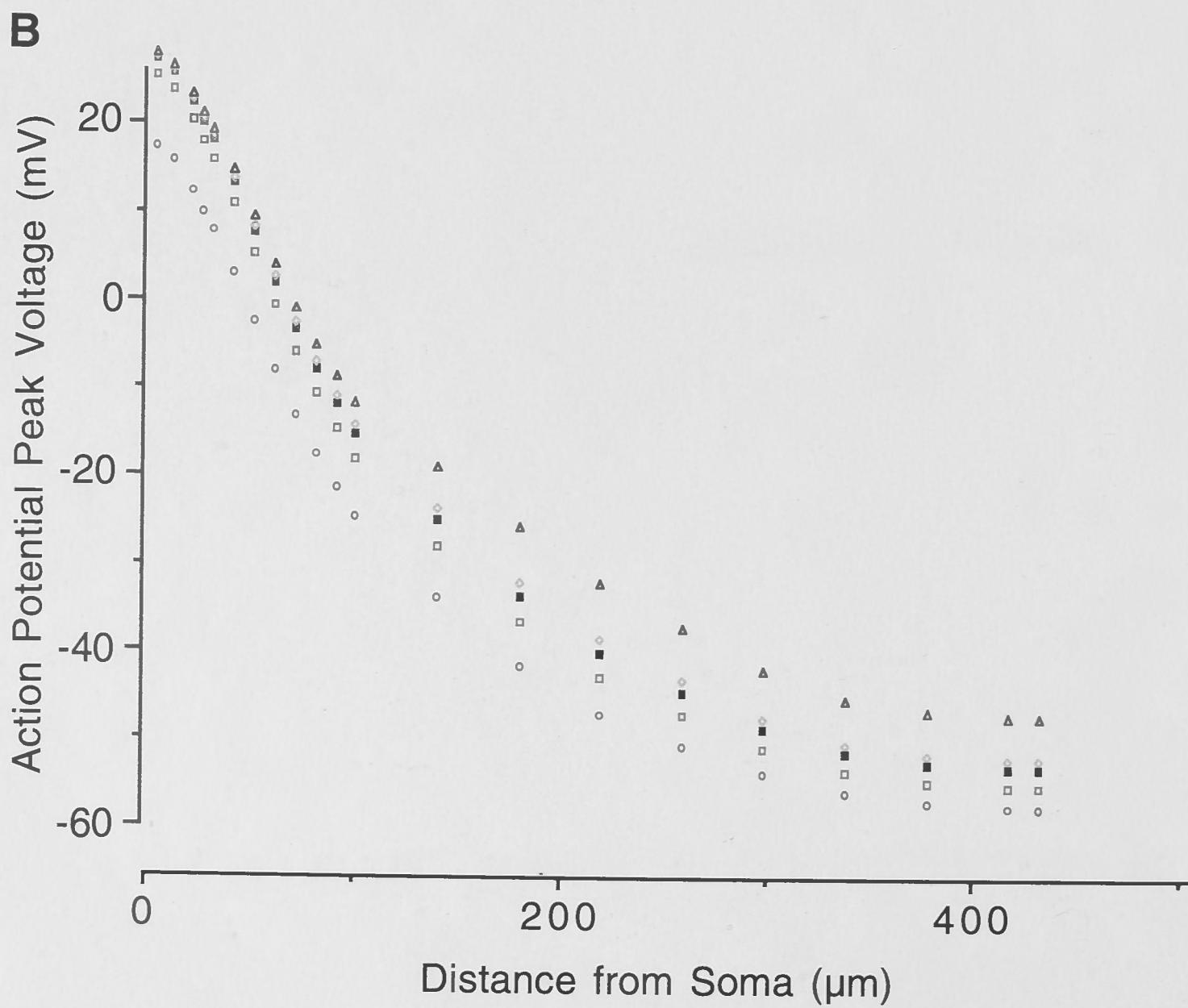
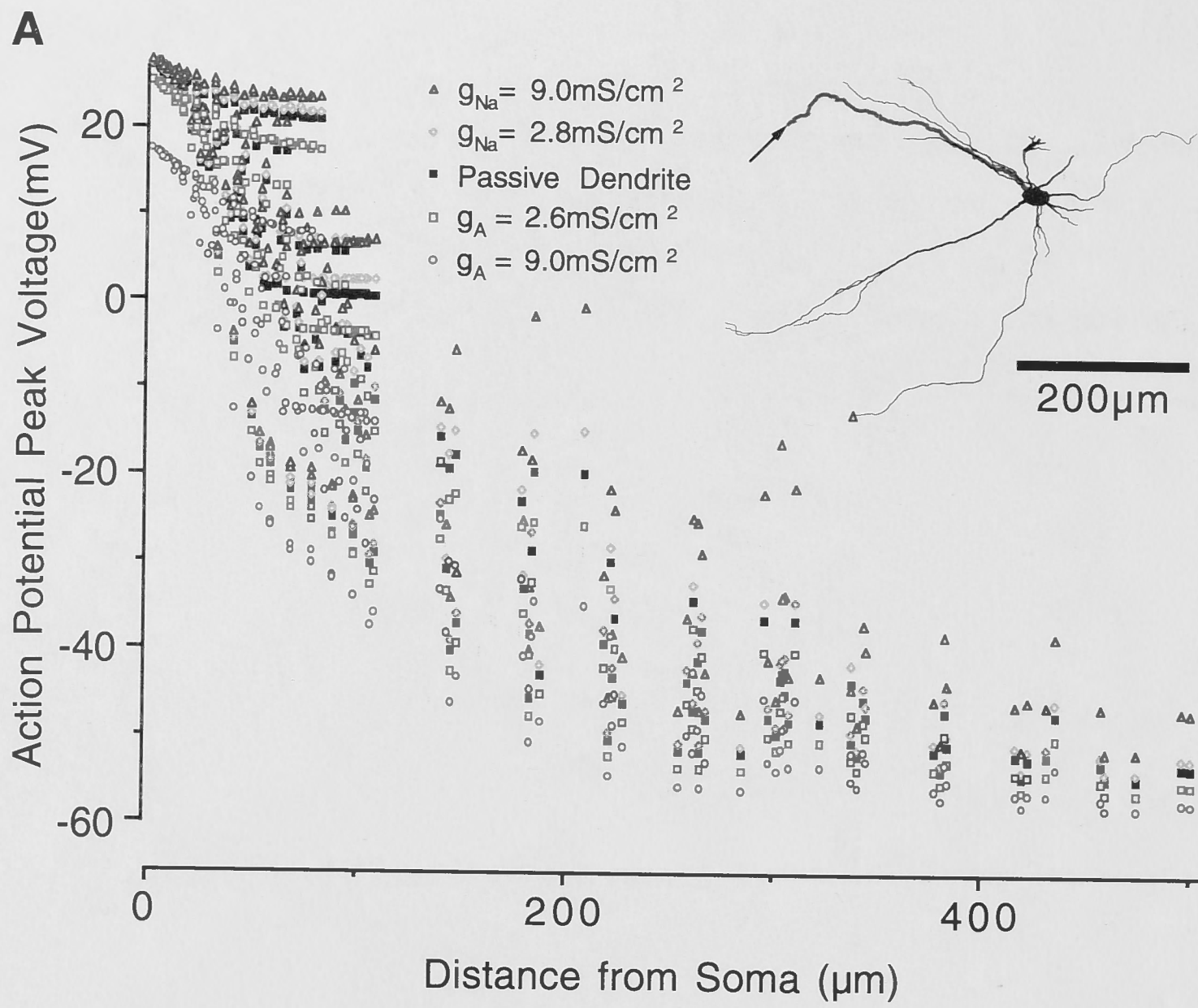


Figure 5.6. **A:** Action potential peak voltage versus distance from the soma for every dendrite of cell C1-2101 and the effect of active dendritic conductances. The legend shows the symbols for each situation: passive (no active conductances),  $g_{Na}=2.8\text{mS/cm}^2$ ,  $g_{Na}=9.0\text{mS/cm}^2$ ,  $g_A=2.6\text{mS/cm}^2$  and  $g_A=9.0\text{mS/cm}^2$ . **B:** Action potential peak voltage versus distance from the soma for the dendrite marked with an arrow in the inset, and the effect of active dendritic conductances.  $I_A$  has its greatest effect in the soma and proximal dendrites while  $I_{Na}$  has its greatest effect at distal locations.



dependent manner. Action potentials in the distal dendritic tree were increased in amplitude more than in the proximal dendritic tree.

Conversely, addition of  $I_A$  (green squares= $2.6\text{mS}/\text{cm}^2$  and blue circles= $9.0\text{mS}/\text{cm}^2$ ) attenuated action potentials more heavily in the proximal dendrites than in the distal dendrites. The action potential waveform has its largest amplitude and fastest time-course in the proximal dendritic tree. Figure 5.6 does not supply any information that would suggest why the different active conductances modify action potential amplitude in the way that they do. The effect of voltage-dependent ion channels on the dendritic action potential will depend on the combination of the voltage activation/inactivation ranges and kinetics of the channel and the time-course and amplitude of the dendritic action potential. This, in turn, depends on the dendritic passive properties and how the action potential is modified by active conductances as it travels to the dendritic site where it is measured.

To further clarify this matter, the currents produced by these ion channels were calculated at different distances from the soma during action potential backpropagation. These currents were calculated for compartments of equal length ( $5\mu\text{m}$ ) at both  $50$  and  $200\mu\text{m}$ . The diameters of these compartments vary at each location and between locations. As membrane current is proportional to membrane surface area, it is necessary to normalise the current by the surface area and present the results as current density to allow comparisons to be made between the two regions. The average surface areas associated with the  $5\mu\text{m}$  length compartments at  $50$  and  $200\mu\text{m}$  in *C1-2101* were  $20.4\mu\text{m}^2$  and  $12.6\mu\text{m}^2$  respectively. The currents calculated in each dendritic segment at  $50$  and  $200\mu\text{m}$  have been averaged and normalised by the compartmental surface areas.

Figure 5.7 shows the average A-current density during the action potential at  $50$  and  $200\mu\text{m}$  for all the dendrites of *C1-2101*, for maximum A-current conductance densities of  $2.6$  and  $9.0\text{mS}/\text{cm}^2$ .

At  $50\mu\text{m}$ , the average peak A-current densities are  $3.6$  and  $10.9\text{pA}/\mu\text{m}^2$  for the low and high conductance densities, respectively. At  $200\mu\text{m}$ , they are  $1.0$  and  $1.8\text{pA}/\mu\text{m}^2$ . For each conductance density, the A-currents are clearly much greater at  $50\mu\text{m}$  than at  $200\mu\text{m}$  and this explains why the A-current has a greater effect on the backpropagated action potential at proximal sites compared with distal sites. The smaller current density in the distal dendrites is caused by the reduced amplitude of the action potential in these regions, leading to a smaller driving potential for  $\text{K}^+$  ions and smaller activation of the A-conductance, even though the slower rise-time of the action potential is more suited to the activation kinetics of the A-current. The slower and smaller backpropagated action potential in the distal dendrites compared with the proximal dendrites is shown in figure 5.8, together with the A-current density that is associated with the potential changes. This figure uses only a single dendrite of *C1-2101* as marked in figure 5.6A. Figure 5.8 shows that the A-current is larger and more rapid in the proximal dendrites than in the distal

dendrites. Furthermore, the A-current peaks after the action potential and contributes to its repolarisation.

The average  $\text{Na}^+$  current densities calculated during a backpropagated action potential at 50 and 200 $\mu\text{m}$  in every dendrite of *CI-2101* are shown in figure 5.9, for maximum  $\text{Na}^+$  conductance densities of 2.8 and 9.0 $\text{mS}/\text{cm}^2$ . The averages mask considerable variability in latency and amplitude of the  $\text{Na}^+$  current density in each dendritic segment at these distances.

For the larger  $\text{Na}^+$  conductance density, the average peak current density at the distal locations (5.1 $\text{pA}/\mu\text{m}^2$ ) is greater than the average peak current density at the proximal locations (3.6 $\text{pA}/\mu\text{m}^2$ ) whereas the peak current densities are similar at the two locations for the smaller  $\text{Na}^+$  conductance density (1.1 vs. 1.2 $\text{pA}/\mu\text{m}^2$ ). The larger effect of the  $\text{Na}^+$  current in the distal dendrites is related to the combination of its voltage activation/inactivation ranges, its kinetics, and the shaping of the action potential in the dendrites by factors other than the  $\text{Na}^+$  current. In the proximal dendrites, the amplitude of the action potential is largely determined by the proximity of the soma and axon hillock conductances and the passive properties of the dendrites. The large action potential in this region fully activates the  $\text{Na}^+$  conductance, but the local  $\text{Na}^+$  current is small because of the reduced driving potential for  $I_{\text{Na}}$ . Figure 5.10 illustrates the action potential and associated  $I_{\text{Na}}$  current densities at 50 and 200 $\mu\text{m}$ , for a maximum sodium conductance density of 9.0 $\text{mS}/\text{cm}^2$ . This figure uses only a single dendrite of *CI-2101* as marked in figure 5.6A. The action potential is heavily attenuated at 200 $\mu\text{m}$  and peaks at about -35mV. At this potential,  $g_{\text{Na}}$  is approximately half activated. However, the driving potential at the peak of the backpropagated action potential is many times greater than the corresponding value at 50 $\mu\text{m}$ , and this explains the larger current at the more distal location. For the smaller conductance density (see Fig 5.9), there is a much smaller activation of the sodium conductance at the distal locations which is only partly compensated by the increased driving potential. At this lower conductance density, the peak current densities at 50 and 200 $\mu\text{m}$  are approximately equal.

The sodium current tends to have a greater influence on the backpropagated action potential at distal compared with proximal locations. In figure 5.10 at 50 $\mu\text{m}$ , the sodium current is seen to peak after the peak of the action potential. This is due to a lag in the activation of the  $\text{Na}^+$  channel because it is driven by the action potential rather than generating it. At this distance, the somatic  $\text{Na}^+$  conductance largely controls the action potential waveform and amplitude. At 200 $\mu\text{m}$ , the  $\text{Na}^+$  current and action potential peak simultaneously because the backpropagating action potential is mostly driven by the  $\text{Na}^+$  conductances in the dendritic membrane.

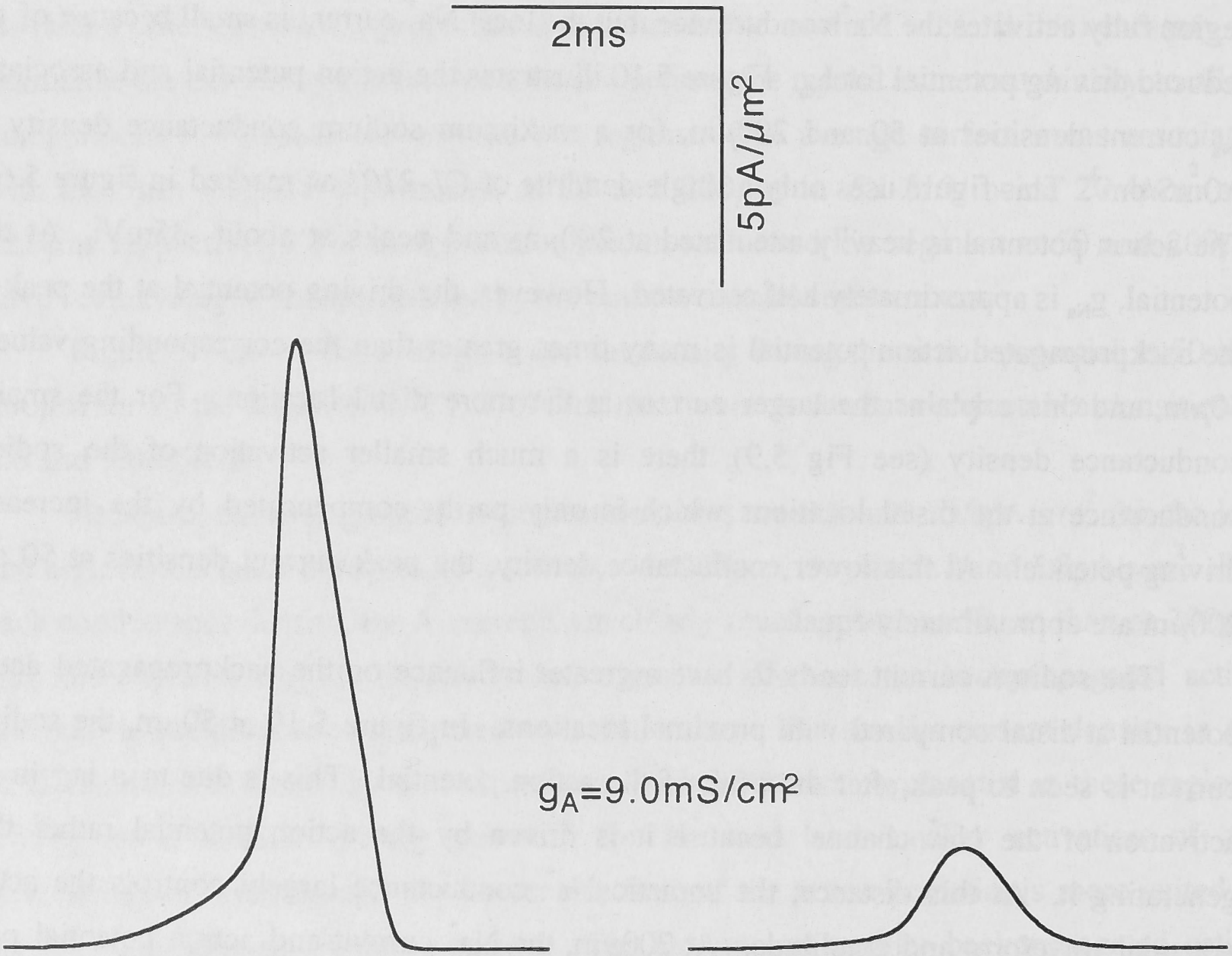
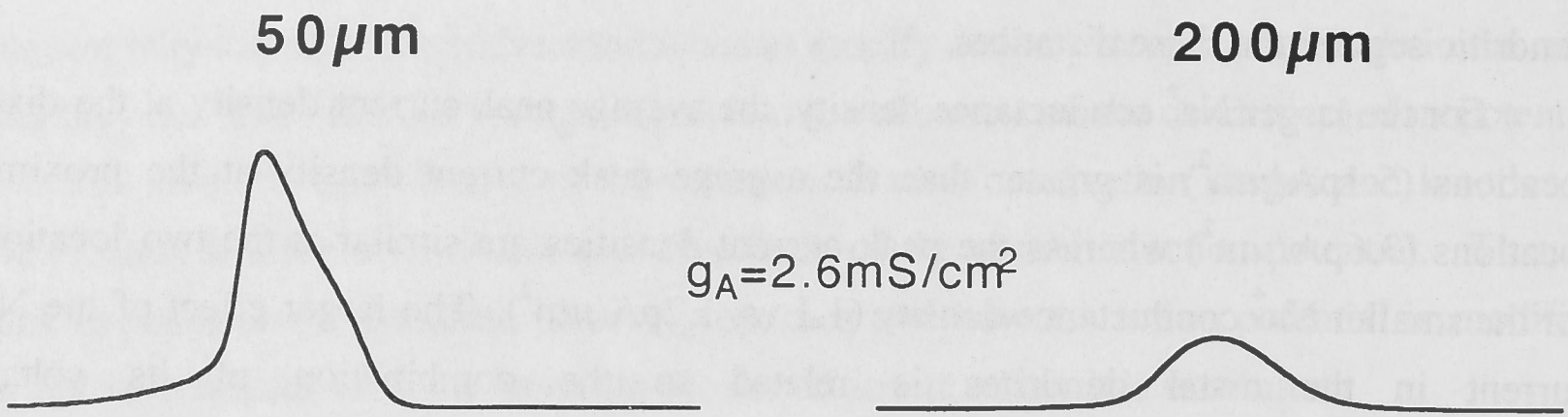
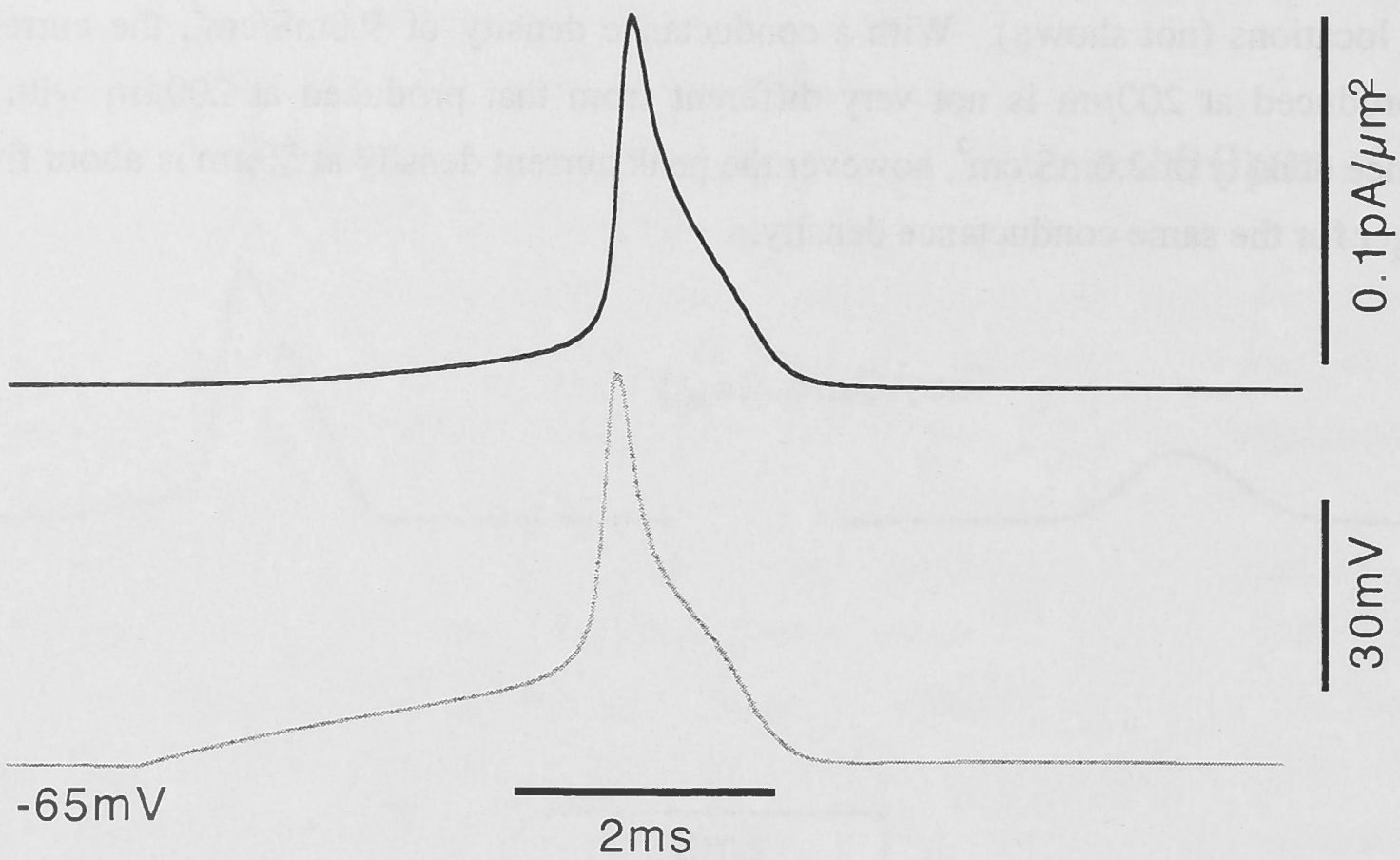


Figure 5.7. The average A-current density at every dendritic location at 50 and 200 $\mu\text{m}$  from the soma with maximum conductance densities of 2.6mS/cm<sup>2</sup> and 9.0mS/cm<sup>2</sup>. The peak current density at the proximal locations is approximately 3.5 to 5 times the peak current density at distal locations. The variability of the peak current density is greatest in the distal locations (not shown). With a conductance density of 9.0mS/cm<sup>2</sup>, the current density produced at 200 $\mu\text{m}$  is not very different from that produced at 200 $\mu\text{m}$  with a conductance density of 2.6mS/cm<sup>2</sup>, however the peak current density at 50 $\mu\text{m}$  is about five times larger for the same conductance density.



50  $\mu\text{m}$

$g_A = 9.0 \text{ mS/cm}^2$



200  $\mu\text{m}$

$g_A = 9.0 \text{ mS/cm}^2$

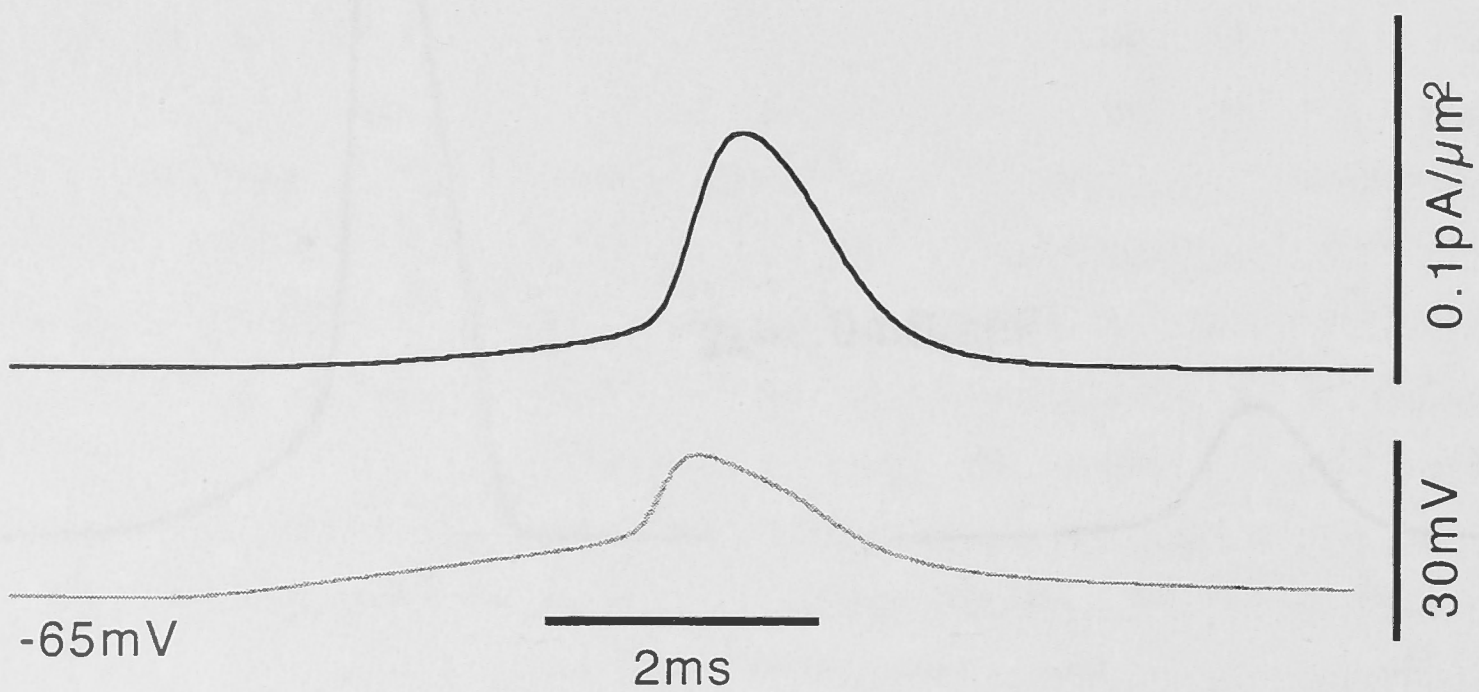
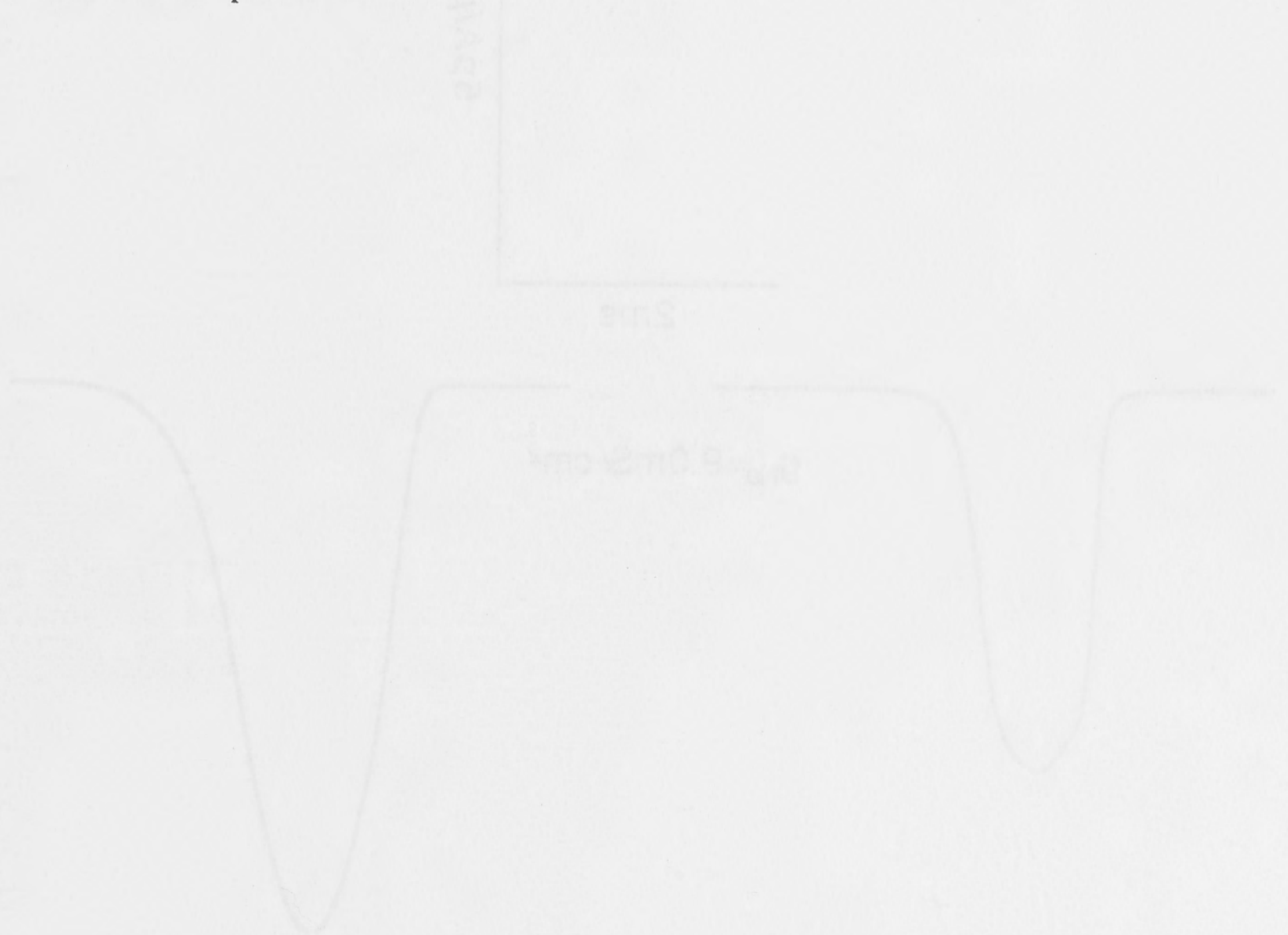


Figure 5.8. The A-current densities produced at 50 and 200 $\mu\text{m}$  with a maximum A-current conductance density of  $9.0\text{mS}/\text{cm}^2$ , compared with the action potential waveform at these locations. This figure used only a single dendrite of *C1-2101* as marked in the inset of *figure 5.6A*. The current density always peaks after the action potential and contributes to its repolarisation. The action potentials are included so that the changes in membrane potential that occur during the current can be compared. This was done so that the driving potential for potassium could be compared with the A-current amplitude. The driving potential for potassium is largest during the peak of the action potential. The reversal potential for potassium was always set to  $-90\text{mV}$  in this model and the peak of the action potential is  $+18\text{mV}$ , making the driving potential for potassium  $108\text{mV}$  at the peak of the action potential. Therefore, although relatively few of the slowly activating  $I_A$  channels will have opened at the peak of the action potential, the driving potential is large so the current amplitude is large. At  $200\mu\text{m}$  from the soma, the action potential amplitude is smaller, the activation of  $g_A$  is smaller, the driving potential for potassium is smaller and the A-current amplitude is smaller.



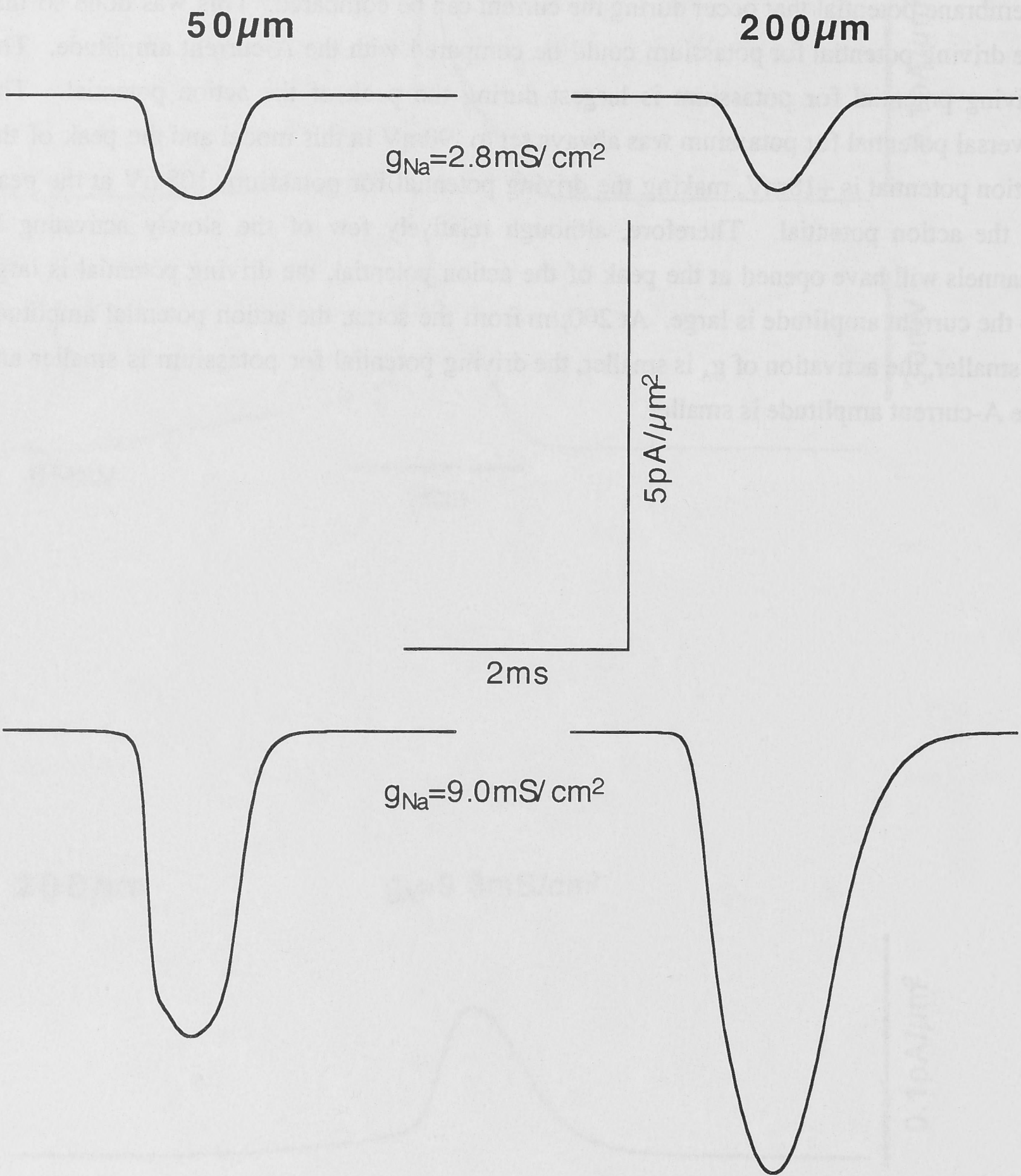
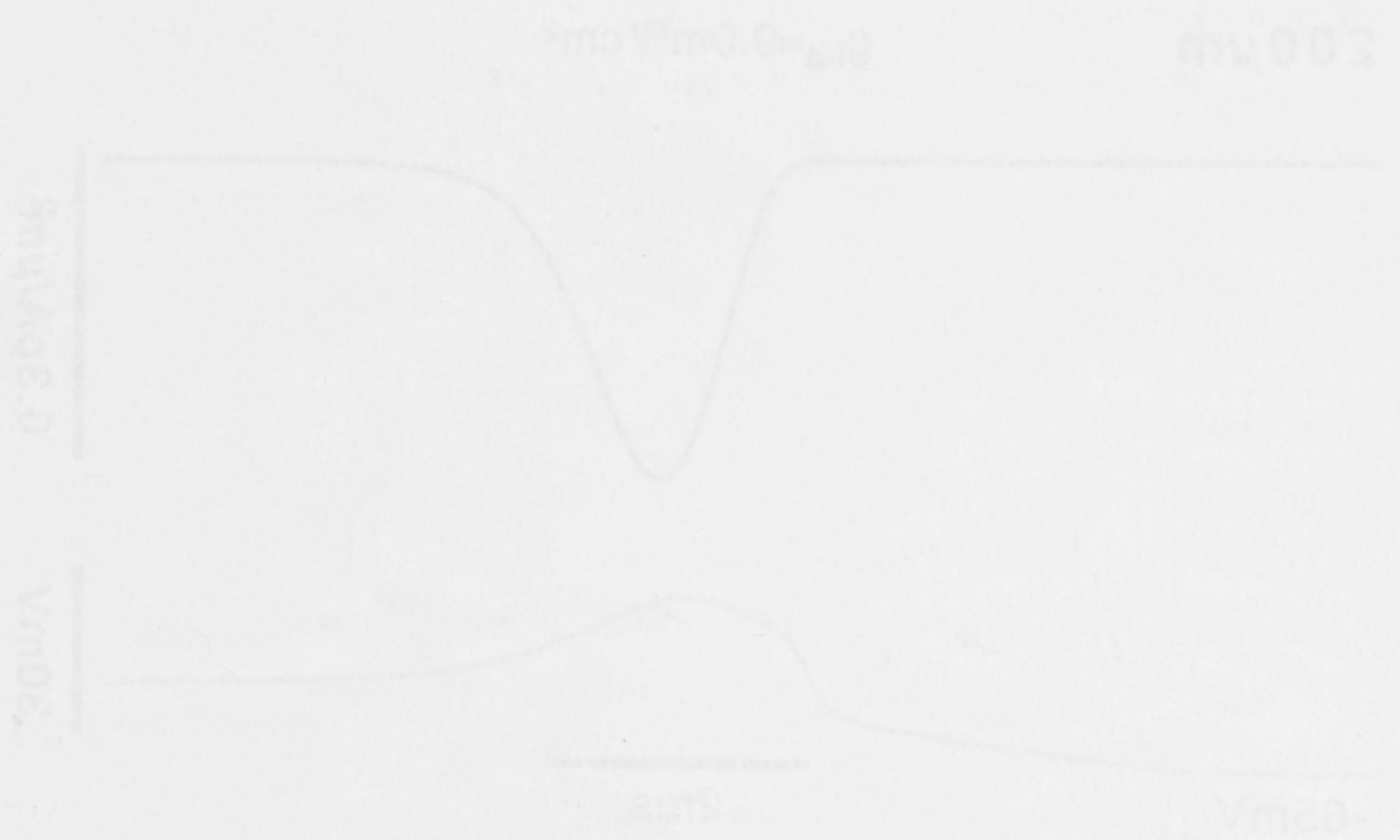


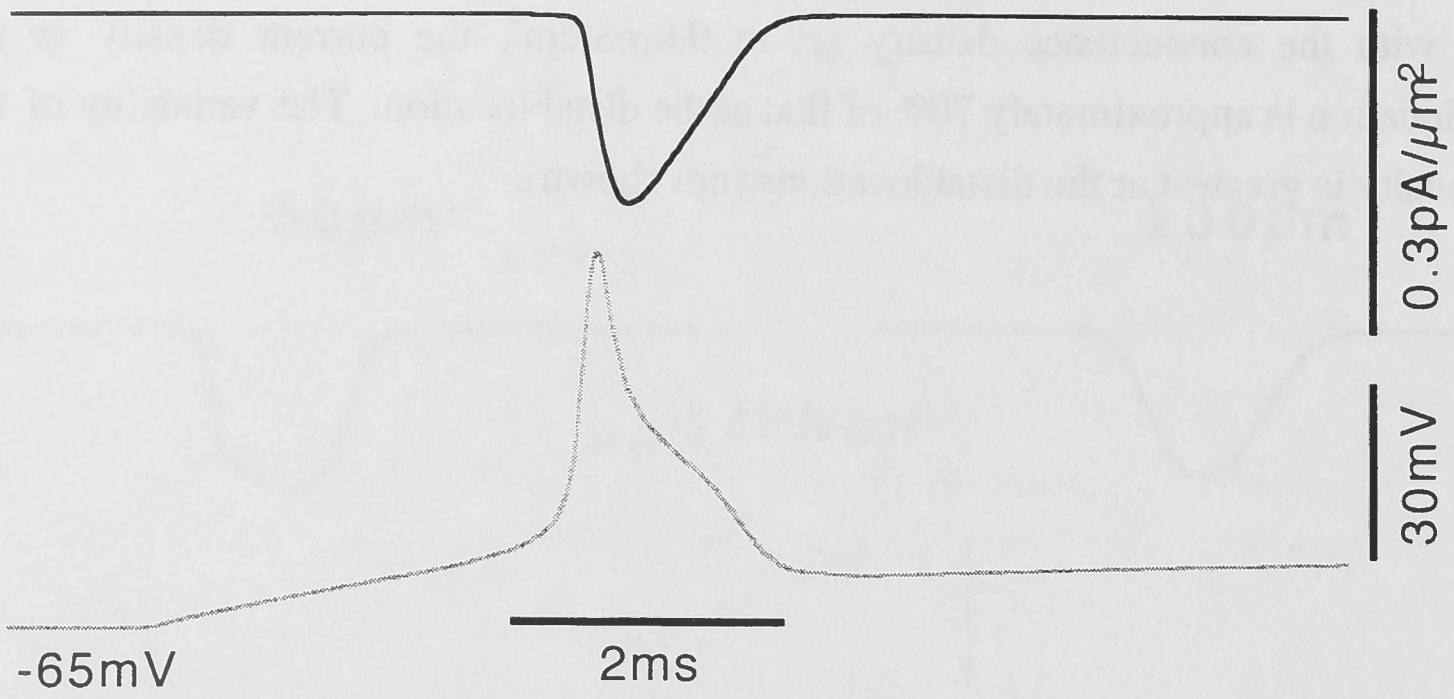
Figure 5.9. The average contrived  $\text{Na}^+$  current density recorded at 50 and 200  $\mu\text{m}$  with maximum  $\text{Na}^+$  conductance densities of  $2.8\text{mS}/\text{cm}^2$  and  $9.0\text{mS}/\text{cm}^2$ . With a conductance density of  $2.8\text{mS}/\text{cm}^2$ , the currents produced at the two locations are approximately equal. However, with the conductance density set to  $9.0\text{mS}/\text{cm}^2$ , the current density at the proximal location is approximately 70% of that at the distal location. The variability of the current density is greatest at the distal locations (not shown).





50  $\mu\text{m}$

$g_{\text{Na}}=9.0\text{mS}/\text{cm}^2$



200  $\mu\text{m}$

$g_{\text{Na}}=9.0\text{mS}/\text{cm}^2$

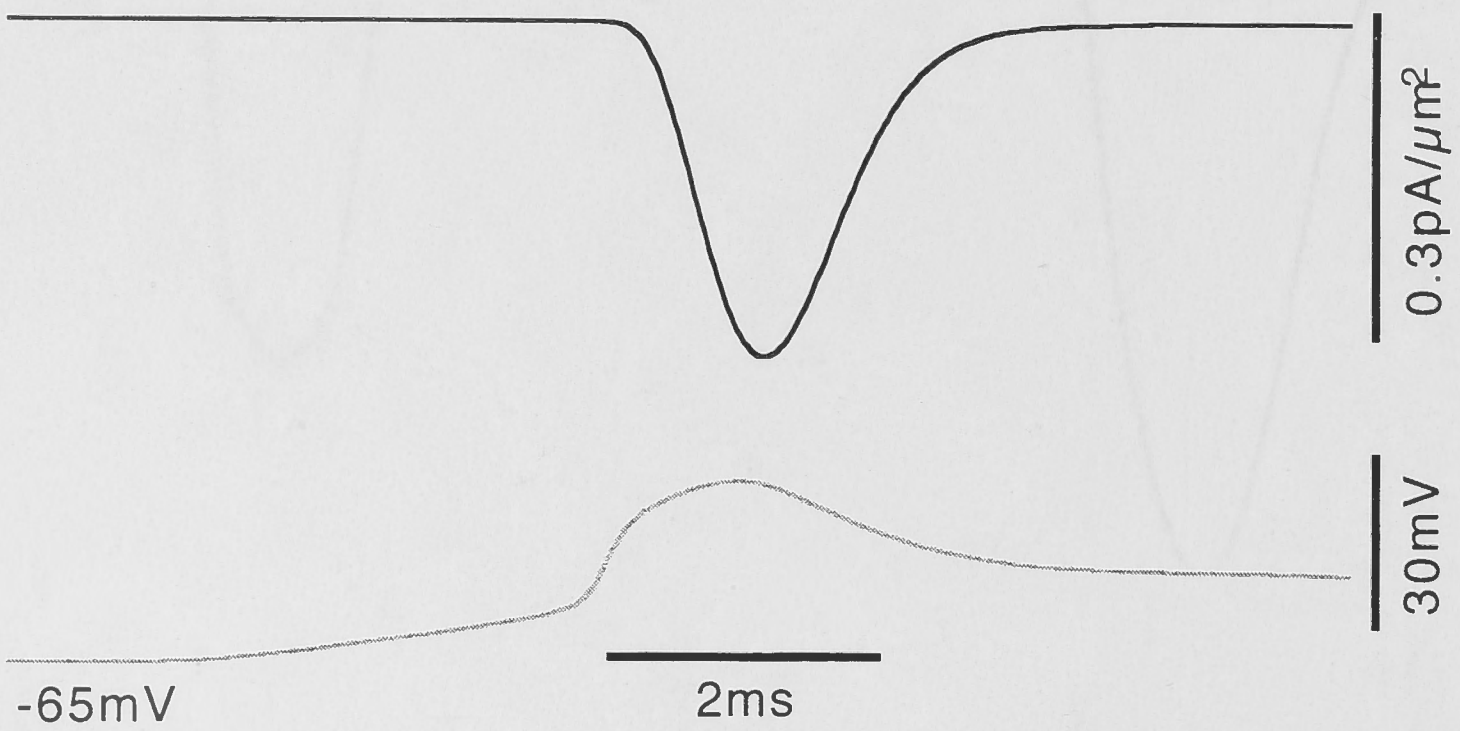


Figure 5.10. The contrived  $\text{Na}^+$  current densities produced at 50 and 200 $\mu\text{m}$  with a maximum sodium conductance density of  $9.0\text{mS}/\text{cm}^2$ , compared with the action potential waveform at these locations. This figure used only a single dendrite of *CI-2101* as marked in the inset of *figure 5.6A*. At 50 $\mu\text{m}$  the  $\text{Na}^+$  current peaks after the action potential because the voltage changes associated with the action potential drive the activation of the  $\text{Na}^+$  conductance. At 200 $\mu\text{m}$ , the  $\text{Na}^+$  current and action potential peak simultaneously because the voltage changes associated with backpropagating action potential are largely driven by the dendritic  $\text{Na}^+$  conductance. The action potentials are included in this figure so that the changes in membrane potential that occur during the  $\text{Na}^+$  current can be compared. This was done so that the driving potential for sodium, and the extent of  $\text{Na}^+$  channel activation, could be compared with the sodium current density. The driving potential for sodium is smallest during the peak of the action potential. The reversal potential for sodium was always set to +50mV in this model. The peak of the action potential at 50 $\mu\text{m}$  is +28mV, making the driving potential for sodium 22mV at the peak of the action potential at 50 $\mu\text{m}$ . Although a large proportion of the  $\text{Na}^+$  channels will have opened at the peak of the action potential, the driving potential is small so the current density is also small. At 200 $\mu\text{m}$  from the soma, the action potential amplitude is smaller, activation is reduced, the driving potential for sodium is larger and the  $\text{Na}^+$  current density is larger.

Lüscher and Larkum (1998) have performed similar modelling of backpropagation in cultured motoneurons. In their model, they found that densities of  $\text{Na}^+$  conductance as low as  $3.0\text{mS}/\text{cm}^2$  could cause significant active backpropagation of the dendritic action potential. This was not observed in the modelling performed in this chapter. To determine the reasons, several tests were performed to see what fundamental differences there were between the model of Lüscher and Larkum (1998) and the model presented in this chapter.

The first of these tests consisted of replacing the dendritic  $\text{Na}^+$  channel that was used in this study with that used by Lüscher and Larkum (1998). The channel is taken from Mainen *et al.* (1995) and has been described already in the Methods section.  $\text{Na}^+$  conductance densities of  $3.0\text{mS}/\text{cm}^2$  and  $9.0\text{mS}/\text{cm}^2$  were used, which are almost identical to the densities used previously. Figure 5.11 shows the action potential peak voltage in *C1-2101* under passive conditions,  $g_{\text{Na}}=3.0\text{mS}/\text{cm}^2$  and  $g_{\text{Na}}=9.0\text{mS}/\text{cm}^2$ . Figure 5.11A shows the action potential peak voltage in every dendrite of *C1-2101*, while figure 5.11B shows the amplitude in the single dendrite marked in the inset of 5.11A. The conductance density of  $3.0\text{mS}/\text{cm}^2$  gives a moderate amplification of the action potential while a density of  $9.0\text{mS}/\text{cm}^2$  produces fully active backpropagation. In figure 5.11B, the  $\text{Na}^+$  conductance density of  $9.0\text{mS}/\text{cm}^2$  does not affect the action potential amplitude until it has propagated beyond about  $80\mu\text{m}$  from the soma. Up to this point, the action potential attenuation is similar to that in a passive dendrite and there is only moderate amplification of the action potential amplitude. Beyond this distance, the backpropagation becomes regenerative and the action potential amplitude begins to increase until it reaches a peak voltage of about  $+30\text{mV}$  in the distal dendrites. The threshold  $\text{Na}^+$  conductance density for active backpropagation could not be sharply defined and was different for each dendrite, varying between about  $3.0$  and  $5.0\text{mS}/\text{cm}^2$ . Even with a conductance density of  $3.0\text{mS}/\text{cm}^2$ , there are a couple of dendrites in figure 5.11A that show active backpropagation as defined by maintained dendritic action potential amplitude.

Overall, the effect of Mainen's sodium channel on the action potential amplitude was the about the same as when the contrived sodium channel was used, except that lower density was required to produce the same effect. Mainen's sodium channel leaves the action potential amplitude in the proximal dendrites relatively unaffected, while in the distal dendrites the action potential amplitude is increased significantly.

Figure 5.12 shows the average sodium current densities obtained with the Mainen model at  $50$  and  $200\mu\text{m}$  when the conductance density is either  $3.0$  or  $9.0\text{mS}/\text{cm}^2$ . The current density has been averaged for every dendrite at these distances, except for the current at  $200\mu\text{m}$ , which is taken from one dendrite only. The currents at  $200\mu\text{m}$  in each dendrite for  $9.0\text{mS}/\text{cm}^2$  were similar in time-course and amplitude, but there was up to  $1\text{ms}$  latency variation for their initiation. These currents were associated with fully active backpropagation of the action potential and their variation in latency was due to different

rates of backpropagation in the dendrites. There were large variations in time-course and amplitude for the  $3.0\text{mS}/\text{cm}^2$  conductance at  $200\mu\text{m}$ , while there was little variation in time-course and amplitude at  $50\mu\text{m}$ , for both conductance levels.

The main differences between the Mainen model and the contrived model are the rates of activation and inactivation. All the current densities in figure 5.12 are much larger than their counterparts in figure 5.9 (contrived model), and the same applies to the corresponding action potential amplification generated by these currents (compare Figs 5.6, 5.11, 5.10 and 5.13). The faster activation and the slower inactivation will enhance the currents at all locations. As was found for the contrived channel, the presence of a sodium current made little difference to the amplitude of the action potential in the proximal  $100\mu\text{m}$  of dendrite, indicating that in this region the main control of the action potential was from the sodium currents generated at the soma, axon hillock and initial segment. Once the action potential propagates beyond this distance, the  $\text{Na}^+$  channel contributes to the amplification of the backpropagated action potential. With a sodium conductance density of  $9.0\text{mS}/\text{cm}^2$ , the backpropagation is fully active. The larger current at  $200\mu\text{m}$  and  $9.0\text{mS}/\text{cm}^2$  (compared with  $50\mu\text{m}$ ) reflects the regenerative activation of the channel by the actively backpropagated action potential. Therefore the  $\text{Na}^+$  channel drives the voltage changes that occur during the actively backpropagated action potential. The smaller current at  $50\mu\text{m}$  with a conductance density of  $9.0\text{mS}/\text{cm}^2$  results from the reduced driving potential for sodium during the large proximal action potential. Figure 5.13 shows the average  $\text{Na}^+$  current densities produced by the sodium channel of Mainen *et al.* at  $50$  and  $200\mu\text{m}$  with conductance densities of  $3.0$  and  $9.0\text{mS}/\text{cm}^2$  compared with the action potentials at these locations. This figure used only a single dendrite of *C1-2101* as marked in the inset of figure 5.11A. The data for  $200\mu\text{m}$  supports the hypothesis that the  $\text{Na}^+$  current drives the voltage changes associated with the actively backpropagating action potential because the current peaks during the rising phase of the action potential. At proximal locations however, the peak  $\text{Na}^+$  current lags behind the action potential peak because its activation is driven by the action potential.

Comparison of the model used in this chapter with that used by Lüscher and Larkum (1998) reveals further differences between the two models. Lüscher and Larkum (1998) used the morphology of a cultured motoneurone and a morphologically realistic axon hillock, initial segment and axon. It was not possible to reproduce the action potential waveform in this model with a realistic hillock and axonal morphology, therefore a simplified hillock was used. Modification of the axon diameter to  $0.8\mu\text{m}$  to match that of Lüscher and Larkum did not result in significant changes in the action potential waveform and so the axon diameter was kept at  $1.0\mu\text{m}$ .

The following text is extremely faint and illegible. It appears to be a dense paragraph of text, possibly a scientific or technical report, but the content cannot be discerned due to the low contrast and blurriness of the scan. The text is oriented vertically on the page.

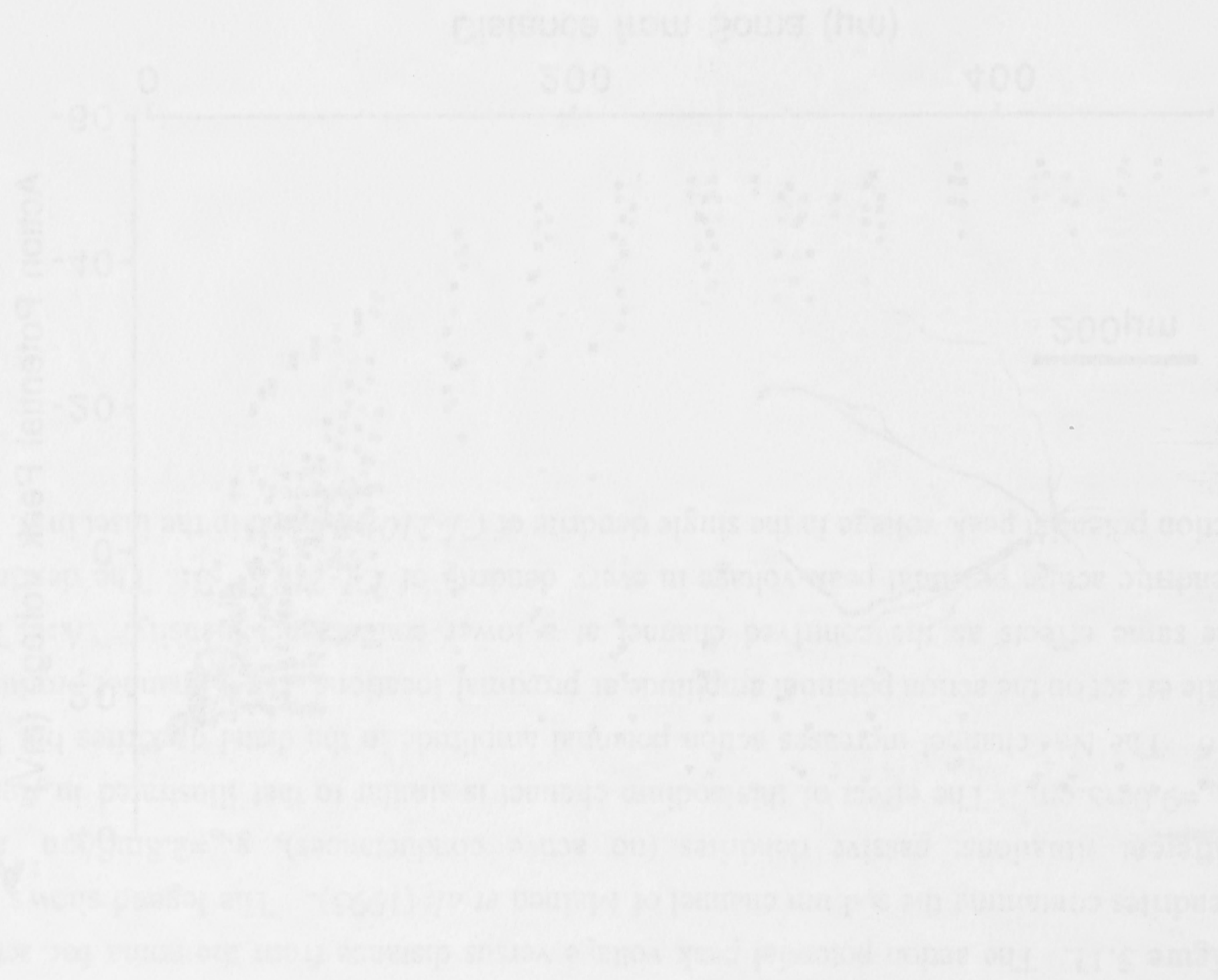
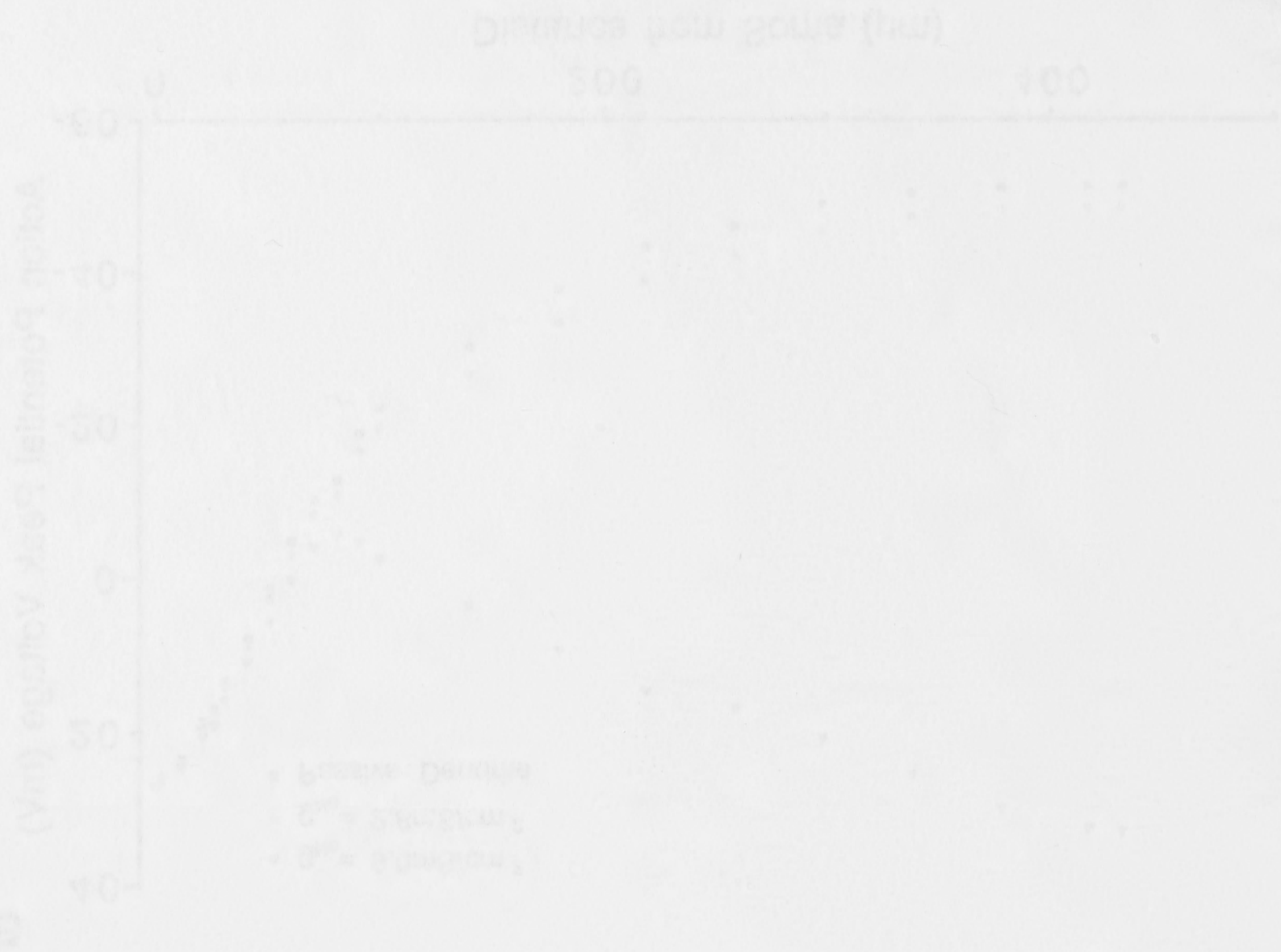


Figure 2.17. The action potential peak voltage decreases from the source but more rapidly in the 3.0% channel of Figure 2.16. The legend shows the different channels: 1.0% (solid circles), 2.0% (open circles), and 3.0% (solid squares). The effect of the reduced channel is similar to that reported in Figure 2.6. The 3.0% channel exhibits action potential propagation in the distal direction but the rate of action potential propagation is reduced. The 1.0% and 2.0% channels show the same effect as the control channel of a lower propagation velocity. When the dendritic action potential peak voltage in each channel is 2.0 mV, the action potential peak voltage in the single channel of 3.0% is reduced to the level of the control channel.

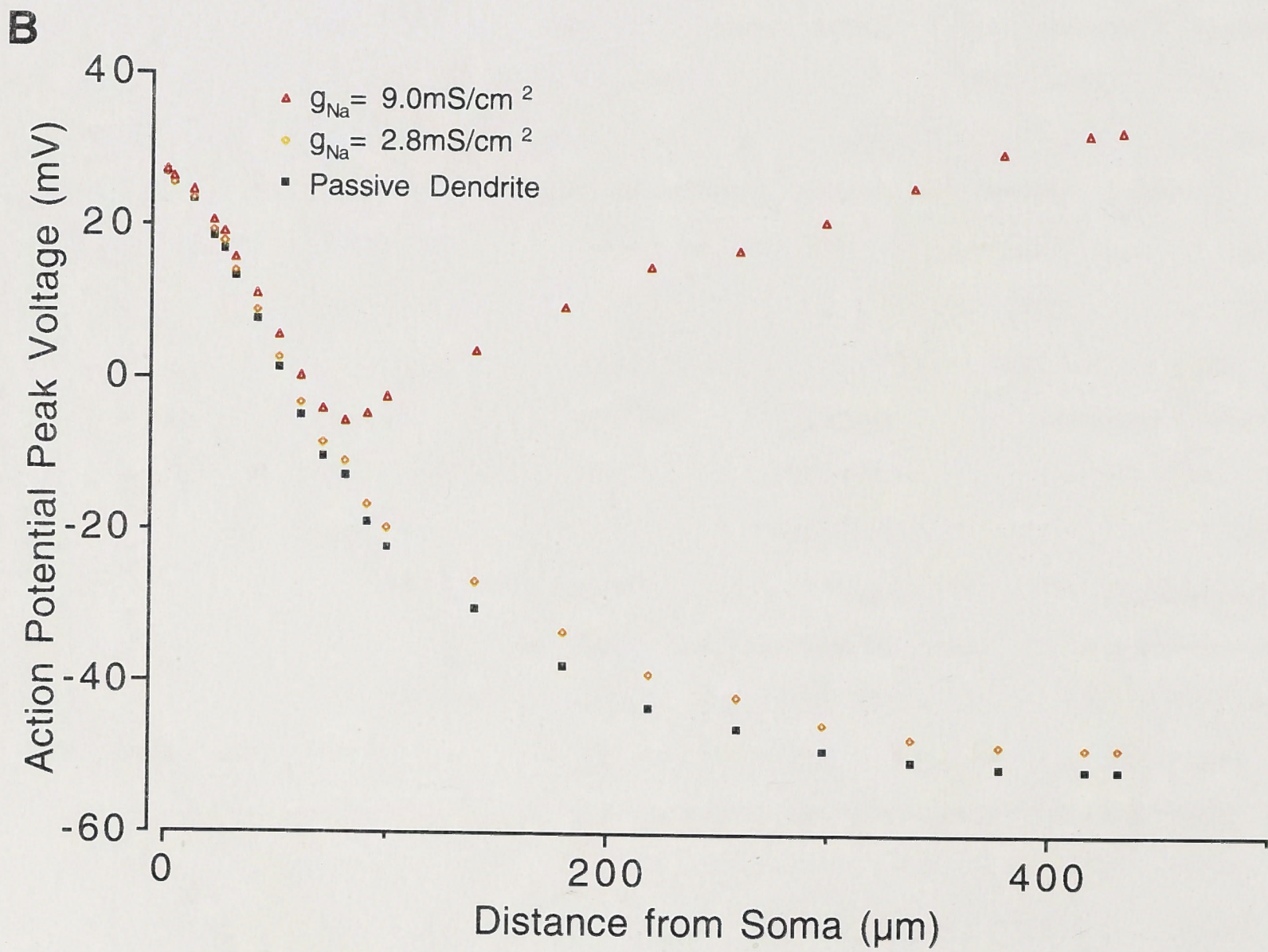
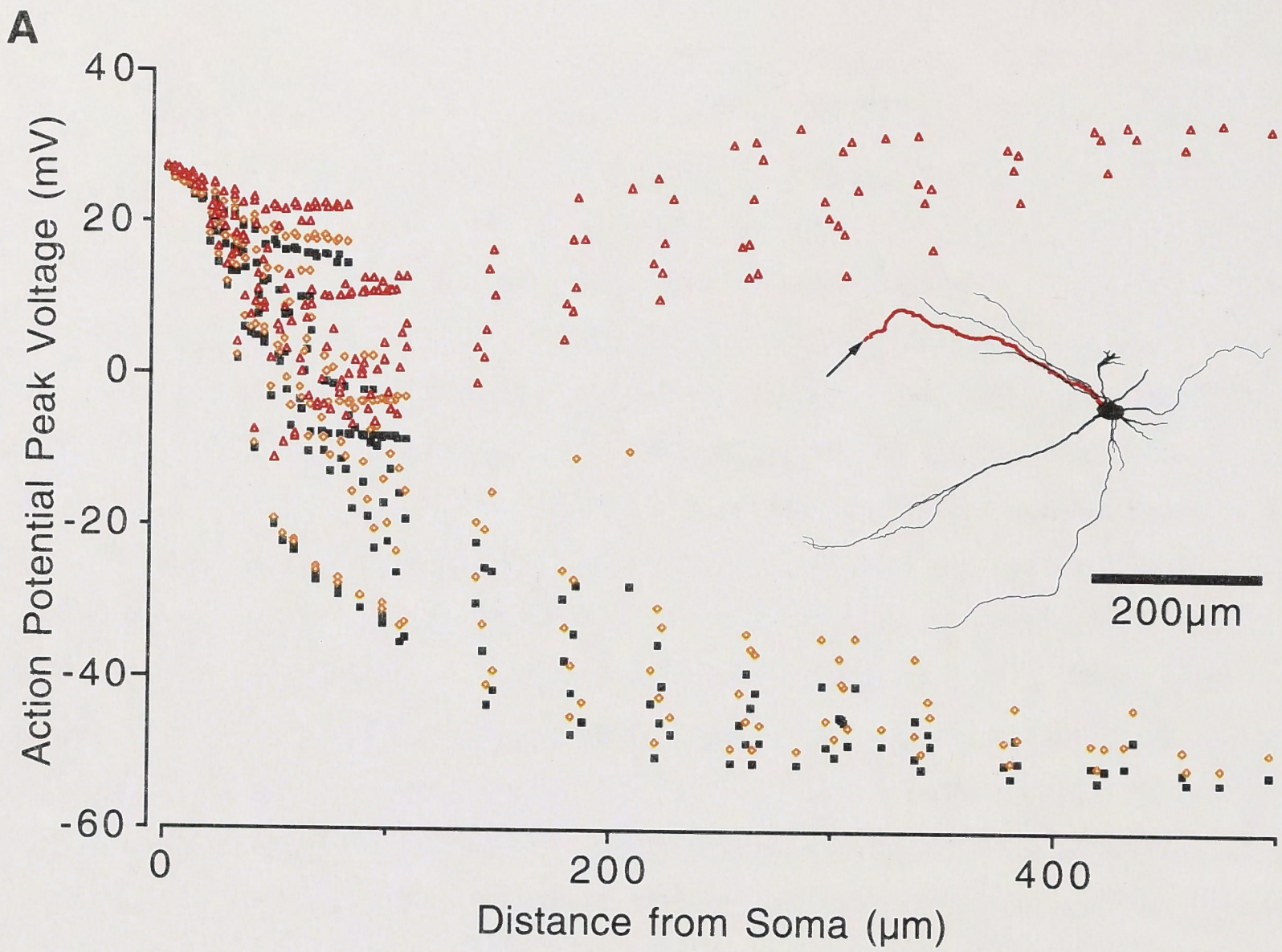


Figure 5.11. The action potential peak voltage versus distance from the soma for active dendrites containing the sodium channel of Mainen *et al.* (1995). The legend shows the different situations; passive dendrites (no active conductances),  $g_{Na}=2.8\text{mS}/\text{cm}^2$  and  $g_{Na}=9.0\text{mS}/\text{cm}^2$ . The effect of this sodium channel is similar to that illustrated in figure 5.6. The  $\text{Na}^+$  channel increases action potential amplitude in the distal dendrites but has little effect on the action potential amplitude at proximal locations. This channel produces the same effects as the contrived channel at a lower conductance density. **A:** The dendritic action potential peak voltage in every dendrite of *CI-2101*. **B:** The dendritic action potential peak voltage in the single dendrite of *CI-2101* marked in the inset in A.





Figure 2.11. The action potential peak voltage versus distance from the soma for various dendrites containing the sodium channel of  $g_{Na} = 3.0 \text{ mS/cm}^2$ . The top plot shows the different situations: passive dendrites (left) and active dendrites (right). The right plot shows the effect of the active dendrite on the action potential amplitude at proximal dendrites. The same effect is shown for a higher sodium channel density of  $g_{Na} = 9.0 \text{ mS/cm}^2$ . The distance between the active dendrite and the soma is  $50 \mu\text{m}$  and  $200 \mu\text{m}$ .

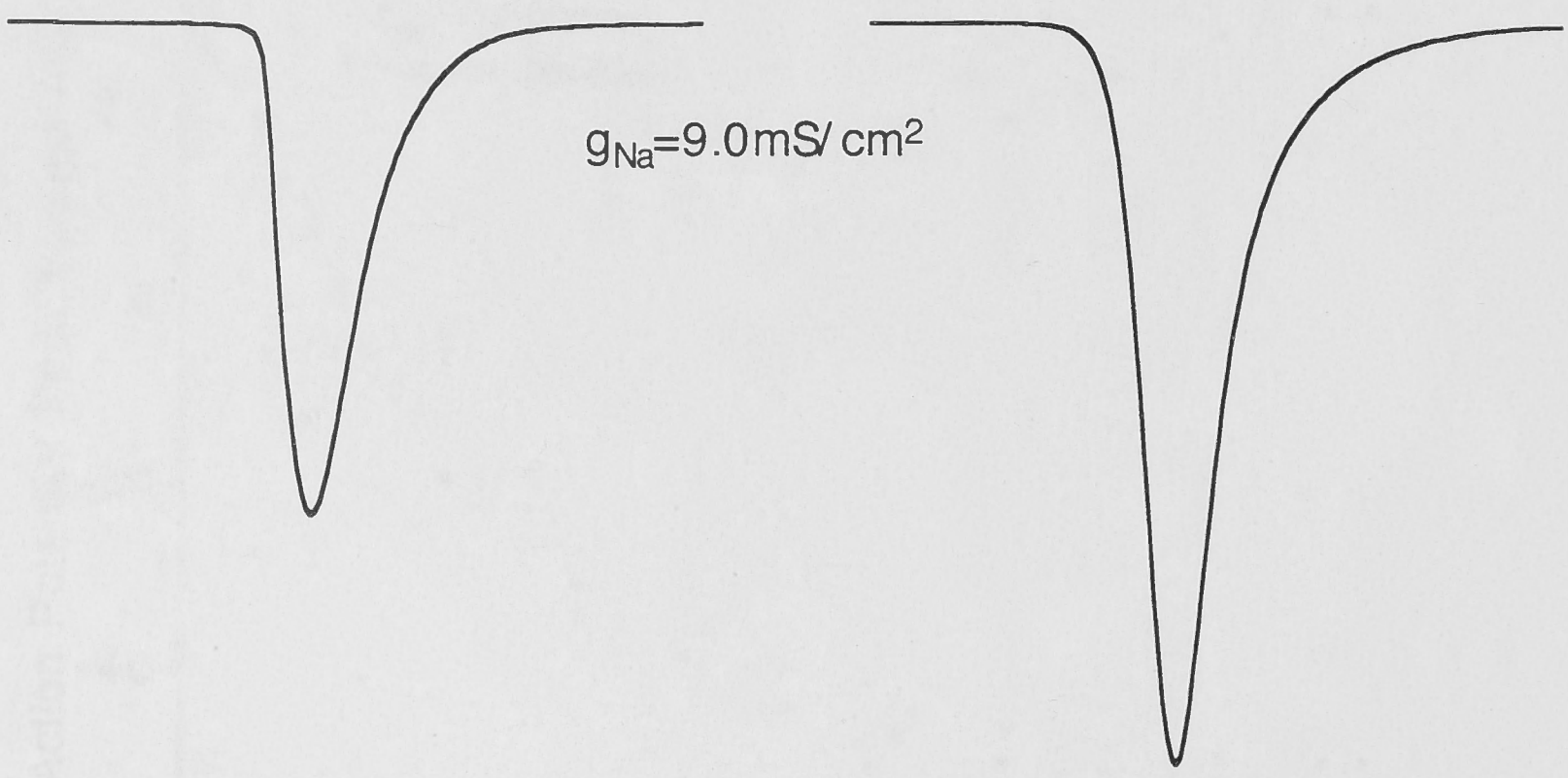
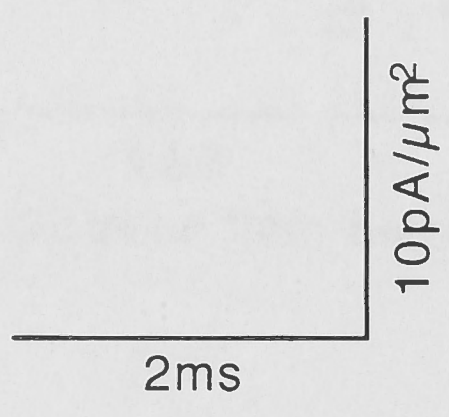
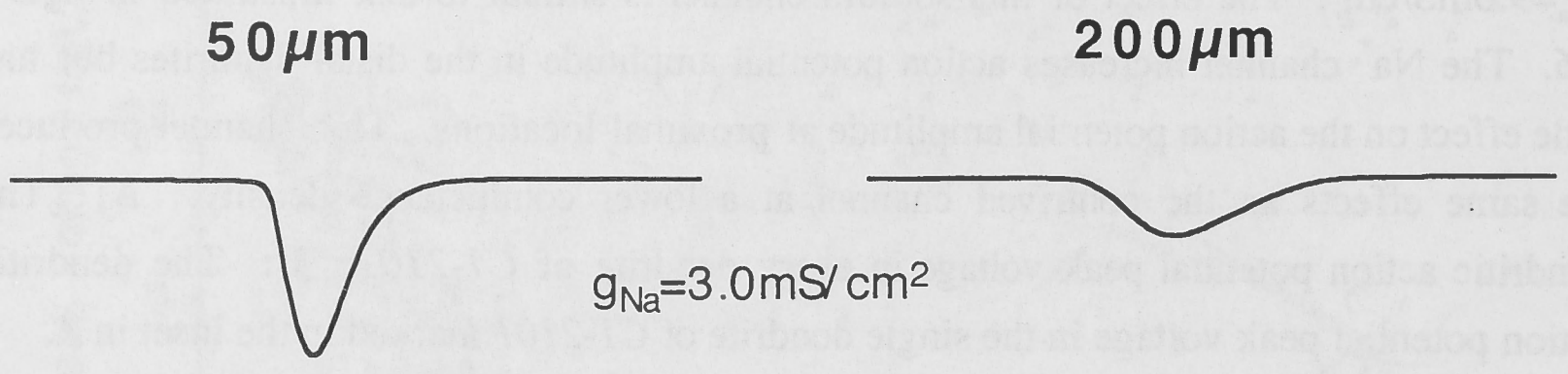
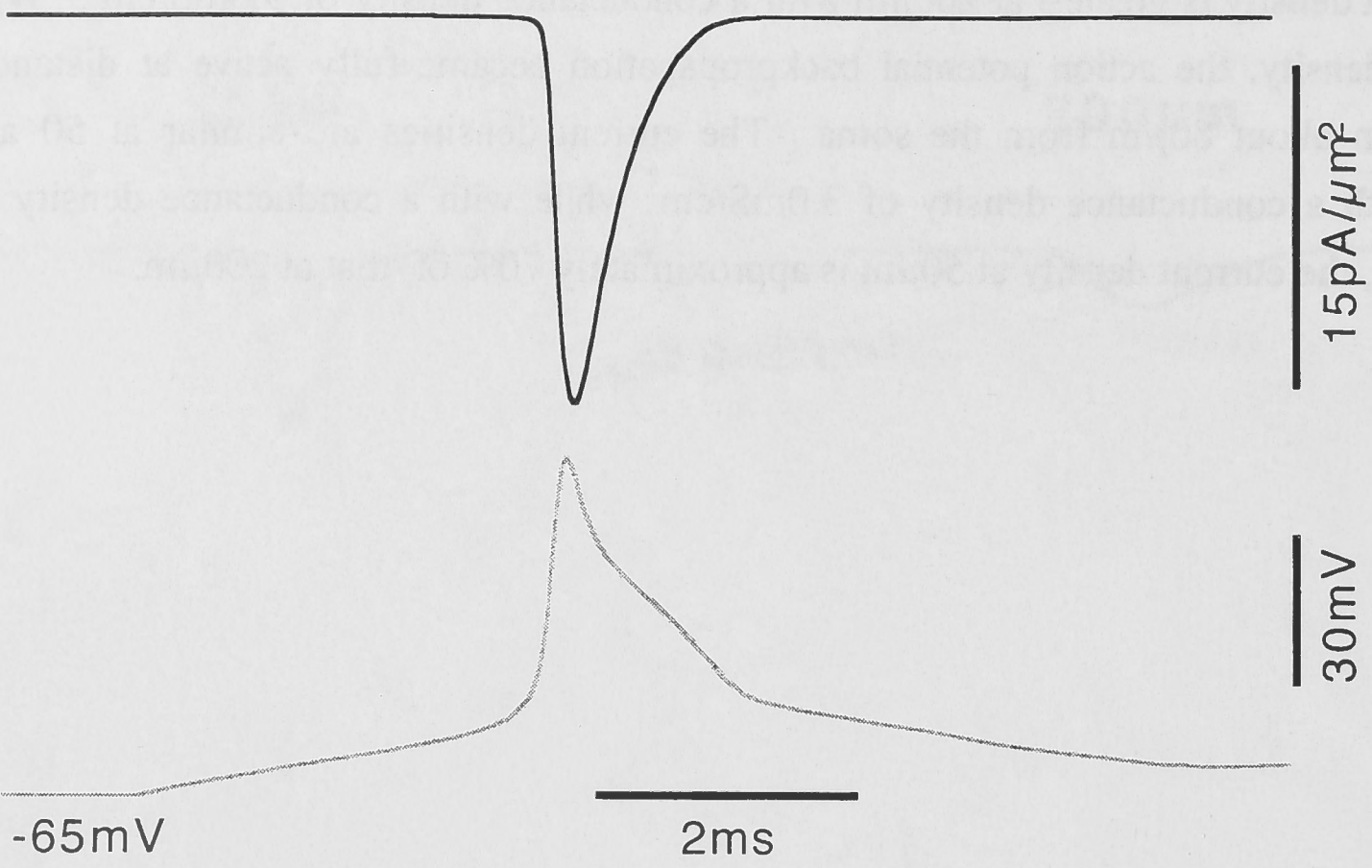


Figure 5.12. The average sodium current density produced by the channel of Mainen *et al.* (1995) at 50 and 200 $\mu\text{m}$  with  $\text{Na}^+$  conductance densities of 3.0 $\text{mS}/\text{cm}^2$  and 9.0 $\text{mS}/\text{cm}^2$ . The current density is greatest at 200 $\mu\text{m}$  with a conductance density of 9.0 $\text{mS}/\text{cm}^2$ . With this high density, the action potential backpropagation became fully active at distances greater than about 80 $\mu\text{m}$  from the soma. The current densities are similar at 50 and 200 $\mu\text{m}$  with a conductance density of 3.0 $\text{mS}/\text{cm}^2$  while with a conductance density of 9.0 $\text{mS}/\text{cm}^2$ , the current density at 50 $\mu\text{m}$  is approximately 70% of that at 200 $\mu\text{m}$ .



50  $\mu\text{m}$

$g_{\text{Na}}=9.0\text{mS}/\text{cm}^2$



200  $\mu\text{m}$

$g_{\text{Na}}=9.0\text{mS}/\text{cm}^2$

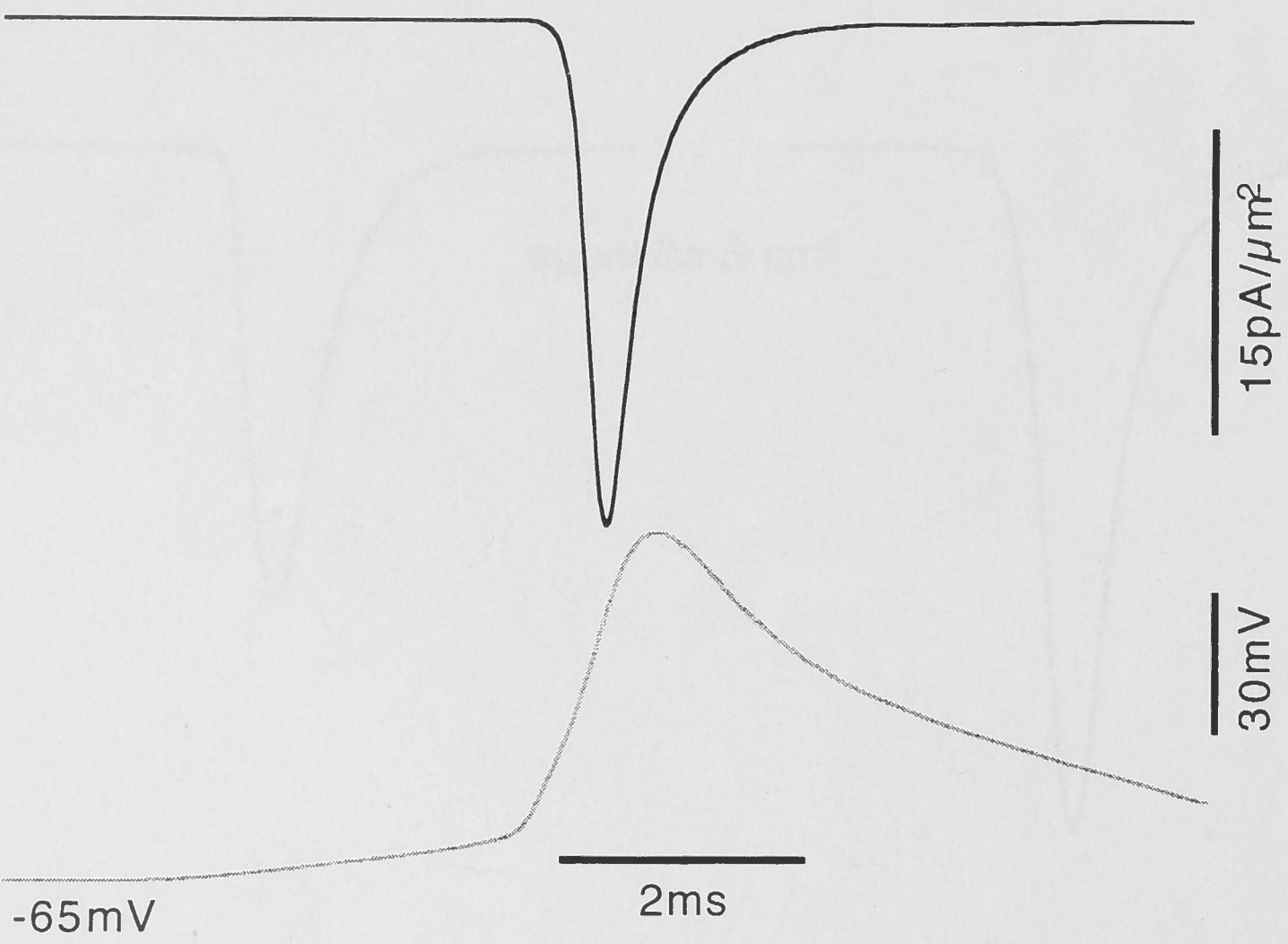


Figure 5.13. The  $\text{Na}^+$  current densities produced by the model of Mainen *et al.* (1995) at 50 and 200 $\mu\text{m}$  with a sodium conductance density of  $9.0\text{mS}/\text{cm}^2$ , compared with the action potential waveform at these locations. This figure uses only a single dendrite of *CI-2101* as marked in the inset of *figure 5.11A*. At 50 $\mu\text{m}$  the  $\text{Na}^+$  current peaks after the action potential because the voltage changes associated with the action potential drive the activation of the  $\text{Na}^+$  conductance. At 200 $\mu\text{m}$ , the  $\text{Na}^+$  current precedes the action potential because the backpropagation is fully active and the action potential voltage is driven by the  $\text{Na}^+$  conductance. The early part of the rising phase of the actively backpropagating action potential activates the  $\text{Na}^+$  conductance. The action potentials are included in this figure so that the changes in membrane potential that occur during the  $\text{Na}^+$  current can be compared. This was done so that the driving potential for sodium and the extent of  $\text{Na}^+$  channel activation could be compared with the sodium current density. The reversal potential for sodium was always set to +50mV in this model. The peak of the action potential at 50 $\mu\text{m}$  is +27mV, making the driving potential for sodium 23mV at the peak of the action potential. Although a large proportion of the  $\text{Na}^+$  channels will have opened at the peak of the action potential, the driving potential is small so the current density is also small. At 200 $\mu\text{m}$  from the soma, the action potential amplitude is larger because of active backpropagation.

Other important differences between the two models are the action potential waveform at the soma and the membrane capacitance. Larkum *et al.* (1996) show somatic action potentials recorded from cultured motoneurons as having a base-width of approximately 2ms and amplitude of approximately 70 to 80mV. In their model the base-width of the action potential is at least 2ms and the amplitude of the somatic action potential is approximately 90 to 100mV; these action potentials are very different from the action potentials that were recorded *in vivo* in Chapter 4. Action potential base-width in the cells recorded here was  $0.67 \pm 0.12$ ms and the action potential amplitude was  $74 \pm 7.9$ mV. This is related to the difference in temperature. Larkum *et al.* (1996) made recordings at 20°C, whereas the recordings described in Chapter 4 were made at 34°C. The action potential will be faster in recordings made at a higher temperature and the action potential attenuation will differ. In addition, dendritic active conductances will have different kinetics at a higher temperature and so their effect on the action potential will be different. Therefore, the results produced in cultured cells and in the model of Lüscher and Larkum (1998) do not necessarily reflect the properties of motoneurons *in vivo*. The faster time-course of the action potential will mean that the membrane capacitance will have a greater effect on the attenuation of the action potential during backpropagation.

To test the effect of a lower capacitance on the action potential attenuation, the modelling was repeated with a capacitance of  $1.0 \mu\text{F}/\text{cm}^2$ . Figure 5.14 shows the peak voltage of the action potential as a function of distance along the single dendrite of *C1-2101* as shown in the inset of figure 5.11A. Passive membrane properties were used for this model. The lower capacitance results in less attenuation of the action potential amplitude and shorter latencies for its initiation at the soma, but does not result in a very different rate of attenuation along the dendritic tree. Figure 5.14B shows the attenuated action potentials recorded at  $50 \mu\text{m}$  and  $200 \mu\text{m}$  from the soma with a capacitances of  $1.7$  and  $1.0 \mu\text{F}/\text{cm}^2$ . There is relatively little difference in their amplitude or time-course when the capacitance is lowered to  $1.0 \mu\text{F}/\text{cm}^2$ . Therefore, the difference in the time-course and amplitude of the action potential as modelled in this chapter and in the results of Lüscher and Larkum (1998) is not caused by then use of different membrane capacitance.

Lüscher and Larkum (1998) have shown that a  $\text{Na}^+$  conductance density as low as  $3.0 \text{mS}/\text{cm}^2$  results in active backpropagation of the dendritic action potential. They defined the threshold for active backpropagation of the action potential by using the phase plane loop of the current versus membrane potential. In the model presented here, backpropagation was defined by adjusting the conductance density until the action potential amplitude was maintained along the dendrites. Figure 5.15A shows the action potential peak voltage along the single dendrite of *C1-2101* illustrated in the inset of figure 5.11A with the capacitance set to  $1.7 \mu\text{F}/\text{cm}^2$ . Six situations of membrane properties were considered; passive dendrites (no voltage-dependent conductances),  $g_{\text{Na}}=3.0 \text{mS}/\text{cm}^2$ ,  $g_{\text{Na}}=9.0 \text{mS}/\text{cm}^2$ ,  $g_{\text{Na}}=12.0 \text{mS}/\text{cm}^2$ ,  $g_{\text{A}}=3.0 \text{mS}/\text{cm}^2$  and  $g_{\text{A}}=9.0 \text{mS}/\text{cm}^2$ . The sodium channel used for this modelling was the contrived channel described in the Methods and the A-current was identical to that used previously. The threshold sodium conductance density required to produce active action potential backpropagation was  $9.7 \text{mS}/\text{cm}^2$ .

Sodium conductance densities lower than this resulted in only small amplification of the action potential amplitude rather than active backpropagation. It can be seen in figure 5.15A that active propagation does not occur until the dendritic action potential has propagated beyond about  $100\mu\text{m}$ . This is due to the low driving potential for sodium during the action potential and the low input impedance at these proximal locations combined with the properties of the channel. Such a non-monotonic change in action potential amplitude as a function of dendritic location has been observed before in models such as those of Hoffman *et al.* (1997) and Migliore *et al.* (1999). The effect of the A-current on the action potential amplitude is not significantly different from that observed with a capacitance of  $1.7\mu\text{F}/\text{cm}^2$ .

To determine how this threshold for active backpropagation would change if the cell capacitance were  $1.0\mu\text{F}/\text{cm}^2$  as used by Lüscher and Larkum (1998), the procedure was repeated with a capacitance of  $1.0\mu\text{F}/\text{cm}^2$ . The results of this modelling are shown in figure 5.15B. The result is similar to that in figure 5.15A except that the threshold  $\text{Na}^+$  conductance density required for active backpropagation is  $4.7\text{mS}/\text{cm}^2$ . Once the sodium conductance density exceeds the critical value of  $4.7\text{mS}/\text{cm}^2$ , there is active backpropagation of the action potential at distances greater than about  $100\mu\text{m}$  from the soma. With a lower capacitance, active backpropagation is achieved with a sodium conductance density that is approximately half of that required when the capacitance is  $1.7\mu\text{F}/\text{cm}^2$ . This is to be expected, as the amount of capacitive charging current needed to achieve threshold is approximately halved. In figure 5.15B, a sodium conductance density of  $3.0\text{mS}/\text{cm}^2$  produced a few millivolts of amplification of the backpropagated action potential. This is greater than that seen when the capacitance is  $1.7\mu\text{F}/\text{cm}^2$  and is due to a slightly larger action potential amplitude with the lower capacitance.

#### *Action Potential Attenuation and Dendritic Diameter*

The relationship between action potential attenuation and dendritic diameter is shown in figure 5.16. At  $50\mu\text{m}$  (Fig 5.16A), there is no correlation between action potential amplitude and dendritic diameter (averaged between the soma and  $50\mu\text{m}$ ). The maximum difference in action potential amplitude between the passive and actively attenuating ( $I_A$ ) situations is no more than about  $15\text{mV}$ . Thus, assuming similar voltage activation/inactivation ranges, kinetics, density and distribution of  $I_A$  in motoneurons, then application of 4-AP to the bath solution would only increase action potential amplitude by at most  $15\text{mV}$  at  $50\mu\text{m}$ . For  $I_{\text{Na}}$ , the change in action potential amplitude is less than  $5\text{mV}$ . Therefore, if dendritic sodium channels could be blocked while somatic and axonal channels were unaffected, the action potential amplitude would decrease by less than  $5\text{mV}$  at  $50\mu\text{m}$ .

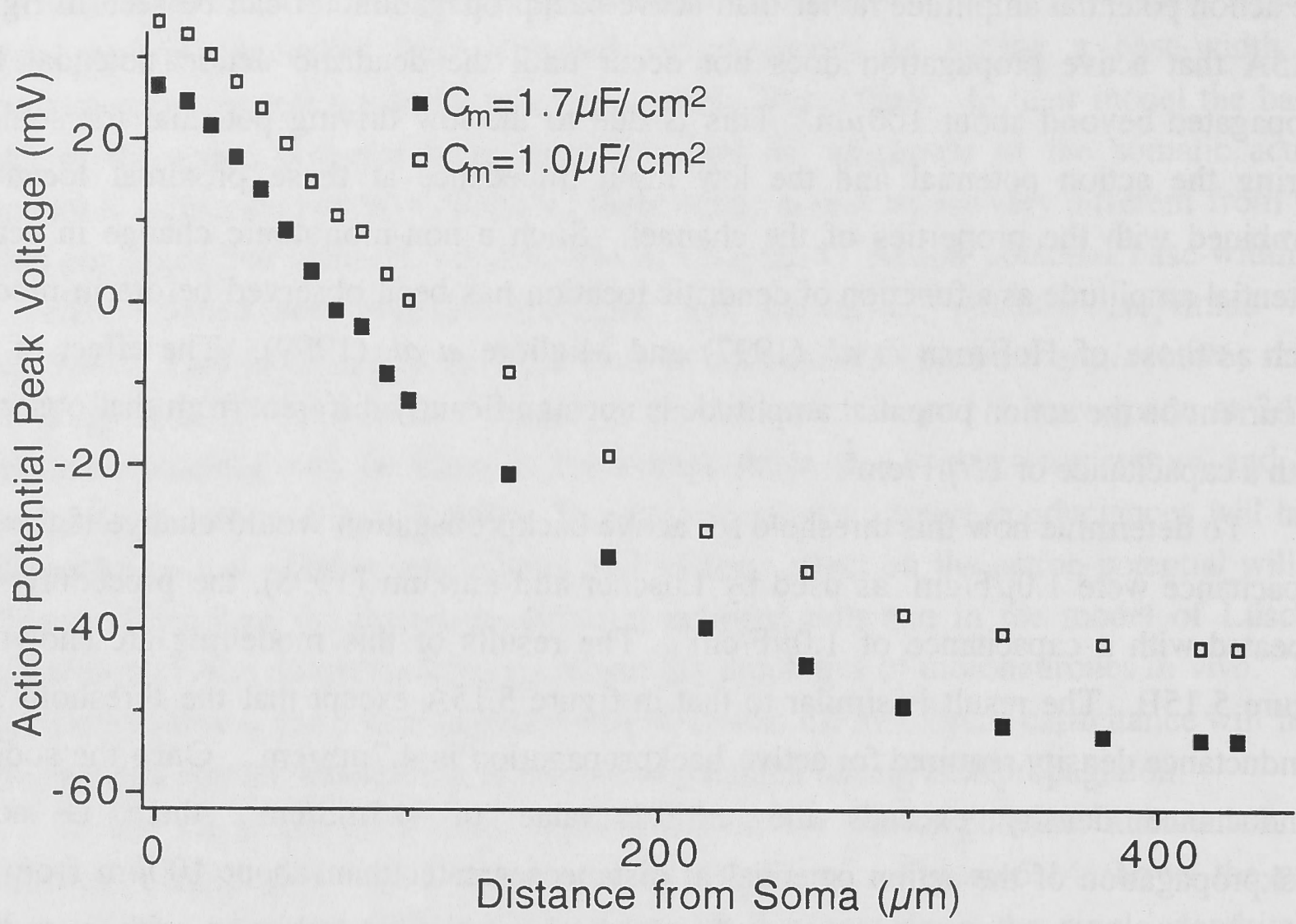
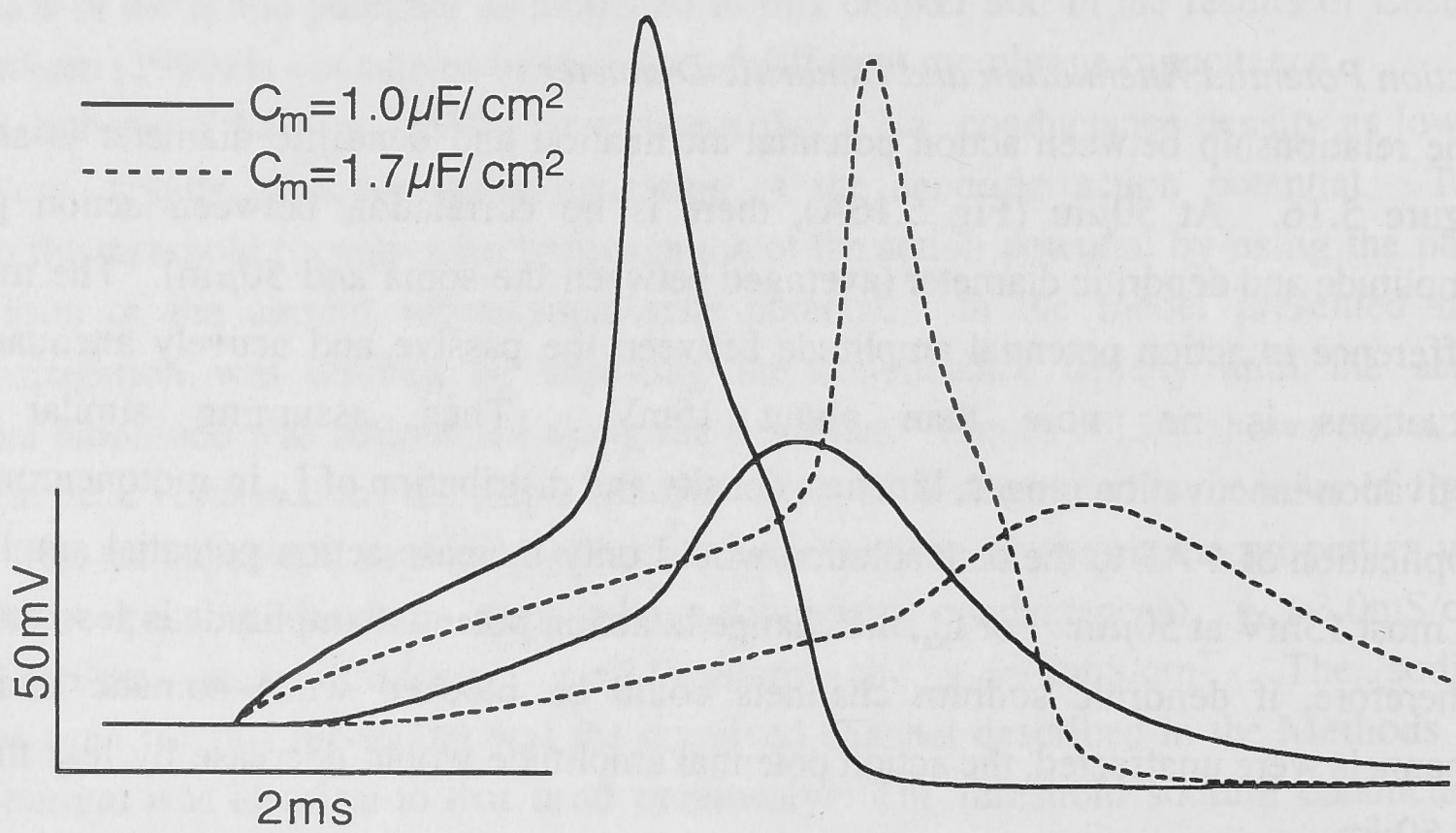
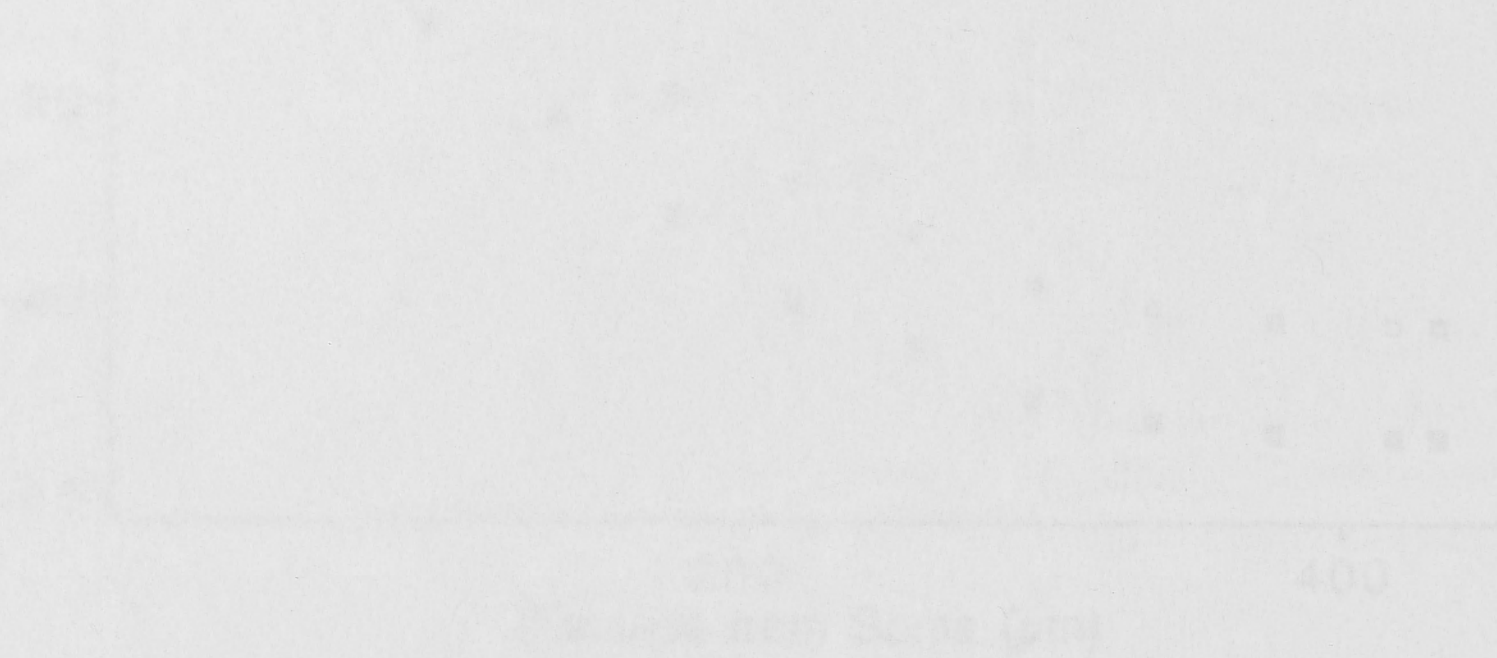
**A****B**

Figure 5.14. The effect of different capacitances on action potential attenuation under passive conditions. **A:** The action potential peak voltage with distance from the soma in a single dendrite of *CI-2101* shown in the inset of *figure 5.11A*. Decreasing the membrane capacitance to  $1.0\mu\text{F}/\text{cm}^2$  results in larger action potential amplitude but does not affect the rate of attenuation in the dendrites. The action potential amplitudes are simply scaled. **B:** The action potentials recorded at 50 and  $200\mu\text{m}$  from the soma with different capacitance values. Changing the capacitance does not significantly change the action potential waveform at either site.



Figure 2.14 The effect of different capacitance on action potential waveform at different positive conditions. At the action potential peak voltage with distance from the soma is a single dendrite of CV 2.01 shown in the inset of Figure 2.14. Decreasing the capacitance capacitance to 1.00 causes the action potential to rise more steeply and to reach the peak rate of rise sooner in the dendrite. The action potential in the soma is shown in Figure 2.14. The action potentials recorded at 50 and 100  $\mu\text{m}$  from the soma with different capacitance values. Changing the capacitance does not significantly change the action potential waveform at either site.





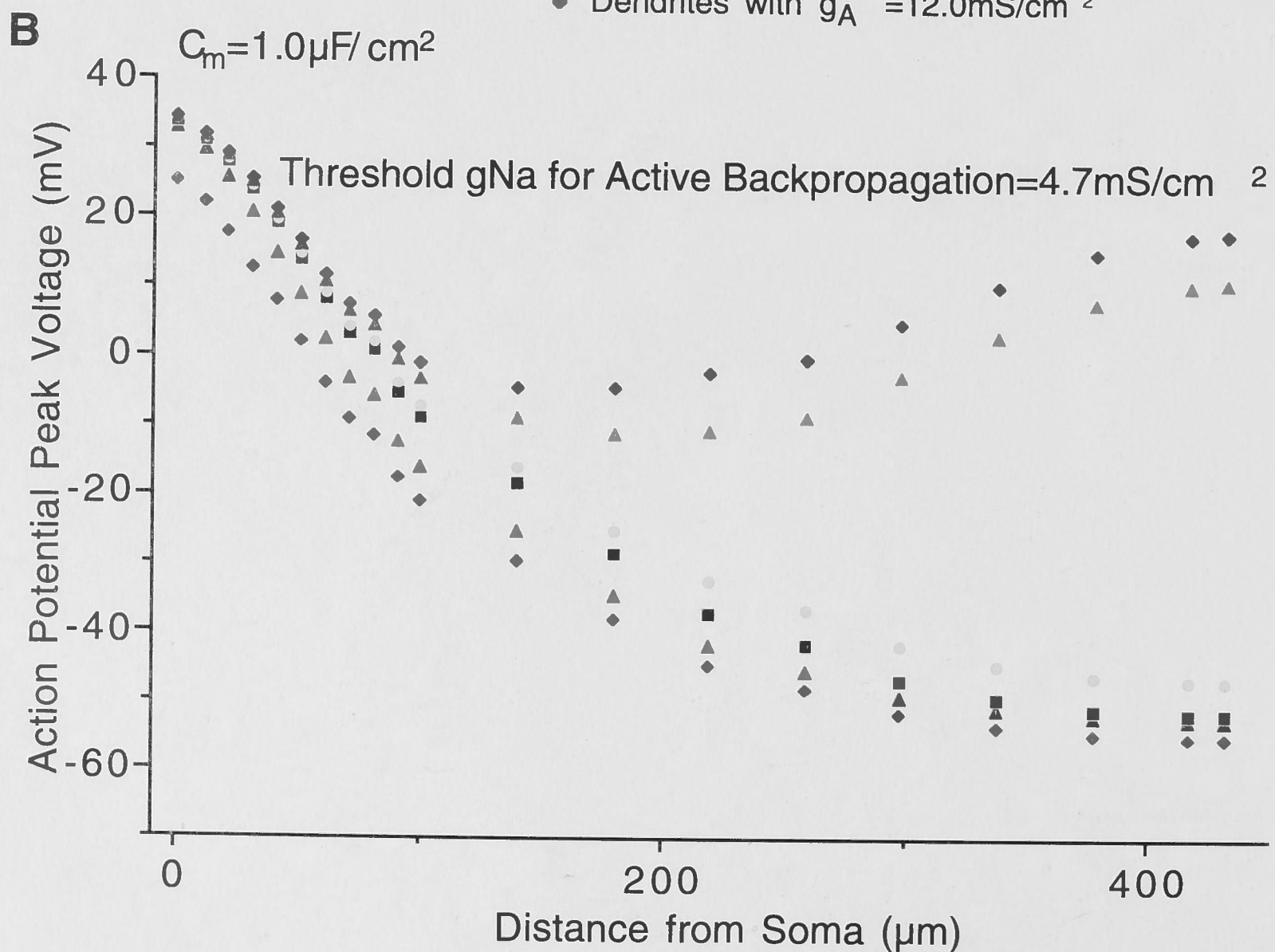
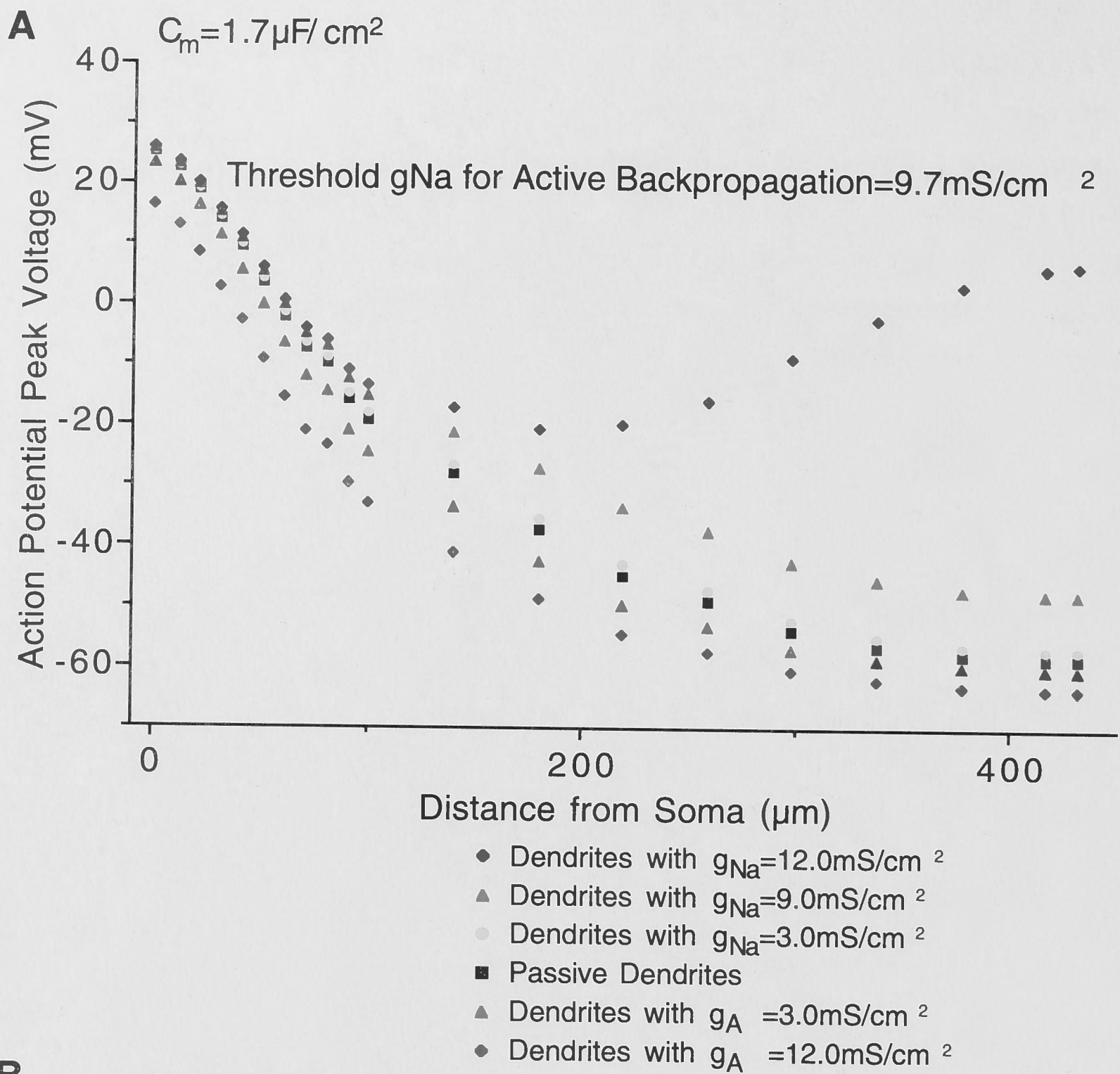
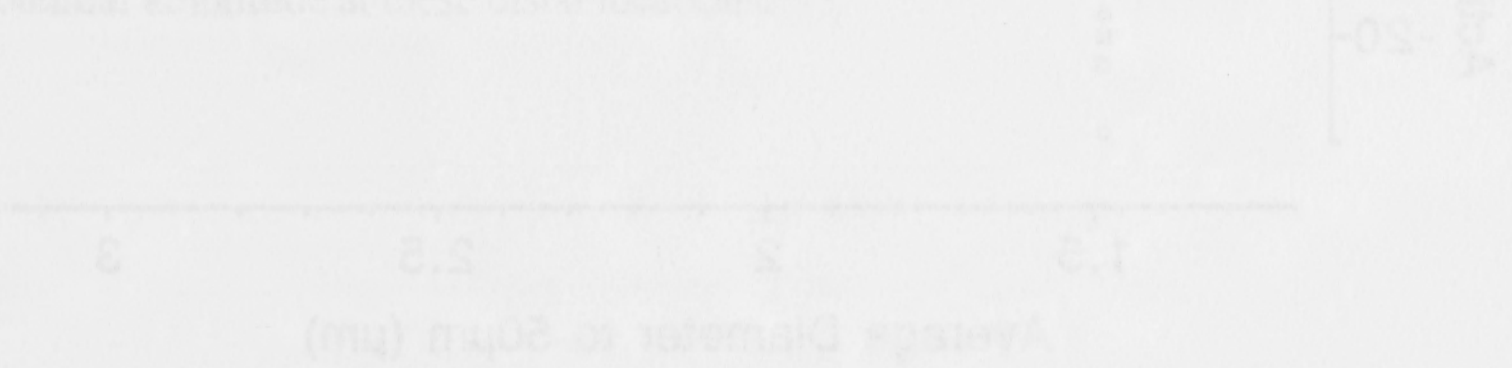


Figure 5.15. Action potential peak voltage versus distance from the soma for different membrane capacitance values and sodium and A-current conductance density. The results are taken from the single dendrite of *C1-2101* illustrated in the inset of *figure 5.11A*. **A:** The action potential peak voltage with distance from the soma for a membrane capacitance of  $1.7\mu\text{F}/\text{cm}^2$ . The sodium channel used for this figure was the contrived model and the A-current was exactly as described previously. The legend shows the different conductance densities used; passive dendritic membrane,  $g_{\text{Na}}=3.0\text{mS}/\text{cm}^2$ ,  $g_{\text{Na}}=9.0\text{mS}/\text{cm}^2$ ,  $g_{\text{Na}}=12.0\text{mS}/\text{cm}^2$ ,  $g_{\text{A}}=3.0\text{mS}/\text{cm}^2$  and  $g_{\text{A}}=9.0\text{mS}/\text{cm}^2$ . For this capacitance, the threshold  $\text{Na}^+$  conductance density necessary for active backpropagation was found to be  $9.7\text{mS}/\text{cm}^2$ . Values of conductance density below this value resulted in amplification of the action potential while values above this resulted in active backpropagation of the action potential. The effect of the A-current in this figure is exactly as in *figure 5.6B*. **B:** The action potential peak voltage with distance from the soma for a membrane capacitance of  $1.0\mu\text{F}/\text{cm}^2$ . The sodium channel used for this figure was the contrived one and the A-current was exactly as described previously. For this capacitance, the threshold  $\text{Na}^+$  conductance density necessary for active backpropagation was found to be  $4.7\text{mS}/\text{cm}^2$ . Values of conductance density below this value resulted in amplification of the action potential while values above this resulted in active backpropagation of the action potential. This figure shows that with the capacitance set to the value used by Lüscher and Larkum (1998) the effect of dendritic  $\text{Na}^+$  conductances is the same but approximately half the conductance density is required to produce the same effect. The A-current still has its maximal effect in the proximal dendrites.

Figure 5.16A also shows that for any one particular diameter, the relative contribution of active conductances is the same. The differences in the amplitude of the action potential for dendrites of the same diameter (e.g. around  $2\mu\text{m}$ ) is related to the rate of taper of the dendrites under consideration, the number of branch points that the action potential passes through before it propagates to  $50\mu\text{m}$  from the soma, the size of the branches at each branch point and the morphology beyond the  $50\mu\text{m}$  point. A further examination of the effects of these morphological considerations has not been made here.

At  $200\mu\text{m}$ , the relationship between average dendritic diameter and action potential amplitude is more monotonic, with smaller average diameters giving smaller action potential amplitudes. Smaller diameter dendrites generally cause greater attenuation of action potential amplitude. Figure 5.16B shows a more monotonic relationship between dendritic diameter and action potential amplitude at this distance than the data in figure 5.16A because of similar taper rates, numbers of branch points, branch diameters and dendritic morphology along the dendritic paths to locations  $200\mu\text{m}$  from the soma. The maximal contribution of the A-current to action potential amplitude at this distance is about  $11\text{mV}$ . Therefore, assuming similar channel properties, density and distribution of  $I_A$  in motoneurons, blockade of  $I_A$  would increase the action potential amplitude by up to  $11\text{mV}$  at  $200\mu\text{m}$ . For the  $\text{Na}^+$  channel, the maximal contribution to action potential amplitude is about  $18\text{mV}$ . Therefore, for similar channel properties, density and distribution of  $I_{\text{Na}}$  in the motoneurone, up to  $18\text{mV}$  decrease in action potential amplitude would be expected if only dendritic  $I_{\text{Na}}$  could be blocked. This applies to a non-actively backpropagating action potential. Larger changes in action potential amplitude would occur if the maximum sodium conductance were increased to ensure active backpropagation.

Figure 5.16 Action potential peak voltage at 50µm and 200µm versus the average dendritic diameter to those distances. These plots show the effect of active conductances on the action potential amplitude. The conductive Na<sup>+</sup> channel was used for the modelling. A: The action potential peak voltage versus average dendritic diameter to 50µm. The average dendritic diameter was calculated from the dendritic diameter at 10µm intervals and the junction of the dendrite with the soma (µm). There is no obvious relationship between dendritic diameter and action potential amplitude. The largest influence on the dendritic action potential amplitude is again the A-current. The action potential peak voltage versus average dendritic diameter to 200µm. The average dendritic diameter was calculated from the dendritic diameter at 10µm intervals including the junction of the dendrite with the soma (µm). There is a monotonic relationship between dendritic action potential amplitude and dendritic diameter. The conductive Na<sup>+</sup> channel had the greatest effect on the action potential amplitude at these distal locations.



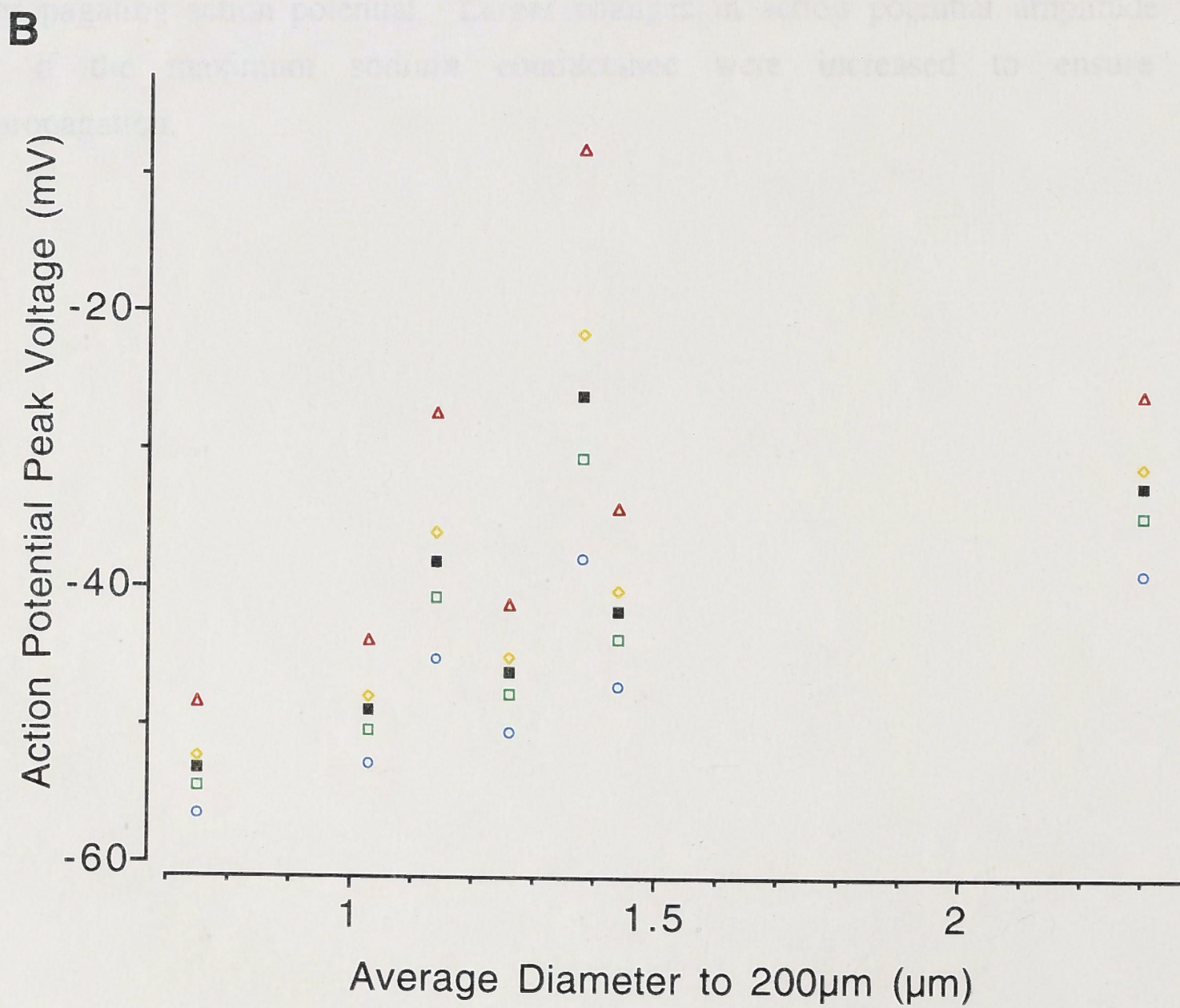
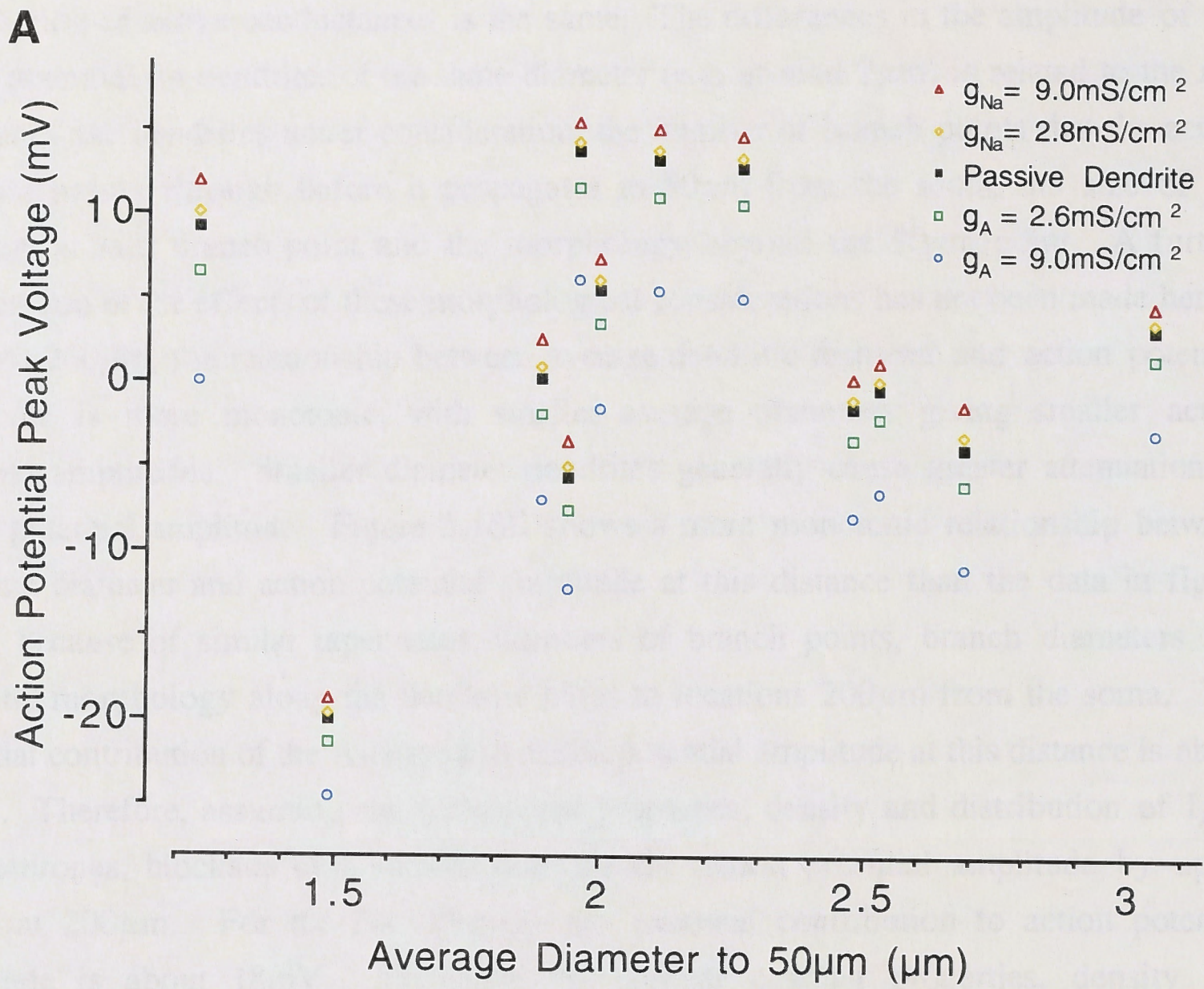


Figure 5.16. Action potential peak voltage at  $50\mu\text{m}$  and  $200\mu\text{m}$  versus the average dendritic diameter to those distances. These plots show the effect of active conductances on the action potential amplitude. The contrived  $\text{Na}^+$  channel was used for the modelling. **A:** The action potential peak voltage versus average dendritic diameter to  $50\mu\text{m}$ . The average dendritic diameter was calculated from the dendritic diameter at  $10\mu\text{m}$  intervals and at the junction of the dendrite with the soma ( $n=6$ ). There is no obvious relationship between dendritic diameter and action potential amplitude and the variability of the action potential amplitude is large. The A-current has the largest influence on the proximal dendritic action potential amplitude. **B:** The action potential peak voltage versus average dendritic diameter to  $200\mu\text{m}$ . The average dendritic diameter was calculated from the dendritic diameter at  $10\mu\text{m}$  intervals including the junction of the dendrite with the soma ( $n=21$ ). There is a monotonic relationship between dendritic action potential amplitude and dendritic diameter. The contrived  $\text{Na}^+$  channel has the greatest effect on the action potential amplitude at these distal locations.



## Discussion:

### *The Simulated Action Potential*

Simulation of the action potential waveform was a difficult procedure. The waveform of the action potential is highly dependent on the morphology of the cell, the properties of the ion channels involved in the production of the action potential and the distribution and density of these channels within the morphology. Many attempts were made to try to reproduce the recorded action potential using realistic ion channels, channel distribution, channel density and axonal morphology but none of these were particularly successful. Therefore a contrived set of ion channels was produced and a simplified axonal morphology was used. The important point in this study was to be able to reproduce the action potential waveform at the soma so that dendritic backpropagation could be studied. This was achieved with reasonable success as shown in figure 5.1. The slight differences between the recorded action potential and the simulated action potential will not cause significant differences in the results.

### *Dendritic Ion Channels*

The dendritic ion channel models that were used in this study were not real ion channels from motoneurons. Safronov and Vogel (1995) have made a study of the voltage-dependent  $\text{Na}^+$  and  $\text{K}^+$  channels that occur in the somatic membrane of motoneurons. However, the data for these ion channels is incomplete. For this reason, it was necessary to use channels from other studies where the descriptions were complete.

The sodium current used to produce the action potential was based on the channel described by Huguenard and McCormick (1992), but with the inactivation rate increased by 40%. This channel produced currents with qualitatively similar amplitudes and time-course to those described by Safronov and Vogel (1995). The fact that this channel reproduced the action potential waveform and the  $\text{Na}^+$  currents described previously in motoneurons indicated that it was appropriate for use in the dendritic membrane of the modelled motoneuron. Since this was a contrived channel, the sodium channel described by Mainen *et al.* (1995) was also placed in the dendritic membrane to determine if there was any difference between the results obtained with this sodium channel and the contrived channel. The amplification of the action potential in the dendrites was not greatly different with either channel except that a lower density of Mainen's channel was required to produce the same effect as the contrived  $\text{Na}^+$  channel.

The delayed rectifier that was used to repolarise the action potential was also a contrived channel with the activation rate increased by 40% to allow the action potential waveform to be reproduced. The action potential in a motoneuron is normally repolarised by a combination of potassium channels, including the A-current, delayed rectifier and  $\text{Ca}^{2+}$  dependent potassium conductance. The A-type potassium channel used in the

dendrites of this model was identical to that described by Huguenard and McCormick (1992). No data were available for the properties of the A-current in the motoneurone.

#### *Action Potential Attenuation Versus Distance from the Soma*

Examination of the attenuation of the action potential with distance from the soma with various combinations of active conductances present showed that  $I_A$  has its greatest effect at the soma and proximal dendrites while the sodium channel has its greatest effect in the distal dendrites. The explanation for these effects is not simple.

The influence of a dendritic voltage-dependent conductance on the action potential amplitude is related to the kinetics of the channel, its voltage activation/inactivation ranges, the density and distribution of the channel, the membrane potential changes that occur during an action potential and the input impedance of the dendrite at the site where the conductance is located. Therefore, there are too many variables to consider to be able to make an intuitive determination of the effect of dendritic conductances on the action potential amplitude.

Examination of the current density produced by  $I_A$  at proximal and distal locations reveals that the current density is greater in the proximal dendrites than it is in the distal dendrites. This is because of the large amplitude of the action potential in the proximal dendrites which activates a large proportion of the A-current. Furthermore, the driving potential for potassium is large during the large proximal action potential ( $\sim 120\text{mV}$  at the peak of the action potential) and so the current that flows through  $I_A$  is large. It should also be noted that the input impedance in the proximal dendrites is lower than that in the distal dendrites. This would tend to diminish the effect of  $I_A$  at the proximal location. The peak current produced by  $I_A$  at proximal locations is 3.5 to 5 times that produced at distal locations. Therefore, although one may expect a larger influence of  $I_A$  at distal locations because of the much higher input impedance, the current produced by  $I_A$  at distal locations is too small to cause a significant effect on the action potential amplitude. This large difference in current amplitude is the main reason why the A-current has its greatest effect in the proximal dendrites.

Examination of the current density produced by the contrived sodium channel showed that the current was generally larger in the distal dendrites than it was in the proximal dendrites for the larger conductance, while the reverse occurred for the smaller conductance.

The explanation for these results lies in the peak amplitude of the action potential achieved with each conductance at each location, the amount of activation of the conductance, and the driving potential. With the large conductance, differences in driving potential determined the relative currents, while for the smaller conductance, differences in the degree of activation and differences in driving potential were both important.

The amplitude of the current and the accompanying action potential amplification at each location are also dependent on the local input impedance, which increases with more distal locations. Thus, similar sized conductance changes placed at a low and high input impedance location will have a greater effect at the higher input impedance location. Thus the effect of the sodium current on the peak amplitude of the action potential is greater at  $200\mu\text{m}$  than at  $50\mu\text{m}$ .

The channel of Mainen *et al.* (1995) produced similar results to the contrived sodium channel except that a lower conductance density was required to produce the same effect (compare figs. 5.6 and 5.11). The major effect of this channel was in the distal dendrites where it caused amplification of the dendritic action potential amplitude. The greater effectiveness of this version of the sodium conductance lies in its more rapid activation and slower inactivation. This results in larger currents generally, but particularly for the slower rising action potentials in the more distal locations.

#### *Comparison of the Model with that of Lüscher and Larkum (1998)*

Various calculations were performed to determine what differences there would have been if the model used here were more like that described by Lüscher and Larkum (1998). One was to use the same sodium channel in the dendrites. This produced similar results to the contrived sodium channel developed in this Chapter and the reasons have been discussed above.

The next calculation examined the action potential amplitude under passive conditions to see if the model would attenuate action potentials differently with the capacitance set at  $1.0\mu\text{F}/\text{cm}^2$  as used by Lüscher and Larkum (1998). Reducing the capacitance to  $1.0\mu\text{F}/\text{cm}^2$  resulted in larger action potential amplitude in all dendrites but did not significantly change the rate of attenuation that was observed. Therefore, changes in specific membrane capacitance do not greatly effect the results obtained with the passive model.

A further calculation determined the dendritic action potential amplitude that would be observed with dendritic active conductances if the capacitance were reduced to  $1.0\mu\text{F}/\text{cm}^2$ . Propagation was similar to that with the capacitance set at  $1.7\mu\text{F}/\text{cm}^2$  except that a lower sodium channel density was required to produce the same effect. The effect of the A-current was not significantly different to when the capacitance was  $1.7\mu\text{F}/\text{cm}^2$ . Figure 5.15 shows that the dendritic location at which active backpropagation begins to occur is not significantly shifted by using a lower capacitance. Lüscher and Larkum (1998) have found that a sodium channel density of  $3.0\text{mS}/\text{cm}^2$  produces amplification of the action potential amplitude in the dendrites while a density as high as  $12.0\text{mS}/\text{cm}^2$  results in active backpropagation as defined by a net inward current. Figure 5.15A shows a similar result in this model although at a higher capacitance. However, the dendritic

amplification of the action potential is non-monotonic unlike the majority of action potential amplitudes shown by Lüscher and Larkum (1998). The sodium channel has no effect in the proximal dendrites and then begins to amplify the action potential once it propagates beyond about  $100\mu\text{m}$ . As discussed above, this is related to the input impedance, sodium driving potential and properties of the channel.

#### *Action Potential Amplitude Versus Dendritic Diameter*

Examination of action potential attenuation with dendritic diameter shows that at short distances from the soma, there is no relation between dendritic diameter and action potential amplitude. This is because of variations in dendritic taper and branching. At distances further from the soma however ( $200\mu\text{m}$ ), overall tapering and branching is similar in each dendrite so action potential amplitude is more closely related to the average dendritic diameter. This has implications for the experimental procedures used in this study. If recordings are made at locations close to the soma, then large variations in action potential amplitude can be expected to occur from cell to cell which are not caused by active conductances but rather, are due to variations in geometry. The experimental results presented in Chapter 4 are probably biased because large dendrites were easier to patch onto and therefore the diameter of the dendrites will be less variable than that shown in figure 5.16. This bias will result in action potentials that have a lower cell to cell variability than the variability observed for different dendrites in the model.

#### *Comparison of Modelled Results with Experimental Measurements*

The modelling presented in this chapter provides insights into the attenuation of the action potential that would be expected for different densities of dendritic active conductances. Chapter 4 showed that blockade of  $I_A$  with 4-AP produced an increase in action potential amplitude of 4mV. This chapter has provided evidence that the conductance density of  $I_A$  required to produce this attenuation of the action potential is in the range of 3.0 to  $9.0\text{mS}/\text{cm}^2$ . Such a density is reasonable considering that Bekkers (2000a, 2000b) has measured the conductance density in pyramidal cells of the neocortex to be 0.5 to  $0.8\text{mS}/\text{cm}^2$  while Hoffman *et al.* (1997) found that A-current conductance density varied from about 6 to  $40\text{mS}/\text{cm}^2$  in hippocampal pyramidal neurones.

#### *Conclusions*

This modelling gave some insights into how the dendritically propagated action potential is attenuated as it moves from the soma of the motoneurone into the dendrites. Most of the passive attenuation of the dendritic action potential occurs within the first  $100\mu\text{m}$  of the dendritic tree. This rapid attenuation is related to the rapid time-course of the action potential and the short membrane time constant of these cells ( $\tau_m=15.28\pm 7.41\text{ms}$ ). If one was to define the dendritic electrical length of the

motoneurone ( $\lambda$ ) using action potential amplitude as the measure, the distance at which the action potential dropped to  $1/e$  of its somatic amplitude would be about  $180\mu\text{m}$  from the soma.

The modelling indicates that the contribution of active conductances to the attenuation or amplification of the action potential is generally less than about 10mV even with realistically high densities of ion channels. Only with densities greater than about  $10\text{mS}/\text{cm}^2$  does the contribution of the sodium conductance to the action potential amplitude exceed 10mV, and the backpropagation of the action potential become a fully regenerative process. This means that action potential backpropagation is dominated by the passive properties of the dendritic membrane and that active conductances may contribute little to changes in action potential amplitude if their density is below the critical threshold for active backpropagation. Although active conductances do not appear to play a major role in modification of dendritic action potential amplitude in this study, they are still important for shaping the action potential waveform in the dendrites of motoneurons. This study has not examined the effect of active dendritic conductances on the time-course of the backpropagated action potential. These conductances will have a greater effect on the decay time-course than they do on peak amplitude. This could have important implications for synaptic integration and modification of synaptic efficacy through the interaction of backpropagated action potentials with postsynaptic potentials.

The modelling performed in this chapter provides an important conceptual framework for understanding the contribution of active conductances to the amplitude of the dendritically propagated action potential. Action potentials in the proximal dendrites are fast and large and are driven by the kinetics of the  $\text{Na}^+$  current in the soma and axon hillock. Therefore, for voltage-dependent conductances to change the action potential amplitude at these proximal locations, their kinetics must be fast enough to turn on during the brief time-course of the action potential. In addition, the large amplitude of the action potential means that it is potentially able to activate channels in the proximal dendrites, but may also inactivate them if their inactivation is sufficiently fast during large depolarisations. The large amplitude of the action potential in the proximal dendrites is also important because it shifts the driving potentials of the various ions. Therefore, although the action potential may activate all the voltage-dependent  $\text{Na}^+$  channels in the proximal dendrites, little current may flow through them because of the reduced driving potential for sodium. For  $\text{K}^+$  channels, the situation is reversed. The action potential increases the driving potential for potassium. Therefore, even if relatively few  $\text{K}^+$  channels are open during the peak of the action potential, the current that flows through them will be large because of the large driving potential.

A further complication, as discussed earlier, is the input impedance at an individual point on a neurone's dendritic tree. The input impedance varies with dendritic location,

and for any given location it depends on the time-course of the backpropagated action potential at that location. This is because impedance is frequency dependent and the waveform of the action potential changes as it propagates into the dendritic tree. If the conductance increase associated with activation of a voltage-dependent conductance by the backpropagating action potential is large compared with the input impedance, that region of the dendrite will tend to be clamped near the equilibrium potential for that conductance. If the conductance change is small in comparison with the input impedance, it will tend to act as a current source and the input impedance will be the major determinant of the local response. This aspect of dendritic responses has not been investigated systematically, but it appears that responses in the distal dendrites for the conductance increases that do not lead to fully active backpropagation are intermediate to the extremes of voltage source and current source activation.

Once the action potential has reached the distal dendrites, its time-course is slowed and it has significantly reduced amplitude. Therefore, for voltage-dependent conductances to contribute to action potential amplitude in this part of the dendritic tree their kinetics may be slower and they must activate with smaller depolarisations. The overall effect of dendritic voltage-dependent conductances on the backpropagated action potential will depend on the combination of voltage activation/inactivation ranges, kinetics, distribution and density of these channels, membrane potential changes that occur during the action potential and the input impedance at the site where the conductances are activated. In the modelling performed in this chapter and in real neurones,  $I_A$  activates much more slowly than  $I_{Na}$ . In addition,  $I_{Na}$  is activated at more depolarised potentials than  $I_A$ . The data shown here suggests that  $I_A$  has its largest contribution to action potential amplitude in the proximal dendrites, while the largest contribution of  $I_{Na}$  occurs in the distal dendrites.



---

## Chapter Six

### General Discussion

---

This thesis examined the passive properties of rat motoneurons, the action potential attenuation that occurs in the dendrites of these cells and the ionic conductances that contribute to this attenuation.

Chapter 3 provided information about the passive properties of motoneurons. It was found that the somatic response of these cells to small voltage deviations near the resting potential was linear. Fitting of small current pulse voltage transients with a computer model allowed the determination of the passive membrane properties. For four cells, the residuals between the experimental and fitted response suggested that homogeneous membrane properties could more accurately describe the subthreshold responses of these cells. These cells had  $R_m = 5.34 \pm 0.91 \text{K}\Omega \cdot \text{cm}^2$ ,  $C_m = 2.35 \pm 0.47 \mu\text{F}/\text{cm}^2$  and  $R_i = 86.50 \pm 21.83 \Omega \cdot \text{cm}$ . Models with these membrane properties matched the cells' experimentally measured membrane time constant and input resistance with high accuracy. The average  $\tau_m$  of these models was  $12.48 \pm 2.90 \text{ms}$  and the average input resistance was  $84.00 \pm 18.96 \text{M}\Omega$ . The passive membrane properties were used to calculate the average electrotonic length of the dendrites to their terminations and the value obtained was  $0.78 \pm 0.27 \lambda$ . This estimate included dendrites that were removed during the slicing procedure. Calculation of the average electrotonic length without inclusion of cut dendrites gave a value of  $0.85 \pm 0.14 \lambda$ . Overall, these results suggest that the passive description of the motoneurone provided here is not greatly different to that provided previously for the cat for DC signals (Fleshman *et al.* 1988, Clements & Redman 1989, Ulrich *et al.* 1994). However, the higher value of capacitance reported here indicates that rapid voltage signals will be attenuated more heavily than was previously thought for these cells.

In Chapter 4, experiments were performed which explored the contribution of the A-type potassium conductance to action potential attenuation in the dendrites of motoneurons. This involved the use of dendritic recordings to explore action potential attenuation in their dendrites. It was unfortunate that dendritic electrodes could not be placed further from the soma than about  $50 \mu\text{m}$ . The average distance at which recordings could be made was  $37 \pm 8 \mu\text{m}$ . The average action potential attenuation at this distance was  $10.7 \pm 6.2\%$ . This is an average of  $8.1 \text{mV}$  of attenuation for a  $74 \text{mV}$  action potential at the soma. Action potentials were always found to peak at the soma first followed by the dendrite indicating that the site of action potential generation is close to the soma. The



average temporal separation between the action potential peaks was  $54.4 \pm 45.6 \mu\text{s}$  for an electrode separation of  $37 \pm 8 \mu\text{m}$  giving a conduction velocity of  $0.68 \text{m/s}$ . Blockade of the A-current produced a  $4 \text{mV}$  increase in the amplitude of the action potential indicating that the A-current contributes to the action potential amplitude at the soma. Measurement of the attenuation using soma-dendritic recordings did not reveal any differences in the amount of attenuation that occurred under control conditions and A-current blockade. An attempt was made to determine if blocking the dendritic A-current intracellularly could reveal a difference in the channel density between the soma and dendrites. However, because the A-current blocker 4-AP does not cross the membrane quickly enough, this experiment was not successful.

Chapter 5 describes a theoretical investigation of the effect of dendritic voltage-dependent conductances on the action potential amplitude in the dendrites. It was possible to reproduce the recorded action potential waveform in the model by using contrived conductances and a simplified axonal morphology. This also produced a voltage-dependent  $\text{Na}^+$  channel that mimicked the amplitude and time-course of currents recorded in rat motoneurons by Safronov and Vogel (1995). Modelling of the influence of dendritic  $\text{Na}^+$  and A-currents on action potential amplitude revealed that  $\text{Na}^+$  currents contribute most to action potential amplitude in the distal dendrites, while A-currents had their largest effect at proximal locations. Only homogeneous distributions of these currents were considered.

Examination of the  $\text{Na}^+$  and A-currents at proximal and distal locations revealed that their contribution to the action potential amplitude was determined by the density of the channels, their properties, the membrane potential that occurs during a backpropagated action potential and also by the input impedance at the dendritic site. A comparison was made between the results from this model and those obtained by Lüscher and Larkum (1998) for another model of backpropagation of the action potential in a dendrite of a cultured motoneurone. This model differed in that it used a membrane capacitance of  $1.0 \mu\text{F}/\text{cm}^2$  and had a different representation of the sodium channel. When the model was retested with this sodium channel, the results were not different except that a lower conductance density was required to produce the same action potential amplification. When a lower capacitance was used, the action potential attenuation under passive conditions did not change. With the lower capacitance, a lower  $\text{Na}^+$  channel density was required to produce the same action potential amplification as in the model with higher capacitance.

Examination of action potential amplitude in relation to diameter showed that at locations close to where the recordings of Chapter 4 were made, the action potential amplitude was not related to dendritic diameter. Overall, the modelling suggests that the

A-current density required to produce the 4mV of attenuation measured in Chapter 4 is somewhere between 3.0 and 9.0mS/cm<sup>2</sup>.

### **Improvements to the Techniques Used**

The experiments and modelling presented in this thesis have some obvious limitations and caveats. This is to be expected when applying new techniques to a new preparation. If this work was to be repeated there are several improvements that could be made to the techniques that have been used. These are discussed here briefly.

#### *Passive Properties*

There are several problems associated with the determination of passive properties that was performed in Chapter 3. A major problem is that the electrode capacitance affects the shape of the injected current transient and distorts the recorded voltage. This could be improved by using Sylgard coated electrodes and lowering the bath level to reduce the capacitance. In dendritic recordings, it was necessary to reduce the bath level to be able to compensate the capacitance but not for somatic electrodes. Since Chapter 3 was performed only with somatic electrodes, and no dendritic electrode experiments had been performed at that time, the bath level was not dropped. Therefore a significant electrode capacitance was present during the recordings. This distorted the waveform of the injected current and the recorded voltage, making the early part of the voltage recording unusable. This part of the transient is most important for determining the passive properties of the cell, particularly  $R_i$ . Therefore, recordings in which the electrode capacitance is reduced will be able to use a larger part of the voltage transient for the fitting procedure and will produce better estimates of the membrane properties.

A better determination of the passive membrane properties could be made by placing electrodes on the dendritic tree. Multiple electrodes, at various locations on the morphology of the cell, would allow a much more accurate determination of the passive properties of the distal dendrites using transfer impedance measurements. Somatic measurements are dominated by the passive properties of the soma and proximal dendrites and are relatively insensitive to the membrane properties of the distal dendrites. It was suggested in Chapter 3 that the membrane properties of some cells may be inhomogeneous. If this is the case, then multiple electrode recordings may be able to better determine the sort of membrane inhomogeneity that occurs. In Chapter 3, a somato-dendritic recording was used as the target response for the fitting procedure. However, not enough experiments of this kind were performed to be able to comment on membrane inhomogeneities.

The fitting procedure may also be improved by applying various types of stimuli to the cell, not just a current pulse. Clements and Redman (1989) applied both brief current pulse and steady-state voltage clamp commands to their cells and used the responses to both stimuli as the target transients for the fitting procedure. This has the advantage that the steady-state voltage clamp affects the membrane potential at a greater distance from the soma than the brief current pulse and therefore samples a larger area of membrane.

### *Visualisation*

The most important factor for improving the quality of the experiments would be to improve the visibility of the dendrites. In this study, dendrites were visualised with infrared differential interference contrast (IRDIC) optics. This is a considerable improvement on methods of visualisation that have been used in the past but it still has its limitations. One way in which the dendrites could be more easily visualised would be by using fluorescence. This could be achieved by filling somatic electrodes with a solution containing fluorescent dye. The tissue would then be visualised under epifluorescence optics. The electrode solution would be allowed to diffuse into the cell through the somatic electrode and fill the dendrites. Once the dendrites could be clearly visualised, it may be possible to attach an electrode to them more easily. This would require visualisation of the dendritic electrode under fluorescence optics and so it would have to be filled with fluorescent dye as well to allow its outline to be viewed while it was attached to the dendrite. If this technique were successful, it may be possible to extend the distance over which dendritic recordings could be made from the soma.

Another method that may improve the visibility of dendrites would be to improve the slicing technique. Bingmann *et al.* (2000) have developed a method of cutting brain tissue using a high-pressure saline jet (macromingotome). This method has the advantage that the cutting is much cleaner than when it is done with a blade. Using this technique, Bingmann *et al.* (2000) have reported that living cells are visible within  $10\mu\text{m}$  of the surface of the slice. If this technique was used to slice the spinal cord, it may produce slices in which dendrites are more visible because the dendrites would lie closer to the surface of the slice where the optics produce the best images.

### *A-currents*

Chapter 4 provided insights into the effects of the A-current on the attenuation of the action potential. To improve on this work it will be necessary to record further from the soma. Techniques for doing this have already been discussed.

The experiment which used intradendritic 4-AP to determine if there was a different density of A-current in soma and dendrites could be improved. This would require the use of a drug that blocks the A-current from the inner face of the membrane. It would be best if this was a large molecule, such as a protein toxin, as this would slow the diffusion of the substance to the soma. This would allow dendritic A-currents to be blocked before the somatic A-currents are blocked, allowing their effect on the dendritic action potential to be determined.

If dendritic recordings could be made further from the soma, it may be possible to apply 4-AP to a local region of the dendritic tree without affecting the somatic channels. This could also provide a method for testing the effect of dendritic A-currents on the backpropagated action potential.

### *Modelling of Active Conductances*

The modelling performed in Chapter 5 makes many assumptions and simplifications about the density, distribution and properties of the ionic channels that are present in the dendritic membrane of motoneurones.

To improve this work it would be necessary to determine the properties of the ionic channels that are present in motoneurones. Safronov and Vogel (1995) have made a study of  $\text{Na}^+$  and  $\text{K}^+$  channels in the somata of rat motoneurones but these data are incomplete. A full determination of the voltage-dependent ionic currents in the motoneurone would allow a more accurate description of action potential backpropagation in these cells.

The modelling could also be improved by using more realistic axon and hillock morphology and a realistic mixture of ion channels to reproduce the action potential. This would give a more realistic voltage and current distribution over the membrane surface of the neurone and would produce results that more adequately match the properties of the real motoneurone.

### *Further Work*

If further time was available to continue the research presented here, then several investigations could be performed that would significantly contribute to the understanding of the processes involved in active backpropagation.

As an extension to the work already performed, it would be good to be able to determine the  $\text{Na}^+$  and  $\text{K}^+$  channel densities in the dendritic membrane as has already been performed for many other cells types (e.g. Stuart & Häusser 1994, Stuart & Sakmann 1994, Häusser *et al.* 1995, Hoffman *et al.* 1997, Magee 1998, Bekkers 2000b, Korngreen & Sakmann 2000, Williams & Stuart 2000b). This requires making cell-attached patches on the dendrites of cells at different distances from the soma and measuring the current density of these channels in relation to the distance along the dendritic tree. A further test would be to measure the current that flows through these channels during backpropagation to see if these channels are activated by backpropagating action potentials. These measurements would also give data on the distribution and density of these ion channels within the dendrites. This would allow realistic distributions and densities to be used in the model and allow more realistic modelling. In addition, a determination of the ion channels involved in action potential generation, their distribution and density would also allow a more accurate reproduction of the action potential waveform and the ionic conductances that produce it.

Another experiment that could be performed would be to test the reciprocity of large signals in the dendrites. This was performed with small signals in Chapter 3, however these small signals are not likely to reveal any break down in the reciprocity of signal transfer that occurs between two points on the dendritic tree of a neurone because they are too small to activate a significant proportion of the dendritic voltage-dependent conductances. Therefore, a test of reciprocity could be performed in which large voltage signals were used.

---

## Appendix One

### The Biocytin/Neurobiotin Glycerol Whole Mount Technique

---

Processing can be done in multi-well plates or in ice cube trays or other similar trays with small wells. A shaker running at low speed may be useful for the procedure. Slices should be handled with a fine paintbrush. In this way, minimal transfer of solutions will occur between the wells. The brush should be free of loose hairs and you should avoid pressing too hard on the slices, particularly with the end of the brush. Slices are best lifted by creating turbulence in the well, so that the slice is floating free and then placing the paint brush underneath it, lifting it free of the liquid. The brush should also be washed with distilled water between steps. Alternatively, a small sucker can be used if minimal solution is transferred in each step. As little as 0.5mL or less of solution may be used in each well for each step of the process.

#### **Materials required:**

0.1M phosphate buffered saline (PBS)

0.1M PBS containing 4% sucrose by weight

Tween 20 buffer: 0.1M PBS / 4% sucrose with 0.1% by volume of Tween 20  
(1 $\mu$ L per mL of polyoxyethylene sorbitan monolaurate).

70% Ethanol

100% Glycerol

50% Glycerol in water

Diaminobenzidine or similar chromophore.

Hydrogen peroxide

Cobalt or nickel chloride

Vectastain ABC kit or other kit suitable for staining biocytin/neurobiotin filled cells.

Once the slices are processed, they are placed on a 13 millimetre diameter round coverslip with a drop of glycerol and observed under a dissecting microscope. The slice is then oriented so that the stained cell is facing downwards on the coverslip. A little more glycerol is then dropped on top of the slice. Now, using a microscope slide with a concave depression (e.g. Sail Brand single concave microscope slides), touch the bottom of the concave depression in the slide onto the glycerol drop on the coverslip. Surface tension will draw up the coverslip and the slice onto the slide. If too much glycerol was used then the excess can be wiped away carefully with a tissue. If too little glycerol was used, then air bubbles may form under the coverslip. If this process is successful, the slice should now be neatly mounted just under the coverslip, and therefore accessible to high power lenses. The coverslip will be held into the depression on the slide by the glycerol. Seal the edges of the coverslip to the slide with two coats of nail polish and label the slide.

## Solutions and times for slice processing:

1. 4% paraformaldehyde / 0.1M PBS / 4% sucrose  
Slices will last for 1 to 2 years in this solution  
At least 2 hours
2. 0.1M PBS / 4% sucrose  
Overnight
3. 70% Ethanol  
30 minutes
4. Rinse slice twice in 0.1M PBS / 4% sucrose  
5 minutes x2
5. Tween 20 buffer plus ABC  
(Vectastain ABC kit: 10 $\mu$ L of "A" and 10 $\mu$ L of "B" per mL)  
48 hours
6. Rinse slice twice in Tween 20 buffer  
10 minutes x2
7. Preincubate slices in 0.05% Diaminobenzidine in  
0.1M PBS / 4% sucrose plus 0.02% Cobalt chloride  
(0.5mg DAB/mL, 0.2mg CoCl<sub>2</sub>/mL)  
in the dark and in the fridge  
2 hours
8. React with 0.003% Hydrogen peroxide in PBS (no sucrose)  
(1 $\mu$ L of 30% H<sub>2</sub>O<sub>2</sub> per 10mL) until desired staining  
is achieved  
1 - 3 minutes
9. Rinse twice in PBS (no sucrose)  
10 minutes x2
10. Clear with 50% Glycerol until slice sinks  
1 - 3 hours
11. Clear with 100% Glycerol  
At least 30 minutes  
Most of the unwanted stain will disappear during this step  
and the slice will become very transparent.
12. Mount in 100% Glycerol as described above

---

## References

---

- Alberts, B., Bray, D., Lewis, J., Raff, M., Roberts, K. and Watson, J.D. (1989). *Molecular Biology of the Cell*. Second edition. Garland Publishing, New York, Chapter 6.
- Andreasen, M. and Lambert, J.D. (1998). Factors determining the efficacy of distal excitatory synapses in rat hippocampal CA1 pyramidal neurones. *J. Physiol. (Lond)*. **507**:441-462.
- Barrett, J.N. and Crill, W.E. (1974). Specific membrane properties of cat motoneurons. *J. Physiol. (Lond)*. **239**:301-324.
- Bekkers, J.M. (2000a). Properties of voltage-gated potassium currents in nucleated patches from large layer 5 cortical pyramidal neurons of the rat. *J. Physiol. (Lond)*. **525**:593-609.
- Bekkers, J.M. (2000b). Distribution and activation of voltage-gated potassium channels in cell-attached and outside-out patches from large layer 5 cortical pyramidal neurons of the rat. *J. Physiol. (Lond)*. **525**:611-620.
- Bi, G.Q. and Poo, M.M. (1998). Synaptic modifications in cultured hippocampal neurons: dependence on spike timing, synaptic strength, and postsynaptic cell type. *J. Neurosci*. **18**:10464-10472.
- Bingmann, D., Wiemann, M., Speckmann, E.-J., Köhling, R., Straub, H., Dunze, K. and Wittkowski, W. (2000). Cutting of living hippocampal slices by a highly pressurised water jet (macromingotome). *J. Neurosci. Meth*. **102**:1-9.
- Bischofberger, J. and Jonas, P. (1997). Action potential propagation into the presynaptic dendrites of rat mitral cells. *J. Physiol. (Lond)*. **504**:359-365.
- Black, J.A., Kocsis, J.D. and Waxman, S.G. (1990). Ion channel organisation of the myelinated fiber. *Trends Neurosci*. **13**:48-54.
- Brock, L.G., Coombs, J.S. and Eccles, J.C. (1953). Intracellular recording from antidromically activated motoneurons. *J. Physiol. (Lond)*. **122**:429-461.
- Brown, T.H., Perkel, D.H., Norris, J.C. and Peacock, J.H. (1981a). Electrotonic structure and specific membrane properties of mouse dorsal root ganglion neurons. *J. Neurophysiol*. **45**:1-15.
- Brown, T.H., Fricke, R.A. and Perkel, D.H. (1981b). Passive electrical constants in three classes of hippocampal neurons. *J. Neurophysiol*. **46**:812-827.
- Burke, R.E., Fyffe, R.E.W. and Moschovakis, A.K. (1994). Electrotonic architecture of cat gamma motoneurons. *J. Neurophysiol*. **72**:2302-2316.
- Caldwell, J.H., Schaller, K.L., Lasher, R.S., Peles, E. and Levinson, S.R. (2000). Sodium channel Na(v)1.6 is localized at nodes of ranvier, dendrites, and synapses. *Proc. Natl. Acad. Sci. U.S.A.* **97**:5616-5620.



- Campbell, D.M. and Rose, P.K. (1997). Contribution of voltage-dependent potassium channels to the somatic shunt in neck motoneurons of the cat. *J. Neurophysiol.* **77**:1470-1486.
- Cash, S. and Yuste, R. (1998). Input summation by cultured pyramidal neurons is linear and position-independent. *J. Neurosci.* **18**:10-15.
- Cash, S. and Yuste, R. (1999). Linear summation of excitatory inputs by CA1 pyramidal neurons. *Neuron* **22**:383-394.
- Carnevale, N.T., Tsai, K.Y., Claiborne, B.J. and Brown, T.H. (1997). Comparative electrotonic analysis of three classes of rat hippocampal neurons. *J. Neurophysiol.* **78**:703-720.
- Chang, H-T. (1951). Dendritic potential of cortical neurons produced by direct electrical stimulation of the cerebral cortex. *J. Neurophysiol.* **14**:1-21.
- Chen, W.R., Midtgaard, J. and Shepherd, G.M. (1997). Forward and backward propagation of dendritic impulses and their synaptic control in mitral cells. *Science* **278**:463-467.
- Chen, X.Y. and Wolpaw, J.R. (1994). Triceps surae motoneuron morphology in the rat: a quantitative light microscopic study. *J. Comp. Neurol.* **343**:143-157.
- Clements, J.D. and Redman, S.J. (1989). Cable properties of cat spinal motoneurons measured by combining voltage clamp, current clamp and intracellular staining. *J. Physiol. (Lond)*. **409**:63-87.
- Clements, J.D., Nelson, P.G. and Redman, S.J. (1986). Intracellular tetraethylammonium ions enhance group Ia excitatory post-synaptic potentials evoked in cat motoneurons. *J. Physiol. (Lond)*. **377**:267-282.
- Colbert, C.M. and Johnston, D. (1996). Axonal action-potential initiation and Na<sup>+</sup> channel densities in the soma and axon initial segment of subicular pyramidal neurons. *J. Neurosci.* **16**:6676-6686.
- Colbert, C.M., Magee, J.C., Hoffman, D.A. and Johnston, D. (1997). Slow recovery from inactivation of Na<sup>+</sup> channels underlies the activity-dependent attenuation of dendritic action potentials in hippocampal CA1 pyramidal neurons. *J. Neurosci.* **17**:6512-6521.
- Colbert, C.M. and Johnston, D. (1998). Protein kinase C activation decreases activity-dependent attenuation of dendritic Na<sup>+</sup> current in hippocampal CA1 pyramidal neurons. *J. Neurophysiol.* **79**:491-495.
- Coleman, P.A. and Miller, R.F. (1989). Measurement of passive membrane parameters with whole-cell recording from neurons in the intact amphibian retina. *J. Neurophysiol.* **61**:218-230.
- Conradi, S., Kellerth, J.O. and Berthold, C.H. (1979). Electron microscopic studies of serially sectioned cat spinal  $\alpha$ -motoneurons. II. A method for the description of

- architecture and synaptology of the cell body and proximal segments. *J. Comp. Neurol.* **184**:741-754.
- Cook, E.P. and Johnston, D. (1997). Active dendrites reduce location-dependent variability of synaptic input trains. *J. Neurophysiol.* **78**:2116-2128.
- Cook, E.P. and Johnston, D. (1999). Voltage-dependent properties of dendrites that eliminate location-dependent variability of synaptic input. *J. Neurophysiol.* **81**:535-543.
- Coombs, J.S., Curtis, D.R. and Eccles, J.C. (1957). The interpretation of spike potentials of motoneurons. *J. Physiol. (Lond)*. **139**:198-231.
- Covarrubias, M., Wei, A., Salkoff, L. and Vyas, T.B. (1994). Elimination of the rapid potassium channel inactivation by phosphorylation of the inactivation gate. *Neuron* **13**:1403-1412.
- Debanne, D., Gähwiler, B.H. and Thompson, S.M. (1998). Long-term synaptic plasticity between pairs of individual CA3 pyramidal cells in rat hippocampal slice cultures. *J. Physiol. (Lond)*. **507**:237-247.
- Dodge, F.A. Jr. and Cooley, J.W. (1973). Action Potential of the Motorneuron. *IBM Journal of Research and Development*. **17**:219-229.
- Drain, P., Dubin, A.E. and Aldrich, R.W. (1994). Regulation of *Shaker* K<sup>+</sup> channel inactivation gating by the cAMP-dependent protein kinase. *Neuron* **12**:1097-1109.
- Durand, D., Carlen, P.L., Gurevich, N., Ho, A. and Kunov, H. (1983). Electrotonic parameters of rat dentate granule cells measured using short current pulses and HRP staining. *J. Neurophysiol.* **50**:1080-1097.
- Edwards, F.A., Konnerth, A., Sakmann, B. and Takahashi, T. (1989). A thin slice preparation for patch clamp recordings from neurones of the mammalian central nervous system. *Pflügers Arch.* **414**:600-612.
- Elliott, E.M., Malouf, A.T. and Catterall, W.A. (1995). Role of calcium channel subtypes in calcium transients in hippocampal CA3 neurons. *J. Neurosci.* **15**:6433-6444.
- Fatt, P. (1957). Electric potentials occurring around a neurone during its antidromic activation. *J. Neurophysiol.* **20**:27-60.
- Fettiplace, R., Andrews, D.M. and Haydon, D.A. (1971). The thickness, composition and structure of some lipid bilayers and natural membranes. *J. Membrane Biol.* **5**:277-296.
- Fleshman, J.W., Segev, I. and Burke, R.E. (1988). Electrotonic architecture of type-identified  $\alpha$ -motoneurons in the cat spinal cord. *J. Neurophysiol.* **60**:60-85.
- Frank, K., Fuortes, M. and Nelson, P.G. (1959). Voltage clamp of motoneuron soma. *Science* **130**:38-39.

- Gao, B-X. and Ziskind-Conhaim, L. (1998). Development of ionic currents underlying changes in action potential waveforms in rat spinal motoneurons. *J. Neurophysiol.* **80**:3047-3061.
- Fujita, Y. (1989). Dendritic spikes in normal spinal motoneurons of cats. *Neurosci. Res.* **6**:299-308.
- Gentet, L. J., Stuart, G. J. and Clements, J. D. (2000). Direct measurement of specific membrane capacitance in neurons. *Biophys. J.* **79**:314-320.
- Golding, N.L. and Spruston, N. (1998). Dendritic sodium spikes are variable triggers of axonal action potentials in hippocampal CA1 pyramidal neurons. *Neuron* **21**:1189-1200.
- Golding, N.L., Jung, H.Y., Mickus, T. and Spruston, N. (1999). Dendritic calcium spike initiation and repolarization are controlled by distinct potassium channel subtypes in CA1 pyramidal neurons. *J. Neurosci.* **19**:8789-8798.
- Häusser, M., Stuart, G., Racca, C. and Sakmann, B. (1995). Axonal initiation and active dendritic propagation of action potentials in substantia nigra neurons. *Neuron* **15**:637-647.
- Häusser, M., Spruston, N. and Stuart, G. (2000). Diversity and dynamics of dendritic signalling. *Science* **290**:739-744.
- Hebb, D.O. (1949) *The Organisation of Behaviour*. Wiley (Interscience), New York.
- Hell, J.W., Westenbroek, R.E., Warner, C., Ahlijanian, M.K., Prystay, W., Gilbert, M.M., Snutch, T.P. and Catterall, W.A. (1993). Identification and differential subcellular localization of the neuronal class C and class D L-type calcium channel alpha 1 subunits. *J. Cell Biol.* **123**:949-962.
- Hermann, L. (1879). *Handbuch der Physiologie*. Vogel, Leipzig.
- Hille, B. (1992) *Ionic channels of Excitable Membranes*. Sinauer Associates Inc, Sunderland, Massachusetts.
- Hines, M. (1993) Neuron - a program for simulation of nerve equations. In: *Neural Systems: Analysis and Modelling*, edited by F.H. Eckman. Kluwer Academic Publishers, Boston. pp. 127-136.
- Hodgkin, A.L. and Rushton, W.A.H. (1946). The electrical constants of a crustacean nerve fibre. *Proc. Roy. Soc. London Ser. B* **133**:444-479.
- Hoffman, D.A., Magee, J.C., Colbert, C.M. and Johnston, D. (1997). K<sup>+</sup> channel regulation of signal propagation in dendrites of hippocampal pyramidal neurons. *Nature* **387**:869-875.
- Hoffman, D.A. and Johnston, D. (1998). Down-regulation of transient K<sup>+</sup> channels in dendrites of hippocampal CA1 pyramidal neurons by activation of PKA and PKC. *J. Neurosci.* **18**:3521-3528.

- Hoffman, D.A. and Johnston, D. (1999). Neuromodulation of dendritic action potentials. *J. Neurophysiol.* **81**:408-411.
- Horikawa, K. and Armstrong, W.E. (1988). A versatile means of intracellular labelling: injection of biocytin and its detection with avidin conjugates. *J. Neurosci. Methods* **25**:1-11.
- Houchin, J. (1973). Procion Yellow electrodes for intracellular recording and staining of neurones in the somatosensory cortex of the rat. *J. Physiol. (Lond)*. **232**:67-69.
- Hounsgaard, J. and Yamamoto, C. (1979). Dendritic spikes in Purkinje cells of the guinea pig cerebellum studied in vitro. *Exp. Brain Res.* **37**:387-398.
- Hsiao, C-f. and Chandler, S.H. (1995). Characteristics of fast transient outward current in guinea pig trigeminal motoneurons. *Brain Res.* **695**:217-226.
- Huguenard, J.R. and McCormick, D.A. (1992). Simulation of the currents involved in rhythmic oscillations in thalamic relay neurons. *J. Neurophys.* **68**:1373-1383.
- Iansek, R. and Redman, S.J. (1973). An analysis of the cable properties of spinal motoneurons using a brief intracellular current pulse. *J. Physiol. (Lond)*. **234**:613-636.
- Jaffe, D.B., Johnston, D., Lasser-Ross, N., Lisman, J.E., Miyakawa, H. and Ross, W.N. (1992). The spread of Na<sup>+</sup> spikes determines the pattern of dendritic Ca<sup>2+</sup> entry into hippocampal neurons. *Nature* **357**:244-246.
- Jack, J.J. and Redman, S.J. (1971). An electrical description of the motoneurone and its application to the analysis of synaptic potentials. *J. Physiol. (Lond)*. **215**:321-352.
- Jackson, M.B. (1992). Cable analysis with the whole-cell patch clamp - theory and experiment. *Biophys. J.* **61**:756-766.
- Johnston, S.W. and North, R.A. (1992). Two types of neurone in the rat ventral tegmental area and their synaptic inputs. *J. Physiol.* **450**:455-468.
- Johnston, D., Magee, J.C., Colbert, C.M. and Christie, B.R. (1996). Active properties of neuronal dendrites. *Annu. Rev. Neurosci.* **19**:165-186.
- Jung, H-Y., Mickus, T., Spruston, N. (1997). Prolonged sodium channel inactivation contributes to dendritic action potential attenuation in hippocampal neurons. *J. Neurosci.* **17**:6639-6646.
- Kandel, E.R. and Spencer, W.A. (1961). Electrophysiological properties of an archicortical neuron. *Ann. N.Y. Acad. Sci.* **94**:570-603.
- Kellerth, J.O., Berthold, C.H. and Conradi, S. (1979). Electron microscopic studies of serially sectioned cat spinal  $\alpha$ -motoneurons. III. Motoneurons innervating fast-twitch (type FR) units of the gastocnemius muscle. *J. Comp. Neurol.* **184**:755-768.
- Kelvin, Lord (William Thompson) (1855). On the theory of the electric telegraph. *Proc. R. Soc.* **7**:382-399.

- Kelvin, Lord (William Thompson) (1856). On the theory of the electric telegraph. *Phil. Mag.* **11**:146-160.
- Koester, H.J. and Sakmann, B. (1998). Calcium dynamics in single spines during coincident pre- and postsynaptic activity depend on relative timing of back-propagating action potentials and subthreshold excitatory postsynaptic potentials. *Proc. Natl. Acad. Sci. U.S.A.* **95**:9596-9601.
- Korngreen, A. and Sakmann, B. (2000). Voltage-gated  $K^+$  channels in layer 5 neocortical pyramidal neurones from young rats: subtypes and gradients. *J. Physiol. (Lond)*. **525**:621-639.
- Kuno, M. and Llinás, R. (1970). Enhancement of synaptic transmission by dendritic potentials in chromatolysed motoneurons of the cat. *J. Physiol. (Lond)*. **210**:807-821.
- Lagerbäck, P.A. (1985). An ultrastructural study of cat lumbosacral  $\gamma$ -motoneurons after retrograde labelling with horseradish peroxidase. *J. Comp. Neurol.* **240**:256-264.
- Lahjouji, F., Bras, H., Barbe, A., Chmykhova, N. and Chazal, G. (1997). Electron microscopic serial analysis of GABA presynaptic terminals on the axon hillock and initial segment of labeled abducens motoneurons in the rat. *Neurosci. Res.* **27**:143-153.
- Larkum, M.E., Rioult, M.G. and Lüscher, H.-R. (1996). Propagation of action potentials in the dendrites of neurons from rat spinal cord slice cultures. *J. Neurophysiol.* **75**:154-170.
- Larkum, M.E., Launey, T., Dityatev, A. and Lüscher, H.-R. (1998). Integration of excitatory postsynaptic potentials in dendrites of motoneurons of rat spinal cord slice cultures. *J. Neurophysiol.* **80**:924-935.
- Larkum, M.E., Kaiser, K.M. and Sakmann, B. (1999a). Calcium electrogenesis in distal apical dendrites of layer 5 pyramidal cells at a critical frequency of back-propagating action potentials. *Proc. Natl. Acad. Sci. U.S.A.* **96**:14600-14604.
- Larkum, M.E., Zhu, J.J. and Sakmann, B. (1999b). A new cellular mechanism for coupling inputs arriving at different cortical layers. *Nature* **398**:338-341.
- Llinás, R. and Nicholson, C. (1971). Electrophysiological properties of dendrites and somata in alligator Purkinje cells. *J. Neurophysiol.* **34**:532-551.
- Llinás, R. and Sugimori, M. (1980a). Electrophysiological properties of *in vitro* Purkinje cell somata in mammalian cerebellar slices. *J. Physiol. (Lond)*. **305**:171-195.
- Llinás, R. and Sugimori, M. (1980b). Electrophysiological properties of *in vitro* Purkinje cell dendrites in mammalian cerebellar slices. *J. Physiol. (Lond)*. **305**:197-213.
- Lüscher, H.-R. and Larkum, M.E. (1998). Modeling action potential initiation and back-propagation in dendrites of cultured rat motoneurons. *J. Neurophysiol.* **80**:715-729.

- Lux, H.-D., Schubert, P. and Kreutzberg, G.W. (1970). Direct matching of morphological and electrophysiological data in cat spinal motoneurons. In: *Excitatory Synaptic Mechanisms*, edited by P. Andersen and J.K.S. Jansen. Universitetsforlaget, Oslo. pp. 189-198.
- Magee, J.C., Christofi, G., Miyakawa, H., Christie, B., Lasser-Ross, N. and Johnston, D. (1995). Subthreshold synaptic activation of voltage gated  $\text{Ca}^{2+}$  channels mediates a localized  $\text{Ca}^{2+}$  influx into the dendrites of hippocampal pyramidal neurons. *J. Neurophysiol.* **74**:1335-1342.
- Magee, J.C. and Johnston, D. (1995a). Characterization of single voltage-gated  $\text{Na}^+$  and  $\text{Ca}^{2+}$  channels in apical dendrites of rat CA1 pyramidal neurons. *J. Physiol. (Lond)*. **487**:67-90.
- Magee, J.C. and Johnston, D. (1995b). Synaptic activation of voltage-gated channels in the dendrites of hippocampal neurons. *Science* **268**:301-304.
- Magee, J.C. and Johnston, D. (1997). A synaptically controlled, associative signal for Hebbian plasticity in hippocampal neurons. *Science* **275**:209-213.
- Magee, J.C. (1998). Dendritic hyperpolarization-activated currents modify the integrative properties of CA1 pyramidal neurons. *J. Neurosci.* **18**:7613-7624.
- Magee, J.C. (1999). Dendritic  $I_h$  normalizes temporal summation in hippocampal CA1 neurons. *Nat. Neurosci.* **2**:508-514.
- Magee, J.C. and Carruth, M. (1999). Dendritic voltage-gated ion channels regulate the action potential firing mode of hippocampal CA1 pyramidal neurons. *J. Neurophysiol.* **82**:1895-1901.
- Magee, J.C. and Cook, E.P. (2000). Somatic EPSP amplitude is independent of synapse location in hippocampal pyramidal neurons. *Nat. Neurosci.* **3**:895-903
- Magistretti, J., Ragsdale, D.S. and Alonso A. (1999). Direct demonstration of persistent  $\text{Na}^+$  channel activity in dendritic processes of mammalian cortical neurones. *J. Physiol. (Lond)*. **521**:629-636.
- Mainen, Z.F., Joerges J., Huguenard J.R. and Sejnowski, T.J. (1995). A model of spike initiation in neocortical pyramidal neurons. *Neuron* **15**:1427-1439.
- Major, G., Larkman, A.U., Jonas, P., Sakmann, B. and Jack, J.J. (1994). Detailed passive cable models of whole-cell recorded CA3 pyramidal neurons in rat hippocampal slices. *J. Neurosci.* **14**:4613-4638.
- Markram, H., Helm, P.J. and Sakmann, B.J. (1995). Dendritic calcium transients evoked by single back-propagating action potentials in rat neocortical pyramidal neurons. *J. Physiol. (Lond)*. **485**:1-20.
- Markram, H., Lübke, J., Frotscher, M. and Sakmann, B. (1997). Regulation of synaptic efficacy by coincidence of postsynaptic APs and EPSPs. *Science* **275**:213-215.

- Martina, M., Vida, I. and Jonas, P. (2000). Distal initiation and active propagation of action potentials in interneuron dendrites. *Science* **287**:295-300.
- McCormick, D.A. and Huguenard, J.R. (1992) A model of the electrophysiological properties of thalamocortical relay neurons. *J. Neurophysiol.* **68**:1384-1400.
- Migliore, M., Hoffman, D.A., Magee, J.C. and Johnston, D. (1999). Role of an A-type K<sup>+</sup> conductance in the back-propagation of action potentials in the dendrites of hippocampal pyramidal neurons. *J. Comp. Neurosci.* **7**:5-15.
- Nelson, P.G. and Lux, H.D. (1970). Some electrical measurements of motoneuron parameters. *Biophys. J.* **10**:55-73.
- Nettleton, J.S. and Spain, W.J. (2000). Linear to supralinear summation of AMPA-mediated EPSPs in neocortical pyramidal neurons. *J. Neurophysiol.* **83**:3310-3322.
- Nitzan, R., Segev, I. and Yarom, Y. (1990). Voltage behaviour along the irregular dendritic structure of morphologically and physiologically characterised vagal motoneurons in the guinea pig. *J. Neurophysiol.* **63**:333-346.
- O'Carroll, D.C., Osorio, D., James, A.C. and Bush, T. (1992). Local feedback mediated via amacrine cell in the insect optic lobe. *J. Comp. Physiol. A. Sens. Neural Behav. Physiol.* **171**:447-455.
- Pongracz, F., Firestein, S., Shepherd, G.M. (1991). Electrotonic structure of olfactory sensory neurons analysed by intracellular and whole cell patch clamp. *J. Neurophysiol.* **65**:747-758.
- Rall, W. (1957). Membrane time constant of motoneurons. *Science* **126**:454.
- Rall, W. (1959). Branching dendritic trees and motoneurone membrane resistivity. *Exp. Neurol.* **1**:491-527.
- Rall, W. (1960). Membrane potential transients and membrane time constant of motoneurons. *Exp. Neurol.* **2**:503-532.
- Rall, W. (1962a). Theory of physiological properties of dendrites. *Ann. N.Y. Acad. Sci.* **96**:1071-1092.
- Rall, W. (1962b). Electrophysiology of a dendritic neuron model. *Biophys. J.* **2**:145-167.
- Rall, W. (1964). Theoretical significance of dendritic trees for neuronal input-output relations. In: *Neural Theory and Modelling*, edited by R. Reiss. Stanford Univ. Press, Stanford. pp. 73-97.
- Rall, W. (1967). Distinguishing theoretical synaptic potentials computed for different soma-dendritic distributions of synaptic input. *J. Neurophysiol.* **30**:1138-1168.
- Rall, W. (1969a). Time constants and electrotonic length of membrane cylinders and neurons. *Biophys. J.* **9**:1483-1508.
- Rall, W. (1969b). Distributions of potential in cylindrical coordinates and time constants for a membrane cylinder. *Biophys. J.* **9**:1509-1541.

- Rall, W. (1970a). Dendritic neuron theory and dendrodendritic synapses in a simple cortical system. In: *The Neurosciences: Second Study Program*, edited by F.O. Schmitt. Rockefeller, New York. pp. 552-565.
- Rall, W. (1970b). Cable properties of dendrites and effects of synaptic location. In: *Excitatory Synaptic Mechanisms*, edited by P. Andersen and J.K.S. Jansen. Universitetsforlag, Oslo. pp. 175-187.
- Rall, W. (1977). Core conductor theory and cable properties of neurons. In: *Handbook of Physiology: The Nervous System, Vol. 1*, edited by E.R. Kandel, J.M. Brookhardt and V.B. Mountcastle. Williams and Wilkins Co, Baltimore.
- Rall, W., Burke, R.E., Holmes, W.R., Jack, J.J.B., Redman, S.J. and Segev, I. (1992). Matching dendritic neuron models to experimental data. *Physiol. Rev.* **72**:159-186.
- Rapp, M., Segev, I. and Yarom, Y. (1994). Physiology, morphology and detailed passive models of guinea-pig cerebellar Purkinje cells. *J. Physiol. (Lond)*. **474**:101-118.
- Regehr, W.G., Konnerth, A. and Armstrong, C. (1992). Sodium action potentials in the dendrites of cerebellar Purkinje cells. *Proc. Natl. Acad. Sci. U.S.A.* **89**:5492-5496.
- Reyes, A., Galarrage, E., Flores-Hernandez, J., Tapia, D. and Bargas, J. (1998). Passive properties of neostriatal neurons during potassium conductance block. *Exp. Brain Res.* **120**:70-84.
- Rice, M.E., Richards, C.D., Nedergaard, S., Hounsgaard, J., Nicholson, C. and Greenfield, S.A. (1994). Direct monitoring of dopamine and 5-HT release in substantia nigra and ventral tegmental area in vitro. *Exp. Brain Res.* **100**:395-406.
- Roper, J. and Schwarz, J.R. (1989). Heterogeneous distribution of fast and slow potassium channels in myelinated rat nerve fibres. *J. Physiol. (Lond)*. **416**:93-110.
- Rose, P.K. and Vanner, S.J. (1988). Differences in somatic and dendritic specific membrane resistivity of spinal motoneurons: an electrophysiological study of neck and shoulder motoneurons in the cat. *J. Neurophysiol.* **60**:149-166.
- Safronov, B.V., Kampe, K. and Vogel, W. (1993). Single voltage-dependent potassium channels in rat peripheral nerve membrane. *J. Physiol. (Lond)*. **460**:675-691.
- Safronov, B.V. and Vogel, W. (1995). Single voltage-activated Na<sup>+</sup> and K<sup>+</sup> channels in the somata of rat motoneurons. *J. Physiol. (Lond)*. **487**:91-106.
- Safronov, B.V., Wolff, M. and Vogel, W. (1997). Functional distribution of three types of Na<sup>+</sup> channel on soma and processes of dorsal horn neurones of rat spinal cord. *J. Physiol. (Lond)*. **503**:371-385.
- Schiller, J., Helmchen, F. and Sakmann, B.J. (1995) Spatial profile of dendritic calcium transients evoked by action potentials in rat neocortical pyramidal neurones. *J. Physiol. (Lond)*. **487**:583-600.



- Schiller, J., Schiller, Y., Stuart, G. and Sakmann, B. (1997). Calcium action potentials restricted to distal apical dendrites of rat neocortical pyramidal neurons. *J. Physiol. (Lond)*. **505**:605-616.
- Schiller, J., Schiller, Y. and Clapham, D.E. (1998). NMDA receptors amplify calcium influx into dendritic spines during associative pre- and postsynaptic activation. *Nat Neurosci*. **1**:114-118.
- Segev, I., Fleshman, J.W., Miller, J.P. and Bunow, B. (1985). Modelling the electrical properties of anatomically complex neurons using a network analysis program: passive membrane. *Biol. Cyber*. **53**:27-40.
- Segev, I., Fleshman, J.W. and Burke, R.E. (1989) Compartmental models of complex neurons. In: *Methods in Neuronal Modelling: From Synapses to Networks*, edited by C. Koch and I. Segev. MIT Press, Bradford. pp. 63-96.
- Sekirnjak, C., Martone, M.E., Weiser, M., Deerinck, T., Bueno, E., Rudy, B. and Ellisman, M. (1997). Subcellular localization of the K<sup>+</sup> channel subunit Kv3.1b in selected rat CNS neurons. *Brain Res*. **766**:173-187.
- Shelton, D.P. (1985). Membrane resistivity estimated for the Purkinje neuron by means of a passive computer model. *Neurosci*. **14**:111-131.
- Sheng, M., Tsaur, M.L., Jan, Y.N. and Jan, L.Y. (1994). Contrasting subcellular localization of the Kv1.2 K<sup>+</sup> channel subunit in different neurons of rat brain. *J. Neurosci*. **14**:2408-2417.
- Smith, P.E., Brunne, R.M., Mark, A.E. and van Gunsteren, W.F. (1993). Dielectric properties of trypsin inhibitor and lysozyme calculated from molecular dynamics simulations. *J. Phys. Chem*. **97**:2009-2014.
- Snedecor, G.W. and Cochran, W.G. (1967) *Statistical Methods*, sixth edition. Iowa State University Press, Ames.
- Spruston, N. and Johnston, D. (1992). Perforated patch-clamp analysis of the passive membrane properties of three classes of hippocampal neurons. *J. Neurophysiol*. **67**:508-529.
- Spruston, N., Jaffe, D.B. and Johnston, D. (1994). Dendritic attenuation of synaptic potentials and currents: the role of passive membrane properties. *Trends Neurosci*. **17**:161-166.
- Spruston, N., Schiller, Y., Stuart, G. and Sakmann, B. (1995). Activity-dependent action potential invasion and calcium influx into hippocampal CA1 dendrites. *Science* **268**:297-300.
- Staley, K.J., Otis, T.S. and Mody, I. (1992). Membrane properties of dentate gyrus cells: comparison of sharp microelectrode and whole-cell recording. *J. Neurophysiol*. **67**:1346-1358.

- Stuart, G.J., Dodt, H.-U. and Sakmann, B. (1993). Patch-clamp recordings from the soma and dendrites of neurons in brain slices using infrared video microscopy. *Pflugers Arch.* **423**:511-518.
- Stuart, G. and Häusser, M. (1994). Initiation and spread of sodium action potentials in cerebellar purkinje cells. *Neuron* **13**:703-712.
- Stuart, G. and Sakmann, B. (1994). Active propagation of somatic action potentials into neocortical pyramidal cell dendrites. *Nature* **367**:69-72.
- Stuart, G. and Sakmann, B. (1995). Amplification of EPSPs by axosomatic sodium channels in neocortical pyramidal neurons. *Neuron* **15**:1065-1076.
- Stuart, G., Spruston, N., Sakmann, B. and Häusser, M. (1997a). Action potential initiation and backpropagation in neurons of the mammalian CNS. *TINS* **20**:125-131.
- Stuart, G., Schiller, J. and Sakmann, B. (1997b). Action potential initiation and propagation in rat neocortical pyramidal neurons. *J. Physiol. (Lond)*. **505**:617-632.
- Stuart, G. and Spruston, N. (1998). Determinants of voltage attenuation in neocortical pyramidal neuron dendrites. *J. Neurosci.* **18**:3501-3510.
- Svirskis, G., Gutman, A. and Hounsgaard, J. (1997). Detection of a membrane shunt by DC field polarization during intracellular and whole cell recording. *J. Neurophysiol.* **77**:579-586.
- Takahashi, T. (1990). Membrane currents in visually identified motoneurons of neonatal rat spinal cord. *J. Physiol. (Lond)*. **423**:27-46.
- Takigawa, T. and Alzheimer, C. (1999). G protein-activated inwardly rectifying K<sup>+</sup> (GIRK) currents in dendrites of rat neocortical pyramidal cells. *J. Physiol. (Lond)*. **517**:385-390.
- Thurbon, D., Field, A. and Redman, S. (1994). Electrotonic profiles of interneurons in stratum pyramidale of the CA1 region of rat hippocampus. *J. Neurophysiol.* **71**:1948-1958.
- Thurbon, D., Lüscher, H.-R., Hofstetter, T. and Redman, S.J. (1998). Passive electrical properties of ventral horn neurons in rat spinal cord slices. *J. Neurophysiol.* **79**:2485-2502.
- Tsubokawa, H. and Ross, W.N. (1996). IPSPs modulate spike backpropagation and associated [Ca<sup>2+</sup>]<sub>i</sub> changes in the dendrites of hippocampal CA1 pyramidal neurons. *J. Neurophysiol.* **76**:2896-2906.
- Tsubokawa, H., Offermanns, S., Simon, M. and Kano, M.J. (2000). Calcium-dependent persistent facilitation of spike backpropagation in the CA1 pyramidal neurons. *Neurosci.* **20**:4878-4884.
- Turner, D.A. and Schwartzkroin, P.A. (1983). Electrical characteristics of dendrites and dendritic spines in intracellularly stained CA3 and dentate hippocampal neurons. *J. Neurosci.* **3**:2381-2394.

- Turner, D.A. (1984). Segmental cable evaluation of somatic transients in hippocampal neurons (CA1, CA3 and Dentate). *Biophys. J.* **46**:73-84.
- Ulfhake, B. and Kellerth, J.-O. (1984). Electrophysiological and morphological measurements in cat gastocnemius and soleus  $\alpha$ -motoneurons. *Brain Research* **307**:167-179.
- Ulrich, D., Quadroni, R. and Lüscher, H.-R. (1994). Electrotonic structure of motoneurons in spinal cord slice cultures: a comparison of compartmental and equivalent cylinder models. *J. Neurophysiol.* **72**:861-871.
- Urban, N.N., Barrionuevo, G. (1998). Active summation of excitatory postsynaptic potentials in hippocampal CA3 pyramidal neurons. *Proc. Natl. Acad. Sci. U.S.A.* **95**:11450-11455.
- Veh, R.W., Lichtinghagen, R., Sewing, S., Wunder, F., Grumbach, I.M. and Pongs, O. (1995). Immunohistochemical localization of five members of the Kv1 channel subunits: contrasting subcellular locations and neuron-specific co-localization in rat brain. *Eur. J. Neurosci.* **7**:2189-2205.
- Velte, T.J. and Masland, R.H. (1999). Action potentials in the dendrites of retinal ganglion cells. *J. Neurophysiol.* **81**:1412-1417.
- Viana, F., Bayliss, D.A. and Berger, A.J. (1993). Multiple potassium conductances and their role in action potential repolarization and repetitive firing behavior of neonatal rat hypoglossal motoneurons. *J. Neurophysiol.* **69**:2150-2163.
- Walton, K. and Fulton, B.P. (1986). Ionic mechanisms underlying the firing properties of rat neonatal motoneurons studied *in vitro*. *Neuroscience* **19**:669-683.
- Weber, H. (1873). Über die stätionären Strömungen der Elektrizität in Cylindren. *Bochardt's J. Math.* **76**:1.
- Westenbroek, R.E., Merrick, D.K. and Catterall, W.A. (1989). Differential subcellular localization of the Ri and Rii Na<sup>+</sup> channel subtypes in central neurons. *Neuron* **3**:695-704.
- Westenbroek, R.E., Hoskins, L. and Catterall, W.A. (1998). Localization of Ca<sup>2+</sup> channel subtypes on rat spinal motor neurons, interneurons and nerve terminals. *J. Neurosci.* **18**:6319-6330.
- Westenbroek, R.E., Ahlijanian, M.K. and Catterall, W.A. (1990). Clustering of L-type Ca<sup>2+</sup> channels at the base of major dendrites in hippocampal pyramidal neurons. *Nature* **347**:281-284.
- Westrum, L.E. (1993). Axon hillocks and initial segments in spinal trigeminal nucleus with emphasis on synapses including axo-axonic contacts. *J. Neurocytol.* **22**:793-803.
- Williams, S.R. and Stuart, G.J. (1999). Mechanisms and consequences of action potential burst firing in rat neocortical pyramidal neurons. *J. Physiol. (Lond)*. **521**:467-482.

- Williams, S. R. and Stuart, G.J. (2000a). Action potential backpropagation and somato-dendritic distribution of ion channels in thalamocortical neurons. *J. Neurosci.* **20**:1307-1317.
- Williams, S.R. and Stuart, G.J. (2000b). Site independence of EPSP time course is mediated by dendritic  $I_h$  in neocortical pyramidal neurons. *J. Neurophysiol.* **83**:3177-3182.
- Wilson, C.J. (1995). Dynamic modification of dendritic cable properties and synaptic transmission by voltage-gated potassium channels. *J. Comput. Neurosci.* **2**:91-115.
- Wolff, M., Vogel, W. and Safronov, B.V. (1998). Uneven distribution of  $K^+$  channels in soma, axon and dendrites of rat spinal neurones: functional role of the soma in generation of action potentials. *J. Physiol. (Lond)*. **509**:767-776.
- Wong, R.S., Prince, D.A. and Basbaum, A. (1979). Intradendritic recordings from hippocampal neurons. *Proc. Natl. Acad. Sci. U.S.A.* **76**:986-990.
- Yuste, R. and Denk, W. (1995). Dendritic spines as basic functional units of neuronal integration. *Nature* **375**:682-684.
- Yuste, R., Majewska, A., Cash, S.S. and Denk, W. (1999). Mechanisms of calcium influx into hippocampal spines: heterogeneity among spines, coincidence detection by NMDA receptors, and optical quantal analysis. *J. Neurosci.* **19**:1976-1987.